Proteomics Analysis of Protein-Producing Chinese Hamster Ovary Cells during Apoptosis in Prolonged Cultivation

by

Yi-Yun Wei

A thesis
presented to the University of Waterloo
in fulfilment of the
thesis requirement for the degree of
Master of Science
in
Biology

Waterloo, Ontario, Canada, 2010

Author's Declaration

I hereby declare that I am the sole author of this thesis. This is a true copy of the thesis, including any required final revisions, as accepted by my examiners.

I understand that my thesis may be made electronically available to the public.

Abstract

Among the factors important for maintaining productivity of recombinant proteins in mammalian cells, culture lifetime, cell density and cell viability are three simple but essential aspects that can greatly influence the final yield. During cell culturing, the degradation of environmental conditions such as nutrient depletion and accumulation of toxic waste products, often lead to premature apoptotic cell death in cultures and suboptimal protein yield. Although apoptosis has been extensively researched, the changes in the whole cell proteome during prolonged cultivation, where apoptosis is a major mode of cell death, have not been examined. The work presented in this thesis is the first whole cell proteome analysis of non-induced apoptosis in mammalian cells.

Flow cytometry (FCM) analyses of the level of activated executioner caspases, caspase 3 and 7, demonstrated the onset of apoptosis in CHO batch cultures after the exponential phase. The monitoring of apoptotic cell death assesses the culture conditions at different time points and allows the association of changes in the protein abundances to the degradation of culture conditions, in particular the degree of apoptosis in the whole cultures. The detection of activated caspase 8 and caspase 9, which trigger the extrinsic and intrinsic pathway respectively, has shown that the onset of apoptosis in CHO cells during prolonged cultivation predominantly is via the intrinsic pathway.

To examine the proteomic changes in a monoclonal antibody-producing CHO cell culture at various phases of a batch culturing process, a differential in gel electrophoresis (DIGE) proteomic approach was employed in this study. CHO protein samples at four time points during cultivation were compared. A total of 40 differentially expressed protein spots were successfully identified by mass spectrometry sequencing, resulting in 28 unique protein identifications. These proteins include four structural proteins of the cytoskeleton, ten endoplasmic reticulum and cytosolic chaperones and folding proteins, seven metabolic enzymes and seven other proteins of varied function. The cleavage of

cytoskeletal proteins is a known consequence of apoptosis and the activation of executioner caspases. On the other hand, the induction of seven ER chaperone and foldases is a solid indication for the onset of unfolded protein response (UPR), which is triggered by cellular and ER stresses, many of which are present during prolonged batch cultures. In addition, the upregulation of six glycolytic enzymes and another metabolic protein emphasizes a change in the energy metabolism likely occurred when culture conditions degraded and apoptosis advanced. Interestingly, although a significant portion of proteins identified are well known housekeeping proteins, recent studies have shown that many of them exhibit a wide variety of other roles, including apoptosis regulation and execution. Overall, this study shows that the most drastic changes in aging CHO cultures, where apoptosis is known to be part of, involve the onset of UPR and upregulation of proteins catalyzing glucose metabolism.

Acknowledgements

I would like to express my gratitude to my supervisors, Dr. Brendan McConkey and Dr. Brian Ingalls for their continuous guidance and encouragement throughout this project. I am grateful for having this opportunity to work on such an interesting research topic and for the diverse experience that I have gained. In addition, I would like to thank Dr. Hector Budman and Dr. Jeno Scharer for their scientific direction and insightful discussion in this collaborative research project.

I thank all my fellow lab mates for listening to my constant complains and random nonsense. I am truly indebted to Owen Woody, Zhenyu Cheng and DongRyoung Kim for answering countless statistical and proteomic questions. I also would like to thank Saeideh Naderi for training me on cell culturing and helping me throughout this project. In addition, I want to thank Mishi Savulescu for her expertise in flow cytometry analyses.

Above all, I would like to convey my thanks to my family and friends for their emotional support and motivation to keep me pursing my master degree. Specifically, I would like to thank Jason Hung for his never-ending encouragement and unconditional support. Also, kisses and hugs for my adorable pet rabbit Muffin, who always brightens up my days.

This thesis would not have been possible without the support and help from the above mentioned people.

Table of Contents

List of Figures

List of Tables

List of Abbreviations

2D GE	two-dimensional gel electrophoresis
ACN	acetonitrile
AIF	apoptosis inducing factor
ANOVA	one-way analysis of variance
AP-1	activator protein-1
ATPB	ATP synthase beta subunit
BH	Bcl-2 homology (domain)
BiP	Binding immunoglobulin protein
BSA	bovine serum albumin
BVA	Biological Variation Analysis (of DeCyder gel analysis software)
CAD	caspase-activated DNAse
CARD	caspase recruitment domain
DED	death effector domain
DD	death domain
DHFR	dihydrofolate reductase
DI	deionized
DIA	Differential In gel Analysis (of DeCyder gel analysis software)
DIGE	Differentially in gel electrophoresis
DISC	death-inducing signalling complex
DMSO	dimethyl sulfoxide
DTT	dithiothreitol
ERp60	Endoplasmic reticulum protein 60kDa
ER	endoplasmic reticulum
ERSE	ER stress response element
ESI	electrospray ionization
FA	formic acid
FADD	Fas-associated death domain
FAM	carboxyfluorescein
FCM	flow cytometry
FDR	false discovery rate
FKBP52	FK506-binding protein 52
FLICA	fluorescent inhibitor of caspase
FMK	fluoromethyl ketone
GAPDH	Glyceraldehydes-3-phosphate dehydrogenase
GOI	gene of interest
GRP	Glucose-regulated protein
GS	glutamine synthetase
GSH	glutathione (antioxidant)
HSC70	Heat shock cognate protein 70kDa
HSP	Heat shock protein
ICAD	inhibitor of CAD
IEF	isoelectric focusing
IPG	immobilized pH gradient
IMM	inner-mitochondrial membrane
IMS	intermembrane space (of mitochondria)
JNK	c-Jun-N-terminal kinase
LAMR1	Laminin receptor 1

IAA	iodoacetamide
IAP	inhibitors of apoptosis proteins
LBC	lower buffer chamber
LDH	L-lactate dehydrogenase chain
MAb	monoclonal antibody
MOMP	mitochondrial outer membrane permeabilization
MS	mass spectrometry
MW	molecular weight
NO	nitric oxide
PBS	phosphate buffered saline
PCD	programmed cell death
PDI	Protein disulfide isomerase
PGM	Phosphoglycerate mutase
PGK	Phosphoglycerate kinase 1
PK	Pyruvate kinase isozyme M1/M2
pI	isoelectric points
PI	propidium iodide
Prx6	Peroxiredoxin-6
PS	phosphatidylserine
QIT	Quadruple Ion Trap
QTof	Quadruple-Time Of Flight
RIP	DD-containing receptor-interacting kinase
ROS	reactive oxygen species
SDS-PAGE	sodium dodecyl sulfate-polyacrylamide gel electrophoresis
SILAC	stable isotope labelling with amino acid in cell culture
SODD	silencer of death domain
TCA	tricarboxylic acid
TNF	tumor necrosis factor
TPI	Triosephosphate isomerase
TRADD	TNF receptor type 1-associated death domain protein
TRAF2	TNF receptor-associated factor 2
UBC	upper buffer chamber (of the DAL*Six* gel electrophoresis system)
UPR	unfolded protein response
UPRE	UPR element (which is a transcriptional factor)

Chapter 1. Introduction

1.1 Chinese Hamster Ovary Cell Line

Mammalian cell cultures are the preferred expression hosts for the production of animal recombinant proteins due to their ability to ensure proper protein folding and posttranslational modifications. Among the first few transfected mammalian cultures that were generated by non-viral gene delivery was the immortalized Chinese hamster ovary cells [1]. It was estimated that nearly 70% of all therapeutics produced today are made in CHO cells [2]. The biologics produced by these rodent cells brought in over $30 billion US dollars of worldwide annual sale [2]. As a result of its popularity and reliability in the commercial industry and research laboratories, CHO cells have been awarded and regarded as the "mammalian equivalent of the model bacterium *Escherichia coli*" [2].

1.1.1 History and Characteristics of CHO Cell Lines

The introduction of tissue cultures, including a continuous Chinese hamster (*Cricetulus griseus*) ovary cell line, began in 1957 when Dr. Theodore Puck created several mammalian cell cultures via organ explants of various human and animal sources [3]. Since the creation of the original CHO strain, CHBOC1, more CHO cell lines with different nutritional requirement and enzymatic deficiencies have been developed. For instance, CHO-K1, which is a widely utilized proline-auxotrophic strain, was subcloned from CHBOC1. As a derivative of CHO-K1, DUKX-B1 is deficient in dihydrofolate reductase (DHFR) due to subsequent mutation and gene inactivation [4]. In comparison, both *dhfr* alleles in the genome of DG44 cells were lost due to gene deletion, resulting in a more stable DHFR-minus cell line [5]. To date, the American Type Culture Collection, which is a central depository for biological materials including many cell lines, microorganisms and bio-products, has 42 CHO cell lines and a few Chinese hamster lung and peritoneum cell lines [6].

Although CHO cells are naturally anchorage dependent cells that grow into a fibroblast or epithelial monolayer [6], adaptation into suspension culture has long been achieved. Furthermore, many CHO cultures can be grown in serum-free, chemically defined synthetic medium [7,8], as opposed to the original CHO cell line which requires serum [3]. Ham's 12, which was used for cultivating CHBOC1 originally, and alpha-modified minimal essential media (MEM) were among the more traditional CHO culturing media. With the increase in popularity of CHO cells, many strain-specific and generalized defined media have been formulated to support and enhance CHO cell growth. CDM4CHO, which is suitable for recombinant protein production and the protein-free medium SMF4CHO-Utility [9] are two examples of commercial CHO media available. Other than choosing a medium that supplies the appropriate nutrients, maintaining proper temperature and pH of the culture medium is also important for optimal cell proliferation. For Chinese hamster ovary cells, the medium should be maintained between 36 ºC and 38.5ºC with a pH range from 7 to 8.2 [10].

A normal diploid Chinese hamster cells has 22 chromosomes. However, karyotypic studies have shown that cells from CHBOC1 can display heterogeneity with varying number of chromosomes such as 21, 23 and 44 [11]. Similarly, this heterogeneity was observed in CHO-K1 with a modal 21 chromosomes [12]. On the other hand, DK44 cells exhibit 20 chromosomes consistently [5].

1.1.2 Utilization of CHO cells in Research and Industries

Since their establishment, CHO cell lines have been heavily utilized in various fields of research, including genetics, cell cycle, DNA damage repair, toxicology and drug addiction. For having a low chromosome numbers, being functional hemizygous in many genes, and displaying karyotype heterogeneity in the population, CHO cells have been used in cytogenetic studies [2]. Moreover, CHO cells can be reversibly synchronized at G1 phase with dimethyl sulfoxide (DMSO) and Lovastatin, to facilitate cell cycle studies [13,14]. By transfecting CHO cells with foreign proteins or exposing cells

to various compounds, studies on changes in mammalian cells due to these particles can be thoroughly monitored and investigated. The examination of toxic effects of chemicals and therapeutics, and cellular responses to viral antigens has been carried out using CHO cultures by numerous research groups [2,15,16]. In addition to the study of the effects of foreign compounds, stable expression of proteins of interest can also allow the study of the associated cellular pathways. Lastly, several CHO mutants deficient in DNA damage repair have been used to explore the mechanism of DNA interstrand cross-linking, which is often induced by anti-cancer drugs [17].

In addition to the usage of CHO cells in research laboratories, the employment of biologics-producing CHO cultures in commercial industries has also been widely executed for over 20 years. In 1987, the production of tissue plasminogen activator (tPa) using CHO cells became the first therapeutic recombinant protein produced in mammalian cells clinically approved. Since then many protein products, including monoclonal antibodies (MAb), hormones and enzymes, have been manufactured using CHO cell cultures [2] for therapeutic and diagnostic purposes [18]. For instance, the CHO strain IgG-9β8 under investigation in this thesis was developed from the cell line CHO dhfr$^-$-1 at Cangene Corporation in Mississauga. It expresses a human IgG specific for the Rhesus D (RhD) antigen [19]. Since RhD factors are implicated in several hematologic disorders, anti-RhD MAb might be an alternative to polyclonal anti-RhD prepared from human plasma for treating diseases such as haemolytic disease in newborns and idiopathic thrombocytopenic purpura [20].

1.1.3 Protein Manufacturing using CHO Cultures

The classical method for establishing a protein-producing CHO cell line is a time-consuming and laborious process which can take industries more than six months to develop a suitable expression host and culturing setting for a candidate therapeutic [2]. The first step in developing a high-producing cell line is the creation and delivery of a gene construct containing the gene of interest (GOI) and

selection genes into the host cell for chromosome integration. Selection of transfected cells is carried out in cultures lacking a critical component and hence will not permit the survival of non-transfected cells. The selection gene encoded in the transfected vector provides the missing component that is necessary for propagation of cells. Dihydrofolate reductase (*dhfr*) and glutamine synthetase (*gs*), which are two frequently used selection genes in CHO cultures, work in conjunction with *dhfr* minus host cells and medium without glutamine respectively. Expression of gene of interest can be significantly increased by exposing cells to a drug that blocks the enzymatic activity of the selection marker, in a process called amplification. DHFR and GS are inhibited by methotrexate (MTX) and methionine sulphoximine (MSX) respectively [1]. By applying more selection pressure, the copy number of the inserted DNA increases, resulting in a cell population with varying integration sites, copy numbers, growth rate and specific GOI productivities. Hence, after selection and amplification steps, screening must be done to isolate a small set of candidate protein-production cell lines. The chosen clones are expanded through passaging to allow further evaluation, until finally a single cell line is selected for clinical trial and eventually into mass commercial production.

Present day protein manufacturing processes can routinely yield 10 to 50 fold higher protein amounts than ones developed in the 1980s. Typical cultures in the early 80s were maintained in simple week-long batch set up which had a maximal cell density of $2x10^6$ cells/mL, a specific productivity of less than 10ρg/cell per day and a final titre of 100mg/L [2,21]. With the development of more advance culturing systems, processes performed in recent years have demonstrated the ability to reach $10x10^6$ cells/mL and maintain high viability for weeks. The final protein harvest can now reach 1-5g/L with specific productivity up to 90ρg/cell per day [21]. The improvement of yield over time was tightly associated with having a better understanding of gene expression, metabolism, growth and apoptosis in mammalian cell cultures, host cell engineering, cell line screening methods and manufacturing procedures.

With the aim of establishing high-yield CHO cell lines, numerous approaches have been suggested and employed by researchers and industries over the years. These methods can roughly be classified as i) genetic means, which include vector designing, genetic modification of host cell, or as ii) environment modification, which can involve the optimization of medium and culturing conditions such as temperature and pH, and chemical supplementation. These strategies may affect culture longevity, cell density, cell viability or protein productivity, leading to an increase in the total product yield.

1.1.4 Cell Death in Cell Cultures and its Effect on Protein Manufacturing

Although apoptosis, which is a type of cellular suicide, was first described and characterised in the 1970s, the concept that many cell lines undergo apoptotic cell death in response to the stressful culture environment in bioreactors was first suggested by Al-Rubeai in 1990 [22]. The identification of apoptosis in commercially important animal cell lines such as hybridoma, plasmacytoma and CHO cell lines have been documented using various detection methods. Some of these assays were electron and fluorescence microscopic examination of nuclear morphology, DNA gel electrophoresis, which can show the presence of DNA fragmentation, Western blot identification of cleaved caspase substrates and flow cytometry detection of apoptotic proteins [22-25]. High levels of apoptotic cell deaths have been observed at the end of CHO batch cultures, though the precise level of apoptosis in the cell population could vary due to differences between cell lines, culture conditions and the employed detection assays. In one study, more than 95% of the cell death that occurred during batch cultivation of a serum-free γ-interferon-producing CHO cell cultures was reported to be due to apoptosis [26]. Meanwhile, a high correlation ($R^2 = 0.986$, n=8) between apoptosis and total cell death in cultures, as determined by Trypan Blue assays, was noted in another serum-free CHO batch culture [24]. In this study, it was further concluded that the predominant apoptotic cell death was unrelated to the production of a protein product. Despite these variations, apoptosis still accounts for the majority of cell death occurring in bioreactors during the production of biopharmaceuticals from animal cell lines [24,27].

The induction of apoptosis in cell cultures can be triggered by many detrimental stresses (details in Section 1.2 below). Nutrient limitation, including deprivation of glucose, essential amino acids and non-essential amino acids, is one of the primary causes leading to cell death during the stationary and death phase of batch culture [23,28,29]. Other possible causes of cell death in bioreactors include extreme oxygen levels (hyperoxia and hypoxia) and mechanical agitation in the hydrodynamic environment [27]. Regardless of what triggers apoptosis in cell cultures, it poses a major limiting factor in the production of recombinant proteins [24]. Ongoing cell death in bioreactors makes the maintenance of high cell density with high viability difficult. Not only can this decrease in total viable cell number reduce the final yield, the release of cellular remains and associated degradative enzymes into the medium can also complicate purification and negatively affect the quality of the products [30-32]. At the very basic, maintaining viability and prolonging cultivation period via preventing or delaying apoptosis can be two straightforward strategies for increasing productivity. Hence, the understanding of cell death has been an important component in the optimization of recombinant protein producing cultures.

1.2 Apoptosis

As a mode of programmed cell death (PCD), apoptosis is a controlled and regulated mechanism for cell death triggered by external death stimuli or internal cell stress signals. Apoptotic cells can be characterized by distinct morphological changes including cell shrinkage, nuclear DNA fragmentation, chromatin condensation, membrane blebbing and the formation of apoptotic bodies [33,34]. The term apoptosis was first defined in 1972 by Kerr, Wyllie and Currie to describe the morphologies that had been observed in this particular type of cell death [35]. Apoptosis differs from necrosis, which is an energy independent and passive way of cell death. The morphologies of necrosis include cell swelling, karyolysis (nonspecific DNA fragmentation), membrane disruption, organelle lysis and finally disruption of the cell membrane [33,34,36]. Moreover, leakage of cellular proteins such as lysosomal

enzymes from necrotic cells also generates inflammatory response to surrounding cells causing further damages. Such nonspecific amplifying of cell deaths does not occur with apoptotic cells as the cellular contents are enclosed in apoptotic bodies and not released directly into the extracellular space.

Apoptosis can act as a form of natural defense mechanism to immune reactions or against disease. Its proper function is also crucial during development and aging to maintain cell populations and achieve homeostasis in tissues [34]. Different cells can have diverse response to the same stimuli and conditions. As a form of PCD, apoptosis triggers cell suicides via "genetically determined elimination" [34].

1.2.1 Morphological Progress of Apoptotic Cells

During the early stage of apoptosis, cell shrinkage occurs due to the breakdown of the structural proteins in the cytoskeleton (Figure 1-1). This shrinkage packs the organelles closer and condenses the cytoplasm. Next, the hallmark of apoptosis, **pyknosis** or the irreversible condensation of nucleus, occurs [35,37]. These changes to cell size and chromatin are both visible under light microscope [35]. Blebs, which are irregular bulging of the plasma membrane, begin developing in these apoptotic cells. Following extensive blebbing, nuclear fragmentation known as **karyorrhexis** and the fragmentation of DNA occur. Lastly, the cells disintegrate into individual apoptotic bodies, which enclose a portion of the cytoplasm including organelles and cellular proteins. In vivo, apoptotic bodies will be engulfed by macrophages via phagocytosis, which ensures a clean and efficient removal of the apoptotic cells that does not cause inflammatory responses in surrounding cells. Due to the lack of phagocytic cells, apoptotic bodies likely remained in culture longer than they normally exist in vivo [24]. The process of apoptosis from initiation to the formation of apoptotic bodies is thought to be completed in hours; studies have suggested it can be as quick as 1-3 hours [35].

Chromatin fragmentation occurs when chromatin breaks into large fragments inside the original nuclear membrane. When each chromatin fragment is enclosed by a membrane, this phenomenon is termed **nuclear fragmentation** [38]. Pyknosis has been associated with the reduction of cellular and nuclear volume [37].

Another biochemical feature of apoptosis worth noting is the exposure of cell surface phagocytic recognition markers. Among these, the externalization of phosphatidylserine (PS), which normally resides in the inner-leaflet of the cellular membrane [34], is a well-known and commonly used characteristic for the detection of apoptosis. Comparing to other apoptosis features, exposure of PS was reported to be prior to cell shrinkage, nuclear changes and the loss of plasma membrane integrity [39,40].

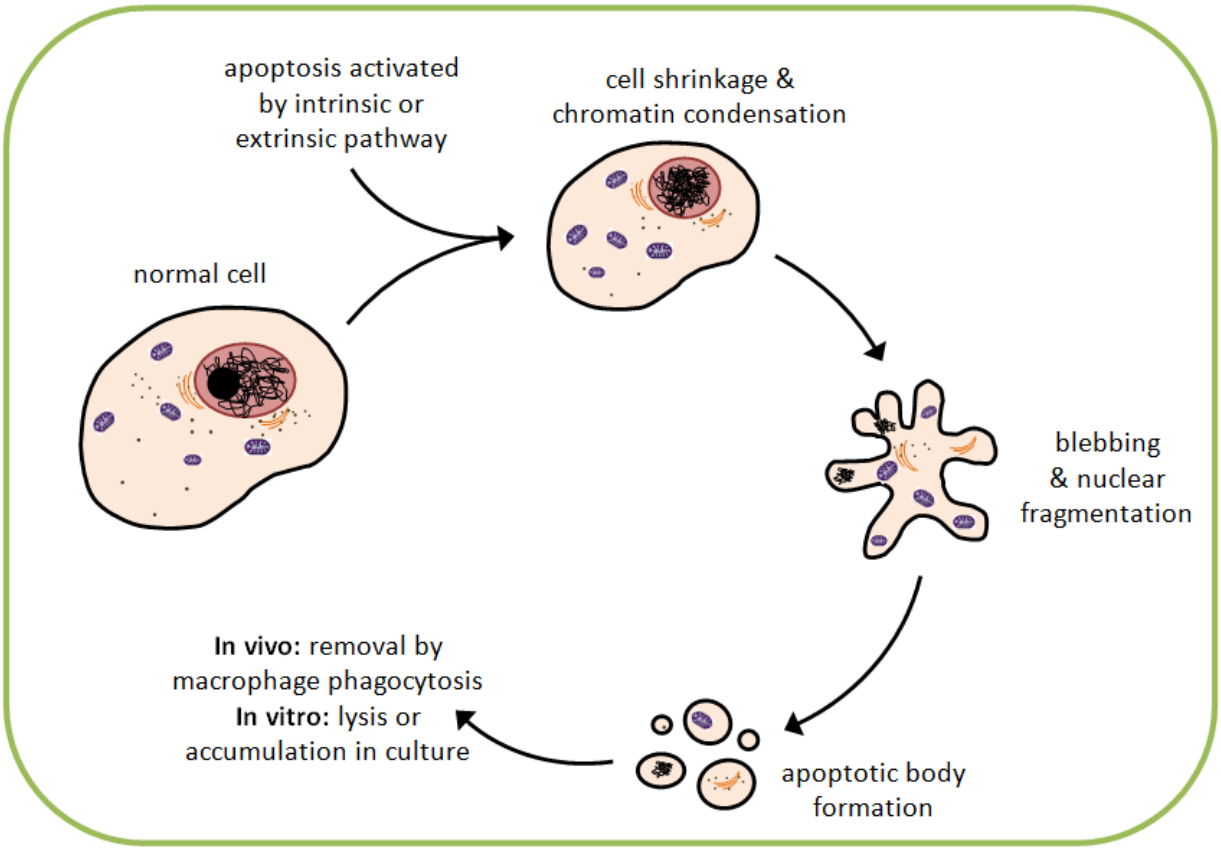

Figure 1-1. Morphological changes of a cell as apoptosis progresses. *Modified from [41].*

1.2.2 Caspases - Important Initiator and Executioner of Apoptosis

Many morphological changes observed in cells undergoing apoptosis are caused by a cysteine protease called caspase 3. In addition to caspase 3, many other members of the **c**ysteinyl **asp**artic acid prote**ase** (caspase) protein family have been associated with apoptosis. Currently, there are at least 14 mammalian caspases that have been identified but not all take part in the process of apoptosis. The apoptotic caspases are categorized into 2 classes: initiator caspases which react to apoptotic stimuli in cells and signal the onset of programmed cell death, and effector caspases which are activated by initiator caspases and are responsible for the proteolytic cleavage of various essential cellular proteins, leading to cell death (see Figure 1-2) [42,43].

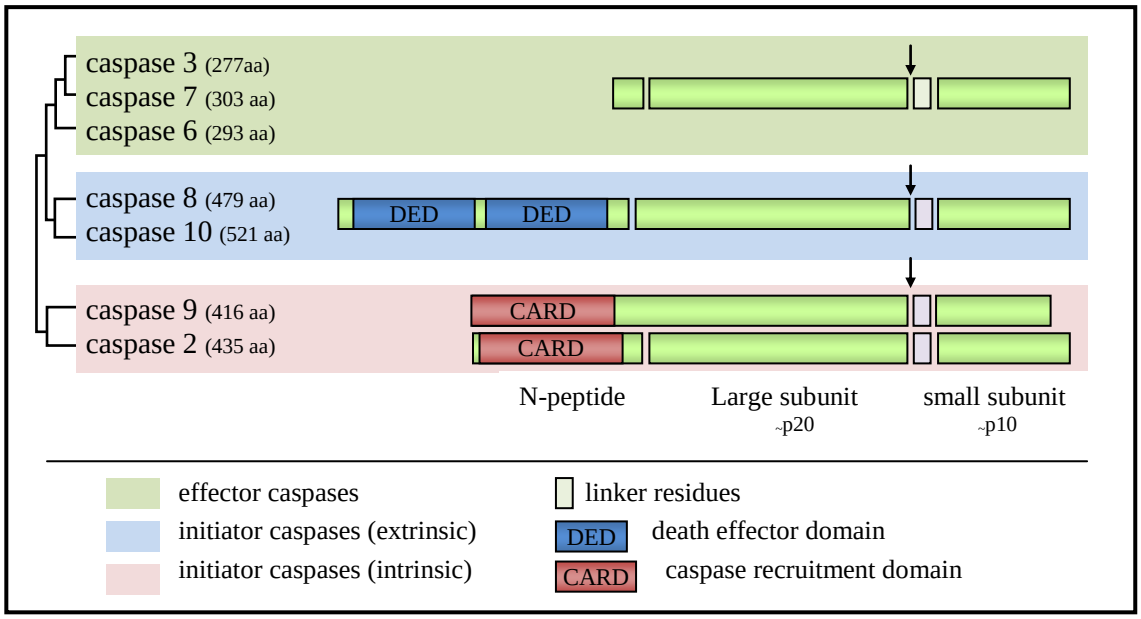

Figure 1-2. Structures of processed mammalian caspases and phylogenetic relationship between apoptotic members of the caspase protein family. *Figure based on [43-45].* The intra-chain activation cleavage which separates the large and small subunit is indicated by the black arrows. Sometimes, additional cleavage removes a short linker sequence between the two subunits.

Caspases typically share a consensus substrate cleavage site consisting of the amino acid sequence X-X-X-Asp where X can be any amino acid. They are synthesized as a single chain zymogen

that requires proteolytic activation during apoptosis [43,46]. Activated caspases are heterotetramers consisting of two set of large and small subunits [47]. Initiator caspases contain either the death effector domain (DED) or caspase recruitment domain (CARD) (see Figure 1-2), which allows them to be recruited by adaptor proteins and be activated. After the recruitment and autoproteolytic cleavage, each molecule of caspases is cleaved into 2 units: a p10 small subunit plus a p20 subunit [43,48].

1.2.3 Mechanism and Pathways of Apoptosis

Mammalian cells can undergo apoptosis through various signalling pathways initiated at different cellular locations including mitochondria, the cell surface and the endoplasmic reticulum, in response to varying stimuli. The extrinsic and intrinsic pathways are two major cell death-inducing signalling pathways that are well characterized and studied. More recently, other mechanisms such as the ER pathway [33] and the perforin/granzyme pathway have also been discovered [34]. The following subsection introduces the two major pathways and the key proteins associated with them.

1.2.3.1 Overview of the Intrinsic Pathway

The intrinsic or mitochondrial pathway (see Figure 1-3) can be triggered by intracellular cell stress signals generated from a variety of non-receptor mediated stimuli including growth factor withdrawal, Ca^{2+} flux, UV irradiation and toxin accumulation [33]. Stimuli can either involve the withdrawal of survival factors which results in the failure to continue suppressing death programs or the direct introduction of apoptotic factors such as toxins, radiation, free radicals and unfolded proteins [34,49].

The Bcl-2 protein family, consisting of at least 25 members (Table 1-1 and 1-2) [34], is known for the sensing of various types of intrinsic stress signals and the control of subsequent mitochondrial

response. Upon the detection of intracellular stimuli, Bcl-2 members migrate to the mitochondria and cause changes to the mitochondrial membrane, eventually leading to mitochondrial outer membrane permeabilization (MOMP). As a result, apoptosis progresses further by the loss of mitochondrial transmembrane potential and the release of pro-apoptotic molecules from the intermembrane space (IMS) into the cytosol [33,50].

Among the released proteins, cytochrome *c*, Smac/DIABLO, HtrA2/Omi are important in the activation of initiator caspase 9 and subsequent apoptotic execution phase. Once cytochrome c is released into the cytosol, it recruits Apaf-1 and procaspase 9 to form the apoptosome complex which then triggers the autoproteolytic activation of procaspase 9. The active caspase 9 then begin the execution of apoptosis by activating caspase 3. Meanwhile, Smac/DIABLO and HtrA2/Omi neutralize the activity of IAP (inhibitors of apoptosis proteins), which can suppress caspases. Moreover, AIF, endonuclease G and CAD are also released from the mitochondria. Both AIF (apoptosis inducing factor) and endonuclease G require no activation by caspases. Upon release from the mitochondria, they translocate to the nucleus and interact with chromatin. AIF cuts DNA into large fragments of 50-300kb and causes condensation of peripheral nuclear chromatin, while endonuclease G produces oligonucleosomal fragments. Meanwhile, the released CAD protein requires translocation to the nucleus and activation by caspase cleavage before it can also produce oligonucleosomal DNA fragments and further chromatin condensation [34].

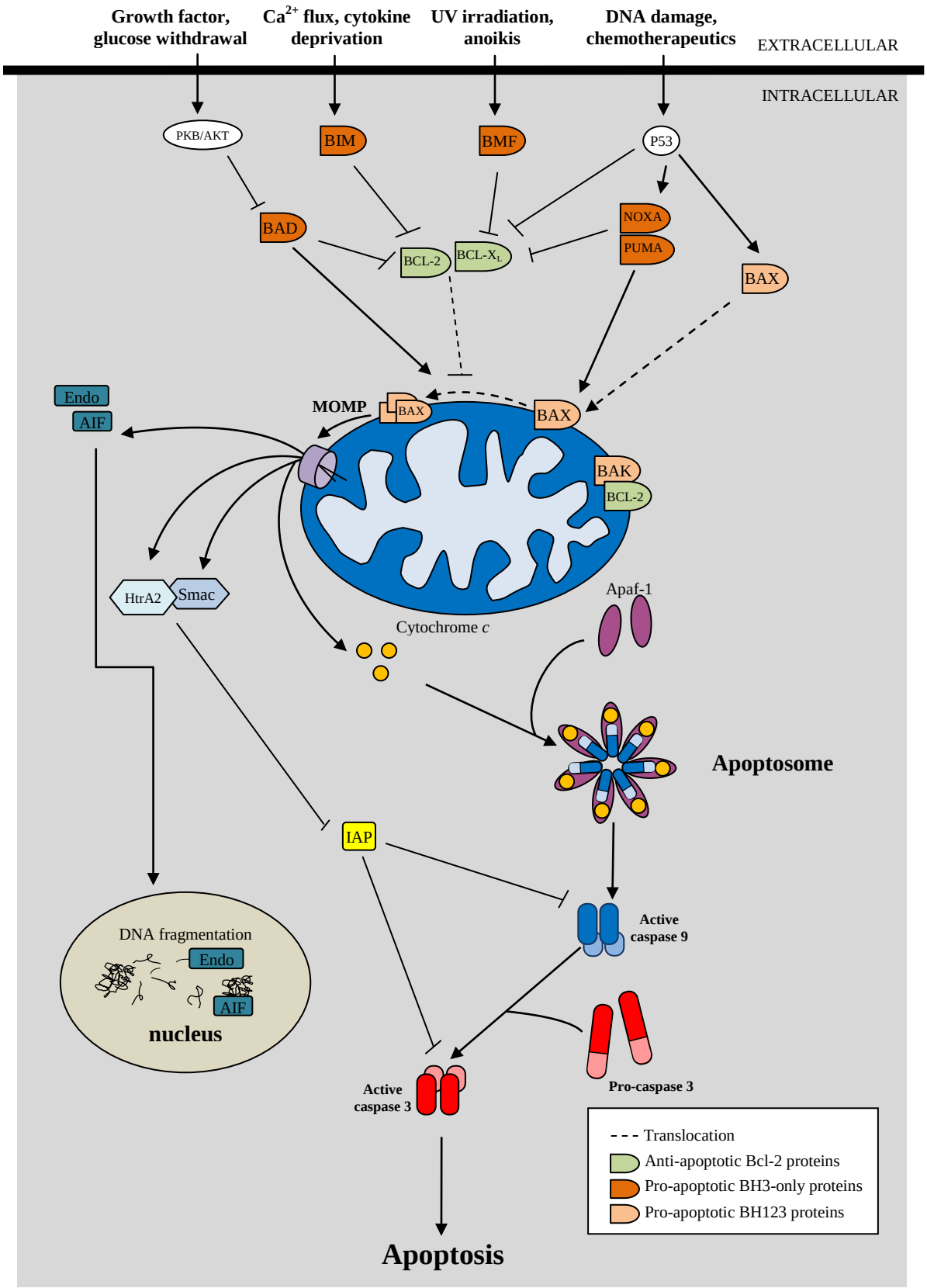

Figure 1-3. Intrinsic Apoptosis Pathway. *Figure based on [33,51,52]. See text for details.*

Bcl-2 Protein Family

Members of the Bcl-2 protein family all contain at least one of the four Bcl-2 homology (BH) domains. Pro-survival Bcl-2 family members are multidomain proteins containing at least three of the four BH domains: BH1, BH2, BH3 and BH4; while pro-apoptotic Bcl-2 members can be subdivided into multidomain proteins with BH1-3 domains, and BH3-only [34,53,54]. BH3-only proteins sense intracellular stress signals and in response, trigger cell death by inducing the oligomerization of pro-apoptotic BH123 proteins at the outer mitochondrial membrane. The anti-apoptotic Bcl-2 members promote cell survival by neutralizing the BH123 molecules. Hence the ratio and interaction between anti- and pro-apoptotic Bcl-2 proteins determine whether cells will commit to apoptosis [51]. Other than being sensors to stimuli, some BH3-only proteins can also release BH123 proteins from their sequestering anti-apoptotic Bcl-2 relatives.

Table 1-1. Pro-apoptotic members of the Bcl-2 protein family [34,49,52,55]

Abbreviation Name	Full name	Domain structure	Aliases
BAX	Bcl2 associated X protein	BH123	BCL2L4
BAK	Bcl2 antagonist killer 1	BH123	BCL2L7
BOK	Bcl2-related ovarian killer	BH123	BCL2L9
BID	BH3 interacting domain death agonist	BH3	p22 BID
BAD	Bcl2 antagonist of cell death	BH3	BBC6, BCL2L8
BIM	Bcl2 interacting mediator of cell death	BH3	BCL2L11, BOD
BIK	Bcl2 interacting killer	BH3	NBK, BP4, BIP1
BLK	Bik-like killer protein	BH3	BIKLK
PUMA	p53 up-regulated modulator of apoptosis	BH3	BBC3
Bcl-X_S	Bcl2-like protein 1, short isoform	BH34	
Noxa*	Phorbol-12-myristate-13-acetate-induced protein 1	BH3	PMAIP1
BMF	Bcl-2 modifying factor	BH3	

** Noxa is Latin for damage.*
Abbreviations: BCL2L, Bcl2-like protein; Bcb, Bcl2-binding component;

Table 1-2. Anti-apoptotic members of the Bcl-2 protein family [34,49,52,55]

Abbreviation Name	Full name	Domain structure	Aliases
Bcl-2	B-cell lymphoma protein 2;	BH1234	
Bcl-X_L	Bcl2-like protein 1, long isoform	BH1234	
MCL1	Myeloid cell leukemia sequence 1	BH123	BCL2L3, EAT
BCL-W	BCL2 like protein 2	BH1234	BCL2L2
BFL-1	Bcl-2 related protein A1	BH123	BCL2L5, GRS, BCL2A1
BCL-B	BCL2 like protein 10	BH1234	BCL2L10, Boo, Diva

Abbreviation: BCL2L, Bcl2-like protein

1.2.3.2 Overview of Extrinsic Pathway

The extrinsic pathway, also known as the death receptor pathway, is mediated by death ligands and death receptors. Apoptosis is initiated by the binding of death ligands (Table 1-3) to their corresponding cell surface death receptors, followed by the trimerization of the ligand-receptor pairs at the membrane (see Figure 1-4 and 1-5). Death receptors contain cysteine-rich extracellular domains and a cytoplasmic **death domain** (DD) with roughly 80 residues. After ligand binding, cytoplasmic adaptor proteins are recruited to the plasma membrane via homophilic DD interaction between receptor and the adaptor [33,56]. Different death receptors associate with different set of adaptor proteins. For example, Fas binds to the adaptor Fas-associated death domain (FADD) while TNF receptor recruits the adaptor protein TRADD which further interacts with FADD and RIP adaptor proteins. Next by dimerization of the **death effector domains** (DED), FADD adaptor proteins associate with procaspase 8 to form a signalling complex. The autoproteolytic activation of caspase 8 is due to induced proximity and dimerization when recruited to this complex. Once activated, caspase 8 is then released from the complex as a heterotetramer containing two p18 and two p10 subunits [33]. The initiator caspases then activate the effector caspases such as caspase 3, 6 and 7. Their activation marks the beginning of apoptosis' execution phase.

In addition to caspase 8, another similar DED-containing protease, caspase 10 has been shown to associate with the signalling complex while not being essential for cell death signalling. In vivo study demonstrated that it cannot replace caspase 8 in inducing apoptosis but its function in the complex remains unclear [33].

Death receptors and their corresponding death ligands

As members of the Tumour Necrosis Factor (TNF) superfamily [57], **death receptors** can bind with at least one type of **death ligand** expressed on adjacent cells. Table 1-3 shows the six currently characterized non-decoy, membrane bound death receptors that are involved in apoptosis. Decoy receptors have both membrane bound and soluble types. They compete and interfere with functional death receptors by binding to death ligands and thus affect the sensitivity of cells to death-receptor-mediated apoptosis. Soluble decoy receptors may inactivate death ligands on the surface of nearby cells while membrane bound decoys may decrease the host cell's sensitivity to external apoptotic signals [42,58]. Moreover, membrane bound Fas ligands can be cleaved by cell surface matrix metalloproteinase-7 (MMP-7) into their soluble less-active forms, which bind to and block the receptors on adjacent cells [42]. Similarly, membrane bound TNFα can be cleaved by metalloprotease TNF alpha converting enzyme into its soluble form.

Table 1-3. Death ligand and receptor pairs [42,50]

Death receptor and aliases	Death ligand
TNFR1	TNFα, LTα
Fas/CD95/Apo1	FasL
DR3/TRAMP/Apo3	TL1A, TWEAK
DR4/TRAILR1/Apo2	TRAIL
DR5/TRAILR2/TRICK2	TRAIL
DR6	Unknown

Fas pathway

Among the identified death receptors, the Fas pathway is the most characterized and best understood [50,59]. Upon Fas ligand binding, the Fas receptor recruits an adaptor protein called Fas-associated death domain (FADD) through the interaction between homologous death domains (DD) present on both proteins. The resulting complex is termed the death-inducing signalling complex (DISC) (Figure 1-4). Depending on cell types, Fas-mediated apoptosis may require the participation of mitochondria (see section 1.2.3.3).

TRAIL pathway

TRAIL-R1 and TRAIL-R2 are two functional (i.e. non-decoy) receptors identified that are capable of inducing TRAIL-mediated apoptosis. TRAIL stands for tumor necrosis factor α-related apoptosis-inducing ligand. Although research studies have found contradictory results, it has now been clear that both TRAIL receptors transduce death signals through the adaptor protein FADD as in the FAS pathway [60,61]. Although the ligation of TRAIL to TRAIL-R1 and TRAIL-R2 can activate other nonapoptotic pathways such as the NF-κB and JNK pathways (details below in "TNF pathway" section), apoptosis is the predominant result of TRAIL binding [62] (Figure 1-4). As with TNF-mediated cell death, the recruitment of adaptor protein RIP to the ligand-receptor complex is necessary for the activation of NF-κB and JNK [52,60]. In addition to RIP, TRAF2 is also required for the JNK pathway [52]. As explained in Section 1.2.3.3, TRAIL can trigger apoptosis via different paths depending on the cell type involved.

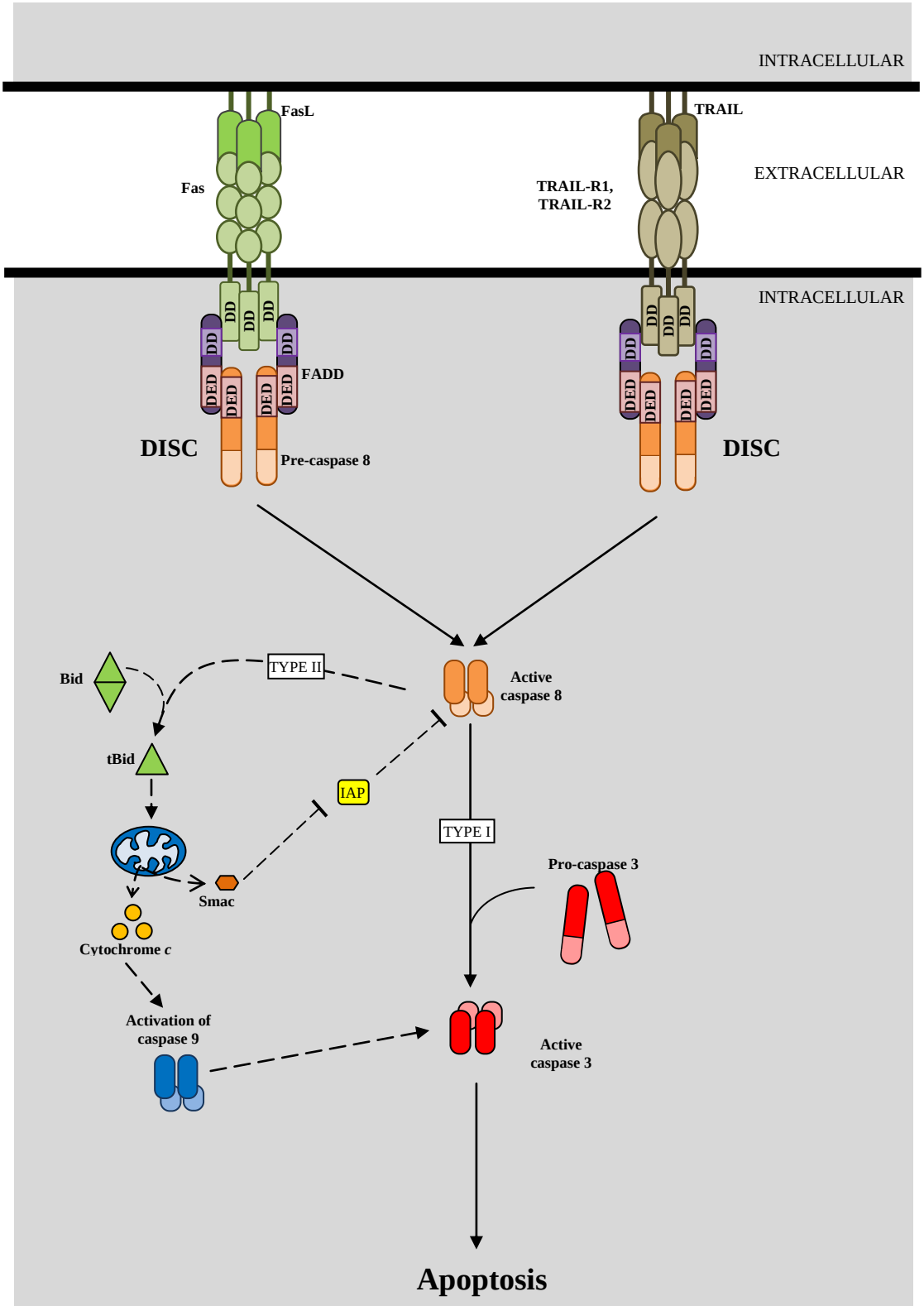

Figure 1-4. Apoptosis initiated by FasL and TRAIL death ligands. *Figure based on [33,56,63].* Dotted lines indicate reactions occurred in Type II cells. *Abbreviations: DD, death domain; DED, death-effector domain; DISC, death-inducing signalling complex.*

TNF pathway

Under the non-induced condition, the death domains of ubiquitously expressed TNF-R1 receptors are blocked by the silencer of death domain (SODD). The release of SODD from TNF-R1 is triggered by the binding of death ligand to the receptor, which subsequently recruits the adaptor protein TRADD (see Figure 1-5). TRAF2 (TNF receptor-associated factor 2) and RIP (DD-containing receptor-interacting kinase) associate with TRADD at its amino-terminal DD and carboxy-terminal DD respectively into TNFR **signalling complex I**. When TRADD, TRAF2 and RIP disassociates from the plasma membrane, they further recruits FADD and procaspase 8, forming the apoptotic cytoplasmic **complex II** [64]. Although it is widely documented that this complex II facilitates the activation of caspase 8 as described for DISC in the Fas pathway, there are still some controversies regarding the composition of the complex.

Signalling complex I activates the pro-survival NF-κB by removing its inhibitor IκB. Once activated the NF-κB translocates into the nucleus where it act as the transcriptional factor for many pro-survival genes. Their targets include cFLIP, IEX-1L, Bf1-1/A1, XIAP, cIAP1, cIAP2 and Bcl-X_L [33]. When present, FLIP binds to procaspase 8 and prevents its activation. Since TNF activates the anti-apoptotic NF-κB pathways, it does not induce cell death spontaneously as Fas and TRAIL signalling pathways. The activation of TNF-induced apoptosis is masked by the simultaneous activation of NF-κB in vivo unless the anti-apoptotic pathway is inhibited.

Furthermore, TNF binding also triggers the c-Jun N-terminal kinase (JNK) pathway by activating JNK kinase, allowing it to translocate into the nucleus and enhance activity of transcription factors such as c-Jun and ATF2. As one of the activator protein-1 (AP-1), c-Jun participates in the regulating of proliferation, differentiation and apoptosis. However, the exact mechanism and whether JNK takes on a pro-survival or anti-survival role in the TNF pathway remains uncertain [65].

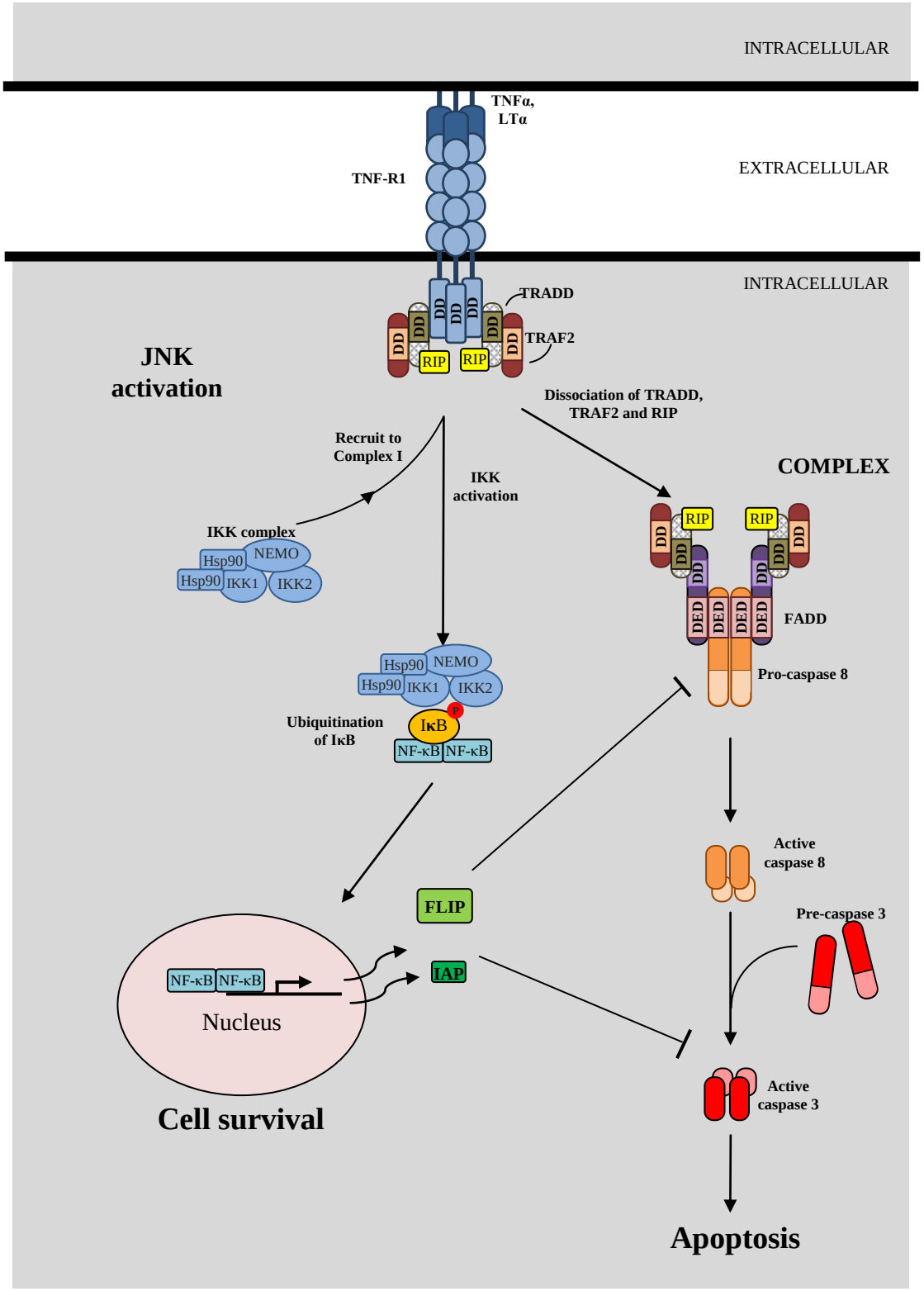

Figure 1-5. Extrinsic apoptotic pathway triggered by TNF. *Figure based on [33,64]. Abbreviations: DD, death domain; DED, death-effector domain; DISC, death-inducing signalling domain; IKK, IκB kinase; JNK, c-Jun N-terminal kinase.*

Other death receptor mediated pathways

Although not as well characterized as the TNF or FAS pathways, the ligand Apo3L and its corresponding receptor DR3 (Apo3) have been shown to be fairly similar to TNF and TNF-R1. Binding of Apo3L to its receptor activates apoptosis via the recruitment of TRADD, FADD and caspase 8, as well as the induction of NF- κB pathway by TRADD, TRAF2 and RIP [52].

1.2.3.3 Crosstalk between the Extrinsic and Intrinsic Pathway

Cells undergoing Fas- and TRAIL induced apoptosis can be divided into two types: type I and type II cells (Figure 1-4). Death of type I cells can proceed without mitochondrial involvement while in type II cells, participation of mitochondria is required [63,66]. In type I cells, sufficient activation of caspase 8 in DISC induce apoptosis directly. Since only small amount of FADD and caspase 8 are recruited to DISC in type II cells, amplification via the mitochondria is necessary to induce cell death. The involvement of mitochondria in death receptor mediated apoptosis begins by the cleavage of a pro-apoptotic Bcl-2 protein, Bid, by the small level of activated caspase 8 present. Following the translocation of cleaved Bid (tBid) to the mitochondria membrane, mitochondrial dysfunction and apoptosome formation occur [33]. However, the activation of caspase 9 from the apoptosome activation alone does not compensate for the weak DISC and caspase 8 activation. The inhibition of caspase 9 was shown not to prevent the activation of caspase 3 nor the execution of TRAIL-mediated apoptosis. Instead, the release of Smac/DIABLO following the translocation of Bax, which was induced by tBid, was necessary for the removal of XIAP from caspase 3 and its subsequent processing and activation by caspase 8 [48]. The fully activated caspase 3 can then cleave proteins such as XIAP [33] and activate more caspase 8 to complete an amplification feedback loop [59]. In contrast, studies have suggested that stress signals can sensitize cells to death signal pathways [33,42] although the exact mechanisms remain unclear.

This cross talk indicates that proteins involved in apoptosis are not all explicit to a particular pathway but exhibit more complicated roles depending on the cell type and death stimulating condition. However, at the moment it is unclear which type CHO cells belong to and whether the different CHO cell line behaves similarly under various conditions.

1.2.3.4. Endoplasmic Reticulum Pathway

Many cellular stresses, such as oxidative stress, nutrient (glucose) deprivation, protein overload, hypoxia, inhibition of proper protein glycosylation and disturbances of calcium mobilization, can lead to an increase in misfolded protein accumulation in the ER lumen [67] by affecting protein glycosylation and inducing protein denaturation [68]. The alteration of ER homeostasis caused by these factors results in ER stress and provokes the unfolded protein response (UPR), which involves signal transduction between ER and the nucleus. The cell responds to such stress by directly reducing protein translation, increasing translation of ER chaperones to facilitate refolding of the unfolded proteins and degrading misfolded proteins that failed to get refolded correctly via ER-associated degradation [67]. If this stress continues and UPR persists, apoptosis will be initiated at the ER by the release of calcium ions into the cytosol. Calcium ions and cytochrome *c* facilitate communication and amplification of apoptotic signals between the ER and mitochondria. The released Ca^{2+} ions are quickly absorbed by mitochondria, leading to a mass efflux of cytochrome *c* from all mitochondria. Upon binding of cytochrome *c* to the $InsP_3$ receptors on the ER membrane, calcium release is further enhanced. It was reported that both pro- and anti-apoptotic Bcl-2 family members also locate on the ER to facilitate the regulation of Ca^{2+} resting store and release [53]. The exact mechanisms of ER-mediated apoptosis are still under investigation. During ER-mediated apoptosis, the ER-localized caspase 12 becomes activated by a calcium-dependent protease called calpain and translocates to the cytosol, where it cleaves procaspase 9 [33,69]. It has been shown that caspase 12 responds and activates only during ER stresses and not by other death stimuli [70]. While the mitochondria has been reported to respond to

calcium flux from ER, the release of cytochrome *c* and the formation of apoptosome were shown not essential for the induction of ER-mediated cell death. To date, studies seem to suggest that ER stress triggered apoptosis can be signalled through both mitochondrial-dependent and independent pathways [71].

1.2.4 Proteolytic Targets of Caspases

As mentioned in 1.2.2, known apoptotic caspases include caspase 2, 3, 6, 7, 8, 9 and 10. Out of these executioner molecules, caspase 3 is the dominant effector targeting and cleaving a huge number of cellular proteins upon its activation. At least 280 substrates were identified [72] and they can be roughly divided into categories such as mediators and regulators of apoptosis, structuring proteins, DNA repair proteins and cell cycle proteins [46]. However when these proteins are cleaved during apoptosis and the completeness of cleavage can vary. Moreover, some proteins appeared to be targeted by caspases in certain cell types or conditions only [72].

1.2.4.1 Substrates whose Cleavage Results in Key Morphological Changes

The early indicators of apoptosis, chromatin condensation and nuclear remodelling, are achieved by the cleavage of Acinus and Helicard proteins [72]. Acinus, which stands for apoptotic chromatin condensation inducer in the nucleus, has been shown to induce chromatin condensation without DNA fragmentation in vitro [73]. The cleavage and activation of cytoplasmic Helicard, which is a CARD-containing DNA helicase, by caspase leads to its localization to the nucleus where it can alter chromatin architecture. It was shown that the active Helicard fragments accelerated DNA degradation in apoptotic cells, likely by unwinding the DNA and allowing easy access of caspase-activated DNAse (CAD) to the DNA [74].

Internucleosomal DNA degradation is a major characteristic of apoptosis that is caused by the work of the endonuclease CAD. In normal healthy cells, the DNA fragmentation factor 45kD subunit (DFF45), also known as the inhibitor of CAD (ICAD) prevents CAD from digesting cellular DNA. The cleavage of ICAD's N-terminal CIDE-N interaction domain by activated caspase 3 during apoptosis removes its suppression on CAD [75]. In apoptotic cells, the DNA digestion occurs at internucleosomal sites, producing small (multiples of 185 bp) double-stranded fragments of DNA. However less extensive DNA degradation resulting in fragments of sizes 50 – 300 kb also occurs in some cell types [76]. Although AIF and endonuclease G released from the mitochondria also assist in DNA fragmentation, their DNAse activities are caspase-independent [74].

Furthermore, activation of pro-apoptotic kinases such as ROCK1 kinase and p21-activated kinase 2 (PAK2) are necessary for the morphological change to cell membranes during apoptosis. Activation of ROCK1 kinase leads to membrane blebbing, while PAK2 is involved in the formation of apoptotic bodies [33].

1.2.4.2 Apoptotic Proteins

Many proteins involved directly in the apoptosis pathways are targeted by caspases upon their activation. Proteins with anti-apoptotic nature are inactivated when they are proteolytically cleaved by caspases. On the other hand, some pro-apoptotic proteins must be activated by caspases in order to carry out their apoptotic responsibilities.

Anti-apoptotic proteins including Bcl-2, Bcl-X_L, IAPs and FLIP-L are also cleaved by caspases [33]. The cleavage of Bcl-2 and Bcl-X_L are related to sensitivity of the mitochondrial pathway. However it is unclear whether this is a ubiquitous feedback mechanism or a stimulus-specific event. Several pro-survival protein kinases have been identified as caspase targets after the initiation of

apoptosis. As part of the signalling component of the DISC complex in the TNF extrinsic pathway, RIP kinase activates the pro-survival NF-κB pathway. It was shown that RIP can be cleaved by caspase 8 leading to the removal of this anti-apoptotic inhibition from NF-κB. In addition to RIP, Focal adhesion kinase (FAK), which typically transduces survival signals from the extracellular matrix, is another anti-apoptotic kinase targeted by caspases. In vivo, FAK transduces survival signals from the extracellular matrix and, as the name suggests, regulates focal adhesion formation in adherent cells. Death ligands such as FAS and TRAIL have been shown to trigger the cleavage of FAK by caspases 3, 6 and 7 in both adherent and suspension cells early in the apoptosis stage [77].

1.2.4.3 Cytoskeletal Proteins

Proteolyses of several structural proteins lead to the several morphologies observed in cell shape during apoptosis. Cleavage of nuclear lamins is responsible for the nuclear shrinkage and budding. The loss of overall cell shape is due to the cleavage of fodrin and gelsolin, which leads to the disruption of actin filament network [33]. The constitutively active fragment of the cleaved gelsolin can depolymerize F-actin. Cells deficient in gelsolin showed greatly delayed membrane blebbing suggesting that actin reorganization by gelsolin is required for membrane blebbing [72]. In addition, intermediate filament proteins such as keratin 18, keratin 19 and vimentin are also cleaved by caspases [33], which affects the maintenance of the cytoskeletal architecture.

1.2.4.4 DNA Repair Proteins

Many DNA repair proteins are cleaved and inactivated during cell death for the conservation of cellular resources and energy. Since apoptosis is a regulated energy-dependant mechanism, proper balance and utilization of cellular energy is important for the successful execution of apoptosis. It was found that the depletion of cellular ATP can abrogate apoptosis and induce necrosis instead [78].

Meanwhile, inhibition of DNA repair promotes the apoptosis process [72]. DNA repair proteins including DNA-dependent protein kinase (DNA-PK), Rad51, ATM and poly(ADP-ribose)polymerase (PARP) are known substrates of caspases [33,72]. The cleavage of PARP especially has become a common protein marker for detection of apoptosis [48,79,80]. When activated by DNA damage, PARP catalyzes the attachment of ADP-ribose polymers to nuclear proteins and facilitates DNA repair. Since this process consumes large amount of NAD^+ thus indirectly depleting ATP resources, the cleavage and inactivation of PARP during apoptosis likely is carried out by caspases to prevent a huge energy loss [33,72].

1.2.4.5 Cell Cycle Proteins

During the late phase of apoptosis, several cell cycle-associated factors become activated by cleavage and inactivation of their inhibitors. Some caspase-cleaved cell cycle inhibitory factors are Wee1, CDC27, $p21^{CIP1}$, $p27^{KIP1}$ and Rb [33]. As a critical component of the G2/M cell cycle checkpoint machinery, Wee1 mediates cell cycle arrest by phosphorylating and inactivating the cell cycle-regulatory kinase CDC2 and CDK2. Following the cleavage and inactivation of Wee1, cell cycle progression continues [72,81]. The cleavage of cyclin inhibitors $p21^{CIP1}$ and $p27^{KIP1}$ results in increased CDK2 activity that will also allow cell cycle progression [82]. Moreover, the inactivation of the anaphase-promoting complex via cleavage of its component CDC27 results in increased activity of CDK activity as well [81]. Since the cell has irreversibly committed to apoptosis, continuing DNA checkpoint and repair is meaningless and even energy-wasting. The cleavage of cell cycle proteins by caspases during apoptosis hence helps direct resources to undergo apoptosis [83]. Surprisingly in several studies, cleavage of cell cycle regulators has shown pro-apoptotic consequences. The loss of proliferation inhibitor retinoblastoma (Rb) has been shown to promote the accumulation of procaspases [84]. In another case, CDC2 phosphorylated and activated the pro-apoptotic Bcl-2 family member Bad by inhibiting its interaction with AKT [85].

1.3 Detection of Apoptosis using Flow Cytometry

Flow cytometry (FCM) analysis allows multi-parametric characterization of individual intact cells. By measuring the intensities of scattered light and emitted fluorescence, a flow cytometer senses particles in a liquid stream as they pass through a laser beam (see Figure 1-6). The intensities of front and side scattered lights for each detected cell correlate to its size and granularity. When cells labelled with fluorochrome-linked antibodies or stained with fluorescent dyes are excited by a laser beam, florescence is emitted over specific wavelengths and can be measured [86]. Every fluorophore has optimal but not necessarily unique excitation and emission wavelengths. When more than one fluorophore is used on the same cell sample, multiple characteristics of each cell within a population can be identified simultaneously.

One common indicator of apoptosis involves the examination of activated caspases within cells. The fluorescent inhibitor of caspase (FLICA) methodology utilizes synthetic peptide caspase inhibitor for the detection of activated caspases. It contains 3 components: a chemical group such as fluoromethyl ketone (FMK) to covalently bind to a cysteine, a short caspase-specific recognition peptide and a fluorescent reporter group [87]. Since the peptide sequence was based on the substrate cleavage sites of caspases, FLICA is an irreversible, competitive pseudo-substrate for active caspases. For caspase 3 and 7, the recognition sequence is aspartic acid-glutamic acid-valine-aspartic acid (DEVD); while leucine-glutamic acid-threonine-aspartic acid (LETD) and leucine-glutamic acid-histidine-aspartic acid (LEHD) are for caspase 8 and 9 respectively [87,88]. The FAM FLICA caspase kits which use carboxyfluorescein (FAM) labelled FMK peptide inhibitor of caspases, were utilized in this project. Sulforhodamine B (SR) and fluorescein (FITC) are alternatives to the green fluorescent FAM.

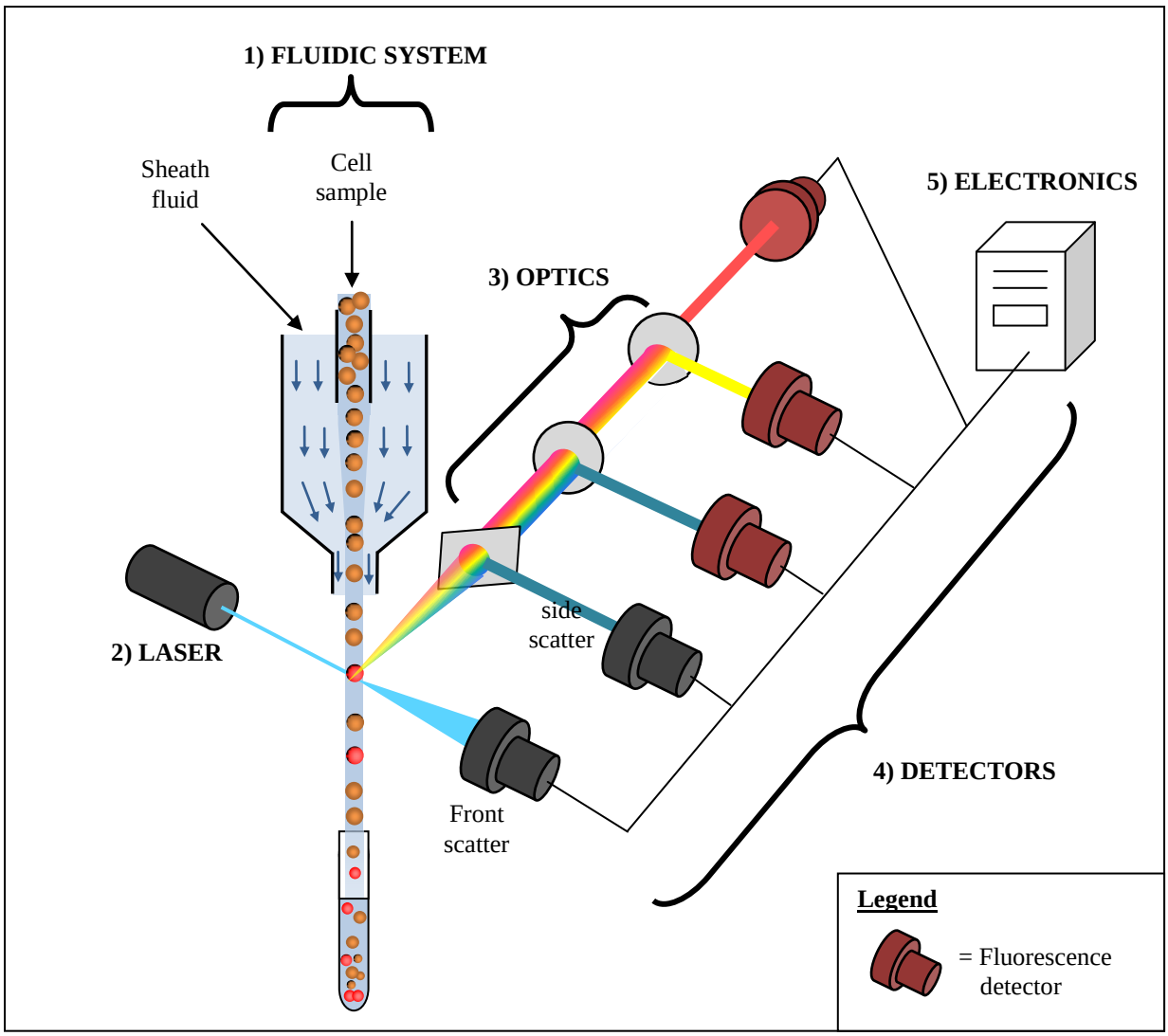

Figure 1-6. Main components of a flow cytometer. *Figure based on [89,90].*

After entering the cell, FLICA molecules covalently bind to reactive cysteine residues on the large subunits of the active caspase heterodimer with 1:1 stoichiometry. Only bound FLICA reagents will be retained within cells while the free FLICA molecules get rinsed out during washing [87]. Hence the fluorescent signal intensity corresponds to the amount of activated caspases present within the cells when reagents are added. Propidium iodide (PI) can be used as a membrane integrity or dead cell stain along with the activated caspase-binding FLICA stain. PI only penetrates damaged cell membranes and intercalates with DNA, thus leaving viable cells unstained. The penetration of PI across leaky plasma

membranes can help assess viability of apoptotic cells and identify the progression of apoptosis since disturbance of membrane integrity is not observable until late stages of apoptosis [91].

In this thesis, cells are considered live or viable by the exclusion of membrane integrity dye such as PI, whereas dead cells show positive PI intensity in FCM analysis. Meanwhile, the occurrence of apoptosis is determined by the presence of activated executioner caspases as indicated by a positive FLICA intensity. Therefore, using this bi-color assay, cells can be categorized as i) C3-PI- (live non-apoptotic) cells that posses intact membrane and no activated caspases 3 and 7, ii) C3+PI- (early apoptotic) cells that contain significant number of activated caspases 3 and 7 yet still maintain their membrane integrity, iii) C3+PI+ (late apoptotic) cells which have non-intact membrane and activated caspases 3 and 7, and iv) C3-PI+ (primary and secondary necrotic) cells that displayed a damaged membrane but no activated caspase (see Table 1-4). These C3-PI+ cells could be either the caspase-independent necrotic or very late apoptotic cells which have lost their ability to bind FLICA [87,92,93]. The absence of FLICA signal has been reported in cells at late stage of apoptosis [87,92] and suggested to reflect the inactivation, degradation or secretion of activated caspases out of the cells. In particular, the extracellular secretion of activated caspase subunits has been observed at the final stages of apoptosis [47,94] when the caspase-mediated cleavage of essential cellular proteins was likely completed. Some studies have termed apoptotic cells at the late stage as **secondary necrotic** cells for their resemblance to primary necrotic cells. The baseline signal intensity of non-stained cells can be used to determine the threshold (minimum intensity) for a positive signal. Using the thresholds in subsequent FCM analyses with labelled samples, cells with non-specific fluorescence can then be classified as negative for a phenotype.

Table 1-4. Interpretation of results for the bi-color flow cytometry analyses for caspase 3

Cell type	Cell Condition	Activated caspase 3 (apoptosis indicator)	Propidium iodide staining (death indicator)
C3-PI-	Healthy, nonapoptotic	-	-
C3+PI-	"early" apoptotic	+	-
C3+PI+	"late" apoptotic	+	+
C3-PI+	Primary necrotic or secondary necrotic	-	+

+: positive as intensity past the cutoff threshold
-: negative as intensity below the threshold
C3: caspase 3

Similarly, FCM caspase 8 and caspase 9 tests can also categorize cells into four subpopulations. However, unlike caspase 3 and 7 which are common to all apoptotic pathways, FCM caspase 8 assay preferentially recognizes caspases specific to the extrinsic pathway. The activation of caspase 9, which may be involved in both mitochondrial and ER-mediated apoptotic pathways, can be detected with the FCM caspase 9 assay. Since they represent the initiation of apoptosis only, interpretation of these subpopulations will be slightly different.

1.4 Comparative Proteomic Analysis

Proteome analysis is a powerful method in screening changes between two protein mixtures thus allowing faster identification of a set of differentially expressed proteins than traditional biochemical assays such as the western blot. Two-dimensional gel electrophoresis, or more specifically differential in gel electrophoresis, is often used to separate and select proteins with varying abundances between samples. These proteins are then identified by sequencing using a mass spectrometer. Proteomic analyses are comparable to microarray analyses except that changes in protein expression instead of mRNA expression are exploited.

1.4.1 Two-dimensional Gel Electrophoresis

As a powerful technique for analyzing whole proteomes, two-dimensional gel electrophoresis (2D GE) separates and displays proteins from a mixture onto a polyacrylamide gel according to their isoelectric points (pI) and molecular weights (MW). This technique requires two separate steps: the first dimension step, isoelectric focusing (IEF), separates proteins horizontally across a gel strip with pH gradient according to their pI; the second dimension, sodium dodecyl sulfate-polyacrylamide gel electrophoresis (SDS-PAGE) allows proteins to migrate vertically down a 2D gel piece from the gel strip based on their sizes. Each spot on the resulting 2D array corresponds to one protein in the original proteome. Information such as MW, pI and abundance on thousands of protein spots resolved in a single gel can be readily obtained after gel visualization.

Differentially in gel electrophoresis (DIGE) is a method modified from the traditional 2D GE technique. It is the method employed in this study. Unlike 2D gels, DIGE gels can accommodate multiple protein samples per gel by pre-staining them with spectrally distinct, fluorescent dyes called the CyDye DIGE Fluors – Cy2, Cy3 and Cy5. Protein spots are detected and quantified by the intensity

of the emitted fluorescence when they are scanned with a specific excitation wavelength corresponding to each CyDye. After scanning a gel on these three channels, the single color images resulted were overlapped to create a gel image showing all three protein samples loaded on that gel. Gel images from all gels in an experiment can then be analyzed together by computer software such as DeCyder (GE Healthcare, Quebec) and subjected to statistical analyses to derive a list of proteins with altered expression between samples (see Figure 1-7).

In the DIGE system, expression levels between two protein samples can be directly compared on a single gel, eliminating the problem of gel-to-gel variability as experienced in the traditional method. Another improvement of DIGE is the inclusion of a third sample, an internal standard, which consists of equal amount of all biological protein samples in the experiment. Introducing the same internal standard into all gels helps to separate experimental variation from real biological difference [95] and thus allow more confident comparison between multiple protein samples both within individual gel and across gels. In the DeCyder software, processed abundance data are represented as normalized ratios relative to the internal standard.

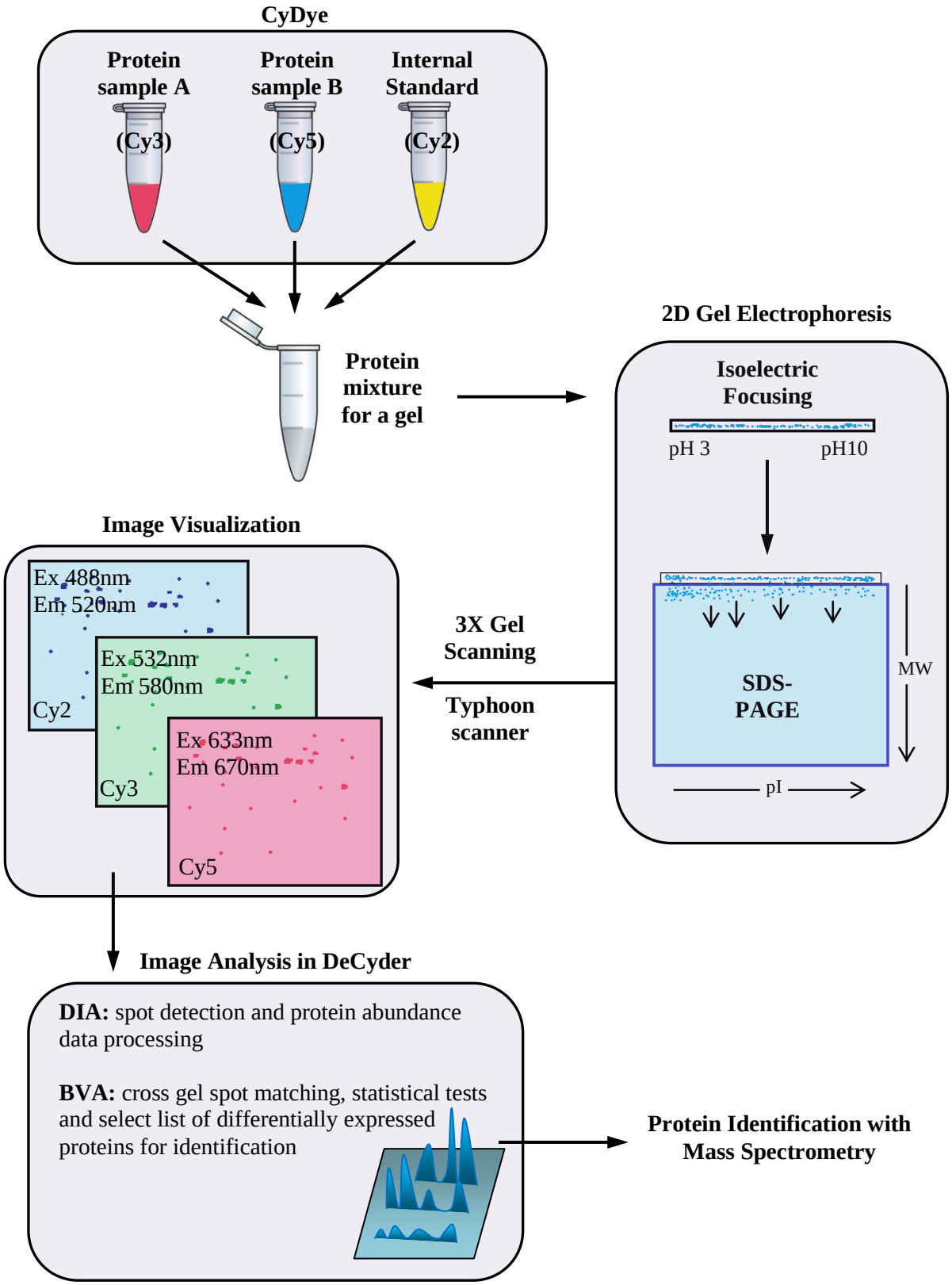

Figure 1-7. Stages of Differential In Gel Electrophoresis Analysis. *Abbreviations: BVA, Biological Variation Analysis; DIA, Differential In gel Analysis; Ex, excitation wavelength; Em, emission wavelength*

CyDye Fluors

CyDye DIGE fluor minimal dye Cy3 and Cy5 can detect a minimum of 0.025ng protein per spot, while Cy2 is slightly less sensitive and has a minimal detectable protein amount of 0.075ng. However, comparing to silver stain, which can detect above 1ng [95] and colloidal Coomassie Brilliant Blue G250 staining with sensitivity around 10ng [96], CyDyes are clearly superior in terms of sensitivity for staining protein gels. CyDye fluor minimal dyes contain an NHS-ester reactive group that can covalently bind to lysine residues in proteins by an amide linkage. As the name implies, a very small amount of dye is required for labelling a protein mixture as compared to the alternative CyDye DIGE fluor saturation dyes. Due to the small ratio of dye to protein, this "minimal labelling" method can ensure that most visualized proteins are labelled with a single dye molecule only [95,96]. The binding of CyDyes to proteins does not alter the pI of the proteins significantly because the addition of the +1 charged dye replaces the loss of a positive charge from the lysine residue (see Figure 1-8). In addition, all three CyDyes have a mass of approximately 500 Da, thus the increase in molecular weights between protein samples will be consistent. As a result, the same protein labelled with any CyDye will migrate to the same location on the 2D gel [97].

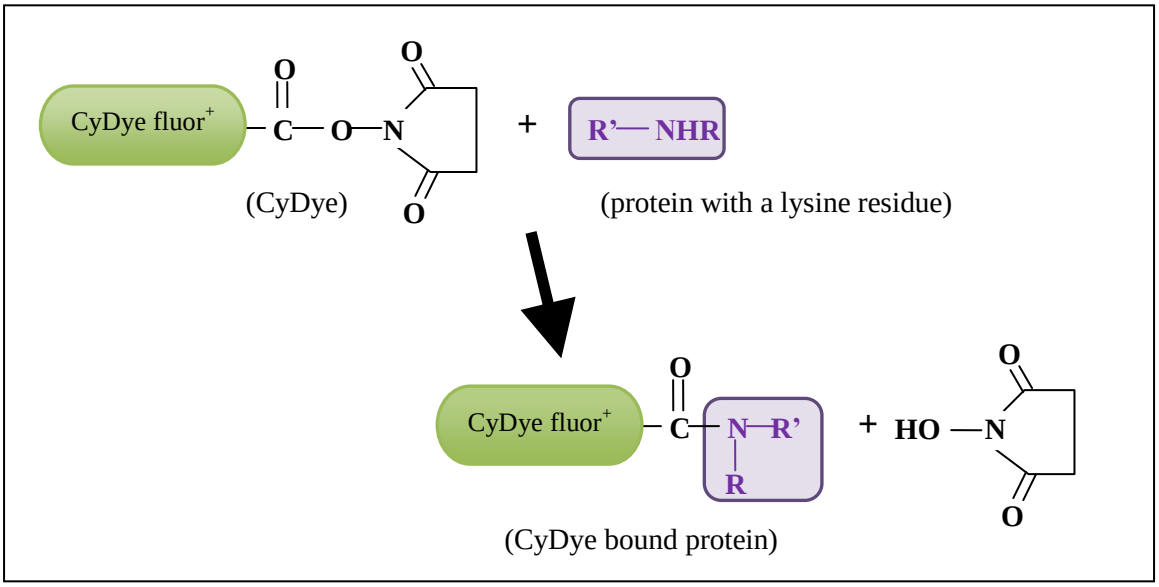

Figure 1-8. Amide bond formation during the binding of CyDye to protein. *Modified from* [98].

Statistical Analyses: t-test and ANOVA

The t-test is a statistical hypothesis test that checks if the means from two groups are equal. Meanwhile, ANOVA generalizes Student's two-sample t-test to compare means from three or more groups. Research data such as protein abundances from two different time points can be converted into a single numerical value called the test statistic, such as t statistic and F statistic. Subsequently, a p-value generated from the test statistic is used to determine the probability of obtaining a difference in protein expression as large as (or larger than) the one observed if there is no real change between the samples. Hence, the smaller the p-value is, the less likely that the observed difference occurs just by chance. Since each spot in the DIGE experiment will be subjected to hypothesis testing, each statistics method will test over 1000 hypotheses. With multiple testing, the accumulated number of false positives might be overwhelming, considering the small total number of positives selected. For example, if 1000 tests are performed with p-value significance level at 5%, overall 50 false positives are expected in the absence of any real effects. Since the 5% p-value significance level is no longer directly indicative of the overall false positive rate, interpretation of DIGE results becomes difficult. In this case, multiple testing correction methods such as the false discovery rate (FDR) correction can be applied to adjust p-values. The FDR is defined as the ratio of false positives over total statistically determined positives [99]. The FDR correction ranks all p-values and selects the largest p-value, denoted p_r, such that the resulting FDR value will be below the desired threshold. All protein spots with a p-value smaller than p_r will then be selected as candidate differentially expressed proteins. By selecting based on an FDR significance level instead, the overall false positive error rate for multiple testing can be kept constant and known.

When there are more than two groups, a large number of t-tests is required to fully compare between each pairing of two groups. Performing multiple pairwise t-tests would largely increase the chance of committing type I errors, also known as false positives. As a result, the ANOVA test is more advantageous when comparing multiple groups, although it does not indicate which groups differ from

the rest. Hence to better distinguish true differentially expressed proteins and identify the variation pattern of the abundance, both t-tests and ANOVA were performed in this study.

1.4.2 Protein Identification via Mass Spectrometry

Protein identification involves three steps: digestion of gel-separated protein spots, peptide sequencing by tandem mass spectrometry, and protein database searches. Tandem mass spectrometry (MS), also known as MS/MS spectrometry, generates protein sequences by subjecting digested protein molecules to two rounds of mass spectrometry analysis. The first MS analysis measures the mass of all the detectable peptides from the original protein digest. Subsequently, each peptide is further fragmented by bombarding with energy before the mass to charge ratios of the resulting fragments are measured [100]. From the tandem mass spectrum, sequences of peptides can be computationally determined using various types of algorithms and searched against protein databases in order to obtain an identity of the original protein species.

A mass spectrometer typically consists of 3 components: an ion source, which creates charged molecules from the protein digest; a mass analyzer that separates ions based on their mass to charge (m/z) ratios with electromagnetic fields; and a detector, which measures the intensity of the ions [101]. Electrospray ionization and matrix-assisted laser desorption ionization are two common ionization methods employed in conjunction with mass separation methods such as the time-of-flight, the quadrupole and the ion trap method. The resulting mass spectrum from MS analysis is a plot showing ion-abundance versus m/z. Sometimes liquid chromatography can be coupled with MS analysis, which occurs as components of the sample elute from the chromatography column [100].

1.5 Objectives of this Project

Since first being described in 1972 [35], apoptosis has been a topic actively and extensively investigated by many research groups. It was reported and widely accepted as the main mode of culture cell death, affecting viability, culture longevity and finally protein production in bioreactors. Some studies placed their focus on understanding the effect of an apoptotic inducer in a particular cell line and set up. For instance, how treatment induces apoptosis in cancer cells, or how an induced apoptotic pathway changes the proteome of treated cells were of common interest. Meanwhile, other researchers focus on delaying and reducing the level of apoptosis within cultures for the sake of process optimization. The effects of various optimization strategies including genetic modification of cell genomes and chemical supplements on productivity, cell growth and viability in cultures were tested. The findings on apoptosis were often generalized, combined, and applied to many other studies with the assumption that the mechanism of apoptosis triggered was similar or in a sense, irrelevant.

The main goal of this research project was to study the whole cell proteome of anti-Rhesus D factor-producing CHO cells at various phases of the cultivation period as apoptotic cell death advanced in the population. Using proteomic techniques such as gel electrophoresis and mass spectrometry, proteins that vary their expression level during the degradation of culture conditions, and upon the onset and execution of apoptosis were identified. Although it is not the only cellular pathways affected during prolonged cultivation, apoptosis is of special interest. The specific apoptotic pathway triggered in protein-producing CHO cells, which was maintained in batch cultures mimicking typical industrial bioreactor setting, was investigated. The presence of apoptosis and the advancement of apoptotic cell death in cultures were regularly examined via flow cytometry assays. The detection of apoptosis with FCM technique allows the association of changes observed in gel electrophoresis to changes in the culture conditions and health of cells over time. In contrast to previous studies, the approach employed in this work did not involve the induction of apoptosis by an apoptotic agent. In fact, the present work

is the first systematic proteomics study of non-induced apoptosis in mammalian cell lines. The ultimate objective of this project is to provide more biological foundation for the construction of a strategy which improves productivity by reducing the amount of apoptotic cell death in bioreactors. Since factors crucial in delaying the onset of apoptosis can be inferred by knowing the proteins involved and the specific pathway initiated in CHO cultures, potential means of inhibiting apoptosis in bioprocesses can be developed.

1.6 Overview of Thesis

In Chapter 2, the progression of cell growth and apoptotic cell death in CHO batch cultures throughout the two-week cultivation period is discussed. In addition to a continuous monitoring of cell density and viability via Trypan Blue cell counting, flow cytometry analysis of apoptosis progression was conducted via the quantification of activated caspases within cells. By measuring two major initiator caspases, the death receptor-associated initiator caspase 8 and the mitochondrial/ER pathway-associated initiator caspase 9, the pathway responsible for triggering cell death in CHO cells cultured in spinner flasks was investigated. Protein samples at four time points (day 2.5: late exponential phase, day 4.5: early stationary phase, day 5.5: mid-stationary phase and day 8.5: early death phase) during the culturing period were collected.

In Chapter 3, results of proteomic analyses comparing whole cell proteomes between the four time points are shown and discussed. Of the differentially expressed proteins identified, they can be classified into three major categories based on their typical functions. Other than the detection of cytoskeletal proteins that are known targets of caspases, a significant number of chaperones and metabolic enzymes displayed changes in their protein abundance over time as nutrient depletion, waste product accumulation and apoptosis occurred over time. Among these, the simultaneous upregulation of seven ER molecular chaperones and foldases strongly suggest that onset of unfolded protein response

(UPR), which can be triggered by a variety of cellular and ER stresses. In addition, the induction of six out of the ten glycolytic enzymes and a post-glycolysis metabolic enzyme implies noteworthy changes in glucose metabolism. The potential involvement of UPR and energy metabolism, as well as the functions of all identified proteins in CHO cells subjected to stresses caused by natural "aging" in the culturing process and the onset of apoptosis are discussed.

Lastly, the implications of the findings of this work and possible future works are mentioned and proposed in Chapter 4. Due to the limited number of CHO protein reference maps available to date, the DIGE gels and protein identifications obtained in this study will be an informative addition to the current CHO 2D gel database. Most importantly, as the first system-wide proteomic study of non-induced apoptosis in mammalian cells, findings from this study will expand current knowledge of intracellular changes of cell cultured in bioreactors that have undergone stresses brought by the natural degradation of culture conditions and the initiation of apoptotic cell death over time.

Chapter 2. Monitoring CHO Cell Growth and Tracking Apoptosis Progression throughout Cultivation

2.1 Introduction

During cultivation of mammalian cells, the health and condition of cell cultures need constant monitoring. Cell counting utilizing the Trypan Blue stain provides information on cell growth, cell density and viability of the culture. Meanwhile the presence and progress of apoptosis requires the more sensitive and informative flow cytometry (FCM) technique. Flow cytometry measures cell size, cell granularity (denseness of cellular contents) and fluorescent intensity of labelled cells individually. By staining cell samples with two fluorescent dyes: fluorescent inhibitor of caspase (FLICA) and propidium iodide (PI), cells can be classified into four subpopulations depending on whether they are apoptotic and their membrane permeability. The objective of this study is to examine the composition of cultures during prolonged cultivation and monitor their changes inflicted by the death of cells. Special attention will be given to the beginning and advancement of apoptotic cell death in cultures over time. Several major time points will be selected for subsequent whole cell quantitative proteome analyses based on the culture composition. Consequently, FCM associates protein samples collected from cultures at different phase to the degradation of culture condition and the progression of apoptotic cell death. Other than the detection of apoptosis, FCM can also be used to examine the type of apoptotic pathway triggered by measuring the levels of two major initiator caspases, caspase 8 and caspase 9.

2.2 Materials and Methods

2.2.1 Cell Culture Maintenance

Chinese hamster ovary cell line IgG-9β8 (Cangene Corp., Mississauga) was cultured in SFX-CHO medium (Hyclone) supplemented with 1% Fetal Bovine Serum (#16000-077, Invitrogen, Burlington) and 4mM L-glutamine. Cells were grown in a 37ºC, 5% CO_2 water jacketed incubator with high humidity. Since CHO cells are naturally adherent cells, frozen cells were revived and grown initially into disposable tissue culture flasks (T-flasks) for several passages to allow recovery and proliferation. To reduce damage during passaging, cells were detached from T-flasks with a trypsin-like enzyme, TrypLE Express (#12605, Invitrogen, Burlington). Once sufficient density and volume of culture were achieved, cells were detached and transferred into 250mL Flat bottom adjustable hanging bar spinner flasks (#1967-00250, Bellco Glass, NY) to begin adaption into a suspended culture. During volume expansion, spinner flasks of sizes 500mL (#1967-00500, Bellco, NY) and 1L (#1967-01000, Bellco, NY) were required to maintain sufficient culture in a single flask. All experiments were performed with a set of four 500mL spinner flask cultures in a batch culture set up. Cultures of the same experiment were typically seeded from the same "parent' culture to obtain replicates with less variation. The number of passages taken was maintained low to avoid possible alterations to the cell line, even though CHO cell line is immortalized, which theoretically can proliferate indefinitely. Initial seeding concentration in T-flasks was 0.2×10^6 cells/mL while that in the spinner flasks was 0.25×10^6 cells/mL.

In between subculturing, used spinner flasks were first diluted with ultra pure water and autoclaved, then soaked and washed in 1% Terg-A-zyme enzyme detergent (Z23287, Sigma, Oakville). These flasks were stored and autoclaved shortly before use.

2.2.2 Culture Viability Assay with Trypan Blue Exclusion Method

Trypan Blue dye penetrates damaged membranes of dead cells providing them a dark blue color while leaving live cells unstained [79]. Hence this assay can differentiate between viable and nonviable cells and quantify the two populations. The Trypan Blue assay cannot distinguish between different forms of cell death such as necrosis and apoptosis. This procedure was mainly used to determine viability and cell count. Cell count was performed by mixing equal ratios of Trypan Blue dye with a culture sample, then loading the mixture onto a hemacytometer. After correcting for the dilution factor, the cell concentration of the original sample was obtained. Two cell counts, dead (xD) and viable (xV) cell densities, were obtained from this assay and they are used to generate the percent viability (%V) and total cell density (xT) of the cultures:

$$xT = xV + xD$$

$$\%V = \frac{xV}{xT} \times 100\%$$

2.2.3 Detection of Apoptosis using Flow Cytometry

Experimental Setup and cell sample preparation

Cultures from the two experiments conducted were prepared and maintained in the same fashion. However, slightly different flow cytometry analyses were performed in each. For run A, only the quantification of executioner proteins, caspase 3 and 7, were completed to detect the presence of apoptosis. In addition to testing the presence and level of apoptosis via activated caspase 3 and 7 amount, two additional FCM assays focusing on the initiator caspases, caspase 8 and 9, were done in run B. For the detection of caspase 3/7, caspase 8 and caspase 9, the FAM FLICA caspase 3&7 kit (ICT094, AbD Serotec, UK), FAM FLICA caspase 8 kit (ICT910, AbD Serotec, UK) and FAM FLICA

caspase 9 kit (ICT913, AbD Serotec, UK) were used respectively. Three aliquots of each culture sample were collected and each subjected to sample preparation for one of the three caspase assays.

The flow cytometry (FCM) negative controls were collected at 2.5 days after seeding, during which time the cells actively proliferated in exponential phase and culture conditions were near optimal. Four aliquots of each culture were prepared: unstained, stained with apoptotic reagent only, stained with propidium iodide (PI) only and stained with both apoptotic reagent and PI. These 4 samples were necessary for setting the thresholds for subsequent FCM data analyses. For the remaining time points, two aliquots of each culture were collected: unstained and labelled with both apoptotic reagent and PI.

For each caspase assay, 10μL of 30X FLICA reagent was added to $3x10^5$ cells in a 5mL FCM round bottom tube for each test. Cells were incubated for 60 minutes in a 37ºC, 5% CO2 incubator where tubes were gently agitated by flicking every 20 minutes to ensure proper distribution of the reagent and to minimize settling of cells. Afterwards, cell mixtures were washed twice with 2mL and 1mL of 1x wash buffer (provided in the FLICA kit). In between each wash, cells were pelleted using 5 minute centrifugation at 1000rpm. After the last wash, 400μL 1x wash buffer was added to resuspend the pellets. Each desired tube was supplemented with 2μL PI and incubated for at least 5 minutes on ice prior to FCM analysis.

The FCM analyses were performed on a Becton Dickinson FACS Vantage SE with a 488nm excitation and FL1-H and FL3-H detection filters for measuring FLICA and PI intensities respectively. A total of 20000 events (cell counts) were captured in each test.

Data analysis of flow cytometry results

Dotplots comparing apoptotic reagent (FLICA) intensity to PI intensity and single parameter histograms were generated using Windows Multiple Document Interface for Flow Cytometry (WinMDI)

v2.9 written by Joseph Trotter (The Scripps Research Institute, San Diego, USA). Each point on the dotplot corresponds to a detected cell particle from the FCM run. Due to background signals from unstained cells, intensity thresholds are set to reduce false positives for each stain. To set the cut off threshold for the x-axis, which corresponds to the intensity of the apoptotic reagent, the maximum x-axis intensity of day 2.5 cells that were stained only with PI was used. Conversely, the maximal y-axis intensity was set according to the maximum y-axis intensity from day 2.5 cells stained with apoptotic reagent only. To eliminate the effect of outliers, the exact values of the two thresholds were set to at least 95^{th} percentile of the background distribution.

2.3 Results

2.3.1 CHO Cell Growth and Viability during Cultivation

Each culturing experiment consists of four duplicate CHO cultures seeded from the same original culture. Figure 2-1a shows the average viable growth curve, 2-1b shows the average total cell density curve and 2-2 shows the average viability trend for two separate experiments, run A and B. The viable and total cell density curves, obtained from Trypan Blue assays, show some variations between runs especially during the first 8 days due to better growth rates in run B. Maximum viable cell densities achieved in run A and B were between 1-1.2 $x10^6$ and 1.4-1.6 $x10^6$ cells/mL respectively. Deviations introduced in the culture conditions such as passage number, actual seeded cell concentrations and the stresses from the subculturing procedure could influence and affect cell growth. For instance, run A and run B were initialized at passage 22 and 27 respectively to ensure sufficient and proper adaptation of CHO cells in suspended cultures. On the other hand, the viability curves were fairly consistent between the two runs, suggesting the occurrence of cell death was similar proportion-wise. During the time course experiment, CHO cultures exhibited high viability above the 90% range until day 8 to 10 when a significant increase in cell death began, which was observed by the sharp drop in viability in Figure 2-2.

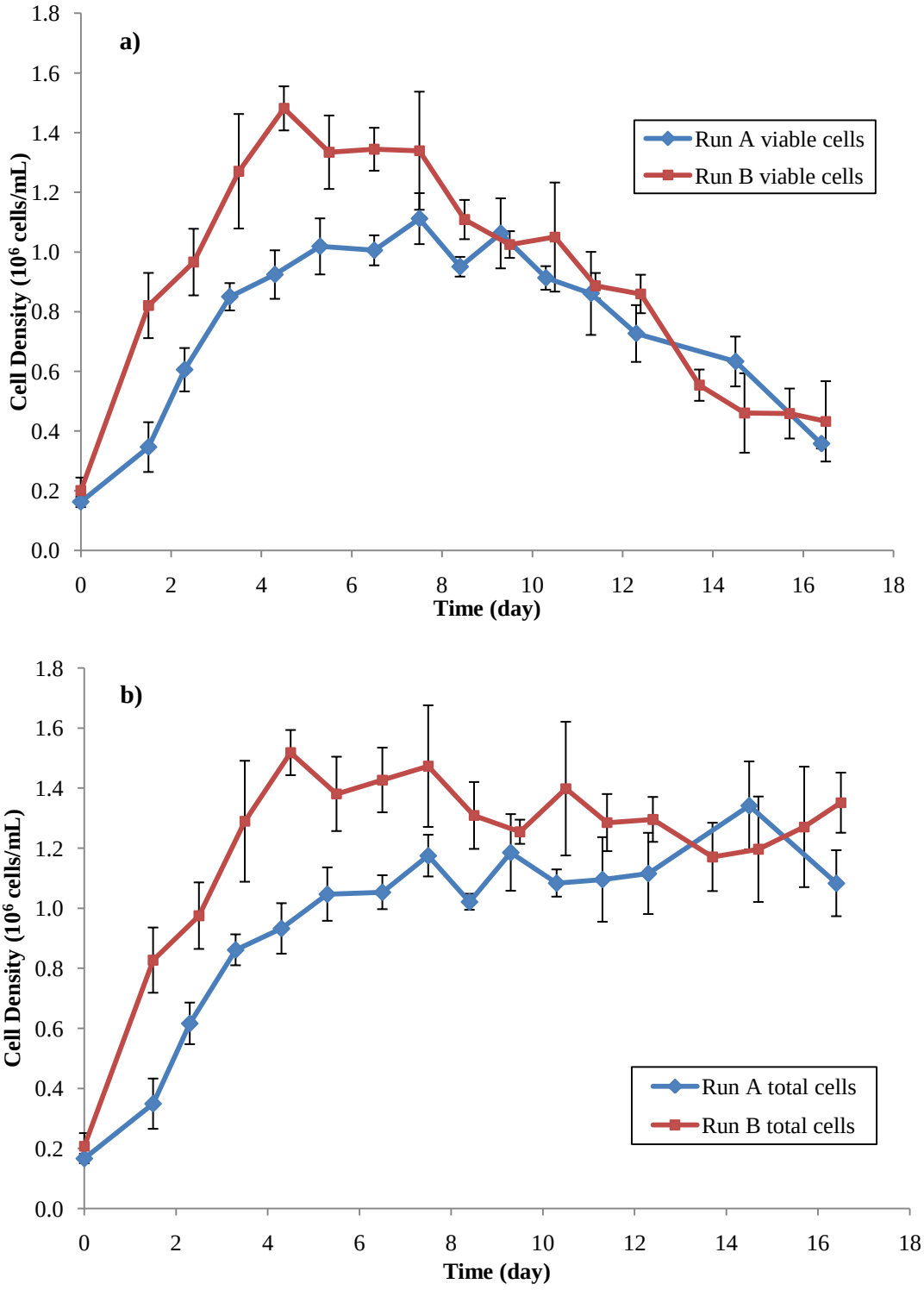

Figure 2-1. Average viable and total cell density curves observed in run A and B based on Trypan Blue exclusion assays. a) Viable cell density; b) total (viable + nonviable) cell density. Each run consisted of 4 replicate CHO cultures, which resulted in one average density curve. Error bars correspond to one standard deviation above and below the means.

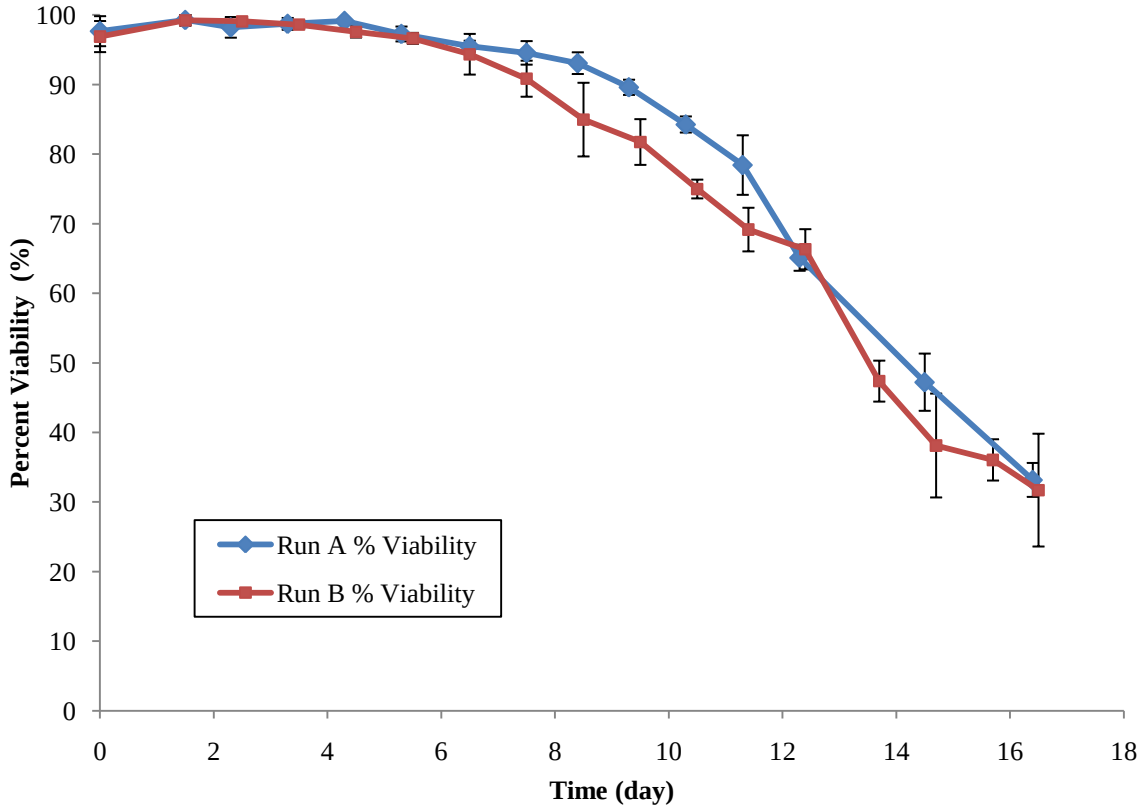

Figure 2-2. Average CHO culture viability throughout run A and B experiments based on Trypan Blue assays. Viability is calculated from the viable and total cell counts.

2.3.2 Detection of Apoptosis in CHO Cells

During the 17 day culturing process, flow cytometry was used to monitor the progress of apoptosis and cell death in the spinner flasks. Both caspase 3 and 7 are executioner caspases responsible for many phenotypes observed in cells undergoing apoptosis. Since their activation and activities are common to both intrinsic and extrinsic pathways, FCM analysis of caspase 3 and 7 activation was used as a method for detecting the presence of apoptosis within a cell population.

2.3.2.1 Setting Parameter Thresholds

The culture sample taken on day 2.5 was considered as the healthy reference sample or negative control, where the amount of apoptosis within culture is expected to be minimal. Figure 2-3 shows a series of dotplot analyses typically done to set the thresholds for the two parameters, namely the minimum FLICA intensity which corresponds to the presence of activated caspases 3 and the minimum PI intensity which indicates permeable membrane. For each dotplot, all 20000 events or cells detected were plotted. Day 2.5 culture incubated only with PI (Figure 2-3b) should reveal cells with fairly low intensity for FLICA, corresponding to background noises. It was used to set the appropriate FLICA (x-axis) cutoff by ensuring most cells have negative readings for activated caspase. To determine the threshold for the PI parameter, day 2.5 culture incubated with only FLICA reagent (Figure 2-3c) was examined in a similar fashion. Negative control from a day 2.5 culture with no dyes added (Figure 2-3a) showed background signals for both parameters. As a result, it was used to check that the correctness of the two thresholds and any potential technical problems that might have occurred during FCM sample preparation. For illustration purposes, Figure 2-3d and 2-3e shows the caspase 3 and PI results for samples of a single culture collected on day 2.5 and day 9.5 respectively. An increase in the apoptotic dead subpopulation and a decrease in the healthy subpopulation were apparent as time progressed. A separate pair of thresholds was set for each culture following the procedure above. Appendix A.2 shows a full set of dotplots for one of the four CHO cultures of run A. Although the thresholds were determined for each CHO culture sample individually, they were comparable between the four replicates (see Appendix A.2.2).

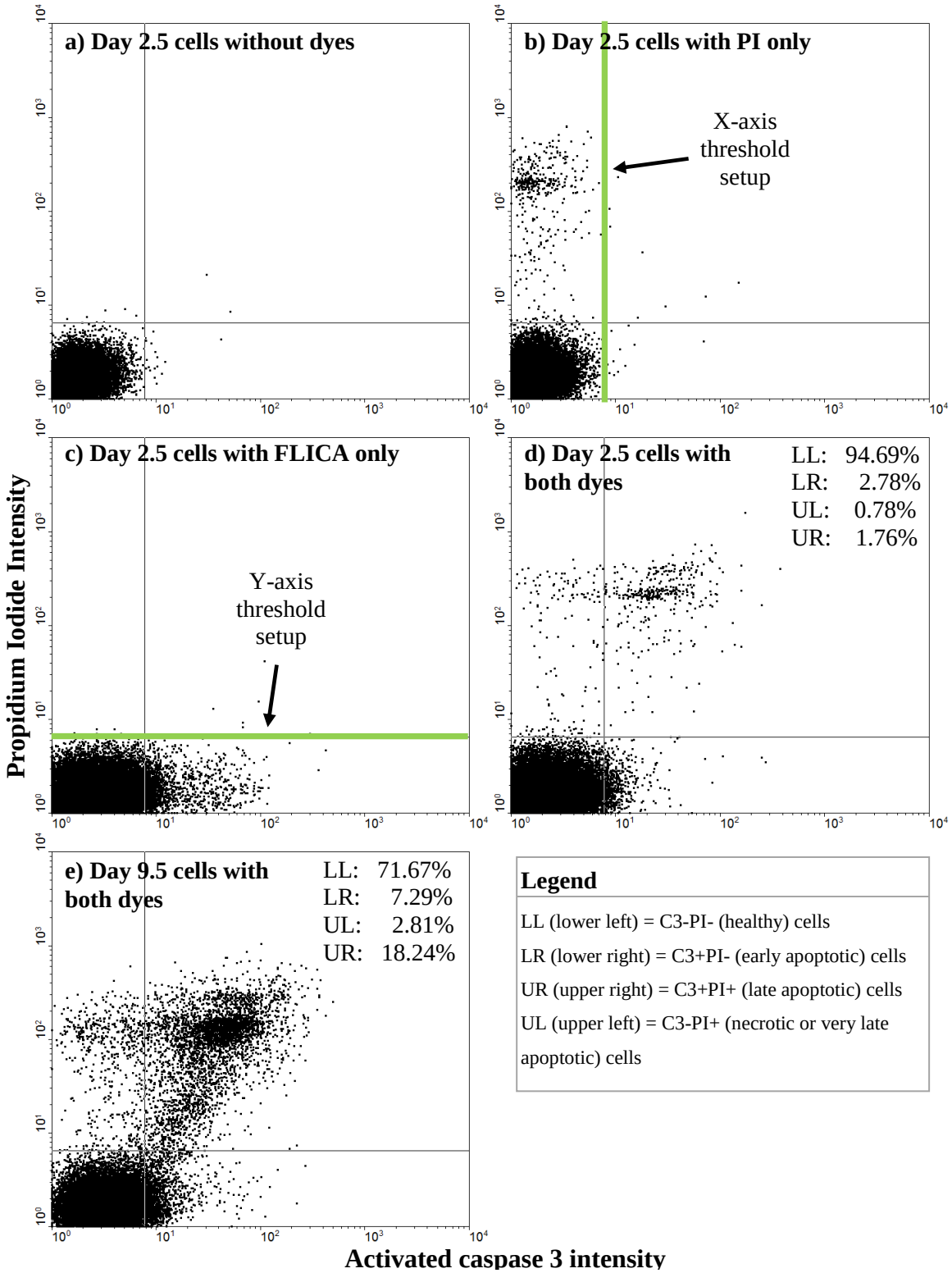

Figure 2-3. Flow cytometry raw data presented as dotplots for the negative controls and an apoptotic culture sample. Each plot, which corresponds to one FCM test, contains 20000 data points. Each dot in the plot represents one cell. Positive propidium iodide (PI) intensity corresponds to loss of membrane integrity while positive activated caspase 3 (C3) indicates apoptosis occurring.

2.3.2.2 Apoptosis Progression over Time in run A and B

Flow cytometry analyses were conducted repeatedly over the cultivation period in both run A and B until the fraction of healthy (live and non-apoptotic) cells dropped below 30% of the culture. As Figure 2-4 demonstrates, the exact timing when cultures in the two experiments reached 30% was different. Figure 2-4a shows the average trend of the four replicate spinner flask cultures in run A experiment. Based on their PI and FLICA intensities, cells were distinguished into C3-PI- (healthy), C3+PI- (early apoptotic), C3+PI+ (late apoptotic) and C3-PI+ (primary or secondary necrotic) cells (see section 1.3). From the figure, an obvious decrease in healthy subpopulation could be seen as the culture aged. The healthy cells made up over 70% of the culture until day 9.5 when a sudden decrease in this cell type occurred. A sharp drop of healthy cell population from 70% to 30% happened over a period of approximately 2 days. Consequently, the amount of apoptotic cells which tested positive for activated caspase 3 increased over time. Initially, the abundance of apoptotic cells was gradually increasing and cells retained membrane integrity. The peak amount of the early apoptotic cell population occurred between day 5.5 and 8.5 as shown in Figure 2-4a. However, after day 8.5, the proportion of late apoptotic cells (which are no longer viable) exceeded that of the early apoptotic cells. The total apoptotic percentage remained 30% of the total cell count until day 9.5, when the rate of death and/or apoptosis went up noticeably as exhibited by the late apoptotic cell population. During run A, C3-PI+ cells, which correspond to primary and secondary necrotic cells (i.e. cells which resembled necrotic cells at the end stage of apoptosis), remained consistently low during all time points sampled.

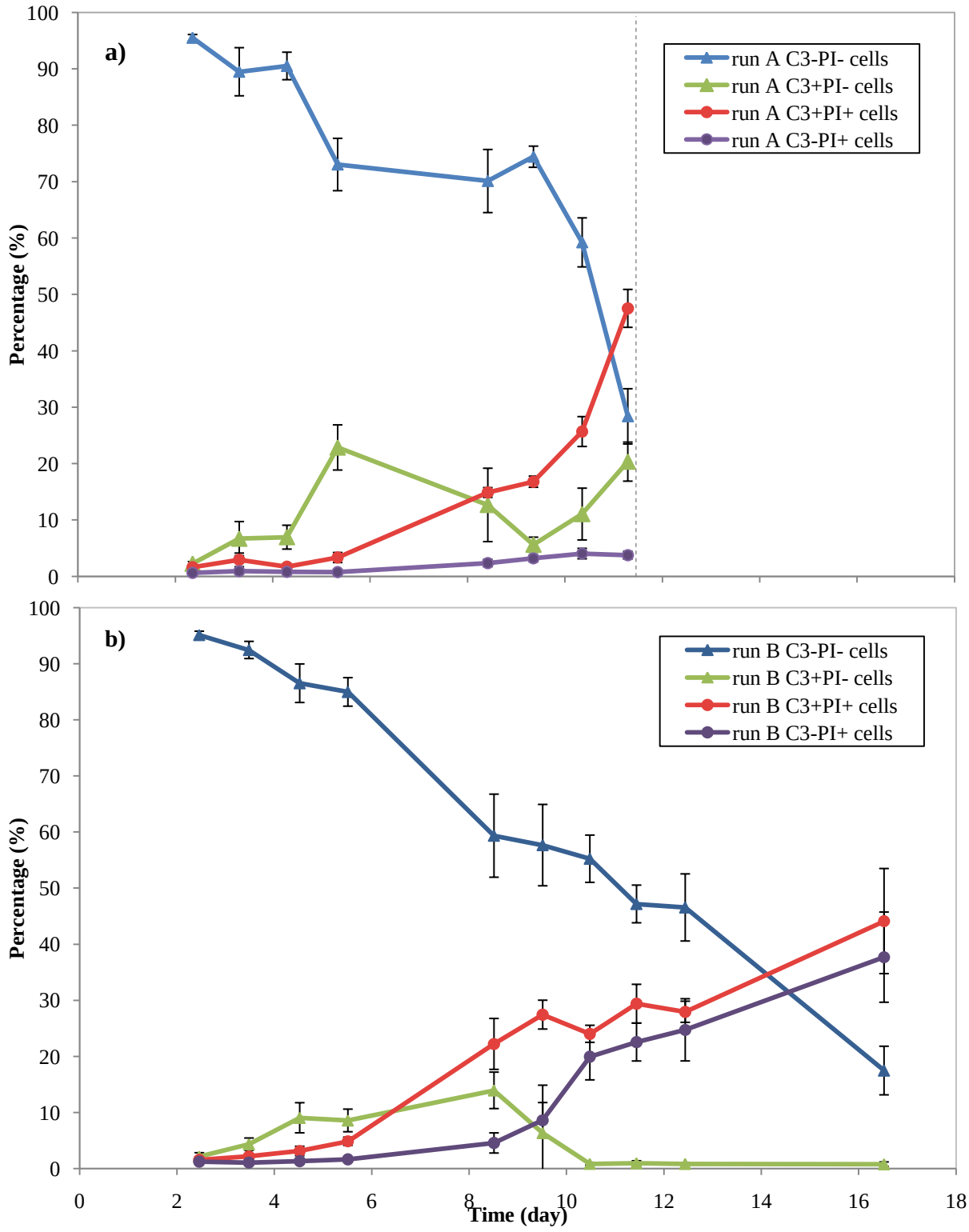

Figure 2-4. Apoptosis progression in run A and run B based on FCM caspase 3/7 assay, represented by percentage. a) run A; b) run B. FCM assays were performed for two additional time points in run B. Dotted line corresponds to the last sampling time point in run A and not the actual cultivation period.

When the same FCM experiment was repeated in run B, a similar general pattern for the progression of apoptosis and cell death was observed (Figure 2-4b) between the two runs. Nevertheless, the exact development of different subpopulations varied slightly between the two experiments. Two additional FCM time points near the end of the culturing process were collected in run B. Based on FCM assays, the decrease in healthy population seemed to be more gradual over time, as opposed to the more sudden drop observed in run A. The decrease of viability from 60% to 20% took about 8 days in run B as opposed to the 40% decrease in viability in run A which happened over 2 days. Similarly the increase in the late apoptotic subpopulation was fairly constant and more gradual in run B. These variations between experiments could be contributed by a 1-2 day delay in apoptosis progression such that the process was merely prolonged in run B. Furthermore, instead of increasing suddenly around day 5.5 as in run A, the percentage of early apoptotic cells remained constant between 10 to 15% from day 4.5 to 8.5 with perhaps a small peak on day 8.5. Soon after, the early apoptotic cells advanced into the late apoptotic phase and were mostly dead by day 10.5. A more apparent deviation between run A and B involves a significant elevation in the amount of C3-PI+ cells within the cultures after day 8.5. In run A, minimal percentage (<5%) of the culture fall into this category from day 2.5 until the last FCM sampling time point, day 11.5; while in run B, the increase started after day 8.5and continued until day 16.5 when the average level of these cells between four culture replicates was 38%.

Instead of comparing percentages, the changes in the four cell subpopulations over time were also examined as cell counts (see Figure 2-5). Comparison between the two representations (percentages versus cell densities) did not show any drastic difference in the overall patterns. The total dead cell counts in both runs were plotted and examined as well (see Figure 2-6). A consistent increase in the number of dead cells (caused by either apoptosis or necrosis) in both set of experiments were observed, though run A showed slightly slower accumulation of dead cells than run B. Moreover, Figure 2-7 shows an alternative view of the flow cytometry results by comparing between total apoptotic cells and the caspase-negative dead cells. In any case, the general trend of apoptosis

progression remained similar between the duplicate batches of experiments, although the exact timing and trend observed during cultivation seemed to deviate somewhat.

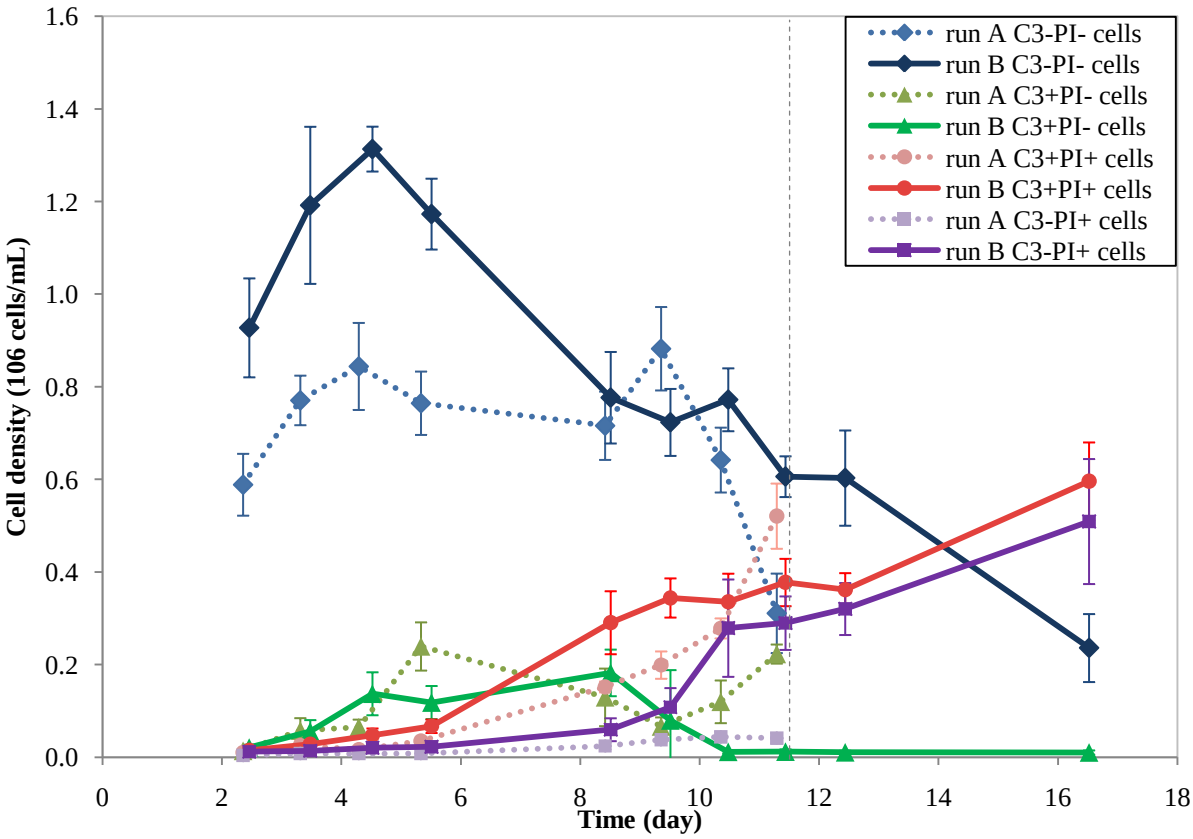

Figure 2-5. Apoptosis progression in run A and run B based on FCM caspase 3/7 assay, represented by cell numbers. This figure uses an alternative representation of subpopulation proportion (i.e. cell count) in cultures as opposed to the percentage shown in Figure 2-4.

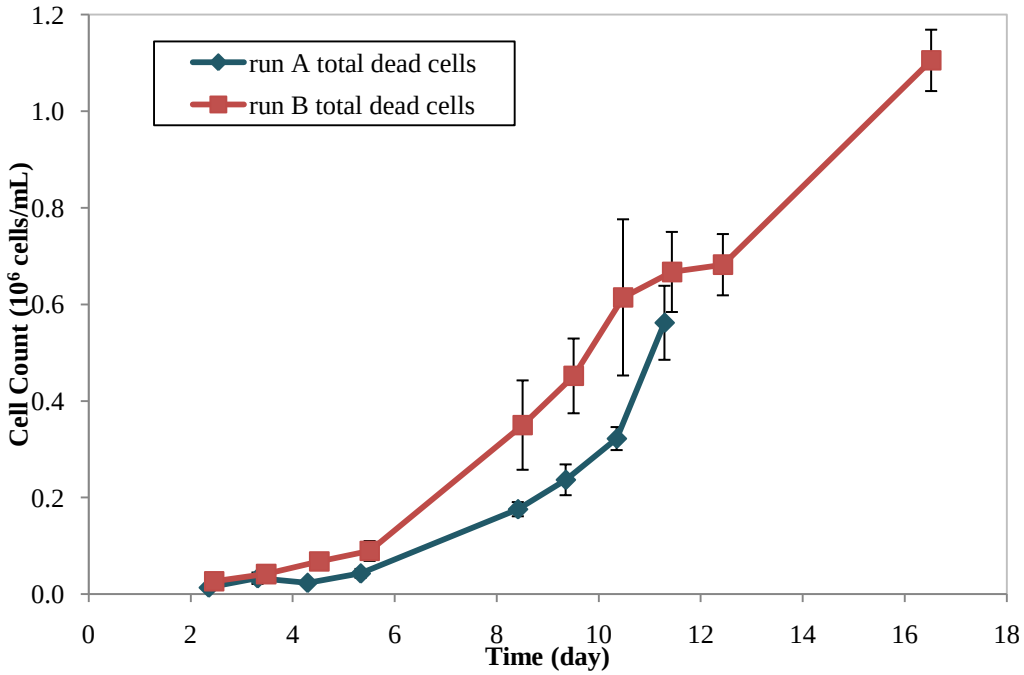

Figure 2-6. Total cell death as measured by FCM caspase 3/7 assay in run A and B. Cell death is determined by a positive propidium iodide intensity (i.e. C3+PI+ cells plus C3-PI+ cells). *Abbreviations: C3, caspase 3; PI, propidium iodide*

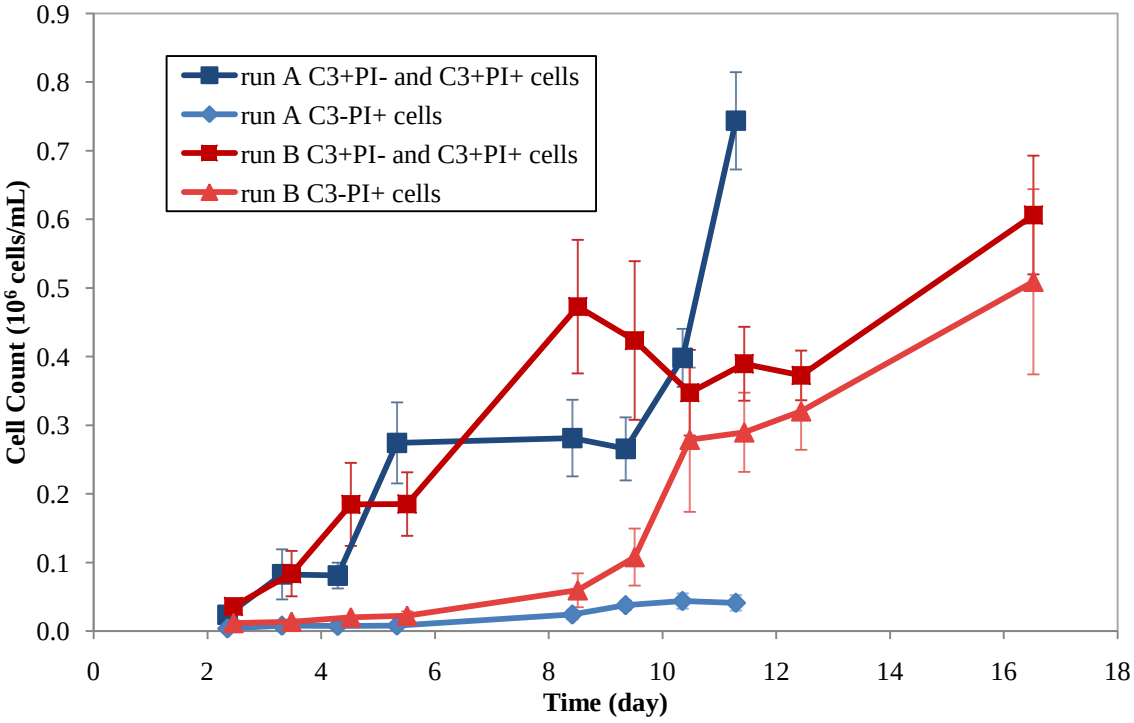

Figure 2-7. Comparison between caspase-positive cells to caspase-negative dead cell density as determined by FCM caspase 3/7 assay in run A and B. C3-PI+ cells can be a mix of primary necrotic and very late apoptotic cells that have lost its ability to bind FLICA. *Abbreviations: C3, caspase 3; PI, propidium iodide*

2.3.3 The Apoptotic Pathways Activated in CHO cultures

Flow cytometry assays on the amount of activated caspase 3/7, caspase 8 and caspase 9 were performed to monitor and compare the onset of various apoptotic pathways in run B. Activated caspase 8 in cells indicate the involvement of extrinsic pathway while activated caspase 9 signals the participation of intrinsic (mitochondrial) and possibly ER pathways in triggering apoptosis. Therefore by tracking the activation of these two proteins, more information on the apoptotic pathway initiated in this particular CHO culture setting was obtained. As mentioned previously in 2.3.2.2, caspases 3/7 results for run B were shown in Figure 2-4b and Figure 2-5. After the same analyses were done to the raw FCM data for both caspase 8 and caspase 9 methods, Figure 2-8 (and Figure A-4 in Appendix A) was generated to better examine and compare the results from the three caspase tests. Figure 2-8a shows the percentage of **C-PI-** cells as determined by the presence of different activated caspases, namely caspase 3, caspase 8 and caspase 9. Although a general decrease in the C-PI- cell population was observed regardless which caspase was measured, the proportion of cells with no caspase 9 activation appeared to be significantly less when compared to that of caspase 3 and caspase 8. A corresponding trend can also be seen in Figure 2-8b which shows the levels of the **C+PI-** cells. T-tests were done to investigate whether the differences between the three FCM caspases assays are statistically significant when used to classify each subpopulation (Table 2-1). It can be seen that when the curves in Figure 2-8 deviate, the corresponding p-values were less than 0.05 indicating statistical significance. The level of cells showing activated caspase 3 and activated caspase 8 did not differ by much when examining Figure 2-8, and in most cases it was not statistically different (Table 2-1).

When looking at the **C+PI+** cells (Figure 2-8c), a steady increase in cells having activated caspases is seen, regardless of the kind of caspase tested for. According to t-tests, these C+PI+ cells did not exhibit significant differences between the three FCM tests until after day 9.5 or 10.5. This increase in late apoptotic (C+PI+) cells corresponds with the decrease in early apoptotic cells (C+PI-) over time

(Figure 2-8b), suggesting that many early apoptotic cells observed in earlier time points (before day 8.5) had lost their membrane integrity and became dead as characterized by the PI result. The rate of healthy cells entering the early apoptotic phase appeared to decrease after day 5.5 when most transformation occurred as early apoptotic cells entered late apoptotic phase, which could be interpreted from the sharp drop in early apoptotic subpopulation after day 8.5. Lastly, the proportion of primary and secondary necrotic cells (**C-PI+**) in cultures also increased as the cultures grew older. At the last time point near day 16, both caspase 3 and caspase 8 FCM methods showed about 35% of the cultures to be dead with no detectable activated caspase signals. However based on the FCM caspase 9 method, only 20% was determined to be caspase-independent dead cells. This phenomenon could be explained by the presence of dead cells with activated caspase 9 the might not be categorized properly when testing for caspase 3 or caspase 8. However, since executioner caspases such as caspase 3 were necessary to cause death of apoptotic cells, it is unclear why activated caspase 3 detection did not pick up as many apoptotic dead cells as the caspase 9 method towards the end of the culturing process. Whether the specific inhibition rate and turnover rate vary between different caspases play a role in this observation is to be considered.

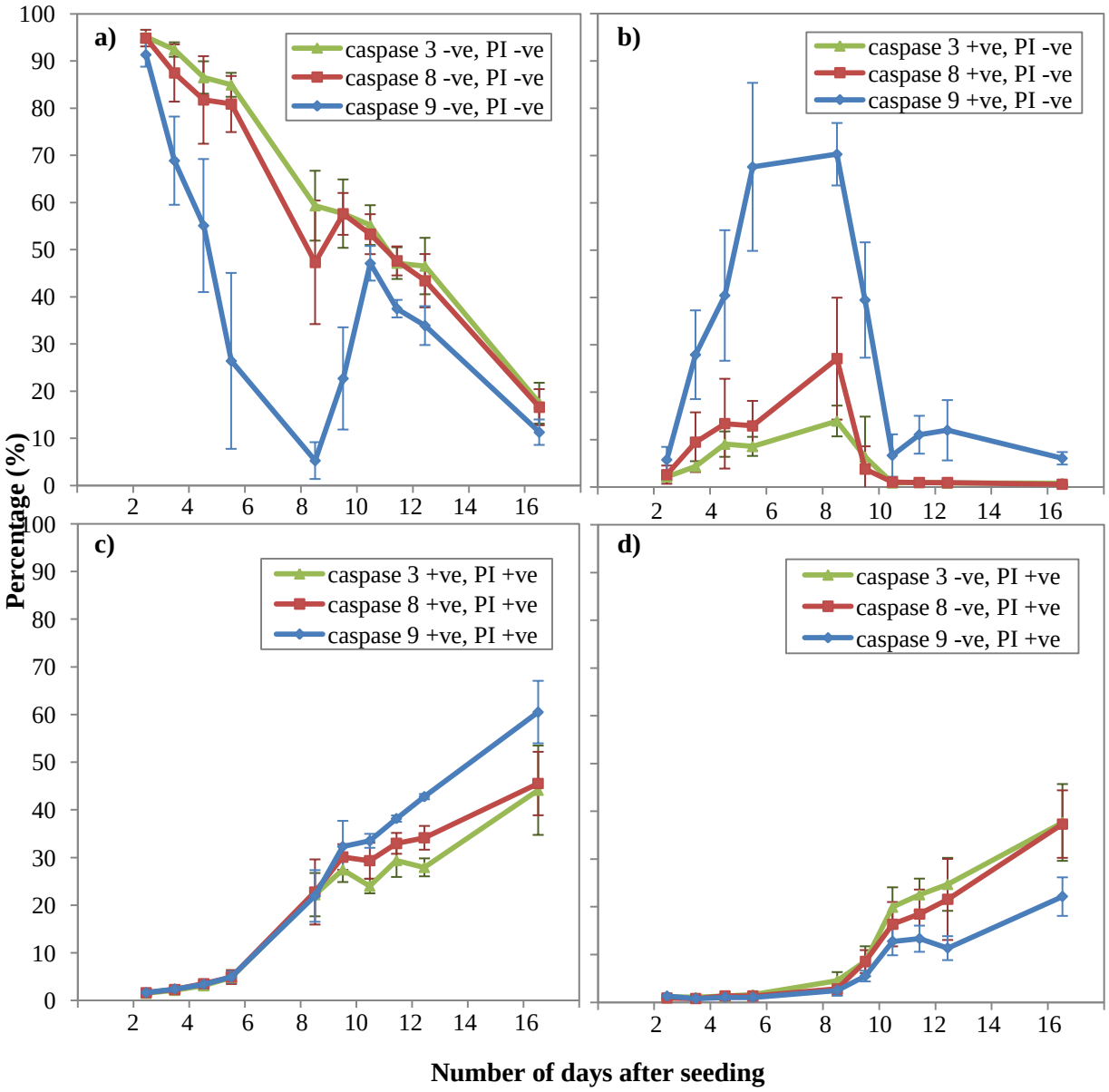

Figure 2-8. Comparison between cell subpopulations based on three FCM caspases assays of run B cultures. a) C-PI-, b) C+PI-, c) C+PI+, d) C-PI+ subpopulations. Caspase 8 and 9 are pathway-specific initiator caspases while caspase 3 is the common executioner caspases in different apoptotic pathways. *Abbreviations: C, caspase; PI, propidium iodide.*

Table 2-1. T-test comparison between a subpopulation from three FCM caspase assays. Each t-test was performed between FCM percentages from the four replicates measured by two FCM assays. A p-value less than 0.05 indicates that the differences between two assays is statistically significant and is highlighted in yellow below. *Abbreviations: C9, caspase 9; C8, caspase 8; C3, caspase 3; C, caspase; +, positive; -, negative*

a) C-PI-

Day	C9 vs. C3 t-test p-value	C8 vs. C3 t-test p-value	C8 vs. C9 t-test p-value
2.5	0.09250	0.84540	0.00395
3.5	0.01245	0.19920	0.00883
4.5	0.01233	0.30130	0.04448
5.5	0.00549	0.16570	0.00513
8.5	0.00074	0.13810	0.00308
9.5	0.00209	0.97700	0.00393
10.5	0.06590	0.00577	0.11860
11.5	0.02082	0.61850	0.00836
12.5	0.07668	0.09405	0.12310
16.5	0.01430	0.17130	0.00924

b) C+PI-

Day	C9 vs. C3 t-test p-value	C8 vs. C3 t-test p-value	C8 vs. C9 t-test p-value
2.5	0.11892	0.74915	0.0147
3.5	0.01199	0.18885	0.00901
4.5	0.01249	0.38015	0.04106
5.5	0.00491	0.1337	0.00521
8.5	0.00086	0.14239	0.00255
9.5	0.00260	0.26422	0.00345
10.5	0.07314	0.56857	0.09728
11.5	0.01276	0.96326	0.01263
12.5	0.03608	0.72875	0.03285
16.5	0.00283	0.38602	0.00266

c) C+PI+

Day	C9 vs. C3 t-test p-value	C8 vs. C3 t-test p-value	C8 vs. C9 t-test p-value
2.5	0.84301	0.65571	0.99251
3.5	0.11532	0.17418	0.26337
4.5	0.55534	0.24066	0.47834
5.5	0.84749	0.8892	0.94527
8.5	0.72803	0.68663	0.34263
9.5	0.05624	0.00254	0.22956
10.5	0.00041	0.02896	0.11342
11.5	0.00820	0.20579	0.02235
12.5	0.00074	0.04503	0.00981
16.5	0.01019	0.59231	0.00882

d) C-PI+

Day	C9 vs. C3 t-test p-value	C8 vs. C3 t-test p-value	C8 vs. C9 t-test p-value
2.5	0.78622	0.27757	0.00456
3.5	0.02872	0.19295	1.00000
4.5	0.11590	0.95081	0.24364
5.5	0.06392	0.21031	0.09999
8.5	0.01431	0.03225	0.41726
9.5	0.12086	0.88313	0.06305
10.5	0.00564	0.14498	0.22647
11.5	0.00805	0.23613	0.03543
12.5	0.00337	0.12210	0.04310
16.5	0.01824	0.89993	0.01173

2.4 Discussion

2.4.1 Progression of Apoptosis in CHO Cultures occurs in Several Phases

By measuring the levels of activated executioner caspases (caspase 3 and 7), flow cytometry (FCM) assays allowed the progress of apoptosis to be quantified and tracked in both spinner flasks culture experiments, run A and B. In addition, propidium iodide (PI), which detects membrane integrity, was added as a cell death differentiation stain. This bi-color FCM assay allows cells to be classified into four subgroups: **A) C3-PI- (healthy) cells** were negative for caspase activation and intact plasma membrane; **B) C3+PI- (early apoptotic) cells** contained activated executioner caspases while still maintained membrane integrity; **C) C3+PI+ (late apoptotic) cells** had advanced into the stage where it could no longer exclude PI stain; **D) C3-PI+ (primary and secondary necrotic) cells** had no intact plasma membrane yet no activated caspases were detected [87]. The C3-PI+ subpopulation could include both necrotic and very late apoptotic cells whose caspases were inhibited, lost or degraded beyond detection by FLICA [87,92,93]. The detection of activated caspase outside of cells at the end stage of apoptosis process has been detected; while the presence of mostly procaspases has been secreted from necrotic cells [47,94]. It has been speculated that the elimination of caspase activity occurred in apoptotic cells where cleavage of cellular proteins have been completed.

Comparison between run A and B

Between different runs, changes in the health condition of the cultures were generally consistent. Viable healthy cells gradually decreased throughout the culturing period while cells became apoptotic and eventually died. The degree of population-wise apoptosis in CHO-IgG-9β8 culture began rising from the initial basal level (<5%) after day 4.5 or 5.5. Following the increase of live early apoptotic cells, which peaked at 15-20% between 5.5-8.5 days, a large and steadily increasing late apoptotic cell population began accumulating until the end of culturing process and contributed to approximately 50-60% of the culture population. However, unlike run A, the accumulation of caspase-negative dead cells in run B was observed soon after day 8.5. To elucidate this deviation, two questions need to be answered: i) which type of cell produces the C3-PI+ signal, and ii) if the lack of C3-PI+ cells in run A was due to fewer FCM analyses, meaning the presence of C3-PI+ subpopulation would be seen if additional analyses were performed past day 11.5.

If there was indeed very few C3-PI+ cells in run A, it is unlikely that these cells were made up of very late apoptotic cells (i.e. secondary necrotic cells). Since high level of C3+PI+ cells were already present in run A by day 10.5, some of these cells should have already advanced into the C3-PI+ stage before the last FCM time point. However it is possible that the observed trend is real if C3-PI+ cells were mainly contributed by primary necrosis. One possible explanation of having primary necrotic cells in run B could be the effect of having higher cell densities in the spinner flasks. The peak viable cell density in run B is between 1.4-1.6x10^6 cells/mL instead of 1-1.2x10^6 cells/mL as seen in run A. Having a higher cell number in run B implies that less nutrient and resources were available per cell, and more waste products and contents of dead cells were released into the medium. For example, elevation of ammonia and lactate, which were known waste products in CHO cultures, has been shown to induce necrotic cell death [23]. When cell densities of the four subpopulations were examined (Figure 2-5) instead of percentage, it appears clearer that a larger number (larger by 0.2x10^6 cells) of apoptotic cell death occurred in run B before the elevation of C3-PI+ dead cells on day 8.5. In addition,

from Figure 2-6, which displays the total number of cell deaths as measured by FCM, it can be seen that run A showed a two-day delay for reaching the same quantity of dead cells than run B. Because the number of apoptotic and possibly necrotic cells increased faster and greater in run B, which had the same amount of nutrient and medium to start with, it would be possible that the resource limitation caused many dying cells to switch from apoptosis to necrosis instead [102]. The occurrence of necrotic cells might also self-amplify and caused more necrosis to take place in run B cultures near the end of the cultivation.

On the contrary, this variation might be due to the fact that FCM sampling was stopped earlier in run A, thus missing the beginning of the elevation and resulting in the low level of C3-PI+ cells. In this case, C3-PI+ cells cannot be caused by primary necrosis alone. By day 11.5 which is the last sampling time point in run A, only 28% of the culture remained healthy (C3-PI-) and available for turning necrotic since the majority of the remaining cultures were already apoptotic. Besides, in run B the accumulation of these caspase-negative cell deaths began as early as day 8.5 when healthy cells still dominate the culture at 60%. These evidence weakened the idea that necrosis has yet to take place. In the alternative case, one could argue that the degradation of apoptotic cells gave rise to most of these caspase-negative cell deaths. Since late apoptotic cells did not accumulate as much nor as fast in run A until after day 10.5 (Figure 2-5) when they suddenly increased in numbers, it might be reasoned that the conversion from late apoptotic into very late apoptotic cells had not occurred by day 11.5 in run A. Since apoptosis was documented to occur within 1-3 hours and FCM analyses were done at least 24 hours apart, the total apoptotic cell counts plotted in Figure 2-7 might better represent the situation. As the early apoptotic cells counted in one time point could already be in the very late apoptotic stage with degraded caspases in the next FCM analysis time point, the total apoptotic cell counts included the transformation of cells from early apoptotic to very late apoptotic stage and from late apoptotic to very late apoptotic cell stage.

General trend of apoptosis progression in culture

Although the time of apoptosis initiation in an unsynchronized and non-induced culture varied considerably, the different phases of apoptosis progression in the culture as a whole could still be observed. From day 0 to day 4.5, the cultures could be considered healthy and viable, where cells proliferate normally. During this period of time, nutrient concentrations were decreasing and waste product levels were increasing, both of which are potential triggers for apoptosis. The deterioration in extracellular conditions led to the initiation of apoptosis in cells after day 4.5. At this time, not many apoptotic cells were yet in the state where degradation of proteins and the loss of membrane integrity had occurred. However, between day 4.5 and 8.5, more apoptotic cell death progressed from the early stage into the late phase where the plasma membrane became permeable. From day 8.5 onward, the proportion of late apoptotic and caspase-negative dead cells continuously increased and eventually accounted for a large portion of the culture.

2.4.2 The Dominant Apoptotic Pathway Triggered in CHO Cultures

Although some cells are likely to undergo apoptosis via the extrinsic pathway as exhibited by the activation of caspase 8 in some cells, the dominant trigger for apoptosis seems to be related with intracellular cell death stimuli as shown by the steep increase of activated caspase 9 early in the culturing process. As early as 5.5 days after seeding, CHO cultures showed an average of 70% cells with active caspase 9 and intact plasma membrane as compared to only less than 15% of the culture exhibited active caspase 8 and caspase 3. The high percentage of live caspase 9 positive cells was maintained until day 8.5 where its decrease concurred with the increase of more late apoptotic cells with no membrane integrity and some caspase-negative dead cells that could be caused by necrosis or the deterioration of late apoptotic cells. Although death receptor-mediated cell death in some cell lines might engage a crosstalk with the mitochondrial pathway, it is more likely that the activation of caspase 9 in this work corresponds to the onset of mitochondrial and/or ER pathway. In addition to having an

earlier and a significantly larger amount of activation in caspase 9, prolonged cultivation of cell cultures are known to encounter nutrient limitation and accumulation of toxic waste products over time, both of which are linked to the intrinsic cell death. Moreover, expression of recombinant protein in cell cultures can overload the ER folding system and lead to ER apoptotic cell death. Therefore, based on the known conditions of the CHO cultures in this study, the possibility of a type II extrinsic pathway occurring is not very high. However, as the ER initiator caspase 12 can activate caspase 9, the detection of caspase 9 in this study alone is not enough to distinguish which intracellular compartment (mitochondria and/or ER) governs the initiation of apoptosis. Currently, interactions and communication between the mitochondria and ER suggest a tight association and extensive crosstalk between these two initiation sites [53]. In addition to the interactions between mitochondria and ER via calcium ion signalling, apoptosis is also being regulated by many Bcl-2 proteins localized on both organelles [103]. The mitochondria and ER are interconnected both physically and physiologically [104]. In fact, it remains unclear how distinct the mitochondrial and ER-mediated apoptosis really are.

Ideally apoptotic cells triggered by both active caspase 9 and caspase 8 should converge to the activation of caspase 3. However the average level of late apoptotic cells with active caspase 3 did not become dominant as expected towards the end of the culturing process. It is possible that the consistent 20% difference between caspase 9 active and caspase 3 active cells beyond day 9.5 was caused by the delay in the activation of executioner caspases and the continuous increase in the late apoptotic cells triggered by intracellular stimuli that had not yet activated caspase 3. Alternatively, cells with activated caspase 3 are not expected to persist in the cultures for very long, as they will disintegrate. Because the fast progression of apoptosis, apoptotic cells with activated executioner caspases are expected to last only few hours after the initial stimulation.

In agreement with FCM results obtained in this work, a CHO cDNA array study comparing mRNA expression over five days done by Wong and colleagues showed an increase in both caspase 8 and caspase 9 mRNA levels within cells after exponential phase [69]. In Wong's study, the upregulation of caspase 9 mRNA in the batch culture showed a slightly larger fold change than that observed for caspase 8, while the increase in caspase 8 mRNA level was much more persistent between day 3-5, which span the stationary and death phase of the CHO cell line employed. From the lack of mRNA changes to proteins important to the ER-mediated apoptosis pathway (such as caspase 12 and BiP), it was concluded that the ER pathway was not significant in Wong's study. Nevertheless, the choice of detection technique in systematic studies can be an important factor that influences the observed results and their interpretations. Unlike protein abundance measurement as in FCM or DIGE techniques, changes in mRNA cannot be directly translated to changes in protein activities, which in many cases are better represented by protein expression. More detail comparison between results from Wong's transcriptomic study and those of the proteomic analysis from this thesis will be presented in Chapter 3.

Chapter 3. Differentially Expressed Proteins during prolonged CHO cells Cultivation

3.1 Introduction

The main objective of proteomic analyses of CHO cultures at various phases of cultivation is to study the systemic changes at the protein level over time and to identify important mechanisms related to these changes, which are often encountered during protein production in the industrial bioreactors. Proteins that vary their expression level during extended cultivation will be examined and identified. These may include proteins that are responsive to the degradation of culture conditions such as the depletion of nutrients and accumulation of metabolic waste products. Since cell death, in particular apoptosis, greatly influences the longevity and condition of mammalian cell cultures, it was anticipated that some changes in apoptotic proteins and apoptosis-modified proteins will be uncovered via a whole cell proteomic analysis. The detection of differentially expressed proteins allow us to capture the intracellular responses prior to and when culture conditions become less than desirable. Moreover, the identification of any proteins specific to an apoptotic pathway will shed light on the method of apoptosis initiation and reveal possible causes for it during prolonged cultivation in bioreactors. Studying the intracellular changes of CHO cells in a time course will broaden our knowledge on the behaviours and "natural aging" of cells in bioreactors, thus may contribute to the improvement of culturing process for industrial purposes.

Protein samples were collected in run A for subsequent proteomic analyses using differential in gel electrophoresis (DIGE) and mass spectrometry (MS). As a modified version of the traditional 2D gel electrophoresis technique, DIGE allows two protein samples to be separated on a single gel. By staining each protein sample with a different fluorescent dyes, protein abundances between samples can be compared and analyzed. Proteins that were either up- or down-regulated at various time points of

the cultivation will be distinguished from the whole cell proteome. Following MS sequencing and database searching, identification of these proteins can then be obtained.

In this study, based on the FCM caspase 3 and cell count results, four time points were selected for examining altered protein expressions in CHO cells undergoing prolonged cultivation and apoptosis. Cell samples from day 2.5 cultures, which were still in the proliferating exponential phase, were used as healthy and apoptosis-negative control samples. Between day 4.5 and day 5.5, the cultures were at the end of exponential phase or the beginning of stationary phase. Day 4.5 was sampled as an early stationary phase time point where levels of both early and late apoptotic cells were just starting to incline. Cells collected on day 5.5 were considered as a mid-stationary phase sample where apoptosis had already progressed in the cultures to the stage with the peak amount of early apoptotic population. Lastly, day 8.5 marked the beginning of the death phase and contained equal ratio of late apoptotic (C3+PI+) to early apoptotic (C3+PI-) cells. To avoid the interference of over-degraded cellular contents, protein samples beyond day 8.5 were not considered due to the large proportion of dead cells and possibly cellular debris in the whole culture.

3.2 Materials and Methods

3.2.1 Protein Extraction and Quantification

Cells were harvested by removing an aliquot of 5 to 20mL depending on the cell concentration, from the 500mL spinner flasks at various time points during the culturing period. Cells were washed three times with cold 1x phosphate buffered saline (PBS) solution (137mM NaCl, 2.7mM KCl, 10mM Na_2HPO_4, 17.6mM KH_2PO_4). During each wash, the PBS-cell mixture was centrifuged at 1000rpm for 5 minutes to remove the PBS wash buffer. After the third wash, cell pellets were stored at -80ºC or immediately lysed as described below.

To extract protein, a lysis buffer containing 7M urea, 2M thiourea, 4% CHAPS (3-[(3-Cholamidopropyl) dimethylammonio]-1-propanesulphonate) and 50mM Tris, pH 8.0 was used with a mammalian cell protease inhibitor cocktail (1μL per 10^6 cells, P8340, Sigma, Oakville). To achieve consistent protein concentration between 2 to 3 μg/μL, roughly 30-35μL of lysis buffer was used per 10^6 cells. Lysis buffer-cell mixtures were mixed by rotating at 4ºC for 1 hour before the cell debris were pelleted by centrifugation for 30 minutes at 14000 rpm at 4ºC. The protein-containing supernatants were then transferred into new Microcentrifuge tubes.

Protein concentrations were measured using Bio-Rad protein assay (Cat. #500-0002, Bio-Rad Laboratories Ltd., Mississauga), which is based on the Bradford method [105], immediately after extraction following the manufacturer's microassay procedure. A linear standard curve was constructed with 2, 4, 6 and 8 μg/mL bovine serum albumin (BSA) standards and their corresponding spectrophotometer absorbance reading at 595nm. Triplicates of each protein sample including the BSA standards were used to ensure accuracy of the assay. The protein extracts were then stored at -80°C.

3.2.2 Differential in Gel Electrophoresis

3.2.2.1 Protein Sample Labelling

Prior to running the Differential In-Gel Electrophoresis (DIGE) experiment, the choice of protein samples loaded in each gel and the corresponding CyDyes were chosen to avoid dye bias. CyDye 3 and 5 need to be alternatively used for labelling biological duplicates. Table 3-1 shows the protein samples and corresponding CyDye labelling used in this project. For each gel, 2 protein samples and an internal standard, each labelled with a different CyDye DIGE Fluor minimal dye (Cy2: #25-8010-82, Cy3: 25-8010-83, Cy5: 25-8010-85, GE Healthcare, Quebec), were loaded. Fifty microgram of each protein component yielded a total of 150μg protein mixture loaded per gel.

Table 3-1. DIGE experimental design

Gel No.	Spinner flask ID	Cy3	Cy5	Cy2
1	1	D2.5	D4.5	internal std
2	1	D5.5	D2.5	internal std
3	1	D2.5	D8.5	internal std
4	2	D2.5	D4.5	internal std
5	2	D5.5	D2.5	internal std
6	2	D2.5	D8.5	internal std
7	3	D4.5	D2.5	internal std
8	3	D2.5	D5.5	internal std
9	3	D8.5	D2.5	internal std
10	4	D4.5	D2.5	internal std
11	4	D2.5	D5.5	internal std
12	4	D8.5	D2.5	internal std

The internal standard was prepared by pooling an equal amount of all protein samples that were to be analyzed by DIGE. Having the same protein mixture in the internal standards for all 12 gels made subsequent gel image mapping and cross-gel spot matching possible. After staining each of the three protein components with 1µL of 200ρmol/µL CyDye working solution, the light sensitive samples were incubated on ice for 30 minutes before 1 µL of 10mM lysine was added to stop further labelling reaction. After another 10 minutes incubation on ice in the dark, all three individually stained protein components were combined into one mixture. Finally, 9µL of 1M dithiothreitol (DTT), 2.25µL of pH 3-10NL IPG buffer (#17-6000-88, GE Healthcare, Quebec) and sufficient rehydration buffer (7M urea, 2M thiourea, 4% CHAPS, 0.002% bromophenol blue) were included to obtain a total sample volume of 450µL for each gel.

3.2.2.2 Gel Strip Rehydration

Combined DIGE protein samples were pipetted evenly into the grooves of the Immobiline DryStrip Reswelling Tray (#80-6371-84, GE healthcare, Quebec), which could hold maximum 12 immobilized pH gradient (IPG) gel strips. 24cm pH 3-10NL Immobiline DryStrip gel strips (#17-6002-

44, GE Healthcare, Quebec) were warmed at room temperature for 5 minutes and positioned gel side down into the reswelling tray. By gently lifting and sliding the strip over the surface of the sample solution with a forceps, the entire strip became coated with the sample. Once no bubbles remained under the strip, the strip was overlaid with roughly 2.5 mL of PlusOne DryStrip Cover fluid (#17-1335-01, GE Healthcare, Quebec) to prevent evaporation and urea crystallization. The strips were allowed to rehydrate on a level surface in the dark for 12 hours.

3.2.2.3 Isoelectric Focusing

After rehydration, the strips were transferred to and placed gel side up in the manifold ceramic tray (#80-6498-57, GE Healthcare, Quebec), which then was covered with 120mL of DryStrip cover fluid oil. Two paper wicks, each wetted with 150µL ultrapure water, were placed partially over the ends of each gel strip. Once all the strips had been positioned and lined up, electrodes were positioned on top of the tray, in contact with the paper wicks. Isoelectric focusing (IEF) was carried out on Ettan IPGphor II Isoelectric Focusing Unit (#80-6505-03, GE Healthcare, Quebec) using the following protocol with no additional rehydration step:

Step 1. 500V (1 hr)
Step 2. Gradient to 1000V (3 hrs)
Step 3. Gradient to 3000V (3 hrs)
Step 4. 3000V (2 hrs)
Step 5. Gradient to 8000V (3 hrs)
Step 6. 8000V (10:30 hrs)
Step 7. 500V (24 hrs)

Once step 6 was finished, IEF phase was completed and strips were maintained at 500V for a maximum of 24 hours. Alternatively, each IPG strip could be removed and placed in an equilibration tube with plastic side in contact with the tube and stored in -80ºC until ready for equilibration.

3.2.2.4 SDS-PAGE Phase

Gel Casting

All DIGE non-fluorescent clear glass plates, plastic spacers and gel casters were washed with deionized (DI) water prior to usage. DIGE gel plates were further washed with ultrapure water, rinsed with 70% ethanol, and wiped dry with KimWipes. For each gel, a short and long glass plates were aligned and pressed together firmly to form a gel cassette. The DALT*six* gel caster (#80-6485-46, GE Healthcare, Quebec) was assembled by alternatively inserting gel plate cassettes and plastic spacers. Plastic spacer blocks were used when there were less than 6 gel cassettes. Spacer sheets were added to ensure the height of the plate sets was the same as the edge of the caster. Fresh 12% acrylamide gel solution was made after the gel caster had been assembled. Enough gel solution was poured slowly into the caster until the solution level was about 0.5cm below the edge of the short plate. To avoid the gel surface drying out, 1mL of water was layered carefully in between each plate cassette. Once the gel solidified, the plate cassettes were removed from the caster and the outer surfaces were rinsed with DI water to remove any gel residues. The top surfaces of the gels were layered again with DI water or 2X running buffer (50mM Tris base, 384mM glycine, 0.4% SDS).

Equilibration

Each IPG strip was incubated in 15mL equilibration buffer (6M urea, 50mM Tris-HCl pH 8.8, 30% glycerol, 2% SDS, 0.002% Bromophenol blue) containing fresh 1% DTT for 30 minutes in the dark on a rocking platform, followed by another half hour incubation in equilibration buffer containing fresh 2.5% iodoacetamide (IAA).

Electrophoresis

Each IPG strip was inserted into a gel cassette where it evenly contacted the top edge of the gel. After all bubbles trapped between the gel and the strip were removed , the liquid covering the gel

surface was decanted and replaced with agarose sealing solution (25mM Tris base, 192mM glycine, 0.1% SDS, 0.5% agarose, 0.002% bromophenol blue) to immobilize the gel strip. A maximum of 6 gel cassettes were placed into the cassette carrier, and any unused slots were filled with spacer blocks. The upper buffer chamber (UBC) (28-9057-86, GE Healthcare, Quebec) was fitted firmly onto the carrier. Prior to electrophoresis, 4.5L of 1x electrophoresis running buffer (25mM Tris base, 192mM glycine, 0.2% SDS) was cooled to 10°C in the lower buffer chamber (LBC) of the DALT*six* Electrophoresis unit (#80-6485-08, GE Healthcare, Quebec) using the MultiTemp III Thermostatic Circulator (#18-1102-77, GE Healthcare, Quebec). After the carrier had been positioned in the electrophoresis unit, more 1x running buffer was added until the maximum fill line indicator was reached. The UBC was filled with 2X running buffer (50mM Tris base, 384mM glycine, 0.4% SDS) until it levelled with the buffer in the LBC. Electrophoresis began at 1W per gel for half an hour and continued at 17.5W per gel until the dye front reached the bottom of the gels.

3.2.2.5 Gel Visualization, Data Analysis and the Generation of Protein Spot Pick List

Gel cassettes containing DIGE gels were rinsed with DI water and wiped dry. Using the Typhoon 9400 scanner (#63-0055-78, GE Healthcare, Quebec), gels were scanned at a PMT setting of 600V and 200 micron resolution with 3 different filters: 520 BP40 Cy2, 580 BP30 Cy3 and 670 BP30 Cy5. Each gel resulted in 3 different gel images with file extension ".gel", corresponding to the 3 CyDye labelled samples. Using the software Image Quant 5.2 (GE Healthcare, Quebec), all gel images were cropped to the same size and loaded into DeCyder v6.0 software (GE Healthcare, Quebec). Each of the 12 gels was subjected to spot detection in the DeCyder Differential In gel Analysis (DIA) module with estimated number of spots set to 2000. Next, spots in all 12 gels were matched to each other in the DeCyder Biological Variation Analysis (BVA) module using the "match all" option. Due to the number of protein isoforms, which showed up as horizontal "trains of protein spots," there were many mismatched spots between the images from the 12 gels. As a result, spot merging and landmark

settings were used to improve the quality and accuracy of automatic matching. Subsequently, t-test statistical analyses were performed between day 2.5 to day 4.5 samples, day 2.5 to 5.5 samples, and day 2.5 to 8.5 samples using the statistical programming language R (see 2.4.5.1 and Appendix A.1). Protein samples collected at different time points from the same spinner flask were treated as paired data in t-tests. Lastly, DeCyder's built in paired ANOVA test was done to examine changes across of proteins from all 4 time points. In addition, p-value results from both t-tests and ANOVA tests were converted to false discovery rate (FDR) in R (see 2.4.5.1 and Appendix A.1). To select proteins of interest, an FDR cut-off of 0.1 was used. The final spot picking list was generated from the combined results of the statistical tests.

Data extraction and statistical test analyses using R

Raw standardized abundance data of all detected spots were extracted from DeCyder software after BVA analysis was performed using R scripts (see Appendix A.1). The DeCyder software represented protein abundance fold changes or ratios that were less than 1 by their negative reciprocal, meaning a 10 fold down regulation of protein X between 2 samples would be displayed as -10 instead of 1/10. This also indicates that the standardized abundances, which were adjusted based on the internal standard of each gel, were presented this way and must be converted back prior to subsequent statistical analyses. Once adjusted and scaled logarithmically, the standardized abundances were subjected to paired t-test analysis with unequal variance in R. For each protein spot, the average ratios between replicates, t-test p-values and the corresponding FDR values were calculated using R.

For the one way paired ANOVA test, the post matching BVA file was analyzed without the DeCyder built in FDR correction. The FDR values were computed using R as shown in Appendix A.1.

3.2.3 Mass Spectrometry

Protein spots that differed in expression between time points were subsequently excised from preparative gels loaded with high amount of protein and trypsin in-gel digestion before finally analyzed by the mass spectrometer.

3.2.3.1 Preparative Gels

A high total amount of protein (500, 750 and 1000 μg) containing a mix of all 16 protein samples were loaded onto 24cm pH3-10NL IPG strips and 12% polyacrylamide gels to obtain spots with sufficient and detectable amount of proteins. The 2D gel electrophoresis procedure was similar to that of the DIGE (see section 3.2.2) with a few modifications. One major difference was that the inner side of the shorter plate must be treated with Bind Silane solution to facilitate binding of the gel piece. Gel plates were washed with detergent, water then 70% ethanol. After drying using KimWipes, 5mL of Bind Silane solution (4mL ethanol, 100μL acetic acid, 5μL Bind Silane and 0.9mL DI water) was distributed evenly across one side of the plate with KimWipes. The treated plate was dried for an hour in the flow hood before washing with 70% ethanol and final drying. The gel plate cassette was assembled with the treated side facing inward. Subsequent SDS-PAGE was performed as mentioned previously.

After the second dimension SDS-PAGE, the untreated glass plate was removed from the cassette. For each gel, 500mL fresh colloidal Coomassie blue staining solution (10% ammonium sulphate, 0.12% Coomassie Blue G-250, 10% phosphoric acid, 20% methanol) was needed to visualize protein spots. After all other ingredients had dissolved, methanol was added slowly drop by drop to avoid destroying the Coomassie blue colloids. The gel piece with the attached plate was immersed and incubated in the staining solution overnight at room temperature on a rocking platform. Subsequent

destaining with ultrapure water was done overnight. The gel piece was scanned at 633nm using the Typhoon 9400 scanner with no filter, PMT 600V and a resolution of 100µm. Spot matching between DIGE and preparative gels was done manually. Excised gel pieces were stored in water at room temperature until gel spot picking.

3.2.3.2 MS Sample Preparation: In gel Protein Digestion

To reduce contamination of keratin, all procedures were followed carefully and potential sources of contamination minimized. All equipments including tweezers, scalpel and flow hood were cleaned thoroughly with 100% acetonitrile (ACN) and let dry. All pipette tips and low retention Microcentrifuge tubes were rinsed twice with 100% ACN and let dry overnight in a flow hood.

Protein spot excision

An in-gel digestion protocol was used to create a peptide mixture from each protein spot selected from the DIGE experiment. Each spot was excised using a clean scalpel, cut into approximately 1 mm^3 cubes and transferred into a 0.6mL low retention Microcentrifuge tube. All the following steps required incubating the gel pieces in a reagent while vortexing for a period of time before the tubes were centrifuged briefly and the liquid phase removed. All steps were performed at room temperature, unless specified otherwise.

Destaining

Gel pieces were washed three times for 5 minutes in fresh 100µL ultrapure water. To remove Coomassie blue stains, gel pieces were vortexed for 10 minutes in 100µL of 50mM NH_4HCO_3 in 50% ACN 3 times.

Reduction and Alkylation

After a 5 minute dehydration step of incubating gel pieces in 100µL of ACN, all excess liquid was removed. Next, 100µL of reduction solution (10mM DTT in 100mM NH_4HCO_3) was added to the dehydrated gel pieces which were incubated for 30 minutes in a 50ºC water bath. The gel pieces were then dehydrated twice in 100µL of ACN for 5 minutes each time at room temperature. 100µL of 55mM iodoacetamide in 100mM NH_4HCO_3 was used to rehydrate and alkylate the gel pieces. After 30 minutes of incubation in the dark at room temperature without vortexing, all liquid was removed following a brief centrifugation. The gel pieces were washed with 100µL of 100mM NH_4HCO_3 for 15 minutes and dehydrated with ACN for 5 minutes. Next, the gel pieces were dried for 20 minutes on a SpeedVac.

Trypsin digestion

Sufficient 50mM trypsin in acetic acid was added to fully rehydrate the gel pieces. Between 2 - 12µL is typically necessary for each protein spot. The digest tubes were incubated on ice for 10 minutes to allow gel pieces to fully absorb the trypsin solution. To remove excess trypsin, 50µL of 100mM NH_4HCO_3 was used to wash the gel pieces for 5 minutes. After all liquids were removed, a fresh aliquot of 50µL 100mM NH_4HCO_3 was mixed to the digest tube which was then allowed to incubate on ice for 5 minutes before transferring to a 37ºC water bath for a 16-18 hour digestion.

Peptide extraction

Immediately following the digestion, sample tubes were briefly vortexed and centrifuged. For each digest, a 0.6mL Microcentrifuge tube (collecting tube) was prepared with 5µL of 5% formic acid (FA) in 50% ACN prior to peptide collection. To extract peptides, 50µL of ultrapure water was added to the digest mixtures. After a 2 minute vortexing and a brief centrifugation, the digests were sonicated for 10 minutes in a 37ºC heated water bath. With a 30 second centrifugation at 14000rpm to spin down all liquid, the peptide-containing supernatant was transferred to the collecting tube. Subsequently,

75µL of 5% FA in 50% ACN was added to the sample tube, which was then subjected to another 2 minute vortexing and brief centrifugation. The second sonication required 5 minutes and was followed by another quick 30 second centrifugation before transferring the supernatant to the collecting tube. Finally, another fresh aliquot (75µL) of 5% FA in 50% ACN was mixed in with the gel pieces. The last extraction step involves no sonication but just vortexing for 2 minutes and pop-spin centrifugation before transferring the supernatant to the collecting tubes. The peptide samples were completely dried in the collecting tubes using the SpeedVac.

ZipTip cleanup

For MS analysis at the University of Waterloo MS facility, samples were de-salted and cleaned up using ZipTip C18 pipette tip (Cat. #ZTC18S096, Millipore). The dried peptides resulted from ZipTip cleanup were resuspended with 10µL of 0.1% FA solution. Samples analyzed by the Proteomic Core facility of the Atlantic Research Center at the Dalhousie University required no ZipTip cleaning nor FA resuspension. To start the ZipTip Cleanup process, a 0.6mL Microcentrifuge elution tube containing 5µL of 50% ACN was prepared for each protein sample. The ZipTip C18 pipette tip was wetted at least 3 times with fresh 10µL 50% ACN, then equilibrated at least 3 times with fresh 10µL 0.1% FA. All liquids were drawn and expelled carefully into a container without introducing air bubbles into the column. To bind the peptides to the ZipTip, the acidified digests were slowly and repeatedly drawn into the tip and expelled back into the collecting tube 10 times. The ZipTip was then washed 2 or 3 times with 10µL 0.1% FA before eluting into the elution tube by drawing the 5µL of 50% ACN into the tip and expelling it back to the elution tube 10 times slowly. At the last ejection, all liquids were expelled completely. To protonate peptides and prevent trypsin autolysis, 1µL of 1% FA was immediately added to the eluted peptide sample to achieve a final concentration of 0.2% FA in 50% ACN. If the initial estimated protein amount was above 100-150ng, samples was diluted further with 5µL of 50% ACN and 1µL of 1% FA. Despite whether ZipTip cleanup was performed, all prepared peptide samples were stored in a -20ºC freezer until ready for MS analysis.

3.2.3.3 MS Protein Sequencing

The majority of the MS/MS analyses were done using Waters/Micromass Q-Tof Ultima Global machine at the University of Waterloo Chemistry department's MS Facility. Nano injection, positive electrospray ionization (ESI) with Quadruple-Time Of Flight (QTof) detection was used.
For low abundance protein spots, MS/MS analyses were performed by the Proteomics Core facility at the Atlantic Research Center of the Dalhousie University using LC Packings Ultimate and Applied Biosystems QTRAP 2000. Separation of peptide extracts by C18 reverse-phased nano-LC was performed before the ESI MS/MS analysis with Quadruple Ion trap (QIT) detection.

3.2.3.4 MS Data Analysis – Identification using PEAKS and MASCOT Tools

Two separate software packages were used for analysis: MASCOT MS/MS Ions Search (Matrix Science Inc.) and PEAKS (Bioinformatics Solutions Inc.). When matching protein identification of MS/MS data using MASCOT online, the parameters used were listed in Table 3-2. Similar protein identification analyses were also performed using the commercial software, PEAKS v2.5 with setting as listed in Table 3-3 below. Results from both MASCOT and PEAKS methods were compared.

Table 3-2. MASCOT parameter setting

Parameters*	Values**
Database	MSDB***
Taxonomy	All entries
Enzyme	Trypsin
missed cleavages allowed up to	1
Fixed modifications	Carbamidomethyl (C)
Variable modifications	Oxidation (M)
Peptide tolerance	0.2 Da for QTof; 0.3 Da for QIT
MS/MS tolerance	0.1 Da for QTof; 0.3 Da for QIT
Peptide charges	+2, +3 for QTof; +1, +2 and +3 for QIT
Data format	.dta for QTof; Mascot generic for QIT

** Any unlisted parameters were unset or following the default setting.*

*** QTof refers to analysis performed with QTof detection. QIT refers to analyses performed by Dalhousie University with the Ion Trap detection*

**** Initial searches were done with the MSDB database. Unsuccessful searches were performed again in NCBI (nr) DB and Swiss-Prot DB.*

Table 3-3. PEAKS protein identification and auto de novo options

Parameters	Values**
Search in database	MSDB
Parent mass error tolerance	0.2 Da for QTof; 0.3 Da for QIT
Fragment mass error tolerance	0.1 Da for QTof; 0.3 Da for QIT
Enzyme and PTM	Trypsin with Cam
Instrument	Quadrupole-TOF for QTof; Ion Trap for QIT
Centroid and deconvolute for analysis	yes

** Any unlisted parameters were unset or following the default setting.*

*** QTof refers to analysis performed with QTof detection. QIT refers to analyses performed by Dalhousie University with the Ion Trap detection*

For PEAKS, results were evaluated by percentage where 100% indicates a perfect match between the protein ID to the sequence data and 0% indicates no match. On the other hand, MASCOT uses a score based system with no upper bound. For each MASCOT protein search, the resulting score was derived from individual ion p-values and converted into a nonprobablistic based value. The higher the score, the more reliable and accurate the identification.

3.3 Results

Based on repeated flow cytometry analyses throughout CHO cultivation, protein samples for four time points during the cultivation of four spinner flask CHO cultures in run A were prepared. To examine the differences at the protein level that may contribute to the onset, progression and effect of apoptotic cell death in prolonged cultures on top of the changes brought by the degradation of culture conditions over time, protein samples were compared with quantitative 2D gel electrophoresis. Protein extract from cells collected on day 2.5 was used as a healthy control. Day 4.5 was considered to be in the early stationary phase, day 5.5 in the mid-stationary phase and day 8.5 in the early death phase. Correlation between various cultivation phases to apoptosis progression was made by flow cytometry assays that detect activated caspases in cells. The levels and stages of apoptotic cell deaths in cultures were shown to be increasing with time. Since apoptosis in individual cell from initiation to death progressed within hours, proteomic analysis of culture examines the changes population-wise. In this study, three DIGE comparisons were done per culture, resulting in a total of 12 gels. By detecting and quantifying abundance of the protein spots resolved on each gel, protein expression changes between time points could be visualized. The four CHO culture replicates allow the significance of these observed changes to be validated by statistical tests. Based on statistics, a list of potential differentially expressed protein spots was generated. After screening to remove non-protein spots and ones with low fold change or abundance, the resulting subset of spots was then subjected to identification by mass spectrometry. The results are presented below.

3.3.1 Spot Detection in DIGE Images

Figure 3-1 shows a typical DIGE gel image displaying Cy3 and Cy5 channels. Spots in 2D gel images correspond to proteins of a particular molecular weight and isoelectric point. When viewing with Image Quant TL, protein spots stained with CyDye 3 showed up green while ones dyed with

CyDye 5 were red. Relative quantities of proteins are measured by fluorescence using a scanner laser, and can be observed to a degree by the colors seen in the overlapped images. When the 2 protein samples contained roughly equal amount of a protein, the corresponding spot on the gel is yellow. If a protein was more abundant in one sample, then the color of that spot would be more red or green depending on the dye used in the dominant sample. As expected for most proteomic analyses, the majority of the spots in all 12 gels were yellow, indicating no large differences in abundance.

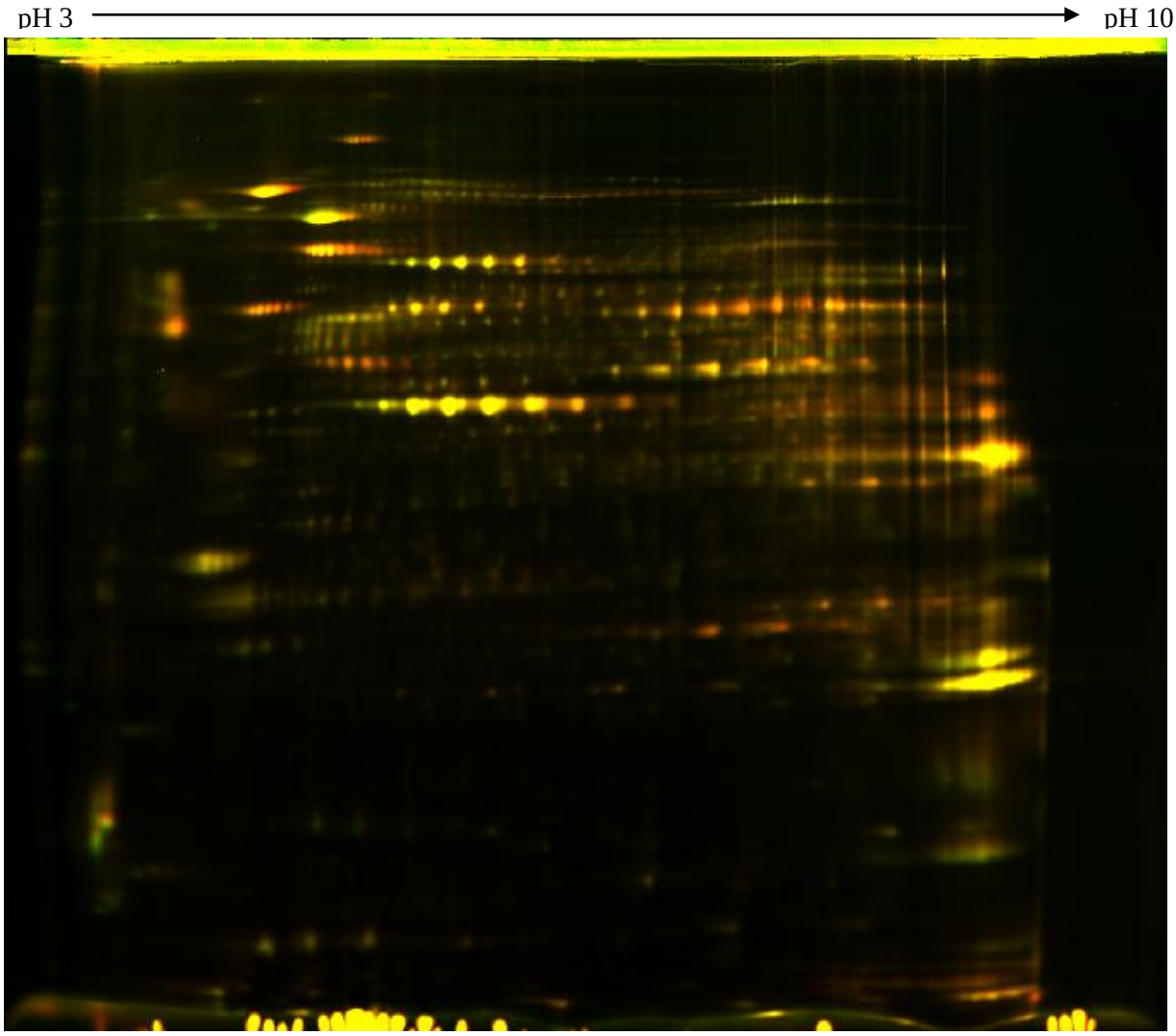

Figure 3-1. A sample DIGE gel image showing day 2.5 and day 4.5 protein extracts from one spinner flask of run A. Isoelectric focusing, which separates proteins by charge horizontally across a gel strip, was conducted over a nonlinear range from pH 3 to pH 10. Subsequent SDS-PAGE, which separates proteins by mass, was performed. Day 2.5 was stained with Cy3 (green) and day 4.5 proteins were stained with Cy5 (red).

Following the initial visual inspection in Image Quant TL, gel images were processed via Differential In Gel Analysis (DIA) in the DeCyder software. Table 3-4 showed the number of protein spots detected in each of the 12 gels. For comparison of spots between gels, spots detected in these 12 DIA were then matched against each other using the DeCyder 2D Software Biological Variation Analysis (BVA). Final numbers of matched spots across gels were also shown in Table 3-4 below. By default, the gel with the most number of spots detected was considered as the master image for BVA matching.

Table 3-4. Number of spots detected and matched in all 12 DIGE gels

Gel number	Protein samples	Number of spots detected	Number of spots matched across 12 gels
1	SP1 D2.5 vs. D4.5	1711	1210
2	SP1 D2.5 vs. D5.5	1814	1281
3	SP1 D2.5 vs. D8.5	1903	1287
4	SP2 D2.5 vs. D4.5	1925	1252
5	SP2 D2.5 vs. D5.5	1890	1278
6	SP2 D2.5 vs. D8.5	1727	1180
7	SP3 D2.5 vs. D4.5	1860	1387
8	SP3 D2.5 vs. D5.5	1866	1417
9	SP3 D2.5 vs. D8.5	1815	1360
10*	SP4 D2.5 vs. D4.5	1924	1924
11	SP4 D2.5 vs. D5.5	1812	1351
12	SP4 D2.5 vs. D8.5	1807	1345

** Gel 10 was the master gel for cross-gel matching*

3.3.2 Generation of Candidate Protein Spot List using T-test and ANOVA

As the biological relevance of small fold changes is difficult to interpret, a common practice in DIGE analysis is to establish both a statistical threshold and a fold change threshold, both which have to be passed in order for a spot to be considered differentially expressed. Since it was expected that some biologically relevant changes might have subtle fold changes, to avoid filtering out proteins that were regulated slightly in response to the changes occurring in cultures as cells aged and became apoptotic, only a fixed FDR threshold was used to determine potential proteins of interest. For each statistical test,

an FDR cutoff of 0.1 or 10% was applied for the initial compilation of a list of differentially expressed proteins from samples collected at different time points. The size of the un-screened list from all three t-tests and ANOVA are listed in Table 3-5. Manual screening of the t-test lists was done to eliminate non-protein spots such as dust, spots with fold change less than 1.1, and spots with very low abundance that were unlikely to be identified successfully by mass spectrometry (Table 3-5). Between day 2.5 and day 4.5, only two proteins changed their expression level significantly. From day 2.5 to day 5.5, significantly different abundance was detected for eight protein spots. Between day 2.5 and day 8.5, 59 proteins had varied expression. As expected, the number of differentially expressed proteins increased as the culture aged and had a greater proportion of apoptotic cells. The total number of unique differentially expressed protein spots, based on t-test scores, was 62 proteins (see Figure 3-2a).

Table 3-5. Number of differentially expressed proteins obtained from t-tests and ANOVA

Statistical test	Number of differentially expressed proteins based on FDR cutoff only	Number of differentially expressed proteins after FDR cutoff and manual screening	Fold change (up/down/mix*)
t-test: day 2.5 vs. 4.5	3	2	2/0/0
t-test: day 2.5 vs. 5.5	15	8	8/0/0
t-test: day 2.5 vs. 8.5	183	59	33/26/0
ANOVA	281	66	41/23/2

** When comparing the changes across all 4 time points in ANOVA test, a few spots did not show uniform direction of expression changes.*

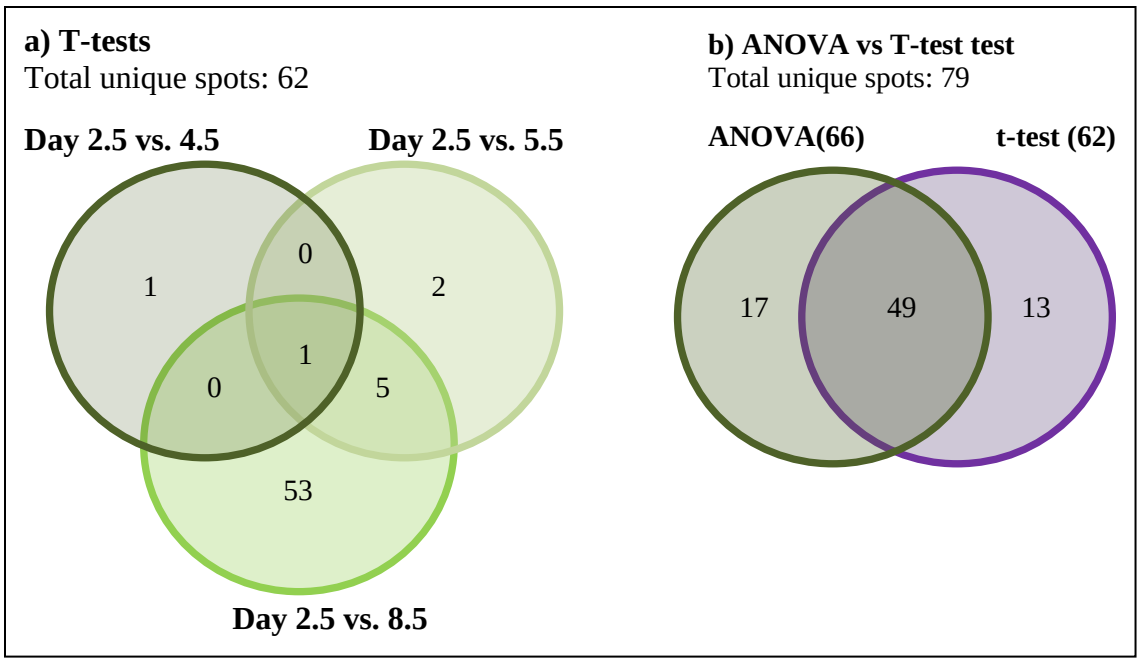

Figure 3-2. The number of differentially expressed proteins from T-test and ANOVA.

On the other hand, manual screening of the ANOVA list focused mostly on the consistency in fold change direction between time points and also whether the spot had very low protein abundance. After screening, the ANOVA test yielded 66 potential candidates from the original 281 spots.

More than 70% of the protein spots were in common between the two lists (see Figure 3-2b), leading to 79 unique spots when combined. The close agreement between the different statistical tests further supported the selected spots as potential candidate for subsequent mass spectrometry analyses. Since not all combinations of paired t-tests possible were calculated, it is expected that ANOVA would identified additional protein spots that were not selected based on the three t-tests performed.

Figure 3-3 shows a single channel DIGE gel image displaying all 79 selected protein spots. Borders of each selected spot were highlighted in purple and labelled by the spot ID number. Borders of remaining protein spots detected were outlined in grey. Table 3-6 displays all 79 protein spots and their corresponding average ratios and FDR values from the statistical tests. A fairly consistent

direction of fold changes from day 2.5 to day 4.5, day 5.5 then day 8.5 was observed for 76 out of 79 protein spots (see Table 3-6). Since the fold changes were calculated from standardized abundances, which were adjusted by the internal standard abundances on each gel, the absolute fold change values should be comparable directly between the three ratios. In general, many spots showed uni-directional changes to abundances through time, which were seen by the systematic increasing or decreasing in the three fold change ratios (see Appendix B, Figure B-1, Figure B-2, Figure B-3 and Figure B-4). From the 79 candidate protein spots selected, 32 (40.5%) were continuously up regulated from day 2.5 until day 8.5, 44 (55.7%) were down regulated within this time period; while the remaining 3 (3.8%) showed mix directions for the expression changes (see Table 3-6).

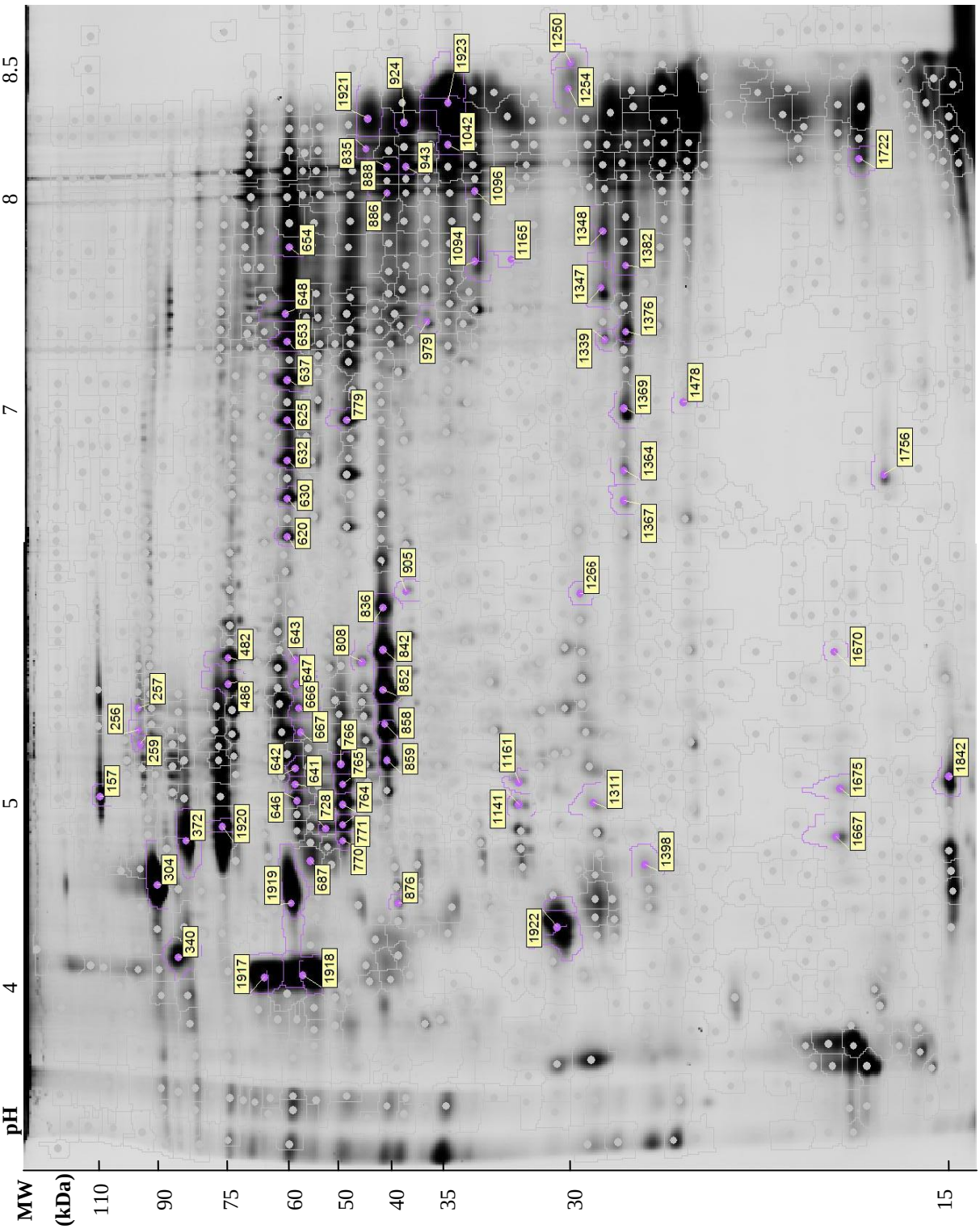

Figure 3-3. Protein spots selected using DeCyder BVA software. Differentially expressed proteins were outlined in purple labelled with spot ID while remaining spots highlighted in grey. Rough estimate of molecular weight and pI were obtained from the protein identifications.

Table 3-6. T-tests and ANOVA statistics of the 79 differentially expressed protein spots

	Day 2.5 vs. 4.5			Day 2.5 vs. 5.5			Day 2.5 vs. 8.5			All 4 time points	
Spot ID	average ratio	t-test p-value	t-test FDR	average ratio	t-test p-value	t-test FDR	average ratio	t-test p-value	t-test FDR	ANOVA p-value	ANOVA FDR
157	1.346	6.72E-03	0.232	1.585	7.88E-03	0.174	1.806	1.78E-02	0.122	1.40E-05	**5.13E-04**
256	-1.174	1.79E-02	0.297	-1.472	1.73E-01	0.475	-1.437	3.06E-04	**0.030**	2.50E-02	9.32E-02
257	-1.196	1.74E-02	0.297	-1.289	5.37E-02	0.310	-1.452	1.86E-04	**0.026**	1.10E-03	1.27E-02
259	-1.150	1.41E-01	0.527	-1.363	3.68E-02	0.261	-1.310	1.31E-03	**0.055**	2.10E-03	2.07E-02
304	1.418	2.70E-03	0.169	1.486	1.67E-02	0.217	2.649	6.57E-05	**0.024**	3.70E-08	**9.48E-06**
340	1.201	2.02E-01	0.584	-1.035	5.88E-01	0.809	1.820	2.25E-02	0.138	1.30E-02	**6.29E-02**
372	-1.131	1.42E-02	0.277	-1.239	2.23E-02	0.229	-1.312	3.93E-03	**0.073**	3.90E-03	**3.05E-02**
482	-1.127	6.16E-02	0.420	-1.153	4.66E-02	0.296	-1.175	5.89E-04	**0.040**	1.20E-02	**6.06E-02**
486	-1.143	2.29E-02	0.316	-1.214	1.95E-02	0.217	-1.205	3.23E-02	0.161	2.90E-03	**2.56E-02**
620	1.407	6.70E-02	0.436	1.368	2.25E-01	0.534	2.210	1.29E-02	0.103	1.90E-02	**7.73E-02**
625	1.400	3.82E-03	0.192	1.539	1.54E-03	0.108	2.252	1.06E-04	**0.024**	1.10E-07	**1.54E-05**
630	1.417	1.85E-02	0.297	1.519	3.39E-02	0.260	2.365	2.51E-03	**0.066**	7.60E-05	**1.73E-03**
632	1.424	1.45E-03	0.165	1.527	2.07E-02	0.220	2.402	8.42E-04	**0.046**	3.30E-06	**1.88E-04**
637	1.411	2.88E-02	0.336	1.538	9.20E-04	**0.099**	2.327	1.24E-04	**0.024**	8.20E-08	**1.40E-05**
641	-1.256	8.25E-02	0.467	-1.245	1.26E-02	0.206	-1.398	3.86E-03	**0.073**	3.90E-04	**6.25E-03**
642	-1.100	2.35E-01	0.617	-1.276	5.25E-03	0.165	-1.318	4.15E-03	**0.073**	5.50E-03	**3.73E-02**
643	-1.089	1.94E-01	0.574	-1.126	1.16E-02	0.206	-1.290	1.11E-03	**0.051**	1.40E-02	**6.52E-02**
646	-1.289	2.91E-02	0.336	-1.177	2.19E-02	0.228	-1.385	2.21E-02	0.136	6.10E-03	**3.96E-02**
647	-1.106	8.98E-02	0.478	-1.151	3.18E-02	0.260	-1.287	7.93E-03	**0.089**	1.40E-04	**2.81E-03**
648	1.333	6.86E-02	0.443	1.415	1.66E-01	0.467	1.915	2.39E-04	**0.027**	1.00E-03	**1.21E-02**
653	1.395	6.27E-02	0.423	1.452	2.77E-03	0.133	2.205	5.10E-05	**0.024**	4.30E-06	**2.10E-04**
654	1.245	5.39E-02	0.403	1.408	3.06E-02	0.260	1.505	2.81E-03	**0.066**	3.60E-03	**2.93E-02**
666	-1.164	2.30E-01	0.615	-1.150	1.89E-01	0.494	-1.213	2.92E-03	**0.066**	8.70E-02	2.13E-01
667	-1.133	3.80E-01	0.728	-1.184	1.37E-02	0.211	-1.219	5.99E-03	**0.083**	2.60E-02	**9.55E-02**
687	-1.085	4.38E-01	0.758	-1.316	4.07E-02	0.279	-1.401	2.27E-02	0.138	2.50E-03	**2.29E-02**
728	-1.012	6.48E-01	0.862	-1.119	7.67E-02	0.360	-1.119	7.67E-02	0.253	1.90E-02	**7.73E-02**
764	1.342	2.32E-03	0.169	1.495	2.54E-04	**0.090**	2.079	1.98E-04	**0.026**	1.90E-08	**6.49E-06**
765	1.372	8.85E-03	0.241	1.538	2.02E-03	0.121	2.164	1.22E-04	**0.024**	3.00E-07	**3.42E-05**
766	1.359	1.15E-02	0.263	1.497	7.09E-03	0.170	2.148	5.75E-04	**0.040**	3.00E-06	**1.88E-04**
770	1.294	7.82E-03	0.233	1.457	1.98E-02	0.217	1.971	1.42E-03	**0.055**	2.60E-05	**8.08E-04**
771	1.341	3.11E-03	0.182	1.512	3.43E-03	0.142	2.096	8.85E-04	**0.046**	9.80E-07	**7.73E-05**
779	1.137	1.38E-01	0.527	1.236	4.39E-02	0.292	1.090	3.89E-01	0.606	1.30E-02	**6.29E-02**
808	-1.091	2.71E-01	0.643	-1.174	2.24E-01	0.533	-1.344	1.43E-03	**0.055**	1.20E-02	**6.06E-02**
835	1.399	6.90E-03	0.232	1.449	7.07E-04	**0.099**	1.402	5.84E-03	**0.083**	2.80E-05	8.20E-04
836	-1.110	3.47E-01	0.712	-1.202	1.47E-01	0.446	-1.410	5.44E-03	**0.083**	2.00E-02	**8.04E-02**
842	-1.118	1.67E-01	0.553	-1.217	3.62E-02	0.260	-1.455	6.22E-04	**0.040**	2.70E-04	**4.77E-03**
852	-1.116	7.28E-02	0.443	-1.224	1.41E-02	0.215	-1.469	8.08E-04	**0.046**	3.20E-06	**1.88E-04**
858	-1.101	1.73E-01	0.558	-1.226	5.68E-02	0.314	-1.470	2.99E-03	**0.066**	1.10E-04	**2.30E-03**

859	-1.084	4.00E-01	0.740	-1.244	1.42E-01	0.441	-1.472	1.42E-02	0.107	4.00E-03	**3.11E-02**
876	-1.110	2.37E-01	0.619	-1.163	5.06E-02	0.302	-1.190	7.22E-03	**0.087**	8.20E-02	2.09E-01
886	1.495	1.89E-03	0.169	1.725	2.03E-03	0.121	1.829	4.12E-03	**0.073**	4.80E-08	**9.84E-06**
888	1.428	5.77E-04	0.124	1.775	2.84E-04	**0.090**	1.706	6.74E-03	**0.086**	1.30E-05	**4.94E-04**
905	1.080	1.02E-01	0.489	1.079	2.43E-01	0.547	1.103	7.19E-03	**0.087**	1.80E-01	3.32E-01
924	1.356	1.86E-02	0.297	1.460	5.56E-03	0.165	1.447	1.12E-02	**0.098**	7.60E-05	**1.73E-03**
943	1.337	1.74E-02	0.297	1.507	2.34E-03	0.130	1.466	4.96E-02	0.199	2.50E-03	**2.29E-02**
979	1.202	6.40E-03	0.232	1.575	4.13E-02	0.280	1.484	2.55E-02	0.146	1.70E-03	**1.82E-02**
1042	1.188	4.14E-02	0.371	1.322	3.04E-02	0.260	1.258	7.39E-02	0.249	3.90E-03	**3.05E-02**
1094	1.216	3.48E-02	0.359	1.309	2.19E-02	0.228	1.141	1.63E-01	0.378	2.10E-03	**2.07E-02**
1096	1.187	1.05E-01	0.489	1.292	2.45E-02	0.234	1.201	1.16E-01	0.313	1.40E-02	**6.52E-02**
1141	1.226	5.64E-03	0.225	1.548	1.04E-02	0.202	1.565	2.99E-03	**0.066**	3.60E-04	**5.95E-03**
1161	1.185	3.27E-02	0.349	1.520	5.23E-02	0.304	1.594	2.84E-03	**0.066**	2.50E-03	2.29E-02
1165	-1.190	5.00E-05	**0.029**	-1.124	3.21E-01	0.619	-1.383	8.44E-03	0.089	4.90E-02	1.47E-01
1250	-1.160	9.21E-03	0.241	-1.204	3.80E-03	0.152	-1.648	1.13E-03	**0.051**	3.50E-07	**3.59E-05**
1254	-1.133	9.46E-02	0.483	-1.133	1.09E-01	0.400	-1.737	3.31E-03	**0.069**	5.20E-05	1.30E-03
1266	-1.013	8.59E-01	0.945	1.213	4.26E-04	**0.098**	1.242	3.92E-02	0.174	7.90E-03	4.68E-02
1311	-1.187	2.68E-03	0.169	-1.164	4.63E-03	0.162	-1.185	1.05E-03	**0.050**	7.50E-03	**4.55E-02**
1339	1.340	1.12E-02	0.263	1.524	1.92E-02	0.217	1.567	1.08E-02	**0.095**	5.00E-04	**7.22E-03**
1347	1.405	5.00E-04	0.124	1.573	9.24E-04	**0.099**	1.573	1.50E-02	0.111	6.30E-06	**2.94E-04**
1348	1.238	4.36E-03	0.201	1.476	1.52E-02	0.216	1.438	7.48E-03	**0.087**	1.50E-04	**2.96E-03**
1364	1.252	7.74E-03	0.233	1.437	1.71E-02	0.217	1.476	5.94E-03	**0.083**	6.50E-05	**1.55E-03**
1367	1.393	1.71E-02	0.297	1.747	5.24E-03	0.165	1.851	5.49E-03	**0.083**	4.20E-06	**2.10E-04**
1369	1.554	3.32E-03	0.188	1.932	1.17E-03	0.103	2.054	2.56E-03	**0.066**	5.20E-07	**4.85E-05**
1376	1.450	2.04E-03	0.169	1.844	6.48E-04	**0.099**	1.950	2.61E-03	**0.066**	2.20E-06	**1.50E-04**
1382	1.358	8.84E-03	0.241	1.863	3.39E-03	0.142	2.085	3.55E-03	**0.070**	7.00E-07	**5.98E-05**
1398	-1.504	6.05E-02	0.418	-1.526	1.72E-01	0.475	-2.040	6.04E-03	**0.083**	N/A	N/A
1478	1.087	2.77E-01	0.649	1.282	1.23E-01	0.417	1.306	1.43E-01	0.352	1.40E-02	**6.52E-02**
1667	-1.252	2.47E-02	0.321	-1.324	1.15E-03	0.103	-1.410	6.45E-04	**0.040**	7.80E-06	**3.48E-04**
1670	-1.361	9.03E-03	0.241	-1.312	5.86E-03	0.165	-1.733	4.13E-03	0.073	6.90E-04	**9.07E-03**
1675	-1.198	1.77E-01	0.566	-1.319	1.52E-03	0.108	-1.469	3.54E-03	**0.070**	2.10E-05	**6.73E-04**
1722	-1.094	5.61E-02	0.412	-1.010	6.93E-01	0.868	-1.160	4.58E-04	**0.040**	4.30E-03	3.20E-02
1756	1.021	6.98E-01	0.890	1.221	3.42E-03	0.142	1.229	1.23E-04	**0.024**	2.00E-03	**2.05E-02**
1842	1.034	3.66E-01	0.724	1.135	2.67E-03	0.133	-1.081	1.03E-02	**0.093**	7.90E-04	**1.00E-02**
1917	1.411	9.36E-02	0.483	1.442	5.48E-02	0.311	3.168	1.92E-03	**0.057**	2.40E-04	**4.39E-03**
1918	1.433	2.09E-02	0.314	1.640	1.38E-02	0.211	3.108	8.47E-04	**0.046**	1.20E-07	**1.54E-05**
1919	1.446	4.30E-06	**0.008**	1.568	1.43E-04	**0.090**	1.930	1.73E-04	**0.026**	2.30E-10	**2.36E-07**
1920	1.428	1.14E-03	0.165	1.566	1.21E-03	0.103	2.549	2.75E-04	**0.029**	1.30E-08	**6.49E-06**
1921	1.445	8.94E-03	0.241	1.592	3.26E-03	0.142	1.491	8.71E-03	**0.089**	1.10E-05	**4.70E-04**
1922	-1.071	7.96E-02	0.461	-1.073	9.82E-02	0.385	-1.146	3.23E-03	**0.068**	2.00E-04	**3.80E-03**
1923	1.191	6.01E-02	0.417	1.361	1.34E-02	0.211	1.269	3.32E-02	0.163	1.00E-03	**1.21E-02**

*Note: yellow highlighted FDR values fall below the 0.1 cutoff while the **boldface** values indicated spots were selected based on that particular statistical test after manual screening.*

3.3.3 Identified Proteins of Interest

Multiple preparative gels containing a mixture of all 16 protein samples were run for spot picking and protein identification. Figure 3-4 shows a typical preparative gel obtained. Manual matching between spots from the DIGE gels to spots on the preparative gels were performed based on relative disposition of landmarking protein spots. Due to the difference in Coomassie and CyDye staining sensitivities, not all 79 spots selected from the BVA analysis could be picked from the preparative gel for subsequent mass spectrometry identification. As a consequence, several preparative gels loaded with 500-1000μg of total proteins were prepared to improve the total number of spots available to be picked.

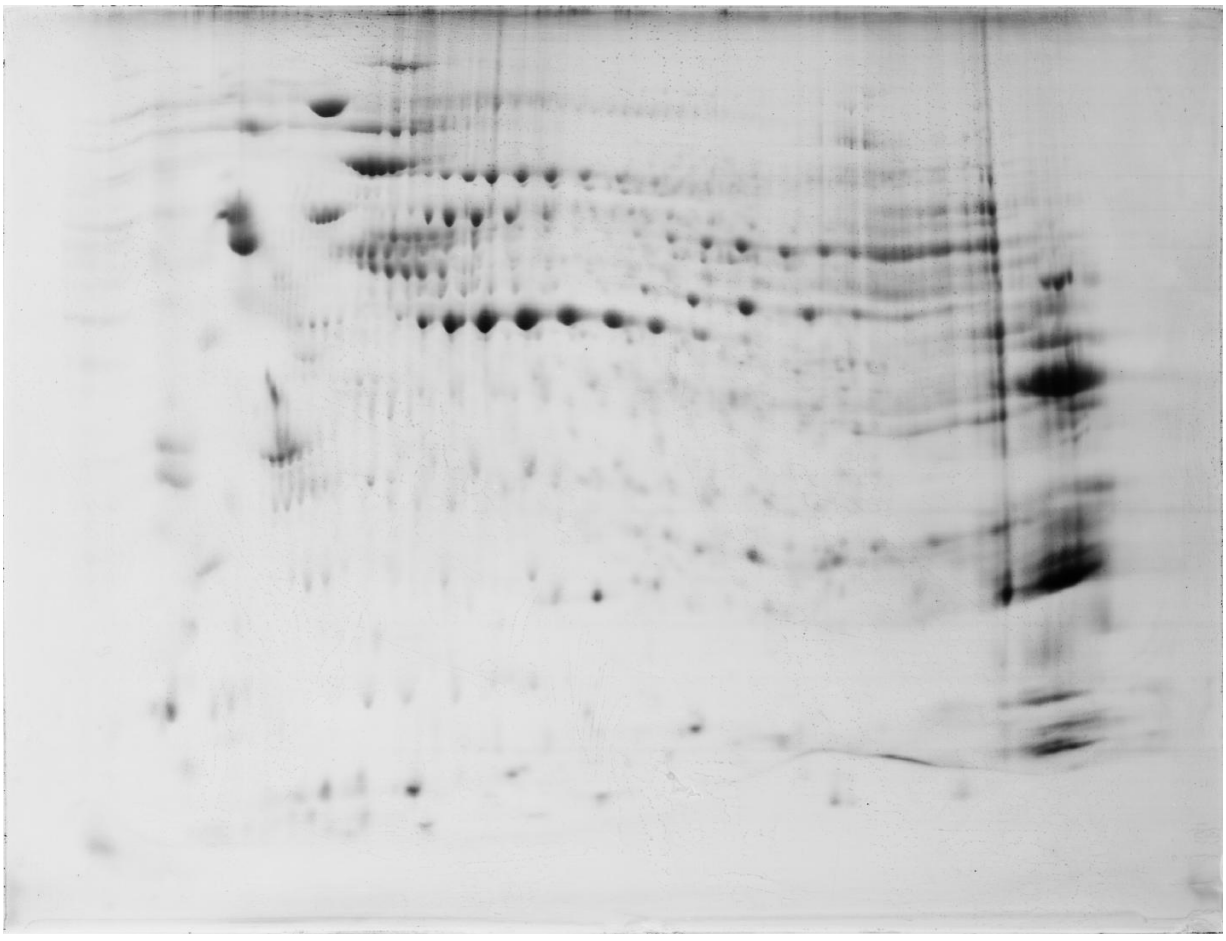

Figure 3-4. A sample preparative gel loaded with 1mg of protein mixture containing all 16 samples, and stained with Coomassie Blue.

Using ESI MS/MS and LC-MS/MS, identification from a total of 40 spots were obtained (Table 3-7 and Figure 3-5). Out of these, only 28 identifications were unique and three spots were each matched to two distinct identifications. From the original 79 protein spots, 32 spots were not subjected to MS analyses due to low abundance or slight differences in migration pattern. Nevertheless, the differentially expressed proteins identified could be classified into four broad categories: cytoskeletal, chaperone-related, glycolytic, and others. All cytoskeletal proteins identified, vimentin/α-tubulin, β-tubulin and actin, were down regulated. A significant proportion of protein spots were of chaperones (18 out of 40) and glycolytic (10 out of 40) proteins. The molecular chaperones include calreticulin, ERp60, PDI, PDIA6, BiP, GRP94, GRP170, HSC70, HSP90β and FKBP52. Except HSC70, HSP90β and FKBP52, all the chaperone proteins were up-regulated. The glycolytic proteins: triosephosphate isomerase, phosphoglycerate mutase, pyruvate kinase isozyme M1/M2, phosphoglycerate kinase 1, glyceraldehyde-3-phosphate dehydrogenase, enolase-1 and lactate dehydrogenase chain A/C all increased their abundance over time during the cultivation period. Lastly, various other proteins were identified to be 14-3-3 protein epsilon isoform transcript variant 1, galectin-1, peroxiredoxin-6, laminin receptor, 80K-H, galectin-3 and ATP synthase beta.

Although the presence of apoptosis within the CHO culture was clearly indicated by flow cytometry results, not all changes brought by apoptosis were reflected explicitly by proteomic analysis. This can most likely be attributed to the fact that apoptosis was controlled both at transcriptional and post-translational levels [106] in addition to the degree of changes necessary to inflict apoptotic cell death. Many of the apoptotic proteins involved were expected to maintain their expression level and function via mechanisms such as localization, association with other proteins and post-translational modification. Since apoptosis requires a quick response and usually takes no longer than a few hours, post-translational modification seems more sensible and logical in many cases. With this said, one should expect to observe any protein modification brought by the execution of apoptosis such as the cleavage of pro-caspases into their active forms, which have different MW and pI values than their

precursors. However, not all desired results, including the cleavage of caspases, were obtained from the DIGE and MS experiment.

On a side note, the absence of the anti-RhD MAb produced by the CHO IgG-9β8 cells was not among the list of differentially expressed proteins detected by DIGE. Since this MAb was being secreted outside of cells, it is expected that only a small amount (that had yet to be secreted) would be present in the protein sample after the extraction procedure, which removes culture medium.

Table 3-7. Protein identification from mass spectrometry analysis (See Appendix B, Table B-1 for full MS results)

A) Cytoskeletal Proteins

Protein Name	Fold change (Day 2.5 vs. 8.5)	DIGE spot ID	PEAKS			MASCOT		
			Score (%)	UniProt Accession	No. of peptides matched	score	UniProt Accession	No. of peptides matched
Vimentin [3]	-1.39	646†	93.8	BAD74030	5	60	P02544	3
α-tubulin			n/a†			74	Q3TIZ0	2
β-tubulin [1,2,3]	-1.12	728†	n/a†			188	P99024	5
Actin (β/γ) [1,2,3]	-1.41	836	98.3	P83751	6	194	Q3UGS0	5
	-1.46	842	95.9	P20359	6	177	O35247	5
	-1.47	852	99.7	O76784	9	203	O35247	7
	-1.47	858	99.9	P60712	9	334	O35247	8
	-1.47	859	99.8	O76784	10	336	Q3UGS0	10

B) ER and Cytosolic Chaperone Proteins

Protein Name	Fold change (Day 2.5 vs. 8.5)	DIGE spot ID	PEAKS			MASCOT		
			Score (%)	UniProt Accession	No. of peptides matched	score	UniProt Accession	No. of peptides matched
Calreticulin[2,3]	3.17	1917	93.1	Q8K3H7	8	131	Q8K3H7	5
	3.11	1918	90.9	Q8K3H7	5	84	Q8K3H7	3
ERp60 [1,2]	2.25	625	95	Q91Z81	8	110	Q91Z81	5
	2.37	630	85	P11598	5	72	P27773	3
	2.40	632	92.4	Q91Z81	5	85	Q91Z81	4
	2.33	637	83	P11598	4	65	P27773	3
	2.21	653	66.7	Q91Z81	3	n/a		
PDI [1,2,3]	1.93	1919	94.2	P05307	4	126	P05307	4
PDIA6	2.08	764	97.3	P38660	6	222	P38660	5
	2.15	766	89.1	P38660	4	96	P38660	3
	1.97	770	88.3	P38660	5	131	P38660	4
	2.10	771	95.8	P38660	6	88	P38660	2
BiP [1,2,3]	2.55	1920	99.8	P07823	11	205	P06761	5
GRP94 [2,3]	2.65	304	99.6	Q3UBU0	7	210	Q3UBU0	4
GRP170 [2]	1.81	157	92.8	Q9JKR6	11	262	Q9JKR6	8
HSC70 [2,3]	-1.18	482	73.3	Q53HF2[††]	10	234	P19120[††]	5
HSP90β [3]	-1.31	372	n/a			53	P34058	6
FKBP52	-1.29	643	n/a			168	P27124	3

C) Glycolytic Proteins and other metabolic enzymes

Protein Name	Fold change (Day 2.5 vs. 8.5)	DIGE spot ID	PEAKS			MASCOT		
			Score (%)	UniProt Accession	No. of peptides matched	score	UniProt Accession	No. of peptides matched
Triosephosphate isomerase[1]	2.05	1369	98.6	Q53HE2	16	153	P00939	2
	1.95	1376[†††]	84.4	P00939	6	121	P00939	3
Phosphoglycerate mutase1	1.57	1339	86.9	P18669	8	167	P18669	8
Pyruvate kinase isozyme M1/M2 [1]	1.51	654	96.2	**P11980**	6	147	**P52480**	5
Phosphoglycerate kinase [1]	1.71	888	89.4	**P50310**	5	141	P50310	4
Glyceraldehyde-3-phosphate dehydrogenase[1]	1.26	1042	65.5	P00355	5	225	**P17244**	5
	1.27	1923	98.3	P00355	7	218	**P17244**	5
Enolase-1 [1,2,3]	1.09	779	90.9	P04764	4	213	Q9PVK2	4
L-lactate dehydrogenase chain A/C [1]	1.14	1094	77.1	**P07864**	2	149	P00340	2
	1.20	1096	35.7	Q5R1W9	4	n/a		

D) Other Proteins

Protein Name	Fold change (Day 2.5 vs. 8.5)	DIGE spot ID	PEAKS			MASCOT		
			Score (%)	UniProt Accession	No. of peptides matched	score	UniProt Accession	No. of peptides matched
14-3-3 epsilon	-1.15	1922	72.2	Q1HPT4	3	213	Q4VJB6	3
Galectin-1 [2,3]	-1.08*	1842	42.1	P48538	2	n/a		
Peroxiredoxin-6 [1]	1.95	1376††††	49.2	O35244	3	63	O08709	3
Laminin receptor 1 [1]	-1.19	876	78.5	P08865	3	165	P26452	3
80K-H	1.82*	340	49.5	Q3U518	2	101	P14314	2
Galectin-3 [1]	-1.65	1250	33	P08699	1(+3)	n/a		
ATP synthase beta [1,3]	-1.12	728†	52.8	P46561	2	77	P00829	2

†*Mascot reported two different proteins from a single MS analysis. The two sets of matched peptides had no overlap. PEAKS matches to only one identification.*
††*The top hit matches to a Hsc70 fragment thus the mass is much less than 70kDa. This record was still an unreviewed UniProtKB entry.*
†††*TPI and Prx6 were identified when analyzing spot 1376 on two gels.*
* *Abundance across 4 time points did not increase or decrease in the same direction throughout. See Table 3-6 for all 3 fold changes. Appendix B Figure B-1 also displayed the changes in abundance for all replicate cultures.*

Note: The accession numbers reported are the most current version in UniProt. Some PEAKS and MASCOT matching resulted in protein records that are obsolete due to various reasons such as deletion and record/database merging.

Protein identification, spot pattern and location were cross referenced with the following CHO 2D reference maps:
1. CHO-K1 cells in Ham's F12 medium, 10% FBS [107]
2. Derivatives of CHO DUKX cells in serum-free DMEM/F-12 based medium with protein hydrolysate and a nutrient mixture [108]
3. human growth hormone expressing CB515 cells in 1:1 DMEM: Coons F12 media, 10% FCS [109]

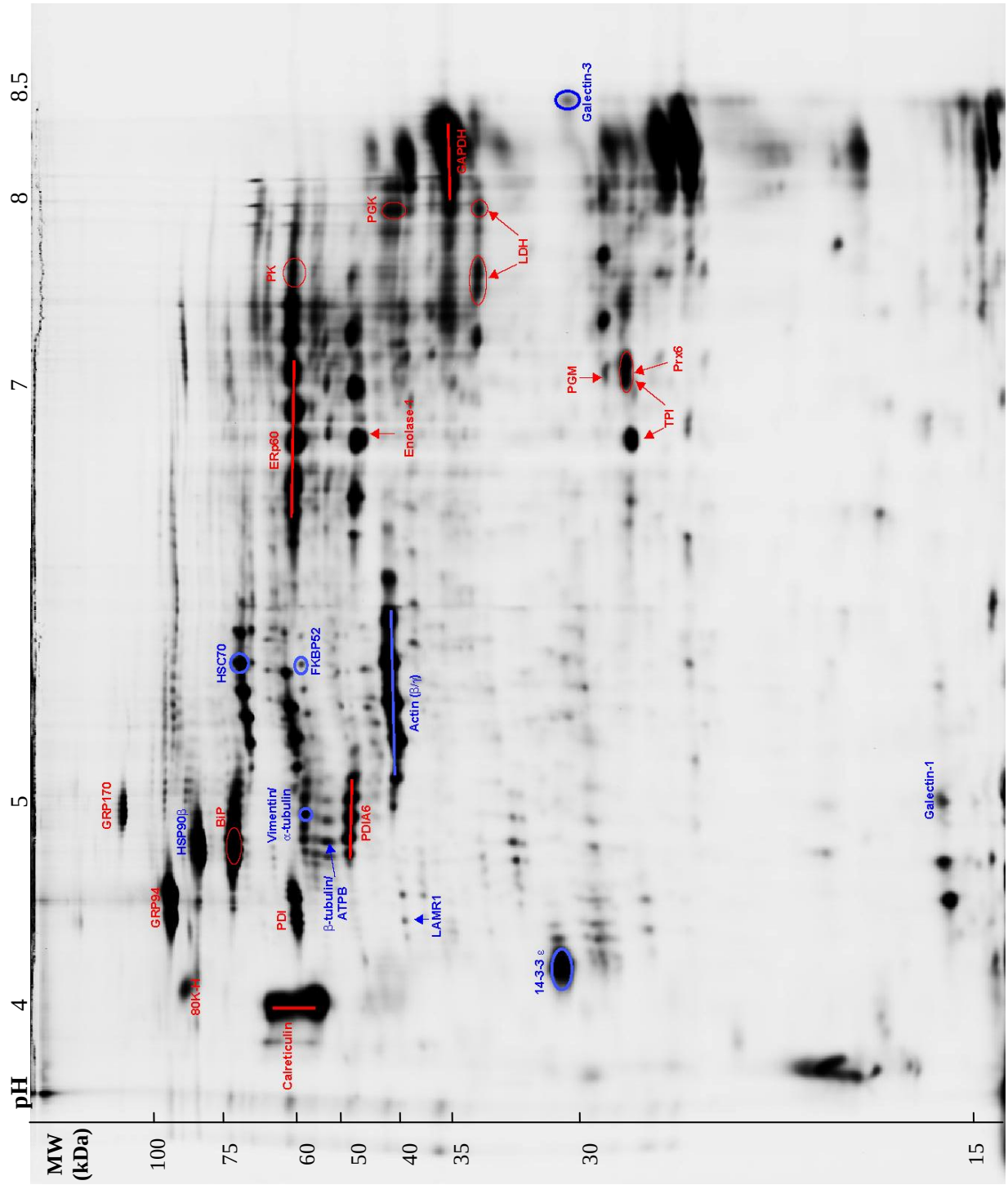

Figure 3-5. MS identified differentially expressed protein spots from the comparison of healthy (day 2.5) to aging/apoptotic (day 4.5, 5.5 and 8.5) CHO protein samples. Red protein ID indicates upregulation occurred over time while blue indicates a reduction in expression. Estimates of molecular weight and pI were obtained from the protein identifications. *Abbreviations: ATPB, ATP synthase beta subunit; BiP, Binding immunoglobulin protein; ERp60, Endoplasmic reticulum protein 60kDa; FKBP52, FK506-binding protein 52; GAPDH, glyceraldehydes-3-phosphate dehydrogenase; GRP, glucose-regulated protein; HSC70, Heat shock cognate protein 70kDa; HSP, heat shock protein; LAMR1, laminin receptor 1; LDH, L-lactate dehydrogenase chain; PDI, protein disulfide isomerase; PGM, phosphoglycerate mutase; PGK, phosphoglycerate kinase 1; PK, pyruvate kinase isozyme M1/M2; Prx6, peroxiredoxin-6; TPI, triosephosphate isomerase.*

Results from run A proteomic analysis shown a wide variety of proteins whose abundances changed after the onset of apoptosis. However, as mentioned, the majority of the differential expressed proteins were not restricted to only apoptotic mechanisms nor did they provide pathway specific information. As a result, run B was subjected to more extensive FCM assays, which measured initiator caspases 8 and 9 on top of the caspase 3/7 test (see Section 2). It appears that the under non-induced and un-manipulated culturing conditions, prolonging cultivation period mainly triggers CHO cell death via the activation of caspase 9.

3.4 Discussion

Of the 79 protein spots determined to have altered expression from the DIGE experiments, 40 protein spots were isolated and identified, providing 28 unique protein identifications. Since several proteins including PDIA6 and actin have many isoforms within the cells, the actual number of unique proteins present was less than the number of protein spots. The existence of these isoforms could easily be noticed from 2D gels as a series of horizontal "trains" of spots, which have similar mass but varying pI. In addition to the presence of isoforms, many of the spots had intensities below the workable or detectable limit either during excision from the preparative gel or mass spectrometry analyses. The differentially expressed proteins sequenced successfully were categorized into four main groups based on their most known cellular functionalities: cytoskeletal, chaperone-related, glycolytic and others. The changes in their abundance caused by the degradation of culture conditions and/or the onset of apoptotic cell death during prolonged cultivation are discussed in the following subsections.

3.4.1 Cytoskeletal Proteins

In healthy mammalian cells, the shape and organization is maintained by the cytoskeleton, consisting of filamentous actin, microtubules, which are polymers of α- and β-tubulin, and intermediate

filaments, which include vimentin, cytokeratins and lamins [110-112]. Numerous cytoskeletal proteins are known substrates of activated caspase 3 during apoptosis. Depolymerization of polymers and degradation of these proteins causes many morphological changes occurred during the execution phase of apoptosis.

When actin is cleaved, two fragments are produced: actin N-terminal 32kDa (Fractin) and 15kDa (tActin) [110], leading to the disruption of actin, which was observed during apoptosis in various cell lines [113-115]. The disintegration of actin polymers is crucial for the reorganization of the actin network during apoptosis to warrant the orderly dismantling of dying cells [116]. Furthermore, the tActin fragment from caspase cleavage can undergo N-myristoylation and translocate to mitochondria [117]. It has been shown that tActin functions downstream of caspase activation and can trigger cell shrinkage observed during apoptotic cell death [115].

Intermediate filaments are responsible for maintaining cell integrity during normal conditions [112]. When cells undergo apoptotic death, the cleavage of vimentin disrupts intermediate filaments into aggregates, which closely resemble ones seen in apoptotic cells, and generates a pro-apoptotic N-terminal fragment able to amplify the cell death signal in a caspase dependent manner [118]. Furthermore, truncated vimentin can also interfere with the assembly of normal vimentin into intermediate filaments [119]. Vimentin is said to be proteolyzed by caspase during the induction of apoptosis when the majority of cells are still viable, hence its cleavage precedes the cytoskeleton reorganization typically seen in apoptotic cell death [118].

Both subunits of tubulin heterodimers, α-tubulin and β-tubulin, have been reported as substrates of caspase-mediated proteolysis. Examination of the cleavage site in α-tubulin indicated a small fragment from its carboxyl end is removed by caspases [120]. In a separate study, the C-terminus of tubulins was shown to be a regulatory region for microtubule polymerization/aggregation [121,122].

Cleaved α-tubulin enhances microtubule polymerization rates in vitro and increases its capacity to polymerize and possibly affect the tubulin dynamics [112,121]. The dismantlement of microtubules during the early apoptotic phase then reassembly in later apoptotic stage have been observed in cells. Based on evidence from HeLa cells, it was hypothesized that microtubules are responsible for the anchorage or transportation of chromatin to apoptotic blebs at the later phase of apoptosis execution [112].

In accordance with the above reviews and studies, the spots identified as tubulin, actin and vimentin in the present study were significantly down regulated in CHO apoptotic cells. Actin was identified from at least five protein spots that differ only in their isoelectric points. Both β- and γ isoforms were matched to similar sets of MS peaks and yielded the same score from the MASCOT protein database searches. However, vimentin and α-tubulin were identified from a single spot due to the small number of peptides sequenced. Since their corresponding molecular weights and pI (53 kDa/pH5.06 and 50 kDa/pH4.96 respectively) are similar, it is not surprising that they resolved into the same spot. PEAKS analysis resulted in a 93.77% score for vimentin while MASCOT scores for both results were not very high. The confident PEAKS hit favours the identification of spot as vimentin but MASCOT results were nevertheless statistically significant. Hence, the decrease in spot intensity could correspond to either a decrease in only one of the two proteins, or a combination of changes in the expression of both proteins. Although exhibiting a smaller fold change than α-tubulin, β-tubulin was also down-regulated in this study. However, the spot identified as β-tubulin also was identified as ATP synthase beta from the same MS analysis. β-tubulin yielded higher score in MASCOT when comparing to that of ATP synthase beta, but it was not identified according to PEAKS. Similar to the case with vimentin and α-tubulin, overlapping likely occurred due to comparable MW and pI. More detail and discussion are included in section 3.4.4 and 3.4.5.

3.4.2 Molecular Chaperone and Folding Enzymes

Many cellular or ER stresses including oxidative stress, amino acid depletion, protein over-expression and inhibition of glycosylation reactions, can lead to the accumulation of misfolded proteins within ER lumen and the activation of the unfolded protein response (UPR) [67]. As an initial response for dealing with these stresses, the UPR enhances cell survival by triggering three separate signalling pathways, namely ATF6, IRE1/XBP1 and PERK/ATF4 systems. These pathways together attenuate global protein translation, increase translation of UPR target genes such as chaperones and folding proteins, and cause the degradation of misfolded proteins [67,123]. Hence, it is not surprising to identify a significant number of ER chaperone proteins from comparative proteomic analyses of stress conditions.

From the DIGE experiment of the present study, a total of ten unique protein identifications obtained from the mass spectrometry analyses belong to the chaperone-related category. HSC70, HSP90 and FKBP52 are the only down-regulated proteins identified in addition to being the only cytosolic chaperones. Meanwhile, the remaining seven chaperone proteins, calreticulin, ERp60, BiP, GRP94, GRP170, PDI and PDIA6 function mostly in the ER and exhibited large fold change as cells aged and died during prolonged cultivation. They are among the most differentially expressed proteins with an upregulation of 1.81 to 3.17 fold change (see Table 3-6 and 4-15) when comparing abundance between day 2.5 and 8.5. As described in more detail below (Section 3.4.2.1-3.4.2.3), these seven proteins participate in the two known chaperone systems in the ER, namely the calnexin/calreticulin chaperone system and the BiP/GRP94 chaperone system [123]. It is worth noting that although ER chaperones can be roughly divided into two systems, association between components from different chaperone cycles have been reported frequently largely due to their multifunctional roles.

All seven ER-localized chaperones and folding proteins identified in the present study are known UPR inducible proteins. Their induction by cellular stresses have been demonstrated in previous studies using microarray, Western blots and 2D gel electrophoresis [124-130] among a list of UPR affected proteins. The presence of cis-acting elements, namely unfolded protein response element (UPRE) and the ER stress response element (ERSE) [67], in the promoter region of a gene suggests it being a target of UPR. Along with the induction of many ER chaperones, the downregulation of FKBP52, which was observed in the present study, had been identified in cells treated with Tunicamycin, which inhibits N-glycosylation of proteins, and cells over-expressed with ATF6 [124]. Although not all known UPR target proteins have been identified in every past study, the detection of a few members can still mark the activation of ER stress response. For instance, the induction of BiP has been viewed as a classic marker for UPR induction [130]. Hence, the presence of seven ER stress proteins in the present study strongly suggests ER stress activation in the prolonged cultivation of CHO cells.

That being said, the roles of ER chaperones and folding enzymes in apoptotic cell death of CHO cultures should not be overlooked. Although it is likely that some changes in the protein expression are better explained as a consequence of UPR, others could also correspond to the progression of apoptosis. In addition, while UPR is the initial response to ER stresses, the apoptotic pathway will be triggered eventually if a problem persists. As a result, many of the observed fold change in protein levels might in fact be the net result of induction and/or repression by both survival and death pathways. In the subsequent sections, the versatile functions of each identified chaperone and folding protein are discussed in the context of normal cell growths and apoptotic cell deaths.

3.4.2.1 Proteins Identified from the Calnexin/Calreticulin Chaperone System in ER

Calreticulin

Calreticulin is a multipurpose 46-60kDa [131,132] ER soluble/luminal protein that participates in lectin-like chaperoning, Ca^{2+} storage and signalling, regulation of gene expression, cell adhesion, and autoimmunity [133,134]. By forming a complex with calnexin and other ER chaperone proteins, calreticulin interacts with glycoproteins and promotes their proper folding in conjunction with ERp60 [133,135]. In contrast to the BiP chaperone system which hydrophobically interacts with polypeptides, lectin chaperone binds to glycans or bulky hydrophilic extensions of proteins [136]. Utilizing its high capacity calcium binding site [133], calreticulin also functions to keep intracellular calcium ions out of the cytosol, as high concentrations in the cytosol can be toxic to the cells [53].

Upregulation of calreticulin has been observed upon the induction of cellular stresses such as the depletion of ER Ca^{2+} store [134], hyperosmotic stress, heat shock, UV exposure and amino acid or glucose deprivation [68]. Since transcription activation of UPR target genes is controlled by two cis-acting elements, UPRE and ERSE [67], the presence of ERSE in the promoter region of calreticulin suggests that its transactivation following ER stress should be the result of UPR activation [137]. As a result, the increased expression of calreticulin observed in CHO cultures of the present study could be due to UPR triggered by the deterioration of culture conditions as nutrients became limiting and waste products accumulated.

In contrast to the UPR survival pathway, calreticulin has also been associated with the progression of apoptosis. When over-expressed, calreticulin increased cell sensitivity to apoptosis by increasing the amount of calcium stored in the ER [133], along with an increase in the mitochondrial cytochrome *c* released [138]. On the other hand, calreticulin deficient cells were more resistant to apoptotic signals due to the decreased ER Ca^{2+} stores [138]. Additionally, when localized to cell

surface, calreticulin has been suggested to function in the clearance of apoptotic cells. Together with the well known apoptotic cell surface recognition factor phosphatidylserine, calreticulin signals and drives the engulfment of apoptotic cells[132,133]. Upregulation and redistribution of calreticulin on the cell surface during apoptosis was observed prior to postapoptotic membrane permeability [132]. It appears sensible to suggest that calreticulin was up-regulated initially to cope with UPR. Since the culture condition continued to worsen, the accumulated levels of calreticulin sensitized cells to apoptosis and may signal for the phagocytosis of apoptotic cells.

When separated on 2D gels, two differentially expressed spots of similar pI but varying molecular weights were identified to be calreticulin. Their changes in abundance were the largest two observed among the 79 spots selected from the DIGE analysis (Table 3-6). The estimated molecular weights from the distance migrated by the two clearly separated spots deviated roughly by 10kDa. It is unclear why there were two isoforms and how they differ in function. However because both isoforms exhibited a similar fold change, around 3 between day 2.5 and 8.5, they might not possess different function or be regulated separately in aging CHO cultures.

ER protein 60 (ERp60)

Another important protein of the calreticulin chaperone systems identified is the ERp60, which is also known as ERp57, ERp61, PDIA3 and glucose-regulated protein (GRP) 58kDa [139]. As a member of the protein disulfide isomerase (PDI) and glucose-regulated protein family, it is responsible for the correct folding of misfolded **glycoproteins** in the ER lumen through the creation and rearrangement of disulfide bonds [139,140]. As mentioned previously, its chaperone function requires the complex formation with ER-retained calreticulin and calnexin which bind glycoproteins as they emerged from the ER membranes [133,140].

Besides localization to the endoplasmic reticulum, ERp60 can also be found in various other locations including the nucleus, the cytosol and the mitochondria. Recent studies have shown that the ERp60 associated mitochondrial μ-calpain, which is an ubiquitous calcium-dependent neutral cysteine protease, is able to cleave the inner-mitochondrial-membrane (IMM)-bound apoptosis inducing factor (AIF) (~62 kDa) and release the functional cleaved form, tAIF (~57 kDa) into the intermembrane space (IMS). It was suggested that mitochondrial ERp60 proteins, which reside mostly at the outer membrane, refold the μ-calpain large subunit into functional conformations via disulfide bond formation. Most importantly, this ERp60-calpain complex may act as the initiator for the mitochondrial apoptotic signalling [139,141]. However, how ERp60 came to be localized in the mitochondria, as well as whether induction of ERp60 expression is necessary for its participation in the mitochondria are unknown. In support of the results from Ozaki and colleagues [139,141], over-expression of ERp60 have been found to attenuate the induction of pro-survival BiP, increase caspase 3 activation and exacerbate hyperoxia and tunicamycin-induced apoptosis in human endothelial cells [140]. In this study [140], a negative correlation between the abundance of ERp60 and BiP proteins was observed, suggesting that ERp60 likely regulates apoptosis through BiP [140]. Also, it was demonstrated that the knockdown of ERp60 suppresses the cell surface exposure of calreticulin, which abolishes phagocytosis labelling. Interestingly, the interaction between calreticulin and ERp60 has been shown necessary for the cotranslocation to the cell membrane [131,140], further suggesting a reason for the simultaneous regulation of these two proteins as observed in the present study. In any case, the simultaneous increase of ERp60 and calreticulin synthesis during apoptotic cell death has been reported in lipopolysaccharide-induced apoptosis in PC12 cells [142].

When comparing CHO proteomes at various time points during culturing, at least five ERp60 isoforms were detected on the 2D gels with comparable positive fold change between 2.21 to 2.4. Although the presence of phosphorylated ERp60 has been reported, the functions of the different

isoforms remain unclear [140]. Nevertheless, as previously reported, the increase in ERp60 abundance correlates with the increase in the apoptotic population within the culture.

3.4.2.2 Proteins Identified from the BiP/GRP94 Chaperone System in ER

The BiP/GRP94 chaperone system functions by the formation of a protein complex consisting of BiP, GRP94, PDI, ERp72, GRP170, UGGT, PDIA6, cyclophilin B and SDF2-L 1. Typical substrates of this system contain hydrophobic residues in the unfolded regions. BiP can bind to certain calnexin/calreticulin substrates if N-glycosylation is blocked [123]. BiP, GRP94, GRP170, PDI and PDIA6 were among the differentially expressed proteins identified by DIGE analyses. All five components were up-regulated by a fold change of roughly 2 as cultures became more apoptotic on day 8.5.

GRP proteins are known to be inducible by undesirable conditions including glucose starvation, low pH, anoxia, calcium ionophores and stresses that disrupt ER function [123]. As a result, it is not unexpected to observe upregulation of a variety of proteins in the BiP/GRP94 chaperone system as CHO culture conditions deteriorated over time. HPLC assays of the various free amino acids (personal communication with Saeideh Naderi) in the culture medium over time showed an increase in lactate and ammonia concentration as the culture aged. Elevated lactate and ammonia levels in cultures are known for their inhibitory effects on cell growth [143].

BiP

Immunoglobulin heavy chain-binding protein (BiP), also known as GRP78 and HspA5, is the most abundant member of the **heat shock protein (HSP) 70** family [144,145]. It is a multifunctional protein that binds and maintains ER calcium homeostasis, acts as a chaperone for preventing protein misfolding and aggregation within the ER, and suppresses activation of UPR [140,145]. The substrate

binding domains (SBD) of BiP interacts with hydrophobic oligopeptides of unfolded proteins. Upon releasing from BiP, the folding and assembly of the substrate occurs [145]. In addition, BiP has been reported to participate in translocation of, at least some, proteins across the membrane into the ER, opening the Sec61 channel, binding to incoming polypeptides and closing the channel to prevent uncontrolled efflux of calcium ions from the ER. Once translocated, the precursor protein then become the substrate of BiP [145,146].

Under normal conditions, BiP binds and suppress ER stress sensor proteins, PERK, IRE1α and ATF6, which can activate ER stress signalling pathways including UPR [67]. When sequestered by misfolded polypeptides, BiP dissociates from these sensor proteins allowing them to activate signal transduction for UPR [140,145]. BiP is one of the UPR target proteins induced upon the activation of IRE1 as the initial pro-survival combat against the ER stress [67,147]. Its over-expression has been shown to protect cells against ER stress-induced apoptosis while the reverse leads to UPR activation and apoptotic cell death [140]. However, induction of BiP expression has been noted in two separate apoptosis studies [148,149]. The observed 2.55 fold induction of BiP protein levels in apoptotic (day 8.5) CHO culture is likely due to the transcriptional activation during UPR as part of the pro-survival mechanism.

GRP94

GRP94, which belongs to the HSP90 family, is an ER luminal resident chaperone. Its many designations include endoplasmin, glycoprotein gp96, calcium binding protein CaBP4, tumor rejection antigen TRA-1 and ERp99 [150,151]. Although GRP94 seems to not be crucial for cell viability, its function is not redundant for the maturation of cell surface ligands and receptors [152], including immunoglobulin heavy chains, integrins, and toll-like receptors [136]. Other than surface proteins, some proteins localized in the secretary pathways are also identified as GRP94 substrates [150].

GRP94 is the most abundant glycoprotein in the ER [136]. Its upregulation occurred in response to various stress conditions including glucose starvation, ER calcium store depletion and over-expression of misfolded proteins [150]. Along with other glucose regulated proteins such as BiP, GRP94 is thought to protect cells against cell death [153]. The combined upregulation of BiP and GRP94 likely was part of the initial effort to cope with the ER stresses in prolonged cultures. Interestingly, GRP94 is constitutively expressed in most cell types and transcriptionally co-regulated with BiP [123]. In agreement with this and the result of another 2D gel study [148], protein abundances of BiP and GRP94 both increased when comparing CHO protein samples from day 2.5 to day 8.5.

GRP170

Glucose regulated protein 170 (GRP170), also known as hypoxia up-regulated 1, is one of the nucleotide exchange factors in the ER lumen that can replace the ADP bound to BiP with ATP [136,145] thus regulate their conformational changes, which facilitate the binding and releasing of substrate proteins. Moreover, it has been shown that GRP170 is a major calcium-binding protein in the ER [154]. The participation of GRP170 in protein refolding, preventing protein aggregation and facilitating translocation across ER membranes has been observed [155]. Although its exact role and mechanism have yet to be resolved, it was suggested that along with co-chaperones, GRP170 can facilitate protein folding without other major chaperones like BiP [155].

GRP170 was up-regulated by 1.8 fold after CHO cultures aged by 8.5 days. Again, this induction may be the result of UPR as cells attempted to cope with the deterioration conditions of an aging culture.

PDI and PDIA6

Members of the protein disulfide isomerase (PDI) family contain CXXC motifs in their thioredoxin domains. Oxidoreductases members catalyze the formation of disulfide bonds via thio-

disulfide exchanges, while members with isomerase activity rearrange non-native linkages into native disulfides [136]. The enzymes PDI, PDIA6 and ERp60 are all members of the PDI family [156].

The multifunctional PDI protein not only functions as oxidoreductase and isomerase, it can also act as a chaperone [136]. It inhibits the aggregation of misfolded proteins, including ones without disulfide bonds [157]. Protein disulfide isomerase family A, member 6 (PDIA6) is also referred as PDI P5, ERP5, calcium-binding protein 1 (CaBP1) and thioredoxin domain-containing protein 7 (TXNDC7). Most PDI family members have C-terminal ER-retention signals. For example, PDI and PDIA6 both have the KDEL sequences. Yet PDI family members have been reported to be involved in many cellular processes taking places in various compartments [158]. It is still unclear which and how members are involved in these non-ER processes. With that said, there are still many unanswered questions regarding each PDI member's roles in protein folding and degradation, as well as the mechanisms and regulations of their many functions [136]. Nevertheless, at least four PDIA6 isoforms with similar molecular weights but varying pI were separated on the DIGE gels and identified with mass spectrometry analyses. All isoforms had a fold change of approximately +2 when comparing abundance from 2.5 days old cultures to that of 8.5 days old samples. On the other hand, PDI appeared to resolve into a single spot on 2D gels, with roughly 2 fold change as well. The expressions of both PDI and PDIA6 likely were up-regulated as occurred to BiP, GRP94 and GRP170 upon the initiation of UPR. In support, PDI has been reported as one of the up-regulated apoptosis-modified proteins [148,149].

3.4.2.3 Cytosolic Chaperone Proteins

Heat shock cognate protein 70kDa (HSC70), **heat shock protein 90 beta (HSP90β)** and **FK506-binding protein 52 (FKBP52)** were the only cytosolic chaperone proteins identified by MS analyses. As a member of the Hsp70 family, the principle role of HSC70 is to shield the hydrophobic

resides of newly synthesized proteins as they emerge from the ribosomes [159]. HSP90β, also known as HSP84, is a mammalian ubiquitous cytosolic member of the HSP90 protein family, which functions as a somewhat substrate-specific molecular chaperone, associating with various intracellular proteins including steroid hormone receptors, actin, tubulin and some kinases [160]. FKBP52, also named p59, FKBP4, HSP56, p52 and Hsp-binding immunophilin (HBI), is a multifunctional protein exhibiting peptidyl-prolyl cis-trans isomerase (PPIase) activity. Its role as one of the HSP90 co-chaperones in the steroid receptor heterocomplex has been well studied. For example, upon the binding of hormone to the glucocorticoid receptor/HSP90 complex, FKBP52 is recruited and promotes the nucleus translocation of the complex by interacting with a motor protein, dynein [161].

Among all 10 chaperone-related proteins identified (see Table 3-4), HSC70, HSP90β and FKBP52 were also the only proteins that decreased in abundance as the culture aged and the degree of apoptosis increased. All three proteins were similarly reduced in abundance, decreasing by 1.17, 1.31 and 1.29 fold respectively on day 8.5 as compared to those on day 2.5. Both HSC70 and HSP90β are constitutively expressed proteins in normal growing mammalian cells [160,162,163]. The concurrent changes observed in the three proteins might be attributed by the fact that HSC70 and FKBP52 proteins can act as co-chaperones for HSP90 [161,164].

Other than being involved in protein folding, HSC70 and HSP90 have additional functions. HSP70 isoforms promote cell proliferation and survival by acting as co-chaperones responsible for substrate loading into HSP90 and neutralizing the effects of several pro-apoptotic proteins such as AIF, APAF-1 and BAX in both the intrinsic and extrinsic pathways [164]. It has been shown that inhibition of either HSP90 or HSC70 can lead to apoptosis in certain cancerous and normal cell lines [165-168]. Hence, it is not surprising to see their down regulation in culture containing significant portion of apoptotic cells. However it is unclear whether the decrease in HSP70 and HSP90 was a means to remove pro-survival signals and chaperones in order for the cells to undergo apoptosis or merely a

consequence of apoptosis. In another study, hyperthermia-induced cell deaths have been observed in cells with low HSC70 expression [162].

Furthermore, HSP90 is a known chaperone of the major activator of the stress response, HSF1 [169]. Activation of the heat shock response is a result of the release and homotrimerization of HSF1 transcription factor from the HSP90-containing multi-chaperone complex [164]. It was postulated that with the increased accumulation of chaperone substrates when UPR occurs, the availability of HSP90 for inhibiting HSF1 polypeptides decreased, thus lifting the suppression on HSF1 and causing the transactivation of *hsp* genes [170]. Since all chaperones except HSP90, HSC70 and FKBP52 identified by DIGE and MS analyses were up-regulated, the removal of HSF1 suppression by decreased HSP90 abundance might be contributing to the increased translation of other heat shock protein chaperones.

3.4.3 Glycolytic Proteins and other Metabolic Enzymes

Six of the ten glycolytic enzymes were positively regulated as CHO cultures became more apoptotic. Figure 3-6 shows the ten reactions of glycolysis while highlighting the last six consecutive steps, which correspond to the reactions catalyzed by the differentially expressed proteins. Listed in the order within the pathway, these proteins are triosephosphate isomerase (TPI), glyceraldehydes-3-phosphate dehydrogenase (GAPDH), phosphoglycerate kinase (PGK), phosphoglycerate mutase (PGM), enolase 1 and pyruvate kinase (PK) isozyme M1/M2. In addition, L-lactate dehydrogenase (LDH) chains have been identified. LDH processes the end product of glycolysis, which is pyruvate, into lactate. The fact that more than half of the glycolytic enzymes were induced strongly indicates the significance of their participation during prolonged cell cultivation and possibly apoptosis. It is also quite intriguing that every enzyme responsible for the latter half of the glycolysis pathway was simultaneously induced.

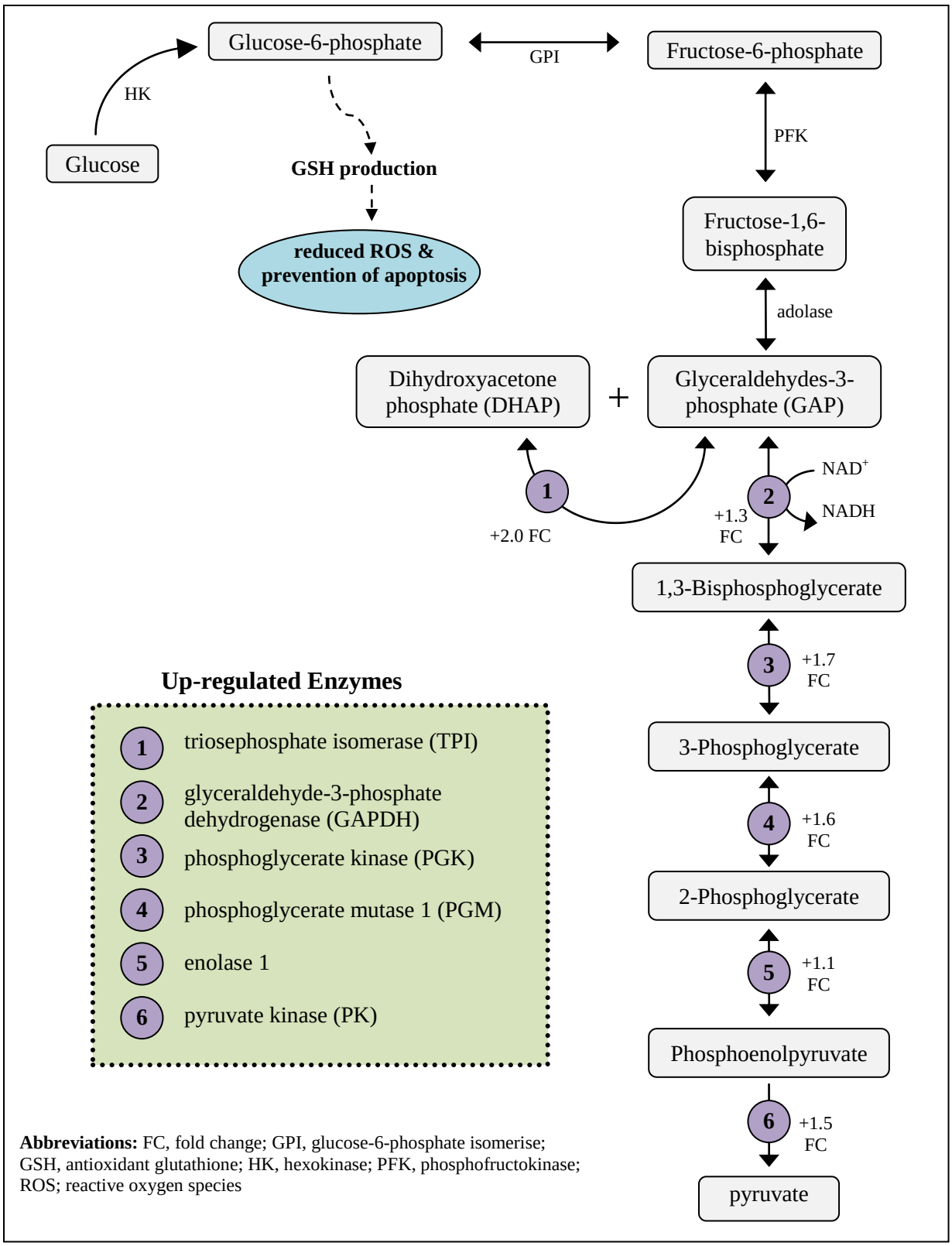

Figure 3-6. Up-regulated enzymes of the glycolysis pathway as apoptosis progressed. The average fold change between day 2.5 and day 8.5 cultures were shown beside each up-regulated enzyme. Dotted lines indicate a multistep pathway, which can regulate the glycolysis pathway. *Figure based on* [171,172].

3.4.3.1 Changes in Energy Metabolism and the Regulation of Glycolytic Enzymes

From the MS analyses, seven metabolic enzymes were found to be up-regulated to various extents. Six of these were directly involved in the breakdown of glucose molecules into two pyruvate molecules, generating two ATPs in the process. In addition, L-lactate dehydrogenase (LDH) A and C chains were also detected from identical mass spectrum peaks. LDH is a metabolic enzyme responsible for converting pyruvate into lactate [173]. It is an alternative route for processing pyruvate. Given that all seven enzymes exhibited an increased abundance as apoptosis progressed, it is not unreasonable to deduce that the amount of glycolysis reactions occurring in the cells rose as the result of more available enzymes. At first glance, the induction of glycolytic proteins when glucose supply was diminishing in cultures over time seems contradictory. However, this phenomenon can be explained if the increase in glycolytic enzymes was a tactic to maintain adequate energy levels within cells when the actual glucose concentration decreased. For this reason, the induction of enzymes might be activated by the depletion of glucose concentration prior to the initiation of apoptotic cell death simply as a cellular response to maintain the necessary glycolysis rate. Alternatively, it is also possible that the upregulation was post-apoptotic attempt to maintain energy level for the proper execution of apoptosis.

Since apoptosis is an energy driven mechanism, the induction of glycolytic enzymes, which can accelerate ATP production, might be necessary for providing the energy required for the execution of apoptosis. Following glycolysis, subsequent energy extraction from pyruvate can either occur via the tricarboxylic acid (TCA) cycle, which yields a high number of ATP per pyruvate, or by its conversion to lactic acid, which only generates one NAD^+ molecule in the process (Figure 3-7). In a study by Swiderek and colleagues, higher glucose consumption rates were reported along with increased mRNA levels of several glycolytic enzymes when cells were under severe hypoxia or anaerobic conditions, which led to apoptosis [174]. It was concluded that as a survival strategy, cells generate more energy by increasing glycolysis in order to compensate for the inefficient energy production under an oxygen

limited state and maintain an adequate energy reservoir [174,175]. It has been noted that in non-cancerous normal cells, the coordinated induction of almost all genes encoding glycolytic enzymes has been found important for the adaptation to hypoxia, which stabilizes and activates the hypoxia-inducible transcription factor HIF-1 [172]. Some of these HIF-1 targets include hexokinase-2, TPI, GAPDH, PGK, aldolase A, enolase 1 and LDH-A [174,176]. However, oxygenation in small-scale stirred tank bioreactors via surface aeration and mixing is often sufficient [177]. The lack of oxygen limitation in CHO cultures maintained in spinner flasks has recently been demonstrated, especially with the use of loose side caps that allow the transfer of oxygen from the atmosphere [178].

The slight increase in the cellular LDH level in this experiment correlates with the accumulation of lactate typically observed in CHO cultures. From amino acid assays (pending publication and personal communication with Saeideh Naderi), CHO IgG-9β8 supplemented with 1-4mM glutamine usually started off with a low lactate concentration around 3-5mM which quickly increased to 12mM in 2-3 days and remained fairly constant until the end of culture process. The induction of LDH levels also reached its peak (at approximate 1.2 fold change) as early as day 4.5 (see Table 3-5). Since only four time points were chosen for DIGE analyses, the LDH induction trend which appeared later than the lactate production might be due to the lack of more data points before day 2.5. In addition to the generation of energy, another possible explanation for the slight increase of LDH relates to whether glycolysis can be completed. While LDH catalyzes the conversion of pyruvate to lactate, it oxidizes NADH and replenishes NAD^+, which is essential for the completion of glycolysis reactions (see Figure 3-6 and Figure 3-7) [172]. Due to its influence on glycolysis reactions and progress, it is not surprising to have LDH expression increase when the demand for energy increases. In Swiderek's study [174], higher lactate production was also noted in hypoxia and anaerobic cultures. The authors suggested that the glucose metabolism switched from the TCA cycle to anaerobic glycolysis. Altogether, these evidences and reports suggest that in the case of prolonged CHO cultures

undergoing apoptosis, LDH may be induced for the same reason, which is to provide enough energy to the cells.

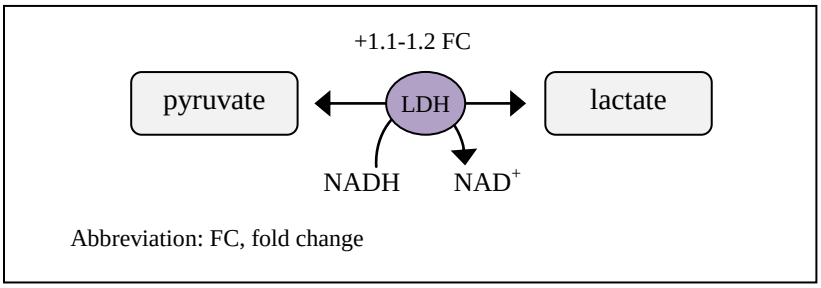

Figure 3-7. Conversion of pyruvate to lactate by lactate dehydrogenase (LDH).

3.4.3.2 Relationship between Glycolytic and Apoptotic Pathways

Besides maintaining energy reservoir when cells are stressed and/or undergoing apoptotic cell death (see Section 3.4.3.1), the changes in glucose metabolism might also have pro-apoptotic consequences. Although how changes in energy metabolism actively induce apoptosis is still unclear at the moment [171], it has been shown that decreases in glucose level, mitochondria membrane potential and oxidative phosphorylation can induce mitochondrial cristae remodelling, releasing cytochrome *c* into the IMS, making it readily available for release into the cytosol [171,179,180]. As for the prolonged CHO cultures in the present study, since the depletion of glucose continued to persist and worsen over time, eventually mitochondrial cristae remodelling and the release of cytochrome *c* into the IMS likely occurred.

In addition to influencing the remodelling of mitochondria and release of cytochrome *c* in the IMS, glucose metabolism can also affect the reduction of reactive oxygen species (ROS). ROS can be elevated during apoptosis or generated by mitochondria under stress conditions such as insufficient oxygen levels within cells which can also lead to apoptosis [171,181,182]. By regulating the levels of metabolic enzymes including glucose-6-phosphate dehydrogenase (G6PDH) and PFK, glucose-6-

phosphate (G6P) molecules are diverted from glycolysis to a pathway that generates cellular antioxidant glutathione (GSH) (Figure 3-6). This increase in GSH level leads to the reduction of ROS and the prevention of apoptosis [171]. Although these proteins were not among the differentially expressed metabolic proteins identified in CHO apoptotic cells, the availability of enzymes catalyzing the latter half of the glycolysis reactions could be crucial in influencing the amount of G6P molecules that fall through the two pathways. With the presence of more glycolytic enzymes, G6P molecules were likely diverted to undergo glycolysis metabolism instead of the pentose phosphate pathway, which generates GSH. Interestingly, it has been shown recently that the oxidation of cytosolic cytochrome *c* by ROS is required to fully activate caspases and apoptosis [183]. Altogether, these findings suggest that the increased glycolytic reactions promote the release of mitochondrial cytochrome *c* and elevation of cellular ROS concentration, both of which are required for the execution of apoptosis.

3.4.3.3 Non-Metabolic Functions of Metabolic Enzymes

For a long time, glycolytic enzymes have been regarded as housekeeping proteins and associated only with the metabolism of glucose in cells [172]. Changes of glycolytic protein levels in studies usually were interpreted as changes to the metabolism of nutrients as availability decreases or culture condition deteriorates. However, more and more studies seem to indicate that additional non-metabolic functions of these glycolytic enzymes exist. For example, the nuclear localization of several glycolytic proteins including enolase-1, GAPDH and LDH has been noted. Evidence presented in several studies suggests that the nuclear form of these enzymes participate in transcription and/or DNA replication. Several studies also show that tyrosine phosphorylation of some glycolytic enzymes may affect their subcellular localization [172]. Some studies were able to explicitly associate cell survival and cell death with a small number of the glycolytic proteins such as hexokinase and GAPDH, although the exact mechanisms are still far from being understood [172,184,185].

In this project, enolase-1 was identified as differentially expressed based on the one-way ANOVA test, and showed slight upregulation when comparing day 4.5, 5.5 and 8.5 protein samples to that of day 2. Based on the initiation of translation at different in-frame AUG start codons, the *ENO1* gene can encode for 48kDa enolase-1 and 37 kDa *MYC* promoter-binding protein MPB1, whose expression induces growth suppression and cell death [172,186]. The spot identified as enolase-1 indeed had an estimate MW of 50kDa from the gel electrophoresis migration. When expressed in vitro, the alternative translations of enolase-1 and MPB1 have been detected simultaneously by Western blot, with the latter expressed at a lower abundance [186]. In contrast, simultaneous downregulation of enolase-1 and MPB1 was caused by retinoic acid treatment of human carcinoma cells [187]. If indeed the observed induction of enolase-1 corresponds to an increase in MPB1 (which was not identified by DIGE and MS analyses in this study), it would correlate nicely to the actively occurring deaths in the CHO culture as determined by flow cytometric assays.

As for GAPDH, although its cytosolic form typically functions as a catalyst in the glycolysis pathway, it has been associated with DNA repair, transcriptional regulation and apoptosis in several studies [172]. Many apoptotic stimuli can activate inducible nitric oxide synthase to produce nitric oxide (NO) in the cells. These nitric oxides *S*-nitrosylate GAPDH, rendering it catalytically inactive and able to bind to a nuclear localization signal containing E3-ubiquitin-ligase called Siah1. The subsequent translocation of GAPDH-Siah1 complex to the nucleus then induces apoptosis by the acetyltransferase p300/CREB binding protein-mediated pathway [188]. Significantly increased GAPDH expression has occurred during apoptosis that was induced by various factors including prolonged culture, nutrient withdrawal and cytotoxic agents [172]. Its pro-apoptotic function was further supported by its over-expression and antisense inhibition, which led to the induction and inhibition of apoptosis respectively [189]. Therefore, in addition to its role in glycolysis, upregulation of GAPDH proteins could also be due to its pro-apoptotic functions. In support of the above studies, two GAPDH isoforms of identical weight and slightly different pI were separated on the CHO DIGE

gels in the present study. They were on average up-regulated by 1.26 and 1.27 fold from day 2.5 to day 8.5.

3.4.4 Other Proteins and their Potential Roles in Apoptosis

14-3-3 epsilon

Expression of 14-3-3 epsilon protein showed a small but statistically significant 1.1 fold down regulation at the late death phase (day 8.5) time point. This downregulation was also significant based on ANOVA comparison of abundance across all four time points. Members of the 14-3-3 protein family interact with a diverse numbers of cellular proteins including transcription factors, biosynthetic enzymes, cytoskeletal proteins, apoptosis factors and signalling molecules via their phosphor-serine or phosphor-threonine binding activity [190,191]. Under normal conditions, 14-3-3 proteins prevent the initiation of apoptosis by binding and inactivating various proteins in the apoptosis pathway, such as Bad and Bax. In the presence of death signals, 14-3-3 proteins become phosphorylated, leading to a conformation change followed by the release of pro-apoptotic substrates and the triggering of apoptosis. The interaction between 14-3-3 proteins and their substrates mostly are regulated by the phosphorylation of ligands and 14-3-3 [190,192]. However, during apoptosis, the dissociation of client-14-3-3 complex has been suggested to occur when 14-3-3 proteins are truncated [192]. 14-3-3 isoforms including 14-3-3 epsilon, have been identified as direct substrates of caspases during apoptosis [193,194]; cleavage results in the decrease of full length 14-3-3 expression as observed in many proteomics studies [195,196]. Based on evidence from previous studies, the observed decrease of 14-3-3 epsilon in CHO cells after the onset of apoptosis could likely be involved in the regulation and release of pro-apoptotic proteins from 14-3-3 suppression. Of course, it cannot be ruled out that the decreased in 14-3-3 abundance might also be related to other pathways. The absence of expression change on day 4.5 and 5.5 might be due to the time required before sufficient activated caspases accumulated and the cleavage of 14-3-3 became noticeable by proteomic analysis. Although the measured fold change was

small, its consistency across replicates (see Appendix B Figure B-4a) and significance based on two statistical tests render 14-3-3 likely to have undergone a real biological change.

Laminin receptor 1

Laminin receptor 1 (LAMR1), also known as 37/67 kDa laminin receptor (LR), laminin binding protein (LBP), p40 ribosome-associated protein and ribosomal protein SA, is a multifunctional protein that can act as a structural component of the ribosome, mediates cellular adhesion and possesses laminin receptor activity [197,198]. The 37kDa form has been clearly identified as a precursor to the 67kDa form, although the exact mechanism is unclear [199,200]. Based on the distance migrated in the DIGE gels, the LAMR1 identified in this study was the 37kDa precursor. Until day 5.5 (the mid-stationary phase) of the culturing process, the abundance of LAMR1 remained constant. Based on t-test analysis between day 2.5 and day 8.5 protein samples, spot 876 which was subsequently identified as LAMR1, was determined statistical significant with a fold change of -1.19. The induction of apoptosis in specific cell lines has been demonstrated by knocking down 37LBP/67LR with antisense cDNA [201] as well as using siRNAs [197]. It has been suggested that LAMR1 is an essential protein for maintaining cell viability. Cleavage of LAMR1 in apoptotic cells has been reported and proposed to have a pro-apoptotic effect [202]. In accordance with these findings, down regulation of LAMR1 was observed in this study.

Galectin-1 and Galectin-3

Galectins are beta-galactoside-binding proteins that regulate various cellular activities including differentiation, apoptosis, cell growth, and tumor progression [203,204]. They can interact with cell surface and extracellular matrix glycoproteins, as well as cytoplasmic and nuclear proteins. Galectin-1 functions as a homodimers of two 14-kDa polypeptides, while galectin-3 forms oligomers [205]. Both galectin-1 and galectin-3 can bind to integrins [204]. Several studies have shown that galectin-1 can inhibit cell growth and promote apoptosis in T cells [206], in particular the activation of type II

extrinsic pathway [206,207]. However, a slight down regulation of galectin-1 was observed during the early death phase (day 8.5) in this study, when significant percentage of the cultures was apoptotic. The reason behind this decrease is unclear, however it could be associated with the role of galectin-1 in other bioprocesses. As a side note, small but statistically insignificant positive fold changes were observed on day 4.5 and day 5.5 of this study before the reduction in abundance was resulted on day 8.5.

Galectin-3, also known as IgE-binding protein, 35 kDa lectin and carbohydrate-binding protein 35 (CBP 35), is the only known member of the galectin family that possesses an anti-apoptotic function [205]. It has been shown to inhibit apoptosis in different cell lines and against stimuli. The means by which galectin-3 inhibits apoptosis remain unclear. However, there is some evidence on the involvement of Bcl-2 [205], phosphorylation of galectin-3 [208] and translocation of galectin-3 into the perinuclear membrane [209]. As the CHO cultures aged, the level of galectin-3 remained constant during the early time points. A slight downregulation was observed on day 8.5. This delayed downregulation might be an indicator that the anti-apoptotic galectin-3 was only removed in the later stage of apoptosis when cell deaths were dominant or unavoidable in the culture. However, due to the unsynchronized nature of cultures in this experiment, a small change in protein abundance might be masked and remained unnoticed until later stages when higher percentage of the population exhibited the same characteristic.

Peroxiredoxin 6

Peroxiredoxin 6 (Prx6) is a thiolspecific antioxidant enzyme and the only member of the peroxidredoxin family that has the ability to remove H_2O_2 and phospholipid hydroperoxide in the plasma membrane [210]. Its expression has been found to be up-regulated upon oxidative stress induced apoptotic cell death [211] while over-expressing Prx6 in cells protects them against oxidative stress [212]. In another study, Prx6 was found to stabilize mitochondrial function by protecting against mitochondrial dysfunction and reducing the production of ROS from mitochondria in mice hepatocytes

subjected to ischemia-reperfusion injury, which is known to generate ROS [210]. Since several mitochondrial changes occur during apoptosis, including changes in ROS production and membrane potential [171,182], the upregulation observed might be a defense against the accumulation of ROS in cells.

As discussed in section 3.4.5, Prx6 was identified in conjunction with TPI from the same spot (#1376) on multiple preparative gels. If overlapping of the two proteins happened, the fold change measured would not reflect the true expression change for either protein. However, when comparing to 2D gel data from Hayduk and colleagues [107], Prx6 was similarly identified in a spot right below PGM as in this study. Although Prx6 had a lower score than TPI, Hayduk's identification supports the match of spot 1376 to Prx6.

Protein kinase C substrate 80K-H

The protein kinase C substrate 80K-H, also known as glucosidase II beta subunit, is the regulatory subunit of α-glucosidase 2. It induces glucose transporter 4 cell membrane translocation by its interaction with protein kinase Cζ and munc18c [213]. A recent study has shown that 80K-H can directly enhance the IP_3- and ATP-induced release of Ca^{2+} by interacting with the cytoplasmic C-terminal tail of IP_3 receptors [213]. As a result, it might participate in the ER apoptotic pathway.

Based on the ANOVA test, spot 340 was determined to be differentially expressed although none of the individual t-test analysis was significant statistically. Although both PEAKS and MASCOT analyses identified 80K-H as the protein in this spot, the scores were not very high. In addition, the reported molecular weight of 60kDa for 80K-H does not match to the estimated MW of 90kDa from the distance migrated during electrophoresis. With the above particulars, the detection of 80K-H and whether its expression did alter significantly over time in the cultures need further verification using techniques such as Western blot.

ATP synthase subunit beta, mitochondrial

Mitochondrial ATP synthase subunit beta (ATPB) is the major catalytic subunit of ATP synthase, which converts ADP into ATP at the mitochondria membrane [214]. It was identified along with β-tubulin in spot 728, which was one of the down-regulated protein spots when comparing CHO cells after prolonged cultivation to ones that were healthy. Reduced level of ATPB is related to the bioenergetic dysfunction of mitochondria [214,215] as the cellular ATP level shows a positive correlation with ATPB abundance [214]. In a proteomic study comparing control versus digoxin-treated human endothelial cells, apoptosis was detected and an increase of ATPB expression was observed two days after treatment. The preservation of ATP allows cells to undergo apoptosis instead of necrosis [214] because unlike necrotic death, apoptosis requires energy to be carried out. It is clear that this unexpected result obtained from the CHO DIGE result in this study conflicts with that of previous studies. However, a constant mitochondrial ATP level but a reduced ATPB abundance in rice mitochondria has been reported two hours after apoptosis was induced by salt stress [216]. The author in the rice study suggested that ATP synthase might not be the main producer of ATP in mitochondria during the early stage of apoptosis. This discrepancy between studies calls for further investigation.

On a side note, both β-tubulin and ATPB were detected in CHO reference maps by Hayduk [107] and Van Dyk [109] with very similar pI although β-tubulin was slightly heavier than ATPB. It is likely that overlapping of these two proteins occurred during electrophoresis or from imprecise spot picking. Overlapping protein spots render any expression change difficult to determine. With this said, it is possible that the observed decreased expression solely reflect the downregulation of β-tubulin, which is a known substrate of activated caspases [120].

3.4.5 Some Concerns with Identified Proteins

Although statistical tests were performed for the selection of differentially expressed proteins, a small number of the protein spots chosen and identified will be false positives. When examining the lists of potential proteins whose expression varied during the course of cell culturing, a few concerns came up. An issue arose from MS analysis when multiple identifications per protein spot were obtained. First, **peroxiredoxin-6 (Prx6)** and **TPI** were detected from two different preparative gels but correspond to the same DIGE spot 1376. Both proteins have molecular weight around 25-26kDa but TPI had much higher scores from both PEAKS and MASCOT analyses. Since different peak sets were matched for each protein, TPI might overlap with Prx6 during separation. This provides some uncertainty in the actual identity of spot 1376 and the cause of increased abundance over time. Because TPI was identified from two nearby protein spots that showed simultaneous upregulation, the contamination from Prx6 should not decrease the likelihood of TPI being a differentially expressed protein. Moreover, Prx6 has been identified in the spot immediately below PGM in a different study [107]. The similar pattern observed supports the match of spot 1376 to Prx6 and that overlapping of two proteins onto the same spot likely occurred.

In addition, spot 728 also matched to two proteins, namely **β-tubulin** and **ATP synthase beta** while the neighboring spot 646 matched to **vimentin** and **α-tubulin**. Although the identifications vimentin, β-tubulin and ATP synthase beta have been reported in CHO reference maps in distinct spots [107,109,217], the exact location of the corresponding spots still cannot be resolved and mapped to the DIGE gels in this study. As the resolution between maps varied and identifications were not complete in all maps, it was hard to confidently match between gels. However, the detection of all three proteins in neighboring spots in other CHO reference maps indicates that some degree of overlapping occurred in this study.

The main sources for the concerns mentioned here are the known limitations of the proteomic experimental techniques employed, such as noise in the DIGE data and low resolution during electrophoresis. With this said, the potential roles of these proteins in prolonged culture and apoptosis were still examined and discussed. In future work, subsequent verification of important proteins of interest can be conducted using other techniques such as Western blot.

3.4.6 Comparison with previous Proteomic and Transcriptomic Studies of Apoptosis

Since the initial CHO protein reference map constructed in 1999 by Champion et al. [108], which successfully sequenced and identified 25 protein spots, few other attempts have been made. Published CHO 2D maps to date include works from Van Dyk et al. [109] with 28 identifications, Lee et al. [217] with 24 identifications and lastly, Hayduk et al. [107] with 224 identifications in 2004.

Genomic or proteomic studies involving CHO cells have been performed to investigate the effects of sodium butyrate (NaBu) treatment, which can enhance protein production while sacrificing cell viability [218], to compare two CHO cell lines with different metabolic profiles and specific antibody productivities [219], to study protein profiles of CHO cells in resting and proliferating phases [220], to understand cellular response to hyperosmotic pressure [217] and to determine the cellular differences of high-producing Bcl-x_L transfected cell line from non-transfected cells under typical culturing conditions [203] and when sodium butyrate was added [221].

Currently, there are no studies on proteomic expression of non-induced apoptotic cells that occurred in prolonged cell cultures, regardless of the cell types. With the exception of a transcriptional profiles of non-induced apoptotic cell death in batch and fed-batch CHO cultures [69], strategies taken by most apoptotic studies focused on examining changes when specific apoptotic pathway was induced by a particular agent. The CHO cDNA microarrays utilized by Wong and colleagues in their CHO

transcriptome study [69] were made from cDNA clones obtained from sequencing CHO cDNA library and contained probes for 4608 express sequence tags [222]. While their objectives were similar to those of this proteome study, comparison studies using microarrays were limited to the probe sets built on the microarray chips, especially when the majority of the apoptotic genes were probed with mouse sequences. From the analyses of 170 apoptosis signalling genes present on CHO and mouse microarrays, the authors reported a total of 47 genes with greater than two fold change (up and down) during batch and fed-batch cultures. During the stationary phase, which coincides with nutrient depletion (glucose and/or glutamine) and loss of viability, the upregulation of apoptotic genes including FasL, FADD, Rip1, caspase 8 seems to support the involvement of the extrinsic apoptotic pathway. Meanwhile, upregulation of caspase 9 was detected briefly during early stationary phase and decreased until death phase. In addition, upregulation of caspase 9/3/7 inhibitor XIAP was observed along with NAIP, another member of the IAP protein family. Although upregulation of Bim and Bad was detected, the absence of Bax and Bak was reported insufficient for Bim and Bad to induce apoptosis. These changes suggest that the mitochondrial pathway was not the major apoptotic pathway triggered. Although the number of probes associated with ER pathway was small, the author also concluded the insignificance of this pathway. Therefore, evidence from this study seems to indicate that the Fas-mediated extrinsic pathway was the dominant mechanism for apoptotic cell deaths in these IFN-γ producing CHO batch cultures. Interestingly, *grp78* mRNA was not differentially expressed in Wang's study however, the protein itself was up-regulated by 2.55 fold on day 8.5 according to DIGE results of this project. When comparing Wang's microarray results to the flow cytometry caspases assays performed in this study, it is clear that the major pathway initiated in the two studies differed. All evidences from FCM analyses support the onset of mitochondrial/ER apoptosis while Wang and colleagues favoured the execution of an extrinsic pathway. It is possible that this difference is cell line specific or influenced by the expression of recombinant proteins. CHO IFN-γ cell line in Wang's study produces a recombinant human interferon gamma, which has been documented to activate Fas death receptor signalling [42,223,224]. Therefore, the observed transcriptional changes in the CHO IFN- γ

batch culture might not be universal or applicable to other CHO cell lines, such as CHO IgG-9β8. Nevertheless, Wang and colleagues utilized the results from their microarray study and created four apoptosis-resistant CHO lines which target early apoptotic signalling genes *Fadd, Faim*, *Alg-2* and *Requiem* [31]. All four gene-targeting strategies resulted in a 24 hour delay in the onset of apoptosis, prolonging batch culture and enhancing IFN-γ production. Since specific productivities of the apoptosis-resistant lines were similar to that of the parental CHO IFN-γ line, improvement in production was due to prolonged culture viability instead.

Proteomic studies on other cell lines treated with apoptotic inducers

Apoptosis triggered by various agents has been studied in various cell lines with different approaches [221,225-227]. For example, comparative 2D gel electrophoresis of sodium selenite-induced apoptosis in human leukemia NB4 cells has been performed and confirmed by RT-PCR and Western blot [226]. Out of the 26 down-regulated and four up-regulated identified proteins which had a minimum 1.5 fold change, only α-tubulin, β-actin and LAMR1 were also identified in CHO IgG-9β8 cultures. However, instead of decreasing in abundance, α-tubulin and β-actin were both up-regulated in NB4 cells. The remaining proteins include regulators of signal transduction such as Rho GDI beta and alpha, members of the mitogen activated protein kinase family, proteins that regulate *c-fos*, *c-myc* and *c-jun* mRNA expression, metabolism related proteins and lastly proteins associated with DNA damage. Although the authors suggested the involvement of JNK pathway in the selenite-induced apoptosis, no definite conclusion on the apoptotic pathway triggered or the mechanisms was made.

In another study, Fas-induced apoptosis in human Jurkat T cells was analyzed using stable isotope labelling with amino acid (SILAC) leucine instead of CyDyes [225]. Using this method, 28 out 38 apoptosis modified protein spots on 2D gels were identified with a minimum 1.5 fold change between normal and Fas-induced apoptotic cultures. Similar to the apoptotic NB4 proteome, most (31) altered protein spots were down-regulated while the remaining seven spots increased expression. On

top of that, one of the up-regulated spot was actually a degraded fragment of heterogeneous ribonucleoprotein (hnRNP) K, which had been identified in two other spots with decreased abundance. Of all 28 identified proteins, only LAMR1, which decreased expression, was also identified in CHO IgG-9B8 cells. The remaining protein identifications include mRNA processing proteins such as 12 different hnRNP proteins, transcription associated proteins such as ribosomal proteins, RNA helicase, elongation factor Tu and transcription factor BTF3, PARP fragments, Rho GDI beta and actin-binding tropomyosin alpha chains. Although there are overlaps between the sets of apoptosis-altered proteins in these experiments, depending on the experimental design, cell lines and apoptotic inducers used, the resulting list of proteins might vary considerably and exhibit low correlation [228]. This was in fact demonstrated by Thiede and colleagues in the comparison of their SILAC results to the results of silver-stained 2D gels analyzing Fas-induced apoptosis in Jurket cells using the sample preparation and gel systems [229]. Although a similar number of protein spots was subjected to MS analyses, only 21 as opposed to 28 spots were successfully identified and among these 21 spots, just 13 identifications were common.

Quantitative proteomic analyses of cisplatin-induced apoptotic Jurket T cells with SILAC and SDS-PAGE has also been conducted [227]. Cisplatin is thought to inhibit DNA replication and transcription, leading to cell death by apoptosis. In this proteomic study, 26 proteins with abundance changes greater than 1.5 fold were identified and 19 were already known to be involved with apoptosis. Upregulation in 14 proteins and downregulation in 12 proteins were observed. Nine RNA-binding proteins including five hnRNP proteins, p54nrb, pre-mRNA splicing factor SRp30C and RNA-binding protein 4 and seven cytoskeletal proteins which include actin, α-tubulin and β-tubulin were identified in this study. However, contradicting to the downregulation of actin, α-tubulin and β-tubulin in "aging" CHO cultures, which include a mix of healthy, apoptotic and dead cells, cisplatin-induced apoptotic Jurket cells showed an increase in these cytoskeletal proteins.

In contrast to the above, some studies have reported a similar subset of proteins affected by apoptosis to the ones observed in the present work. For instance, a proteomic study examining ionizing radiation-induced apoptosis of human prostate cells revealed mostly ER stress response/chaperon and cytoskeletal proteins [148]. Upregulation of ER proteins including GRP94, calreticulin, calnexin, GRP78, GRP75, HSP70 and PDI, as well as downregulation of cytoskeletal proteins were reported in this particular study. Similarly, in a quantitative proteomics study examining staurosporine-induced apoptosis, the detection of many molecular chaperones and ER proteins such as GRP94, BiP, ERp60 and HSP70 proteins, and cytoskeletal proteins like vimentin and α-tubulin was made [125]. It was concluded that the treatment of staurosporine provokes an ER stress and induces the UPR in this study.

Many researchers have tried studying apoptosis with a particular proteomic approach. However, correlation between different studies was usually low and inconsistent. This deviation might be due to differences in the cell line, apoptotic inducer, proteomic techniques and experimental designs used [228]. For instance, the heterogeneous nature of non-induced CHO cultures likely influence the DIGE results obtained in the present study as they were the combined results from cells at different stages. Furthermore, as opposed to the proteomic analyses of prolonged cultures that lasted two weeks in this project, the majority of the induced apoptosis studies performed by other research groups were done in much shorter time frames, which usually were few hours after treatment. In these induced studies, it is expected to observe responses more restricted to apoptosis as abrupt changes were brought uniformly to all cells. On the other hand, in the prolonged cultures, cells were slowly subjected to the degradation of culture conditions and the eventual onset of apoptosis. Many of the up-regulated proteins identified were ER chaperone and metabolic enzymes, which likely increased their activities to cope with the initial cellular stresses and changes of metabolism as nutrient depleted. Lastly, technical variations can significantly affect the number of observed changes made in these studies. For instance, the probes used in a microarray study directly influence which and what types of genes will be monitored. In the case of 2D gel electrophoresis, sample preparation and electrophoresis set up such as

the pH range and cell lysis buffer used greatly control the set of proteins that will resolve on the gels allowing subsequent comparison and analysis. Therefore, depending on the experimental design and set up, the list of differentially expressed proteins identified may not capture all the biological significant changes.

Chapter 4. Conclusions and Future Directions

4.1 Flow Cytometric examination of Apoptosis in CHO IgG-9β8 Cultures

The detection and monitoring of the progress of apoptosis in culture over time were done by quantifying the level of activated executioner caspases in cells with a flow cytometer. It was shown that in the exponential phase or the first 4.5 days of cultivation, CHO cultures were predominantly viable and healthy. An increasing number of cells showed signs of apoptosis initiation after day 4.5 (early stationary phase). Between day 5.5 to day 8.5, more early apoptotic cells progressed into the late apoptotic phase where membrane integrity was lost, indicating the death of the cell. After day 8.5 (early death phase), the number of dead cells including both necrotic and apoptotic cells continued to increase. Eventually dead cells contributed to an overwhelming portion of the culture, which was about 70% of the culture on day 16.5.

When the cellular levels of two major initiator caspases, namely caspase 8 and caspase 9, were examined by FCM, it was apparent that the activation of caspase 9 was the dominant trigger for apoptotic cell death in non-induced CHO cultures. These results suggest the involvement of mitochondrial and/or ER-mediated apoptotic cell death, both of which trigger the activation of pro-caspase 9 upon the detection of various intracellular stress stimuli. Subsequent proteomic analysis has detected the induction of many ER chaperone and folding proteins, indicating that the unfolded protein response (UPR) might be a factor contributing to the onset of caspase 9-dependent apoptosis.

4.2 Proteomic Changes in CHO Cells Undergoing Apoptosis in Batch Cultures

From the changes of protein abundance between samples in the DIGE experiment, a total of 79 protein spots were selected for subsequent MS sequencing. The successful MS analyses of 40 spots yielded 28 unique protein identifications. These proteins include four cytoskeletal proteins, ten ER and cytosolic chaperone proteins, seven glycolytic and metabolic enzymes and seven other miscellaneous proteins.

Since actin, α-tubulin, β-tubulin and vimentin, are known caspase substrates, their reduction in aging and apoptotic cell cultures were expected. The degradations of these cytoskeletal proteins affected actin filaments, microtubules and intermediate filament networks, resulting in many of the observed phenotypes of apoptosis such as the loss of cell shape, cell shrinkage and the reorganization of cytoskeletal structures prior to blebbing and apoptotic body formation.

Except for the three cytosolic chaperone proteins, the seven identified ER chaperones all showed an increase in expression during prolonged cultivation. In addition to being responsible for the proper folding of glycoproteins in the ER, calreticulin and ERp60 have various apoptotic roles. For example, calreticulin labels cells for phagocytosis following its translocation and insertion into the plasma membrane. As for ERp60, it indirectly assists the release of membrane bound apoptosis inducing factors (AIF) into the intermembrane space, allowing them to be released into the cytosol during apoptosis via the intrinsic pathway. The remaining ER chaperones, BiP, GRP94, PDI, GRP170 and PDIA6 form complexes that facilitate folding of hydrophobic residues. As opposed to calreticulin and ERp60, these five chaperones are known for their pro-survival functions only. Both BiP and GRP94, in particular, have been thought to protect cells against apoptosis upon ER stress. On the contrary, three cytosolic chaperones, HSC70, HSP90β and FKBP52 were identified as down-regulated proteins modified by either cellular stress or apoptosis. HSC70 and FKBP52 function as co-chaperones

of HSP90β and assist the folding of substrates such as hormone receptors, actin, tubulin and some kinases. Members of the HSP70 family have a strong cytoprotective role, thus their downregulation in CHO cells could allow cells to remove anti-apoptotic proteins. In contrast, the decrease in availability of HSP90β upon stress has been shown to transactivate *hsp* genes. Since HSC70 is also a member of HSP family, its 1.17 fold downregulation appears contradictory. In any case, whether the reduction in these three proteins influences the fate of CHO cells, or was an indirect effect of apoptosis is unclear. Since unresolved ER stress can lead to apoptotic cell death, the presence of UPR might be an important factor contributing to the initiation of apoptosis in this study.

Interestingly, six of the ten glycolytic enzymes showed an increase in protein abundance and were identified as triosephosphate isomerase (TPI), phosphoglycerate mutase (PGM), pyruvate kinase isozyme, phosphoglycerate kinase (PGK), glyceraldehydes-3-phosphate dehydrogenase (GAPDH) and enolase-1. Moreover, L-lactate dehydrogenase (LDH), which converts the end product of glycolysis into lactate, was also up-regulated in prolonged CHO cultures. It is likely that the increase in these metabolic enzymes was needed to ensure that sufficient energy was available for cell proliferation and maintenance as glucose level dropped from consumption over time and for the execution of the energy-driven apoptosis. Although the exact mechanisms and roles have not yet been elucidated, more and more studies have discovered non-metabolic functions of these enzymes. Evidence suggests that nuclear forms of some of these enzymes participate in the regulation of transcription and DNA replication. For instance, nuclear localization of enolase-1, GAPDH and LDH has been detected. Furthermore, hexokinase and GAPDH have also been explicitly associated with cell survival and apoptosis in recent studies. It has been shown that over-expression of GAPDH induces apoptosis and the induction of GAPDH has also been reported in apoptotic cells in other studies.

Finally, there are seven differentially expressed proteins with diverse roles that did not fall into the above three categories. These identified proteins are 14-3-3 epsilon, laminin receptor 1 (LAMR1),

galectin-1, galectin-3, peroxiredoxin-6 (Prx6), 80K-H and ATP synthase beta subunit (ATPB). Since LAMR1, 14-3-3 epsilon and galectin-3 all exhibit an anti-apoptotic role on top of their many diverse functions, the decrease of their expressions during prolonged cultivation could be interpreted as a way to remove pro-survival signals in dying cells and eliminate any unnecessary interference during the execution of apoptosis. Under normal conditions, 14-3-3 isoforms prevent the initiation of apoptosis by suppressing pro-apoptotic proteins such as Bad and Bax. When cleaved by caspase 3, 14-3-3 epsilon releases its pro-apoptotic client and can no longer prevent cell death. While LAMR1 has been suggested essential for cell survival and galectin-3 has been shown to prevent apoptosis against various stimuli, the exact mechanisms of these activities are still unknown. In contrast, the upregulation of Prx6 in this study probably was part of the initial pro-survival response as culture conditions degraded with time. It has been shown that Prx6 protects against mitochondrial dysfunction and reduces the production of ROS from mitochondria. As for galectin-1, ATPB and 80K-H, their identifications as stress response or apoptosis-modified proteins were not as confident in this study due to conflicting results with literature studies and inconsistent fold changes over time.

4.3 Implications of this Work

In this study, flow cytometry analyses successfully identified the activation of caspase 9 as the dominant apoptotic mechanism involved in triggering cell death in an anti-RhD MAb-producing CHO cell line, CHO IgG-9β8. Progression of apoptosis was also monitored at the population level via the quantification of active caspases. Since the apoptotic pathways reported in this study and that of Wang's microarray study on an IFN-γ producing CHO line seem to differ, it suggests that the exact mechanism of apoptosis might be dependent on the cell line and/or culture conditions involved. This information is extremely useful in the optimization of a cell line, as inhibiting the wrong apoptotic pathway would not enhance cell survival as much.

The main objective behind the quantitative proteomic study of this report was to associate cellular changes at the protein level during prolonged cultivation, which involves the onset and execution of apoptotic cell death, in MAb-producing CHO cultures. The work presented in this study is the first proteome-wide investigation of non-induced apoptosis in mammalian cells. Since no treatment was made to artificially induce cell death, the trigger for apoptosis in these cells was the process of prolonged cultivation as experienced in typical industrial bioreactors. Despite the fact that many proteomic analyses of apoptosis in various cell lines have been done, strategies taken by these studies all involved inducing the cultures with particular apoptotic agents. Treating cells with an apoptotic inducer results in a somewhat "artificial" response specific to the type of induced apoptosis. Moreover, the exact mechanism and apoptotic pathway participated in these induced cell death usually were not understood explicitly. Hence findings from these apoptosis studies may not be applicable to other culture settings. From the DIGE and MS analyses of this work, many proteins expected to be modified by the degradation of culture condition and the onset of apoptosis in protein-producing CHO batch cultures were identified. These include numerous chaperone proteins which, as expected, increased in their expression upon cellular stresses like nutrient depletion, and cytoskeletal proteins that are known substrates of caspases. Apart from the common apoptosis-cleaved substrates and the stress-induced responses, the upregulation of six glycolytic enzymes responsible for the final six steps of glycolysis, and one post-glycolysis metabolic protein were surprising and unseen in previous studies. Meanwhile the expression of several other pro- and anti-apoptotic proteins have altered and been detected in this study. To name a few, 14-3-3 epsilon, peroxiredoxin-6, calreticulin and GAPDH are a few examples. On a side note, due to the small number of proteomics CHO maps available, the CHO IgG-98 DIGE gels and the corresponding protein identifications obtained in this study will be valuable additions to the current 2D gel database.

This work is a component of a larger project that seeks to construct an appropriate culture optimization scheme that specifically targets the apoptotic mechanisms activated based on the identified differentially expressed proteins that were crucial for the onset and execution of apoptosis. Overall, this study demonstrated that the major changes in aging CHO cultures, consisting significant levels of apoptotic cells, involve the regulation of stress response and energy metabolism related proteins. Proteins that solely modulate apoptosis were not readily apparent as differentially expressed proteins within the proteomic analyses. Furthermore, the intracellular responses prior to the initiation of apoptosis include a complex network of changes that might be as important as the regulation of apoptotic proteins. Although no direct apoptosis-regulating proteins were identified, the DIGE results have established the potential importance of UPR and energy metabolism in prolonged cultures and apoptotic cell death. Along with the knowledge of the type of apoptotic pathway triggered, apoptotic proteins associated with ER stress, mitochondrial dysfunction and energy metabolism should be considered in the optimization of CHO IgG-9β8 cultivation. As an example, apoptotic proteins crucial to the intrinsic and ER pathway can be inferred from literature and genetically modified to derive a new pro-survival cell line from CHO IgG-9β8. The choice of target for modification can also be considered based on its influence and/or involvement in energy metabolism. However as discussed in Section 4.4, additional apoptotic proteins that are more suitable for this purpose than the ones obtained thus far may be identified with further study.

More importantly, this work provides the first proteomic analysis of non-induced apoptotic cell death occurring in a typical protein-producing cultivation process. Despite the countless studies exploring apoptosis and the general acceptance that apoptosis is the major mode of cell death in bioreactors, the exact cellular changes occurred and the mechanisms involved during apoptosis in bioreactor cultures have not been investigated thoroughly and extensively. Because the majority of apoptosis studies published so far rely on inducing cell death and triggering a specific type of apoptosis, this work can serve as a reference check to ensure the findings made from induced apoptosis are indeed

practical and applicable to cultures maintained in typical industry bioreactors. As discussed in the subsequent sections, future work can be performed to further increase the number of identified proteins and extract more information. Nonetheless, this work shows the potential of utilizing a proteomics approach in understanding intracellular changes occurring in prolonged CHO cultures where apoptosis was actively involved in inflicting cell death after the exponential phase. It is the first step towards building the fundamental framework for optimizing cultivation process, prolonging longevity and maximizing protein production.

4.4 Future Directions

Additional flow cytometry analysis

From the FCM data presented in this study, noticeably larger percentage of the cultures contained activated caspase 9 than caspase 8, strongly suggesting the role of mitochondrial and/or pathway in the onset of apoptotic cell death in CHO IgG-9β8 cultures. Additional pathway-specific assays such as the detection of ER pathway-specific caspase 12 and the changes in mitochondrial membrane potential can be performed to determine the involvement of the two compartments. To further elucidate and verify that caspase 9 was activated as the dominant initiator caspases for apoptosis in CHO cells, additional FCM analyses investigating the simultaneous presence of both activated caspase 8 and caspase 9 in individual cells could be done. It is expected that a dot plot comparison between caspase 8 and caspase 9 intensity signals would demonstrate a larger cluster of cells showing higher caspase 9 signals versus caspase 8 signals. Although the detection of all major caspases (for example caspase 3, 8, 9 and 12) in each cell would be more informative, currently there are only two fluorochromes, namely carboxyfluorescein and Sulforhodamine B, available for FLICA assays.

Elaboration on proteomic analysis

For future studies, a few modifications on the proteomic analysis can be done to increase the number of apoptosis-modified proteins detected. First, the DIGE experiment could be repeated with a smaller range of pI charges instead of pH 3-10. Isoelectric focusing using IPG gel strips at smaller ranges can better separate protein spots of close pI and increase the resolution of gels. Especially at the extreme pI, protein spots were usually not well resolved and separated. By targeting a specific region of pI, the occurrence of overlapping proteins will be reduced. The increased number of spots resolved on the gel implies that more protein spots will likely be determined as differentially expressed by statistical tests.

Secondly, the option of enriching apoptotic cells prior to proteomic analyses can be considered. Based on the number of potential differentially expressed protein spots obtained from t-test and ANOVA, the progress of apoptosis in day 4.5 and day 5.5 old cultures was either minimal or difficult to discern due to limitations in experimental techniques and design. For example, cells from un-treated cultures contain unsynchronized cells at various cell cycle stages and apoptotic stages. It is likely that due to the high percentage of healthy subpopulation, the early changes that occurred in the apoptotic subpopulation were masked and not observed. To resolve this issue, apoptotic cell enrichment, which allows only the apoptotic subpopulations from a culture sample collected to be separated out for analysis, can be applied. The noise from the non-apoptotic subpopulation will be eliminated. Therefore, smaller fold changes that might be masked previously will be enhanced and fold changes that better reflect true alteration in protein abundances will result. As of now, flow cytometry cell sorting and phosphatidylserine-binding magnetic beads can both separate and isolate apoptotic cells. To avoid excessively decreasing culture volume with repeated sampling over the whole cultivation period, apoptotic cell enrichment was not performed in this study. Since enrichment will filter out non-apoptotic cells, higher number of cells must be collected for subsequent filtering and protein extraction. However, for future studies, more focus on the late stationary/early death phase of the cultivation period,

which was day 8.5 in this project, can reduce the total volume of cultures required and allow a larger volume to be collected for cell enrichment. Since consistent changes in protein expression were observed from day 2.5 to day 4.5, 5.5 and 8.5, proteomic analysis between day 2.5 and day 8.5 likely will be sufficient.

Finally, studying the changes to subcellular proteomes, such as mitochondrial, nuclear and ER proteomes, provides information on translocation which will be overlooked when studying the whole cell proteome. Also, it may help to elucidate the exact role of many multi-functional differentially expressed proteins during apoptosis.

References

[1] Hacker, D.L., De Jesus, M., and Wurm, F.M. (2009). 25 Years of Recombinant Proteins from Reactor-Grown Cells - Where do we Go from Here? *Biotechnol. Adv.* 27, 1023-7.

[2] Jayapal, K.P., Walschin, K.F., Hu, W., and Yap, M.G.S. (2007). Recombinant Protein Therapeutics from CHO cells - 20 years and counting. *Chemical Engineering Progress* 103, 40-7.

[3] Puck, T.T., Cieciura, S.J., and Robinson, A. (1958). Genetics of somatic mammalian cells. III. Long-term cultivation of euploid cells from human and animal subjects. *J. Exp. Med.* 108, 945-56.

[4] Urlaub, G. and Chasin, L.A. (1980). Isolation of Chinese hamster cell mutants deficient in dihydrofolate reductase activity. *Proc. Natl. Acad. Sci. U. S. A.* 77, 4216-20.

[5] Derouazi, M., Martinet, D., Besuchet Schmutz, N., Flaction, R., Wicht, M., Bertschinger, M., Hacker, D.L., Beckmann, J.S., and Wurm, F.M. (2006). Genetic characterization of CHO production host DG44 and derivative recombinant cell lines. *Biochem. Biophys. Res. Commun.* 340, 1069-77.

[6] ATCC. Cell Lines and Hybridomas. 2010.

[7] Kim, D.Y., Lee, J.C., Chang, H.N., and Oh, D.J. (2006). Development of serum-free media for a recombinant CHO cell line producing recombinant antibody. *Enzyme and microbial technology* 39, 426-33.

[8] Gandor, C., Leist, C., Fiechter, A., and Asselbergs, F.A. (1995). Amplification and expression of recombinant genes in serum-independent Chinese hamster ovary cells. *FEBS Lett.* 377, 290-4.

[9] Hyclone. Products: CHO Cell Culture Platform. 2008.

[10] Gottesman, M.M. (1985) Growth properties of Chinese hamster ovary (CHO) cells. In *Molecular Cell Genetics* (Gottesman, M.M., ed.) pp. 139-54. John Wiley & Sons, Inc, New York.

[11] Tjio, J.H. and Puck, T.T. (1958). Genetics of somatic mammalian cells. II. Chromosomal constitution of cells in tissue culture. *J. Exp. Med.* 108, 259-68.

[12] Kao, F.T. and Puck, T.T. (1967). Genetics of somatic mammalian cells. IV. Properties of Chinese hamster cell mutants with respect to the requirement for proline. *Genetics* 55, 513-24.

[13] Wu, J.R. and Gilbert, D.M. (2000). Lovastatin arrests CHO cells between the origin decision point and the restriction point. *FEBS Lett.* 484, 108-12.

[14] Fiore, M., Zanier, R., and Degrassi, F. (2002). Reversible G(1) arrest by dimethyl sulfoxide as a new method to synchronize Chinese hamster cells. *Mutagenesis* 17, 419-24.

[15] Fernandez, M.J., Lopez, A., and Santa-Maria, A. (2003). Apoptosis induced by different doses of caffeine on Chinese hamster ovary cells. *J. Appl. Toxicol.* 23, 221-4.

[16] Kang, S.G., Lee, D.Y., Kang, M.L., and Yoo, H.S. (2007). Biological characteristics of Chinese hamster ovary cells transfected with bovine Prnp. *J. Vet. Sci.* 8, 131-7.

[17] Bessho, T., Mu, D., and Sancar, A. (1997). Initiation of DNA interstrand cross-link repair in humans: the nucleotide excision repair system makes dual incisions 5' to the cross-linked base and removes a 22- to 28-nucleotide-long damage-free strand. *Mol. Cell. Biol.* 17, 6822-30.

[18] Kim, D.Y., Lee, C.L., Chang, H.N., and Oh, D.J. (2005). Effects of Supplementation of Various Medium Components on Chinese Hamster Ovary Cell Cultures Producing Recombinant Antibody . *Cytotechnology* 47, 37-49.

[19] Nickerson, L. and Wiersma, E.J. (2002). Epitope mapping of four monoclonal antibodies specific for the human RhD antigen. *Immunol. Lett.* 80, 33-9.

[20] Kumpel, B.M. (2008). Lessons learnt from many years of experience using anti-D in humans for prevention of RhD immunization and haemolytic disease of the fetus and newborn. *Clin. Exp. Immunol.* 154, 1-5.

[21] Wurm, F.M. (2004). Production of recombinant protein therapeutics in cultivated mammalian cells. *Nat. Biotechnol.* 22, 1393-8.

[22] al-Rubeai, M., Mills, D., and Emery, A.N. (1990). Electron microscopy of hybridoma cells with special regard to monoclonal antibody production. *Cytotechnology* 4, 13-28.

[23] Mercille, S. and Massie, B. (1994). Induction of apoptosis in nutrient-deprived cultures of hybridoma and myeloma cells. *Biotechnol. Bioeng.* 44, 1140-54.

[24] Moore, A., Donahue, C., Hooley, J., Stocks, D., Bauer, K., and Mather, J. (1995). Apoptosis in CHO cell batch cultures: Examination by flow cytometry. *Cytotechnology* 17, 1-11.

[25] Singh, R.P., Al-Rubeai, M., Gregory, C.D., and Emery, A.N. (1994). Cell death in bioreactors: a role for apoptosis. *Biotechnol. Bioeng.* 44, 720-6.

[26] Goswami, J., Sinskey, A.J., Steller, H., Stephanopoulos, G.N., and Wang, D.I. (1999). Apoptosis in batch cultures of Chinese hamster ovary cells. *Biotechnol. Bioeng.* 62, 632-40.

[27] al-Rubeai, M. and Singh, R.P. (1998). Apoptosis in cell culture. *Curr. Opin. Biotechnol.* 9, 152-6.

[28] Simpson, N.H., Singh, R.P., Perani, A., Goldenzon, C., and Al-Rubeai, M. (1998). In hybridoma cultures, deprivation of any single amino acid leads to apoptotic death, which is suppressed by the expression of the bcl-2 gene. *Biotechnol. Bioeng.* 59, 90-8.

[29] Wood, T.E., Dalili, S., Simpson, C.D., Hurren, R., Mao, X., Saiz, F.S., Gronda, M., Eberhard, Y., Minden, M.D., Bilan, P.J., Klip, A., Batey, R.A., and Schimmer, A.D. (2008). A novel inhibitor of glucose uptake sensitizes cells to FAS-induced cell death. *Mol. Cancer. Ther.* 7, 3546-55.

[30] Arden, N. and Betenbaugh, M.J. (2004). Life and death in mammalian cell culture: strategies for apoptosis inhibition. *Trends Biotechnol.* 22, 174-80.

[31] Wong, D.C., Wong, K.T., Nissom, P.M., Heng, C.K., and Yap, M.G. (2006). Targeting early apoptotic genes in batch and fed-batch CHO cell cultures. *Biotechnol. Bioeng.* 95, 350-61.

[32] Gramer, M.J. and Goochee, C.F. (1994). Glycosidase activities of the 293 and NS0 cell lines, and of an antibody-producing hybridoma cell line. *Biotechnol. Bioeng.* 43, 423-8.

[33] Jin, Z. and El-Deiry, W.S. (2005). Overview of cell death signaling pathways. *Cancer. Biol. Ther.* 4, 139-63.

[34] Elmore, S. (2007). Apoptosis: a review of programmed cell death. *Toxicol. Pathol.* 35, 495-516.

[35] Kerr, J.F., Wyllie, A.H., and Currie, A.R. (1972). Apoptosis: a basic biological phenomenon with wide-ranging implications in tissue kinetics. *Br. J. Cancer* 26, 239-57.

[36] Mori, I., Ozaki, T., Tabuse, K., Utsunomiya, H., Taniguchi, E., and Kakudo, K. (2009). Microwave cell death: molecular analysis using DNA electrophoresis, PCR amplification and TUNEL. *Pathol. Int.* 59, 294-9.

[37] Kroemer, G., Galluzzi, L., Vandenabeele, P., Abrams, J., Alnemri, E.S., Baehrecke, E.H., Blagosklonny, M.V., El-Deiry, W.S., Golstein, P., Green, D.R., Hengartner, M., Knight, R.A., Kumar, S., Lipton, S.A., Malorni, W., Nunez, G., Peter, M.E., Tschopp, J., Yuan, J., Piacentini, M., Zhivotovsky, B., Melino, G., and Nomenclature Committee on Cell Death 2009. (2009). Classification of cell death: recommendations of the Nomenclature Committee on Cell Death 2009. *Cell Death Differ.* 16, 3-11.

[38] Yamada, T., Takatsu, Y., Kasumi, M., Ichimura, K., and van Doorn, W.G. (2006). Nuclear fragmentation and DNA degradation during programmed cell death in petals of morning glory (Ipomoea nil). *Planta* 224, 1279-90.

[39] Martin, S.J., Reutelingsperger, C.P., McGahon, A.J., Rader, J.A., van Schie, R.C., LaFace, D.M., and Green, D.R. (1995). Early redistribution of plasma membrane phosphatidylserine is a general feature of apoptosis regardless of the initiating stimulus: inhibition by overexpression of Bcl-2 and Abl. *J. Exp. Med.* 182, 1545-56.

[40] Rucker-Martin, C., Henaff, M., Hatem, S.N., Delpy, E., and Mercadier, J.J. (1999). Early redistribution of plasma membrane phosphatidylserine during apoptosis of adult rat ventricular myocytes in vitro. *Basic Res. Cardiol.* 94, 171-9.

[41] Xu, Y., Mahmood, M., Li, Z., Dervishi, E., Trigwell, S., Zharov, V., Ali, N., Saini, V., Biris, A., Lupu, D., Boldor, D., and Biris, A. (2008). Cobalt nanoparticles coated with graphitic shells as localized radio frequency absorbers for cancer therapy. *Nanotechnology* 19.

[42] Curtin, J.F. and Cotter, T.G. (2003). Live and let die: regulatory mechanisms in Fas-mediated apoptosis. *Cell. Signal.* 15, 983-92.

[43] Riedl, S.J. and Shi, Y. (2004). Molecular mechanisms of caspase regulation during apoptosis. *Nat. Rev. Mol. Cell Biol.* 5, 897-907.

[44] Stennicke, H.R. and Salvesen, G.S. (2000). Caspases - controlling intracellular signals by protease zymogen activation. *Biochim. Biophys. Acta* 1477, 299-306.

[45] Wang, Y. and Gu, X. (2001). Functional divergence in the caspase gene family and altered functional constraints: statistical analysis and prediction. *Genetics* 158, 1311-20.

[46] Degterev, A., Boyce, M., and Yuan, J. (2003). A decade of caspases. *Oncogene* 22, 8543-67.

[47] Krysko, D.V., Vanden Berghe, T., D'Herde, K., and Vandenabeele, P. (2008). Apoptosis and necrosis: detection, discrimination and phagocytosis. *Methods* 44, 205-21.

[48] Deng, Y., Lin, Y., and Wu, X. (2002). TRAIL-induced apoptosis requires Bax-dependent mitochondrial release of Smac/DIABLO. *Genes Dev.* 16, 33-45.

[49] Danial, N.N. (2007). BCL-2 family proteins: critical checkpoints of apoptotic cell death. *Clin. Cancer Res.* 13, 7254-63.

[50] Vermeulen, K., Van Bockstaele, D.R., and Berneman, Z.N. (2005). Apoptosis: mechanisms and relevance in cancer. *Ann. Hematol.* 84, 627-39.

[51] Danial, N.N. and Korsmeyer, S.J. (2004). Cell death: critical control points. *Cell* 116, 205-19.

[52] Ashe, P.C. and Berry, M.D. (2003). Apoptotic signaling cascades. *Prog. Neuropsychopharmacol. Biol. Psychiatry* 27, 199-214.

[53] Szegezdi, E., Macdonald, D.C., Ni Chonghaile, T., Gupta, S., and Samali, A. (2009). Bcl-2 family on guard at the ER. *Am. J. Physiol. Cell. Physiol.* 296, C941-53.

[54] Fesik, S.W. (2000). Insights into programmed cell death through structural biology. *Cell* 103, 273-82.

[55] The UniProt Consortium. (2009). family:"Bcl-2 family". 2009.

[56] Ashkenazi, A. and Dixit, V.M. (1998). Death receptors: signaling and modulation. *Science* 281, 1305-8.

[57] Locksley, R.M., Killeen, N., and Lenardo, M.J. (2001). The TNF and TNF receptor superfamilies: integrating mammalian biology. *Cell* 104, 487-501.

[58] Ashkenazi, A. and Dixit, V.M. (1999). Apoptosis control by death and decoy receptors. *Curr. Opin. Cell Biol.* 11, 255-60.

[59] Engels, I.H., Stepczynska, A., Stroh, C., Lauber, K., Berg, C., Schwenzer, R., Wajant, H., Janicke, R.U., Porter, A.G., Belka, C., Gregor, M., Schulze-Osthoff, K., and Wesselborg, S. (2000). Caspase-8/FLICE functions as an executioner caspase in anticancer drug-induced apoptosis. *Oncogene* 19, 4563-73.

[60] Corazza, N., Kassahn, D., Jakob, S., Badmann, A., and Brunner, T. (2009). TRAIL-induced apoptosis: between tumor therapy and immunopathology. *Ann. N. Y. Acad. Sci.* 1171, 50-8.

[61] Walczak, H. and Haas, T.L. (2008). Biochemical analysis of the native TRAIL death-inducing signaling complex. *Methods Mol. Biol.* 414, 221-39.

[62] Andera, L. (2009). Signaling activated by the death receptors of the TNFR family. *Biomed. Pap. Med. Fac. Univ. Palacky Olomouc Czech. Repub.* 153, 173-80.

[63] Fulda, S. and Debatin, K.M. (2006). Extrinsic versus intrinsic apoptosis pathways in anticancer chemotherapy. *Oncogene* 25, 4798-811.

[64] Stojanov, S. and McDermott, M.F. (2005). The tumour necrosis factor receptor-associated periodic syndrome: current concepts. *Expert Rev. Mol. Med.* 7, 1-18.

[65] Shaulian, E. and Karin, M. (2002). AP-1 as a regulator of cell life and death. *Nat. Cell Biol.* 4, E131-6.

[66] Scaffidi, C., Fulda, S., Srinivasan, A., Friesen, C., Li, F., Tomaselli, K.J., Debatin, K.M., Krammer, P.H., and Peter, M.E. (1998). Two CD95 (APO-1/Fas) signaling pathways. *EMBO J.* 17, 1675-87.

[67] Kim, R., Emi, M., Tanabe, K., and Murakami, S. (2006). Role of the unfolded protein response in cell death. *Apoptosis* 11, 5-13.

[68] Heal, R. and McGivan, J. (1998). Induction of calreticulin expression in response to amino acid deprivation in Chinese hamster ovary cells. *Biochem. J.* 329 (Pt 2), 389-94.

[69] Wong, D.C., Wong, K.T., Lee, Y.Y., Morin, P.N., Heng, C.K., and Yap, M.G. (2006). Transcriptional profiling of apoptotic pathways in batch and fed-batch CHO cell cultures. *Biotechnol. Bioeng.* 94, 373-82.

[70] Szegezdi, E., Fitzgerald, U., and Samali, A. (2003). Caspase-12 and ER-stress-mediated apoptosis: the story so far. *Ann. N. Y. Acad. Sci.* 1010, 186-94.

[71] Malhotra, J.D. and Kaufman, R.J. (2007). The endoplasmic reticulum and the unfolded protein response. *Semin. Cell Dev. Biol.* 18, 716-31.

[72] Fischer, U., Janicke, R.U., and Schulze-Osthoff, K. (2003). Many cuts to ruin: a comprehensive update of caspase substrates. *Cell Death Differ.* 10, 76-100.

[73] Sahara, S., Aoto, M., Eguchi, Y., Imamoto, N., Yoneda, Y., and Tsujimoto, Y. (1999). Acinus is a caspase-3-activated protein required for apoptotic chromatin condensation. *Nature* 401, 168-73.

[74] Kovacsovics, M., Martinon, F., Micheau, O., Bodmer, J.L., Hofmann, K., and Tschopp, J. (2002). Overexpression of Helicard, a CARD-containing helicase cleaved during apoptosis, accelerates DNA degradation. *Curr. Biol.* 12, 838-43.

[75] Sakahira, H., Enari, M., and Nagata, S. (1998). Cleavage of CAD inhibitor in CAD activation and DNA degradation during apoptosis. *Nature* 391, 96-9.

[76] Hockenbery, D. (1995). Defining apoptosis. *Am. J. Pathol.* 146, 16-9.

[77] Wen, L.P., Fahrni, J.A., Troie, S., Guan, J.L., Orth, K., and Rosen, G.D. (1997). Cleavage of focal adhesion kinase by caspases during apoptosis. *J. Biol. Chem.* 272, 26056-61.

[78] Zong, W.X., Ditsworth, D., Bauer, D.E., Wang, Z.Q., and Thompson, C.B. (2004). Alkylating DNA damage stimulates a regulated form of necrotic cell death. *Genes Dev.* 18, 1272-82.

[79] Huerta, S., Goulet, E.J., Huerta-Yepez, S., and Livingston, E.H. (2007). Screening and detection of apoptosis. *J. Surg. Res.* 139, 143-56.

[80] Duriez, P.J. and Shah, G.M. (1997). Cleavage of poly(ADP-ribose) polymerase: a sensitive parameter to study cell death. *Biochem. Cell Biol.* 75, 337-49.

[81] Zhou, B.B., Li, H., Yuan, J., and Kirschner, M.W. (1998). Caspase-dependent activation of cyclin-dependent kinases during Fas-induced apoptosis in Jurkat cells. *Proc. Natl. Acad. Sci. U. S. A.* 95, 6785-90.

[82] Levkau, B., Koyama, H., Raines, E.W., Clurman, B.E., Herren, B., Orth, K., Roberts, J.M., and Ross, R. (1998). Cleavage of p21Cip1/Waf1 and p27Kip1 mediates apoptosis in endothelial cells through activation of Cdk2: role of a caspase cascade. *Mol. Cell* 1, 553-63.

[83] Kurokawa, M. and Kornbluth, S. (2009). Caspases and kinases in a death grip. *Cell* 138, 838-54.

[84] Nahle, Z., Polakoff, J., Davuluri, R.V., McCurrach, M.E., Jacobson, M.D., Narita, M., Zhang, M.Q., Lazebnik, Y., Bar-Sagi, D., and Lowe, S.W. (2002). Direct coupling of the cell cycle and cell death machinery by E2F. *Nat. Cell Biol.* 4, 859-64.

[85] Konishi, Y., Lehtinen, M., Donovan, N., and Bonni, A. (2002). Cdc2 phosphorylation of BAD links the cell cycle to the cell death machinery. *Mol. Cell* 9, 1005-16.

[86] Macey, M.G. (2007) Principles of Flow Cytometry. In *Flow Cytometry: Principles and Applications* (Macey, M.G., ed.) pp. 1-15. Humana Press, Totowa, New Jersey.

[87] Grabarek, J., Amstad, P., and Darzynkiewicz, Z. (2002). Use of fluorescently labeled caspase inhibitors as affinity labels to detect activated caspases. *Hum. Cell* 15, 1-12.

[88] Ekert, P.G., Silke, J., and Vaux, D.L. (1999). Caspase inhibitors. *Cell Death Differ.* 6, 1081-6.

[89] Villas, B.H. (1998). Flow cytometry: an overview. *Cell Vis.* 5, 56-61.

[90] Invitrogen Corp. Fluorescence Tutorials. 2009.

[91] Brink, A., Schulz, B., Kobras, K., Lutz, W.K., and Stopper, H. (2006). Time-dependent effects of sodium arsenite on DNA breakage and apoptosis observed in the comet assay. *Mutat. Res.* 603, 121-8.

[92] Smolewski, P., Grabarek, J., Halicka, H.D., and Darzynkiewicz, Z. (2002). Assay of caspase activation in situ combined with probing plasma membrane integrity to detect three distinct stages of apoptosis. *J. Immunol. Methods* 265, 111-21.

[93] Darzynkiewicz, Z., Juan, G., Li, X., Gorczyca, W., Murakami, T., and Traganos, F. (1997). Cytometry in cell necrobiology: analysis of apoptosis and accidental cell death (necrosis). *Cytometry* 27, 1-20.

[94] Denecker, G., Vercammen, D., Steemans, M., Vanden Berghe, T., Brouckaert, G., Van Loo, G., Zhivotovsky, B., Fiers, W., Grooten, J., Declercq, W., and Vandenabeele, P. (2001). Death receptor-induced apoptotic and necrotic cell death: differential role of caspases and mitochondria. *Cell Death Differ.* 8, 829-40.

[95] Marouga, R., David, S., and Hawkins, E. (2005). The development of the DIGE system: 2D fluorescence difference gel analysis technology. *Anal. Bioanal Chem.* 382, 669-78.

[96] Miller, I., Crawford, J., and Gianazza, E. (2006). Protein stains for proteomic applications: which, when, why? *Proteomics* 6, 5385-408.

[97] Swatton, J.E., Prabakaran, S., Karp, N.A., Lilley, K.S., and Bahn, S. (2004). Protein profiling of human postmortem brain using 2-dimensional fluorescence difference gel electrophoresis (2-D DIGE). *Mol. Psychiatry* 9, 128-43.

[98] Tonge, R., Shaw, J., Middleton, B., Rowlinson, R., Rayner, S., Young, J., Pognan, F., Hawkins, E., Currie, I., and Davison, M. (2001). Validation and development of fluorescence two-dimensional differential gel electrophoresis proteomics technology. *Proteomics* 1, 377-96.

[99] Chen, J.J., Roberson, P.K., and Schell, M.J. (2010). The false discovery rate: a key concept in large-scale genetic studies. *Cancer Control* 17, 58-62.

[100] Mann, M., Hendrickson, R.C., and Pandey, A. (2001). Analysis of proteins and proteomes by mass spectrometry. *Annu. Rev. Biochem.* 70, 437-73.

[101] Griffiths, W.J. and Wang, Y. (2009). Mass spectrometry: from proteomics to metabolomics and lipidomics. *Chem. Soc. Rev.* 38, 1882-96.

[102] Nicotera, P. and Melino, G. (2004). Regulation of the apoptosis-necrosis switch. *Oncogene* 23, 2757-65.

[103] Rasheva, V.I. and Domingos, P.M. (2009). Cellular responses to endoplasmic reticulum stress and apoptosis. *Apoptosis* 14, 996-1007.

[104] Jeong, S.Y. and Seol, D.W. (2008). The role of mitochondria in apoptosis. *BMB Rep.* 41, 11-22.

[105] Bradford, M.M. (1976). A rapid and sensitive method for the quantitation of microgram quantities of protein utilizing the principle of protein-dye binding. *Anal. Biochem.* 72, 248-54.

[106] Twomey, C. and McCarthy, J.V. (2005). Pathways of apoptosis and importance in development. *J. Cell. Mol. Med.* 9, 345-59.

[107] Hayduk, E.J., Choe, L.H., and Lee, K.H. (2004). A two-dimensional electrophoresis map of Chinese hamster ovary cell proteins based on fluorescence staining. *Electrophoresis* 25, 2545-56.

[108] Champion, K.M., Arnott, D., Henzel, W.J., Hermes, S., Weikert, S., Stults, J., Vanderlaan, M., and Krummen, L. (1999). A two-dimensional protein map of Chinese hamster ovary cells. *Electrophoresis* 20, 994-1000.

[109] Van Dyk, D.D., Misztal, D.R., Wilkins, M.R., Mackintosh, J.A., Poljak, A., Varnai, J.C., Teber, E., Walsh, B.J., and Gray, P.P. (2003). Identification of cellular changes associated with increased production of human growth hormone in a recombinant Chinese hamster ovary cell line. *Proteomics* 3,

147-56.

[110] Franklin-Tong, V.E. and Gourlay, C.W. (2008). A role for actin in regulating apoptosis/programmed cell death: evidence spanning yeast, plants and animals. *Biochem. J.* 413, 389-404.

[111] Kueh, H.Y. and Mitchison, T.J. (2009). Structural plasticity in actin and tubulin polymer dynamics. *Science* 325, 960-3.

[112] Moss, D.K. and Lane, J.D. (2006). Microtubules: forgotten players in the apoptotic execution phase. *Trends Cell Biol.* 16, 330-8.

[113] Lin, K.H., Hsiao, G., Shih, C.M., Chou, D.S., and Sheu, J.R. (2009). Mechanisms of resveratrol-induced platelet apoptosis. *Cardiovasc. Res.* 83, 575-85.

[114] Neradil, J., Veselska, R., and Svoboda, A. (2005). The role of actin in the apoptotic cell death of P19 embryonal carcinoma cells. *Int. J. Oncol.* 27, 1013-21.

[115] Mashima, T., Naito, M., and Tsuruo, T. (1999). Caspase-mediated cleavage of cytoskeletal actin plays a positive role in the process of morphological apoptosis. *Oncogene* 18, 2423-30.

[116] Ndozangue-Touriguine, O., Hamelin, J., and Breard, J. (2008). Cytoskeleton and apoptosis. *Biochem. Pharmacol.* 76, 11-8.

[117] Utsumi, T., Sakurai, N., Nakano, K., and Ishisaka, R. (2003). C-terminal 15 kDa fragment of cytoskeletal actin is posttranslationally N-myristoylated upon caspase-mediated cleavage and targeted to mitochondria. *FEBS Lett.* 539, 37-44.

[118] Byun, Y., Chen, F., Chang, R., Trivedi, M., Green, K.J., and Cryns, V.L. (2001). Caspase cleavage of vimentin disrupts intermediate filaments and promotes apoptosis. *Cell Death Differ.* 8, 443-50.

[119] Hofmann, I. and Herrmann, H. (1992). Interference in vimentin assembly in vitro by synthetic peptides derived from the vimentin head domain. *J. Cell. Sci.* 101 (Pt 3), 687-700.

[120] Adrain, C., Duriez, P.J., Brumatti, G., Delivani, P., and Martin, S.J. (2006). The cytotoxic lymphocyte protease, granzyme B, targets the cytoskeleton and perturbs microtubule polymerization dynamics. *J. Biol. Chem.* 281, 8118-25.

[121] Sackett, D.L., Bhattacharyya, B., and Wolff, J. (1985). Tubulin subunit carboxyl termini determine polymerization efficiency. *J. Biol. Chem.* 260, 43-5.

[122] Bhattacharyya, B., Sackett, D.L., and Wolff, J. (1985). Tubulin, hybrid dimers, and tubulin S. Stepwise charge reduction and polymerization. *J. Biol. Chem.* 260, 10208-16.

[123] Ni, M. and Lee, A.S. (2007). ER chaperones in mammalian development and human diseases. *FEBS Lett.* 581, 3641-51.

[124] Okada, T., Yoshida, H., Akazawa, R., Negishi, M., and Mori, K. (2002). Distinct roles of activating transcription factor 6 (ATF6) and double-stranded RNA-activated protein kinase-like endoplasmic reticulum kinase (PERK) in transcription during the mammalian unfolded protein response. *Biochem. J.* 366, 585-94.

[125] Short, D.M., Heron, I.D., Birse-Archbold, J.L., Kerr, L.E., Sharkey, J., and McCulloch, J. (2007). Apoptosis induced by staurosporine alters chaperone and endoplasmic reticulum proteins: Identification by quantitative proteomics. *Proteomics* 7, 3085-96.

[126] Flores-Diaz, M., Higuita, J.C., Florin, I., Okada, T., Pollesello, P., Bergman, T., Thelestam, M., Mori, K., and Alape-Giron, A. (2004). A cellular UDP-glucose deficiency causes overexpression of glucose/oxygen-regulated proteins independent of the endoplasmic reticulum stress elements. *J. Biol. Chem.* 279, 21724-31.

[127] Lee, A.H., Iwakoshi, N.N., and Glimcher, L.H. (2003). XBP-1 regulates a subset of endoplasmic reticulum resident chaperone genes in the unfolded protein response. *Mol. Cell. Biol.* 23, 7448-59.

[128] Kozutsumi, Y., Segal, M., Normington, K., Gething, M.J., and Sambrook, J. (1988). The presence of malfolded proteins in the endoplasmic reticulum signals the induction of glucose-regulated proteins. *Nature* 332, 462-4.

[129] Dorner, A.J., Wasley, L.C., and Kaufman, R.J. (1989). Increased synthesis of secreted proteins induces expression of glucose-regulated proteins in butyrate-treated Chinese hamster ovary cells. *J. Biol. Chem.* 264, 20602-7.

[130] Dukes, A.A., Van Laar, V.S., Cascio, M., and Hastings, T.G. (2008). Changes in endoplasmic reticulum stress proteins and aldolase A in cells exposed to dopamine. *J. Neurochem.* 106, 333-46.

[131] Obeid, M. (2008). ERP57 membrane translocation dictates the immunogenicity of tumor cell death by controlling the membrane translocation of calreticulin. *J. Immunol.* 181, 2533-43.

[132] Gardai, S.J., McPhillips, K.A., Frasch, S.C., Janssen, W.J., Starefeldt, A., Murphy-Ullrich, J.E., Bratton, D.L., Oldenborg, P.A., Michalak, M., and Henson, P.M. (2005). Cell-surface calreticulin initiates clearance of viable or apoptotic cells through trans-activation of LRP on the phagocyte. *Cell* 123, 321-34.

[133] Michalak, M., Groenendyk, J., Szabo, E., Gold, L.I., and Opas, M. (2009). Calreticulin, a multi-process calcium-buffering chaperone of the endoplasmic reticulum. *Biochem. J.* 417, 651-66.

[134] Waser, M., Mesaeli, N., Spencer, C., and Michalak, M. (1997). Regulation of calreticulin gene expression by calcium. *J. Cell Biol.* 138, 547-57.

[135] Wearsch, P.A. and Cresswell, P. (2008). The quality control of MHC class I peptide loading. *Curr. Opin. Cell Biol.* 20, 624-31.

[136] Hebert, D.N. and Molinari, M. (2007). In and out of the ER: protein folding, quality control, degradation, and related human diseases. *Physiol. Rev.* 87, 1377-408.

[137] Qiu, Y. and Michalak, M. (2009). Transcriptional control of the calreticulin gene in health and disease. *Int. J. Biochem. Cell Biol.* 41, 531-8.

[138] Nakamura, K., Bossy-Wetzel, E., Burns, K., Fadel, M.P., Lozyk, M., Goping, I.S., Opas, M., Bleackley, R.C., Green, D.R., and Michalak, M. (2000). Changes in endoplasmic reticulum luminal environment affect cell sensitivity to apoptosis. *J. Cell Biol.* 150, 731-40.

[139] Ozaki, T., Yamashita, T., and Ishiguro, S. (2008). ERp57-associated mitochondrial micro-calpain truncates apoptosis-inducing factor. *Biochim. Biophys. Acta* 1783, 1955-63.

[140] Xu, D., Perez, R.E., Rezaiekhaligh, M.H., Bourdi, M., and Truog, W.E. (2009). Knockdown of ERp57 increases BiP/GRP78 induction and protects against hyperoxia and tunicamycin-induced apoptosis. *Am. J. Physiol. Lung Cell. Mol. Physiol.* 297, L44-51.

[141] Ozaki, T., Yamashita, T., and Ishiguro, S. (2009). Mitochondrial m-calpain plays a role in the release of truncated apoptosis-inducing factor from the mitochondria. *Biochim. Biophys. Acta* 1793, 1848-59.

[142] Huang, Y.H., Chang, A.Y., Huang, C.M., Huang, S.W., and Chan, S.H. (2002). Proteomic analysis of lipopolysaccharide-induced apoptosis in PC12 cells. *Proteomics* 2, 1220-8.

[143] Xing, Z., Li, Z., Chow, V., and Lee, S.S. (2008). Identifying inhibitory threshold values of repressing metabolites in CHO cell culture using multivariate analysis methods. *Biotechnol. Prog.* 24, 675-83.

[144] Gao, S., Zhong, X., Ben, J., Zhu, X., Zheng, Y., Zhuang, Y., Bai, H., Jiang, L., Chen, Y., Ji, Y., and Chen, Q. (2009). Glucose regulated protein 78 prompts scavenger receptor A-mediated secretion of tumor necrosis factor-alpha by Raw 264.7 cells. *Clin. Exp. Pharmacol. Physiol.* .

[145] Dudek, J., Benedix, J., Cappel, S., Greiner, M., Jalal, C., Muller, L., and Zimmermann, R. (2009). Functions and pathologies of BiP and its interaction partners. *Cell Mol. Life Sci.* 66, 1556-69.

[146] Alder, N.N., Shen, Y., Brodsky, J.L., Hendershot, L.M., and Johnson, A.E. (2005). The molecular mechanisms underlying BiP-mediated gating of the Sec61 translocon of the endoplasmic reticulum. *J. Cell Biol.* 168, 389-99.

[147] Shuda, M., Kondoh, N., Imazeki, N., Tanaka, K., Okada, T., Mori, K., Hada, A., Arai, M., Wakatsuki, T., Matsubara, O., Yamamoto, N., and Yamamoto, M. (2003). Activation of the ATF6, XBP1 and grp78 genes in human hepatocellular carcinoma: a possible involvement of the ER stress

pathway in hepatocarcinogenesis. *J. Hepatol.* 38, 605-14.

[148] Prasad, S.C., Soldatenkov, V.A., Kuettel, M.R., Thraves, P.J., Zou, X., and Dritschilo, A. (1999). Protein changes associated with ionizing radiation-induced apoptosis in human prostate epithelial tumor cells. *Electrophoresis* 20, 1065-74.

[149] Gerner, C., Frohwein, U., Gotzmann, J., Bayer, E., Gelbmann, D., Bursch, W., and Schulte-Hermann, R. (2000). The Fas-induced apoptosis analyzed by high throughput proteome analysis. *J. Biol. Chem.* 275, 39018-26.

[150] Yang, Y. and Li, Z. (2005). Roles of heat shock protein gp96 in the ER quality control: redundant or unique function? *Mol. Cells* 20, 173-82.

[151] Strbo, N. and Podack, E.R. (2008). Secreted heat shock protein gp96-Ig: an innovative vaccine approach. *Am. J. Reprod. Immunol.* 59, 407-16.

[152] Randow, F. and Seed, B. (2001). Endoplasmic reticulum chaperone gp96 is required for innate immunity but not cell viability. *Nat. Cell Biol.* 3, 891-6.

[153] Lee, A.S. (2001). The glucose-regulated proteins: stress induction and clinical applications. *Trends Biochem. Sci.* 26, 504-10.

[154] Easton, D.P., Kaneko, Y., and Subjeck, J.R. (2000). The hsp110 and Grp1 70 stress proteins: newly recognized relatives of the Hsp70s. *Cell Stress Chaperones* 5, 276-90.

[155] Park, J., Easton, D.P., Chen, X., MacDonald, I.J., Wang, X.Y., and Subjeck, J.R. (2003). The chaperoning properties of mouse grp170, a member of the third family of hsp70 related proteins. *Biochemistry* 42, 14893-902.

[156] Ellgaard, L. and Ruddock, L.W. (2005). The human protein disulphide isomerase family: substrate interactions and functional properties. *EMBO Rep.* 6, 28-32.

[157] Cai, H., Wang, C.C., and Tsou, C.L. (1994). Chaperone-like activity of protein disulfide isomerase in the refolding of a protein with no disulfide bonds. *J. Biol. Chem.* 269, 24550-2.

[158] Hatahet, F. and Ruddock, L.W. (2007). Substrate recognition by the protein disulfide isomerases. *FEBS J.* 274, 5223-34.

[159] Meimaridou, E., Gooljar, S.B., and Chapple, J.P. (2009). From hatching to dispatching: the multiple cellular roles of the Hsp70 molecular chaperone machinery. *J. Mol. Endocrinol.* 42, 1-9.

[160] Vanmuylder, N., Werry-Huet, A., Rooze, M., and Louryan, S. (2002). Heat shock protein HSP86 expression during mouse embryo development, especially in the germ-line. *Anat. Embryol. (Berl)* 205, 301-6.

[161] Davies, T.H. and Sanchez, E.R. (2005). Fkbp52. *Int. J. Biochem. Cell Biol.* 37, 42-7.

[162] Belay, H.T. and Brown, I.R. (2006). Cell death and expression of heat-shock protein Hsc70 in the hyperthermic rat brain. *J. Neurochem.* 97 Suppl 1, 116-9.

[163] Saito, K., Dai, Y., and Ohtsuka, K. (2005). Enhanced expression of heat shock proteins in gradually dying cells and their release from necrotically dead cells. *Exp. Cell Res.* 310, 229-36.

[164] Powers, M.V., Clarke, P.A., and Workman, P. (2009). Death by chaperone: HSP90, HSP70 or both? *Cell. Cycle* 8, 518-26.

[165] Powers, M.V., Clarke, P.A., and Workman, P. (2008). Dual targeting of HSC70 and HSP72 inhibits HSP90 function and induces tumor-specific apoptosis. *Cancer. Cell.* 14, 250-62.

[166] Rohde, M., Daugaard, M., Jensen, M.H., Helin, K., Nylandsted, J., and Jaattela, M. (2005). Members of the heat-shock protein 70 family promote cancer cell growth by distinct mechanisms. *Genes Dev.* 19, 570-82.

[167] Frese, S., Schaper, M., Kuster, J.R., Miescher, D., Jaattela, M., Buehler, T., and Schmid, R.A. (2003). Cell death induced by down-regulation of heat shock protein 70 in lung cancer cell lines is p53-independent and does not require DNA cleavage. *J. Thorac. Cardiovasc. Surg.* 126, 748-54.

[168] Hostein, I., Robertson, D., DiStefano, F., Workman, P., and Clarke, P.A. (2001). Inhibition of signal transduction by the Hsp90 inhibitor 17-allylamino-17-demethoxygeldanamycin results in cytostasis and apoptosis. *Cancer Res.* 61, 4003-9.

[169] Taherian, A., Krone, P.H., and Ovsenek, N. (2008). A comparison of Hsp90alpha and Hsp90beta interactions with cochaperones and substrates. *Biochem. Cell Biol.* 86, 37-45.

[170] Voellmy, R. and Boellmann, F. (2007). Chaperone regulation of the heat shock protein response. *Adv. Exp. Med. Biol.* 594, 89-99.

[171] King, A. and Gottlieb, E. (2009). Glucose metabolism and programmed cell death: an evolutionary and mechanistic perspective. *Curr. Opin. Cell Biol.* 21, 885-93.

[172] Kim, J.W. and Dang, C.V. (2005). Multifaceted roles of glycolytic enzymes. *Trends Biochem. Sci.* 30, 142-50.

[173] Jeong, D.W., Cho, I.T., Kim, T.S., Bae, G.W., Kim, I.H., and Kim, I.Y. (2006). Effects of lactate dehydrogenase suppression and glycerol-3-phosphate dehydrogenase overexpression on cellular metabolism. *Mol. Cell. Biochem.* 284, 1-8.

[174] Swiderek, H., Logan, A., and Al-Rubeai, M. (2008). Cellular and transcriptomic analysis of NS0 cell response during exposure to hypoxia. *J. Biotechnol.* 134, 103-11.

[175] Kim, J.W. and Dang, C.V. (2006). Cancer's molecular sweet tooth and the Warburg effect. *Cancer Res.* 66, 8927-30.

[176] Schofield, C.J. and Ratcliffe, P.J. (2004). Oxygen sensing by HIF hydroxylases. *Nat. Rev. Mol. Cell Biol.* 5, 343-54.

[177] Marks, D.M. (2003). Equipment design considerations for large scale cell culture. *Cytotechnology* 42, 21-33.

[178] Deshpande, R.R. and Heinzle, E. (2009). Online monitoring of oxygen in spinner flasks. *Biotechnol. Lett.* 31, 665-9.

[179] Gottlieb, E., Armour, S.M., Harris, M.H., and Thompson, C.B. (2003). Mitochondrial membrane potential regulates matrix configuration and cytochrome c release during apoptosis. *Cell Death Differ.* 10, 709-17.

[180] Baricault, L., Segui, B., Guegand, L., Olichon, A., Valette, A., Larminat, F., and Lenaers, G. (2007). OPA1 cleavage depends on decreased mitochondrial ATP level and bivalent metals. *Exp. Cell Res.* 313, 3800-8.

[181] Klimova, T. and Chandel, N.S. (2008). Mitochondrial complex III regulates hypoxic activation of HIF. *Cell Death Differ.* 15, 660-6.

[182] Zamzami, N., Marchetti, P., Castedo, M., Decaudin, D., Macho, A., Hirsch, T., Susin, S.A., Petit, P.X., Mignotte, B., and Kroemer, G. (1995). Sequential reduction of mitochondrial transmembrane potential and generation of reactive oxygen species in early programmed cell death. *J. Exp. Med.* 182, 367-77.

[183] Borutaite, V. and Brown, G.C. (2007). Mitochondrial regulation of caspase activation by cytochrome oxidase and tetramethylphenylenediamine via cytosolic cytochrome c redox state. *J. Biol. Chem.* 282, 31124-30.

[184] Majewski, N., Nogueira, V., Robey, R.B., and Hay, N. (2004). Akt inhibits apoptosis downstream of BID cleavage via a glucose-dependent mechanism involving mitochondrial hexokinases. *Mol. Cell. Biol.* 24, 730-40.

[185] Gottlob, K., Majewski, N., Kennedy, S., Kandel, E., Robey, R.B., and Hay, N. (2001). Inhibition of early apoptotic events by Akt/PKB is dependent on the first committed step of glycolysis and mitochondrial hexokinase. *Genes Dev.* 15, 1406-18.

[186] Feo, S., Arcuri, D., Piddini, E., Passantino, R., and Giallongo, A. (2000). ENO1 gene product binds to the c-myc promoter and acts as a transcriptional repressor: relationship with Myc promoter-binding protein 1 (MBP-1). *FEBS Lett.* 473, 47-52.

[187] Trojanowicz, B., Winkler, A., Hammje, K., Chen, Z., Sekulla, C., Glanz, D., Schmutzler, C., Mentrup, B., Hombach-Klonisch, S., Klonisch, T., Finke, R., Kohrle, J., Dralle, H., and Hoang-Vu, C. (2009). Retinoic acid-mediated down-regulation of ENO1/MBP-1 gene products caused decreased invasiveness of the follicular thyroid carcinoma cell lines. *J. Mol. Endocrinol.* 42, 249-60.

[188] Sen, N., Hara, M.R., Kornberg, M.D., Cascio, M.B., Bae, B.I., Shahani, N., Thomas, B., Dawson, T.M., Dawson, V.L., Snyder, S.H., and Sawa, A. (2008). Nitric oxide-induced nuclear GAPDH activates p300/CBP and mediates apoptosis. *Nat. Cell Biol.* 10, 866-73.

[189] Tajima, H., Tsuchiya, K., Yamada, M., Kondo, K., Katsube, N., and Ishitani, R. (1999). Over-expression of GAPDH induces apoptosis in COS-7 cells transfected with cloned GAPDH cDNAs. *Neuroreport* 10, 2029-33.

[190] Morrison, D.K. (2009). The 14-3-3 proteins: integrators of diverse signaling cues that impact cell fate and cancer development. *Trends Cell Biol.* 19, 16-23.

[191] Bortner, J.D.,Jr, Das, A., Umstead, T.M., Freeman, W.M., Somiari, R., Aliaga, C., Phelps, D.S., and El-Bayoumy, K. (2009). Down-regulation of 14-3-3 isoforms and annexin A5 proteins in lung adenocarcinoma induced by the tobacco-specific nitrosamine NNK in the A/J mouse revealed by proteomic analysis. *J. Proteome Res.* 8, 4050-61.

[192] Kuzelova, K., Grebenova, D., Pluskalova, M., Kavan, D., Halada, P., and Hrkal, Z. (2009). Isoform-specific cleavage of 14-3-3 proteins in apoptotic JURL-MK1 cells. *J. Cell. Biochem.* 106, 673-81.

[193] Nomura, M., Shimizu, S., Sugiyama, T., Narita, M., Ito, T., Matsuda, H., and Tsujimoto, Y. (2003). 14-3-3 Interacts directly with and negatively regulates pro-apoptotic Bax. *J. Biol. Chem.* 278, 2058-65.

[194] Won, J., Kim, D.Y., La, M., Kim, D., Meadows, G.G., and Joe, C.O. (2003). Cleavage of 14-3-3 protein by caspase-3 facilitates bad interaction with Bcl-x(L) during apoptosis. *J. Biol. Chem.* 278, 19347-51.

[195] Park, J., Kim, S., Oh, J.K., Kim, J.Y., Yoon, S.S., Lee, D., and Kim, Y. (2005). Identification of differentially expressed proteins in imatinib mesylate-resistant chronic myelogenous cells. *J. Biochem. Mol. Biol.* 38, 725-38.

[196] Choi, S.L., Choi, Y.S., Kim, Y.K., Sung, N.D., Kho, C.W., Park, B.C., Kim, E.M., Lee, J.H., Kim, K.M., Kim, M.Y., and Myung, P.K. (2006). Proteomic analysis and the antimetastatic effect of N-(4-methyl)phenyl-O-(4-methoxy) phenyl-thionocarbamate-induced apoptosis in human melanoma SK-MEL-28 cells. *Arch. Pharm. Res.* 29, 224-34.

[197] Susantad, T. and Smith, D.R. (2008). siRNA-mediated silencing of the 37/67-kDa high affinity laminin receptor in Hep3B cells induces apoptosis. *Cell. Mol. Biol. Lett.* 13, 452-64.

[198] Kurdoglu, M., Bayram, I., Kolusari, A., Erten, R., Adali, E., Bulut, G., Yildizhan, R., Kurdoglu, Z., Kucukaydin, Z., and Sahin, H.G. (2009). Expression of laminin receptor 1 in gestational trophoblastic diseases and normal placenta and its relationship with the development of postmolar tumors. *Gynecol. Oncol.* 114, 306-9.

[199] Castronovo, V., Claysmith, A.P., Barker, K.T., Cioce, V., Krutzsch, H.C., and Sobel, M.E. (1991). Biosynthesis of the 67 kDa high affinity laminin receptor. *Biochem. Biophys. Res. Commun.* 177, 177-83.

[200] Fatehullah, A., Doherty, C., Pivato, G., Allen, G., Devine, L., Nelson, J., and Timson, D.J. (2009). Interactions of the 67 kDa laminin receptor and its precursor with laminin. *Biosci. Rep.* 30, 73-9.

[201] Kaneda, Y., Kinoshita, K., Sato, M., Saeki, Y., Yamada, R., Wataya-Kaneda, M., and Tanaka, K. (1998). The induction of apoptosis in HeLa cells by the loss of LBP-p40. *Cell Death Differ.* 5, 20-8.

[202] Gerner, C., Gotzmann, J., Frohwein, U., Schamberger, C., Ellinger, A., and Sauermann, G. (2002). Proteome analysis of nuclear matrix proteins during apoptotic chromatin condensation. *Cell Death Differ.* 9, 671-81.

[203] Carlage, T., Hincapie, M., Zang, L., Lyubarskaya, Y., Madden, H., Mhatre, R., and Hancock, W.S. (2009). Proteomic profiling of a high-producing Chinese hamster ovary cell culture. *Anal. Chem.* 81, 7357-62.

[204] Le Mercier, M., Fortin, S., Mathieu, V., Kiss, R., and Lefranc, F. (2009). Galectins and Gliomas. *Brain Pathol.* .

[205] Yang, R.Y. and Liu, F.T. (2003). Galectins in cell growth and apoptosis. *Cell Mol. Life Sci.* 60, 267-76.

[206] Lange, F., Brandt, B., Tiedge, M., Jonas, L., Jeschke, U., Pohland, R., and Walzel, H. (2009). Galectin-1 induced activation of the mitochondrial apoptotic pathway: evidence for a connection between death-receptor and mitochondrial pathways in human Jurkat T lymphocytes. *Histochem. Cell Biol.* 132, 211-23.

[207] Brandt, B., Buchse, T., Abou-Eladab, E.F., Tiedge, M., Krause, E., Jeschke, U., and Walzel, H. (2008). Galectin-1 induced activation of the apoptotic death-receptor pathway in human Jurkat T lymphocytes. *Histochem. Cell Biol.* 129, 599-609.

[208] Yoshii, T., Fukumori, T., Honjo, Y., Inohara, H., Kim, H.R., and Raz, A. (2002). Galectin-3 phosphorylation is required for its anti-apoptotic function and cell cycle arrest. *J. Biol. Chem.* 277, 6852-7.

[209] Yu, F., Finley, R.L.,Jr, Raz, A., and Kim, H.R. (2002). Galectin-3 translocates to the perinuclear membranes and inhibits cytochrome c release from the mitochondria. A role for synexin in galectin-3 translocation. *J. Biol. Chem.* 277, 15819-27.

[210] Eismann, T., Huber, N., Shin, T., Kuboki, S., Galloway, E., Wyder, M., Edwards, M.J., Greis, K.D., Shertzer, H.G., Fisher, A.B., and Lentsch, A.B. (2009). Peroxiredoxin-6 protects against mitochondrial dysfunction and liver injury during ischemia-reperfusion in mice. *Am. J. Physiol. Gastrointest. Liver Physiol.* 296, G266-74.

[211] Yoon, S., Cong, W.T., Bang, Y., Lee, S.N., Yoon, C.S., Kwack, S.J., Kang, T.S., Lee, K.Y., Choi, J.K., and Choi, H.J. (2009). Proteome response to ochratoxin A-induced apoptotic cell death in mouse hippocampal HT22 cells. *Neurotoxicology* 30, 666-76.

[212] Manevich, Y. and Fisher, A.B. (2005). Peroxiredoxin 6, a 1-Cys peroxiredoxin, functions in antioxidant defense and lung phospholipid metabolism. *Free Radic. Biol. Med.* 38, 1422-32.

[213] Kawaai, K., Hisatsune, C., Kuroda, Y., Mizutani, A., Tashiro, T., and Mikoshiba, K. (2009). 80K-H interacts with inositol 1,4,5-trisphosphate (IP3) receptors and regulates IP3-induced calcium release activity. *J. Biol. Chem.* 284, 372-80.

[214] Xu, C., Zhang, X., Yu, C., Lu, G., Chen, S., Xu, L., Ding, W., Shi, Q., and Li, Y. (2009). Proteomic analysis of hepatic ischemia/reperfusion injury and ischemic preconditioning in mice revealed the protective role of ATP5beta. *Proteomics* 9, 409-19.

[215] Shin, Y.K., Yoo, B.C., Chang, H.J., Jeon, E., Hong, S.H., Jung, M.S., Lim, S.J., and Park, J.G. (2005). Down-regulation of mitochondrial F1F0-ATP synthase in human colon cancer cells with induced 5-fluorouracil resistance. *Cancer Res.* 65, 3162-70.

[216] Chen, X., Wang, Y., Li, J., Jiang, A., Cheng, Y., and Zhang, W. (2009). Mitochondrial proteome during salt stress-induced programmed cell death in rice. *Plant Physiol. Biochem.* 47, 407-15.

[217] Lee, M.S., Kim, K.W., Kim, Y.H., and Lee, G.M. (2003). Proteome analysis of antibody-expressing CHO cells in response to hyperosmotic pressure. *Biotechnol. Prog.* 19, 1734-41.

[218] Yee, J.C., de Leon Gatti, M., Philp, R.J., Yap, M., and Hu, W.S. (2008). Genomic and proteomic exploration of CHO and hybridoma cells under sodium butyrate treatment. *Biotechnol. Bioeng.* 99, 1186-204.

[219] Pascoe, D.E., Arnott, D., Papoutsakis, E.T., Miller, W.M., and Andersen, D.C. (2007). Proteome analysis of antibody-producing CHO cell lines with different metabolic profiles. *Biotechnol. Bioeng.* 98, 391-410.

[220] Naryzhny, S.N. and Lee, H. (2001). Protein profiles of the Chinese hamster ovary cells in the resting and proliferating stages. *Electrophoresis* 22, 1764-75.

[221] Baik, J.Y. and Lee, G.M. (2010). A DIGE approach for the assessment of differential expression of the CHO proteome under sodium butyrate addition: Effect of Bcl-x(L) overexpression. *Biotechnol. Bioeng.* 105, 358-67.

[222] Wlaschin, K.F., Nissom, P.M., Gatti Mde, L., Ong, P.F., Arleen, S., Tan, K.S., Rink, A., Cham, B., Wong, K., Yap, M., and Hu, W.S. (2005). EST sequencing for gene discovery in Chinese hamster ovary cells. *Biotechnol. Bioeng.* 91, 592-606.

[223] Ossina, N.K., Cannas, A., Powers, V.C., Fitzpatrick, P.A., Knight, J.D., Gilbert, J.R., Shekhtman, E.M., Tomei, L.D., Umansky, S.R., and Kiefer, M.C. (1997). Interferon-gamma modulates a p53-independent apoptotic pathway and apoptosis-related gene expression. *J. Biol. Chem.* 272, 16351-7.

[224] Spanaus, K.S., Schlapbach, R., and Fontana, A. (1998). TNF-alpha and IFN-gamma render microglia sensitive to Fas ligand-induced apoptosis by induction of Fas expression and down-regulation of Bcl-2 and Bcl-xL. *Eur. J. Immunol.* 28, 4398-408.

[225] Thiede, B., Kretschmer, A., and Rudel, T. (2006). Quantitative proteome analysis of CD95 (Fas/Apo-1)-induced apoptosis by stable isotope labeling with amino acids in cell culture, 2-DE and MALDI-MS. *Proteomics* 6, 614-22.

[226] Dong, H., Ying, T., Li, T., Cao, T., Wang, J., Yuan, J., Feng, E., Han, B., Hua, F., Yang, Y., Yuan, J., Wang, H., and Xu, C. (2006). Comparative proteomic analysis of apoptosis induced by sodium selenite in human acute promyelocytic leukemia NB4 cells. *J. Cell. Biochem.* 98, 1495-506.

[227] Schmidt, F., Hustoft, H.K., Strozynski, M., Dimmler, C., Rudel, T., and Thiede, B. (2007). Quantitative proteome analysis of cisplatin-induced apoptotic Jurkat T cells by stable isotope labeling with amino acids in cell culture, SDS-PAGE, and LC-MALDI-TOF/TOF MS. *Electrophoresis* 28, 4359-68.

[228] Thiede, B. and Rudel, T. (2004). Proteome analysis of apoptotic cells. *Mass Spectrom. Rev.* 23, 333-49.

[229] Thiede, B., Dimmler, C., Siejak, F., and Rudel, T. (2001). Predominant identification of RNA-binding proteins in Fas-induced apoptosis by proteome analysis. *J. Biol. Chem.* 276, 26044-50.

Appendix A. Flow Cytometry Data Analysis

A.1 Sample Flow Cytometry Dot Plot Raw Data

For each spinner flask, FCM testing has been done throughout the cultivation period, measuring FLICA and propidium iodide (PI) intensities. Resulting data were represented by dot plots, each containing 20000 data points (which correspond to cells). Thresholds were set based on single-color control samples from day 2.5 of each spinner flask and applied to the remaining FCM data collected. A sample set of FCM dot plots for each FCM methods (caspase 3, caspase 8 and caspase 9 analyses) was shown.

A.1.1 FCM Caspase 3 Assay for a Culture in run A over Time

FCM analyses measuring the activation of caspase 3/7 and PI permeability were performed to detect and monitor the progress of apoptosis within cultures. Since executioner caspases such as caspase 3 and 7 are common proteins involved in the execution of apoptosis despite the initial trigger, it is the main method for detecting apoptotic cell death in this study. Sample dot plots showing results of FCM caspase 3 analysis for a single spinner flask during the run A time course experiment were displayed in Figure A-1 below. Table A-1 displays the thresholds for FLICA and PI intensity used in the four cultures of run A.

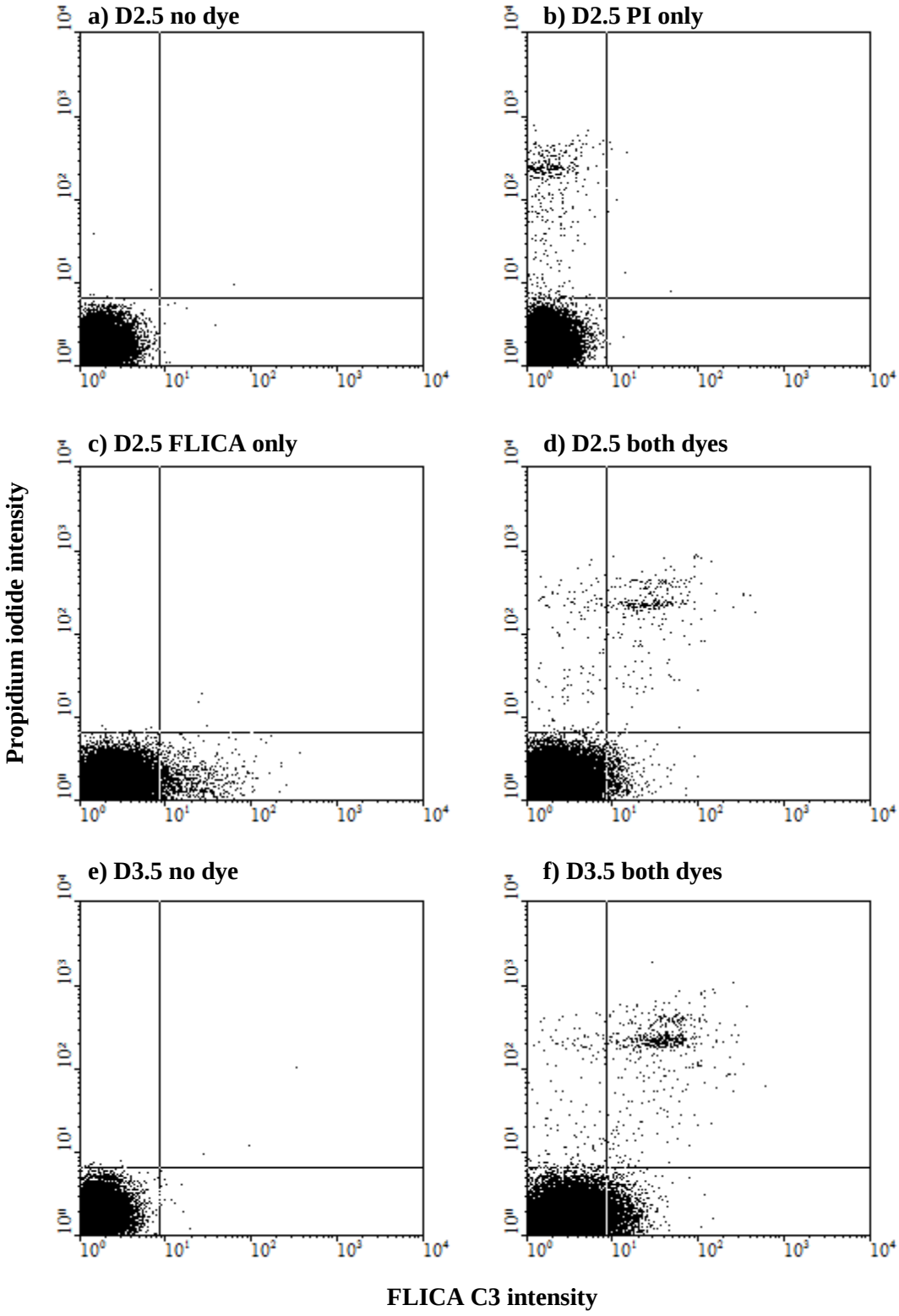
a) D2.5 no dye
b) D2.5 PI only
c) D2.5 FLICA only
d) D2.5 both dyes
e) D3.5 no dye
f) D3.5 both dyes
Propidium iodide intensity
FLICA C3 intensity

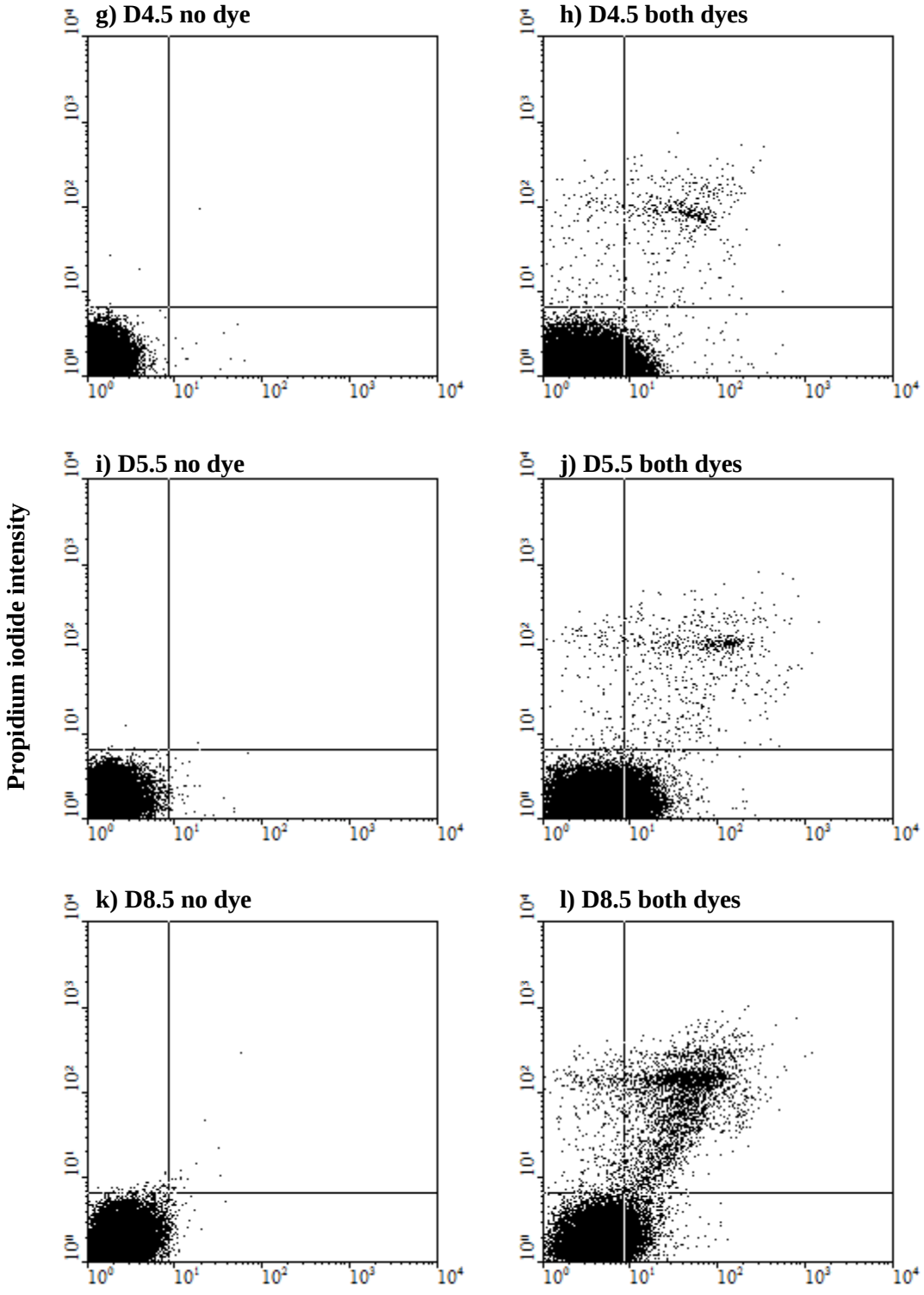
g) D4.5 no dye
h) D4.5 both dyes
i) D5.5 no dye
j) D5.5 both dyes
k) D8.5 no dye
l) D8.5 both dyes
Propidium iodide intensity
FLICA C3 intensity

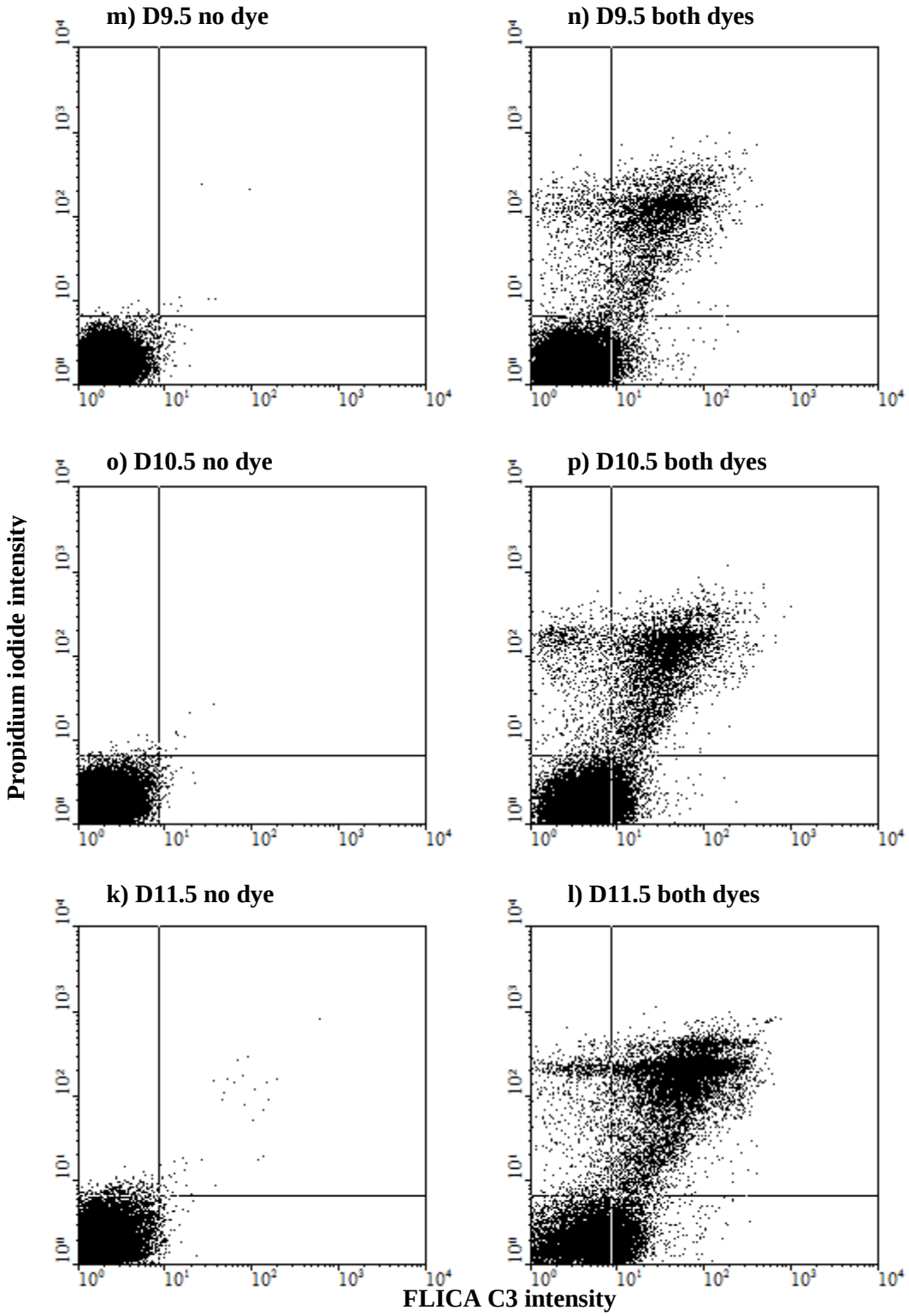

Figure A-1. FCM plots showing raw caspase 3 assay data from a sample culture in run A.
Abbreviations: C3, caspase 3; D, day; PI, propidium iodide.

Table A-1. Intensity thresholds for FCM caspase 3 assay in Run A

Culture replicates	FLICA caspase 3 threshold	Propidium iodide threshold
1	228	208
2	240	208
3	248	240
4	252	220

A.1.2 FCM Caspase 8 and FCM Caspase 9 Assays for a Culture in run B over Time

Levels of activated caspase 8 and caspase 9 were used to differentiate the type of apoptotic pathway triggered in CHO cultures, namely extrinsic and intrinsic pathway respectively. Figure A-2 shows the list of dot plots obtained from the FCM caspase 8 assays and Figure A-3 lists the figures for the FCM caspase 9 assays.

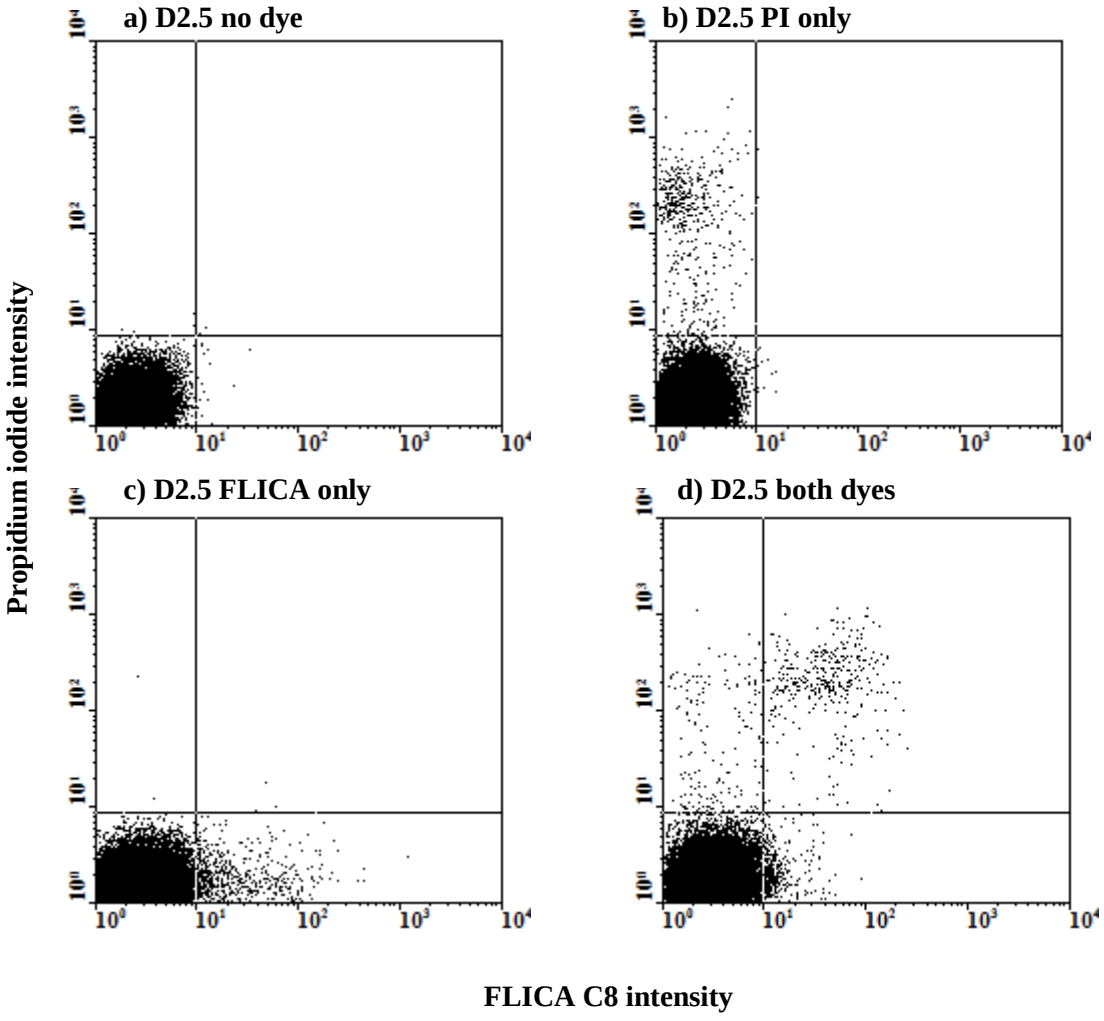

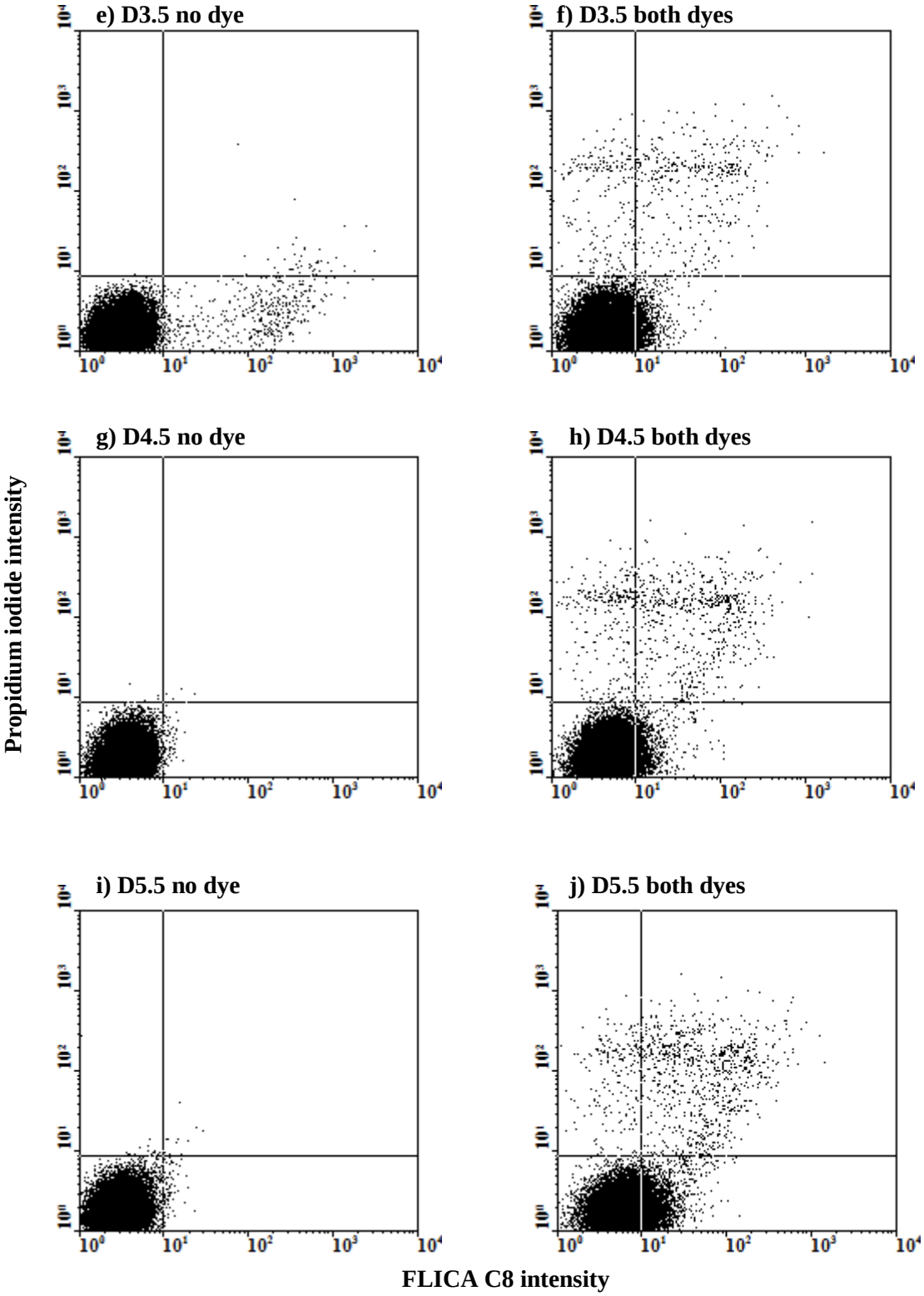
e) D3.5 no dye
f) D3.5 both dyes
g) D4.5 no dye
h) D4.5 both dyes
i) D5.5 no dye
j) D5.5 both dyes
Propidium iodide intensity
FLICA C8 intensity

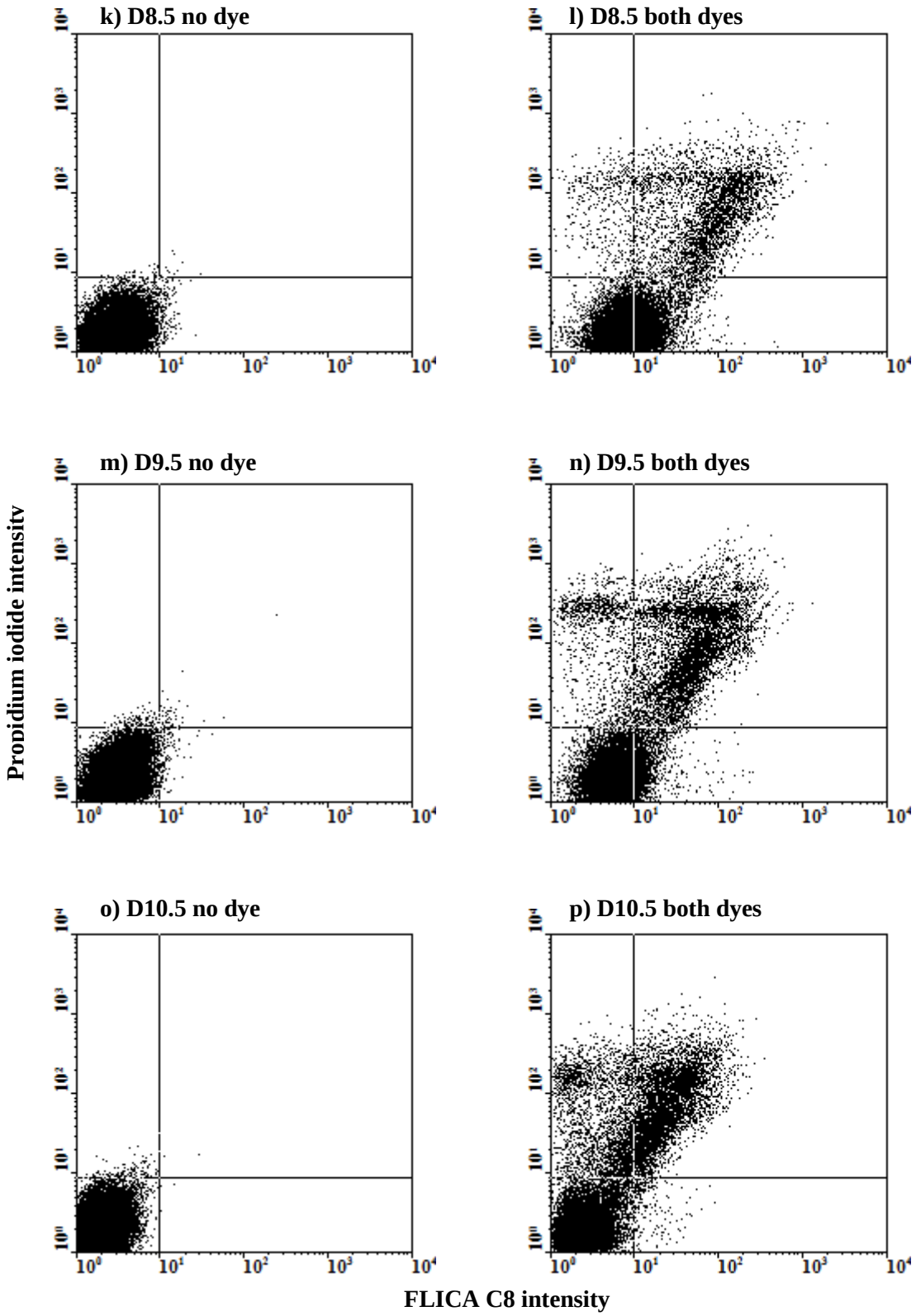
k) D8.5 no dye
l) D8.5 both dyes
m) D9.5 no dye
n) D9.5 both dyes
o) D10.5 no dye
p) D10.5 both dyes
Propidium iodide intensity
FLICA C8 intensity

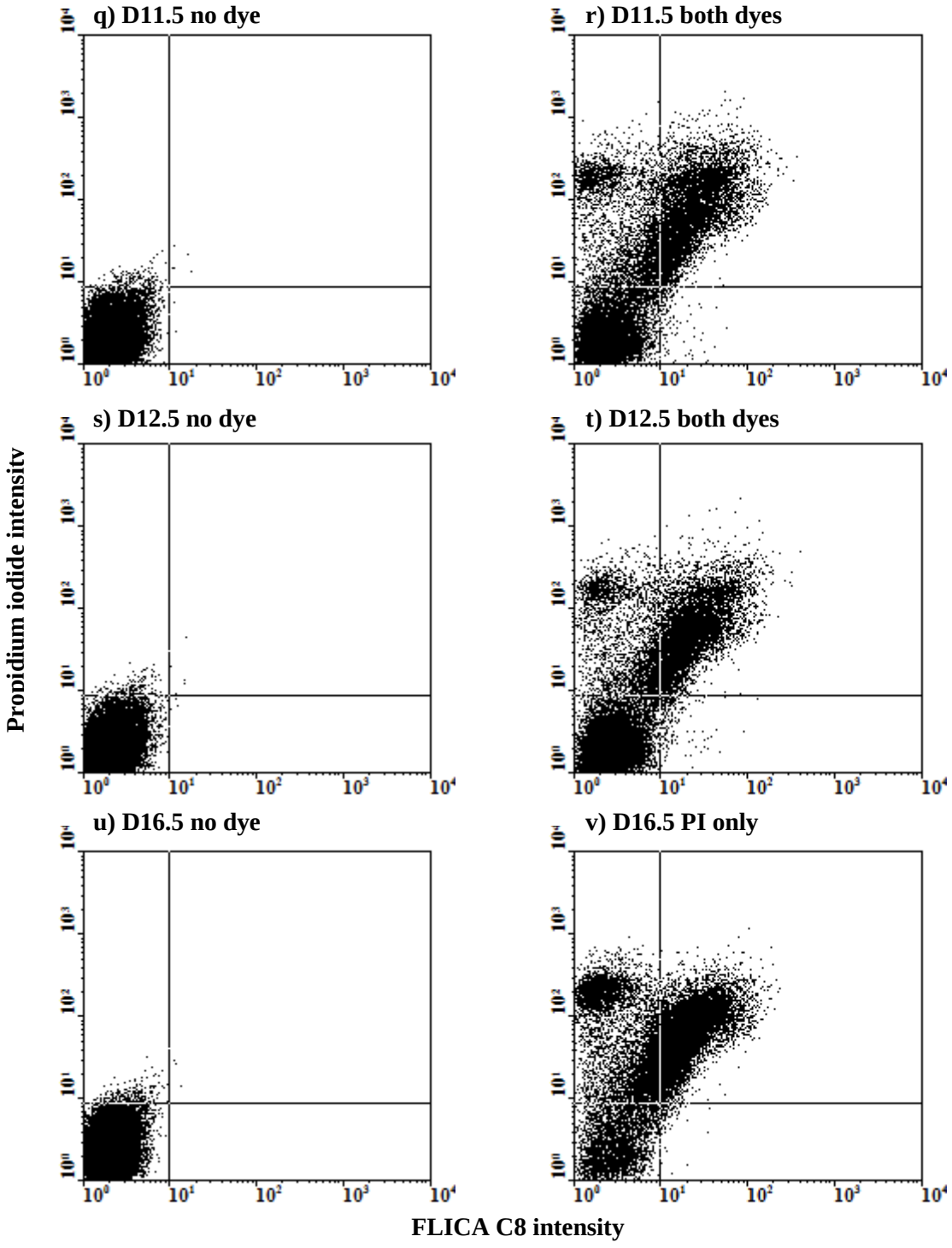

Figure A-2. FCM plots showing raw caspase 8 assay data from a sample culture in run B.
Abbreviations: D, day; PI, propidium iodide.

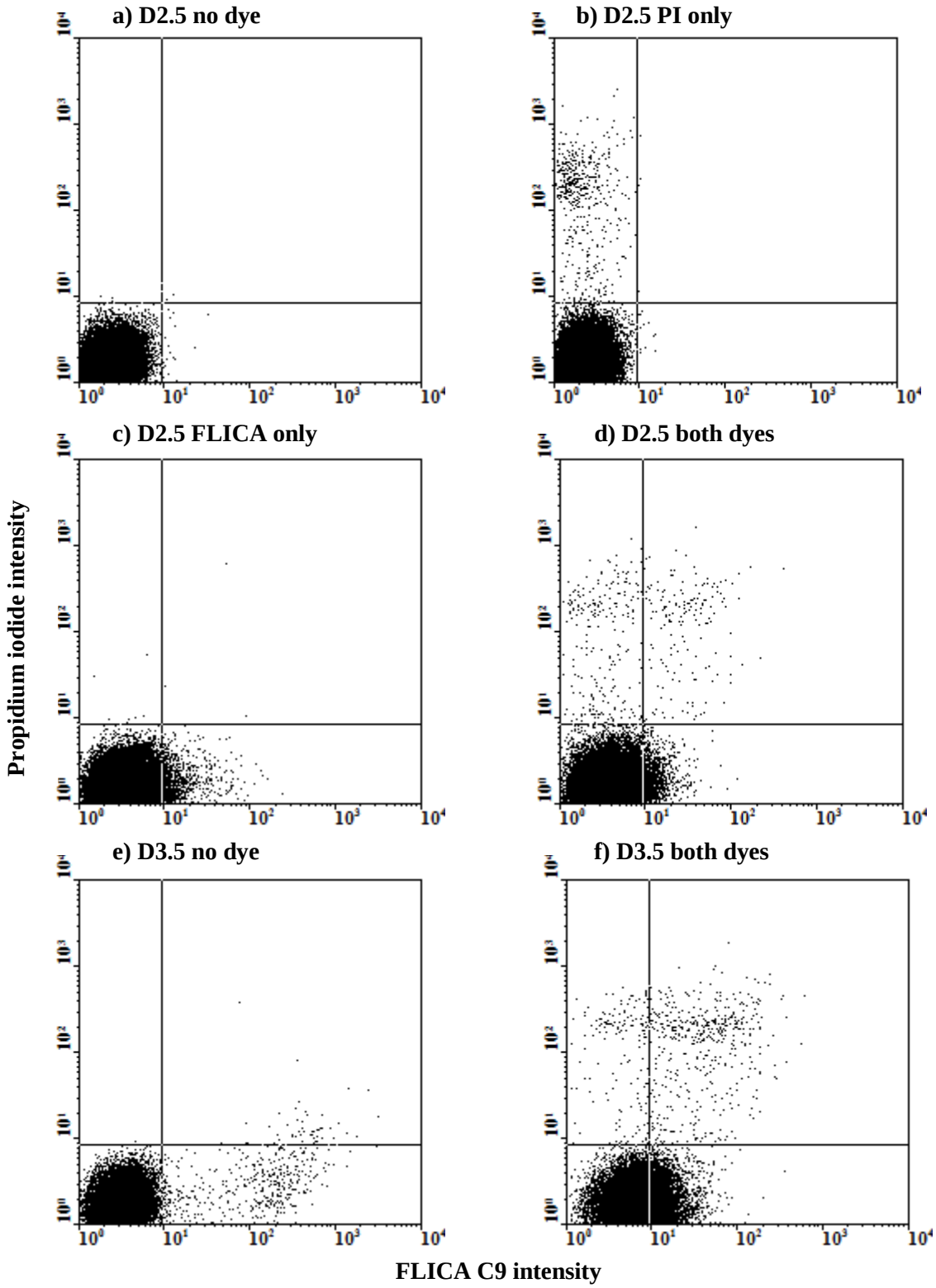
a) D2.5 no dye
b) D2.5 PI only
c) D2.5 FLICA only
d) D2.5 both dyes
e) D3.5 no dye
f) D3.5 both dyes
Propidium iodide intensity
FLICA C9 intensity

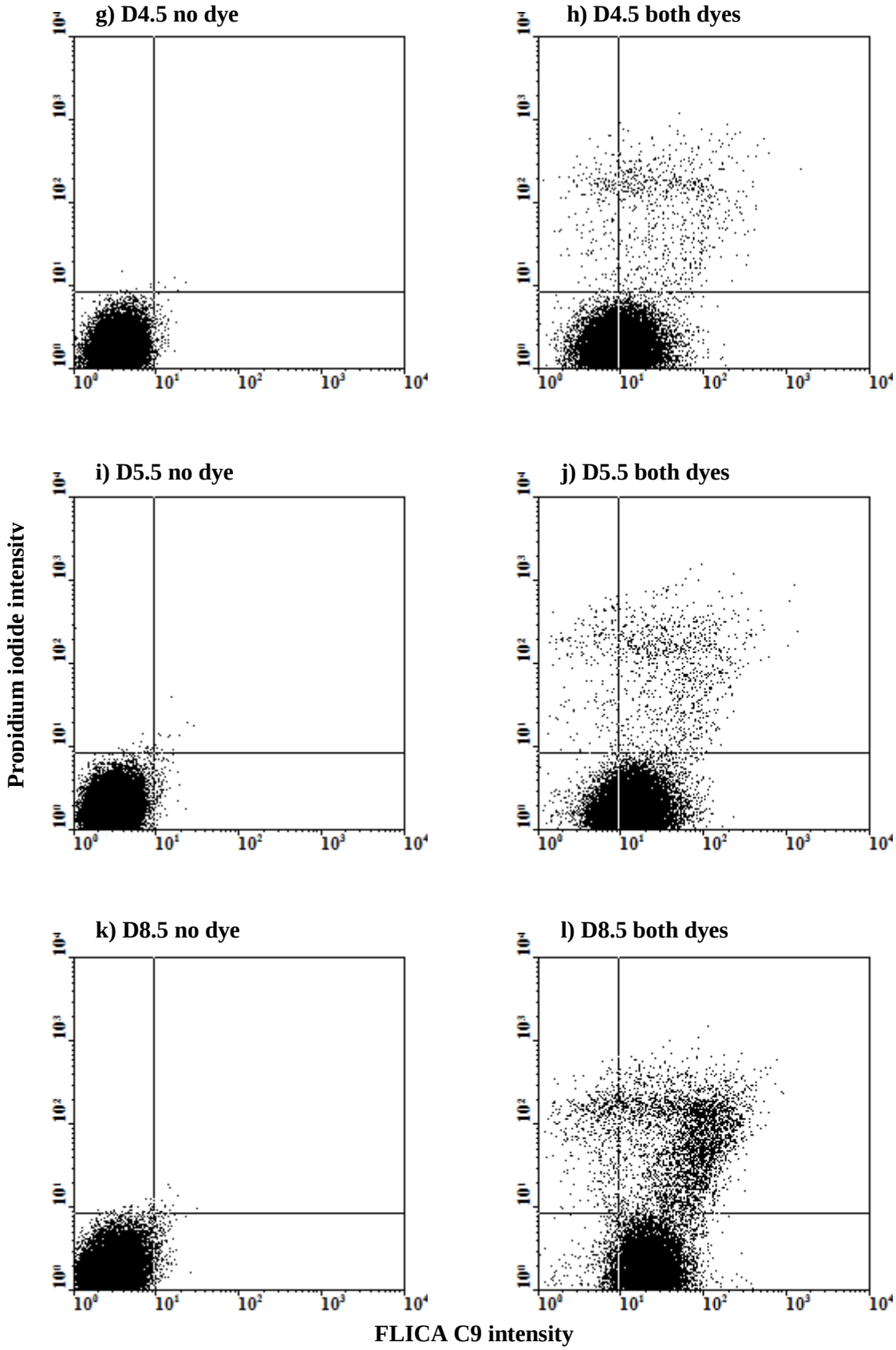
g) D4.5 no dye
h) D4.5 both dyes
i) D5.5 no dye
j) D5.5 both dyes
k) D8.5 no dye
l) D8.5 both dyes
Propidium iodide intensity
FLICA C9 intensity

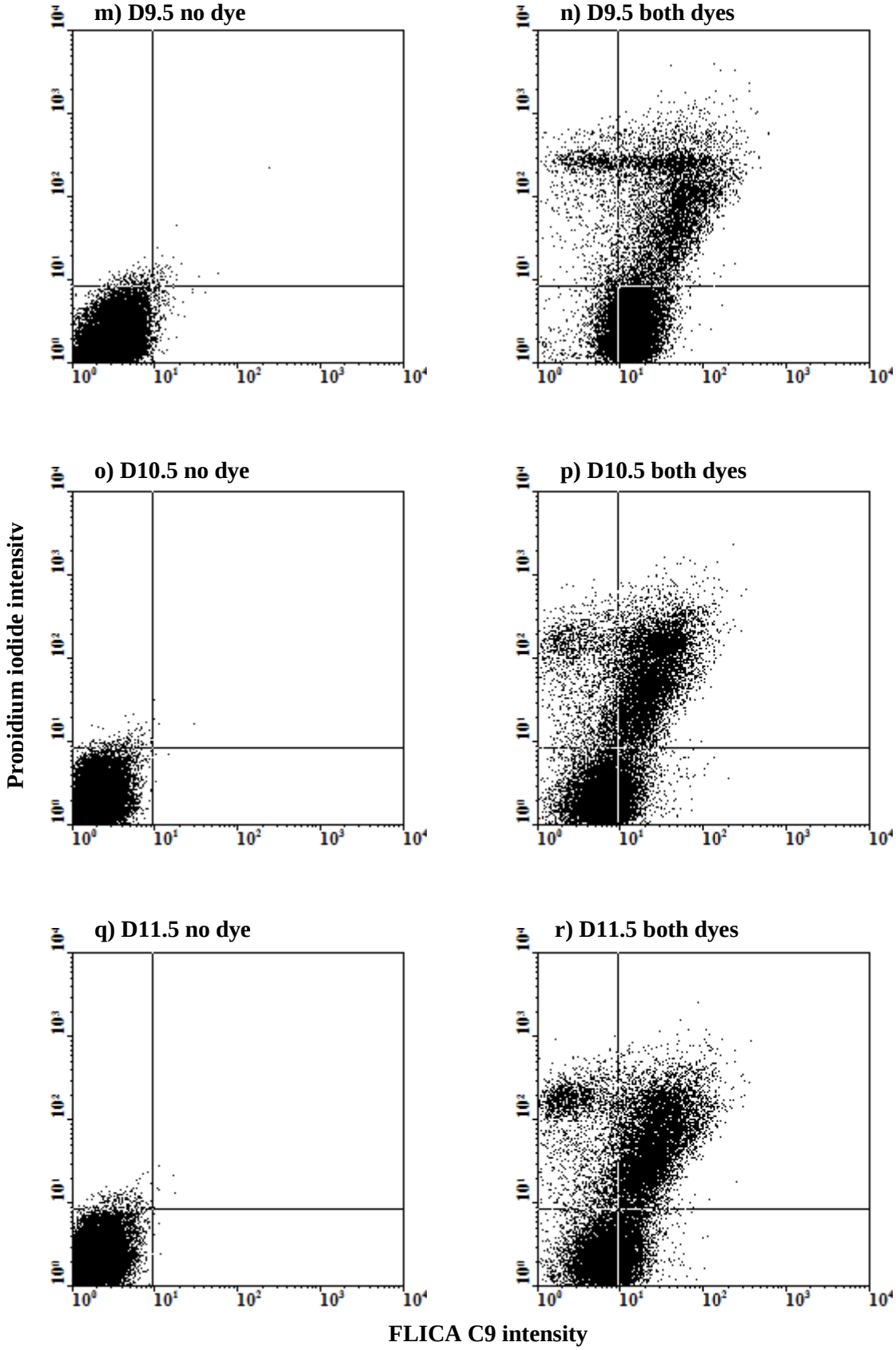
m) D9.5 no dye
n) D9.5 both dyes
o) D10.5 no dye
p) D10.5 both dyes
q) D11.5 no dye
r) D11.5 both dyes
Propidium iodide intensity
FLICA C9 intensity

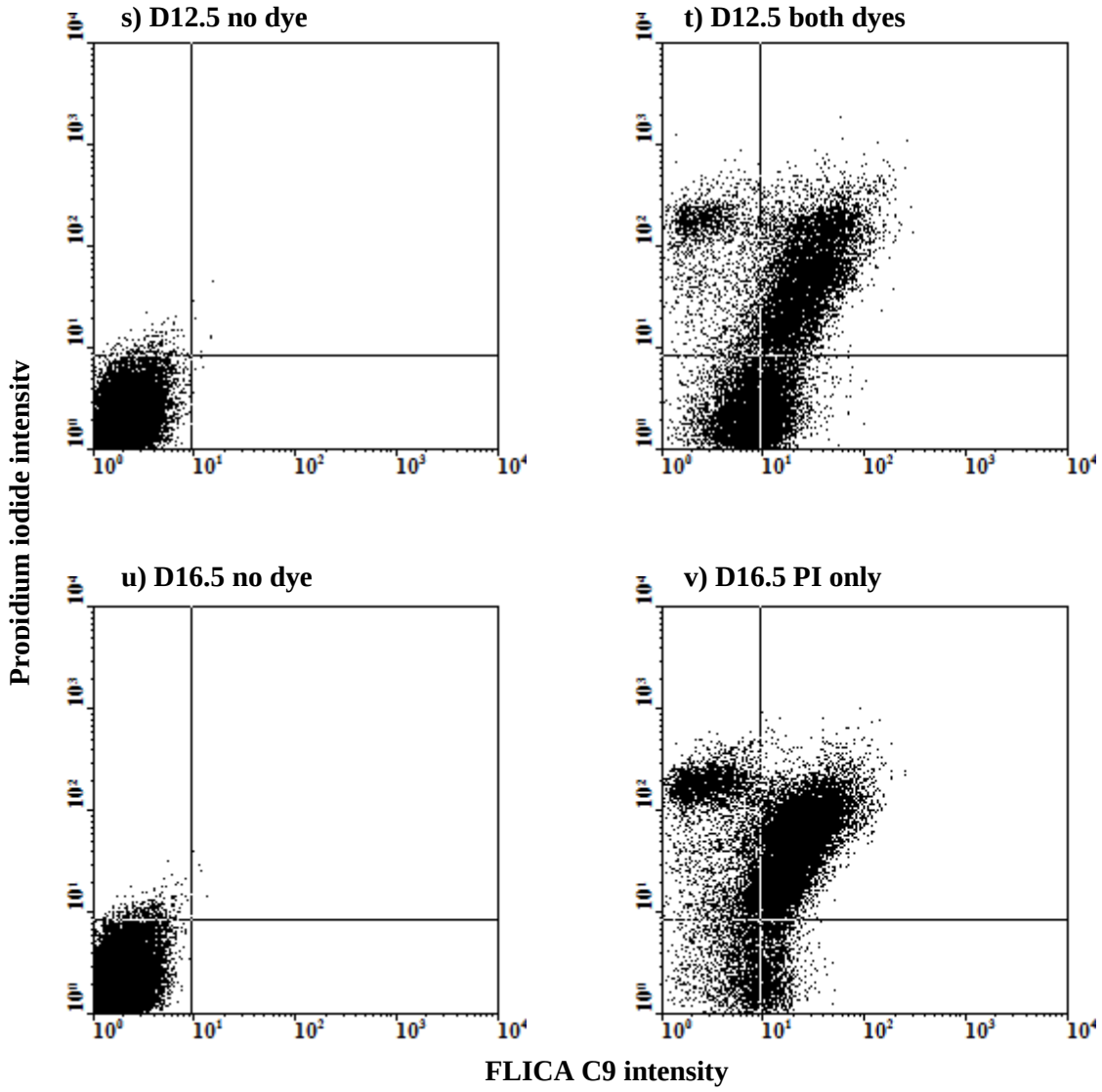

Figure A-3. FCM plots showing raw caspase 9 assay data from a sample culture in run B.
Abbreviations: D, day; PI, propidium iodide.

The following two tables separately display the thresholds for FLICA and PI intensity used in the four cultures of run B. As the name implies, FLICA in the FCM caspase 8 method targets and measures the amount of activated caspase 8, while it corresponds to caspase 9 in the FCM caspase 9 method. Based on the FLICA and PI intensities, cells can be classified into four different subpopulations: C-PI-, C+PI-, C+PI+ and C-PI-.

Table A-2. Intensity thresholds for FCM caspase 8 assay in Run B

Culture replicates	FLICA caspase 8 threshold	Propidium iodide threshold
1	256	240
2	236	236
3	260	236
4	268	244

Table A-3. Intensity thresholds for FCM caspase 9 assay in Run B

Culture replicates	FLICA caspase 9 threshold	Propidium iodide threshold
1	252	236
2	252	232
3	264	252
4	256	248

A.2 Alternative Display of FCM Caspase 8 and FCM Caspase 9 Results

The following figures show the proportion of the four cell subpopulations in the cultures over time based on the levels of activated caspase 8 and caspase 9. Figure 2-8 is an alternative display of the combined data of Figure A-4a and A-4b below.

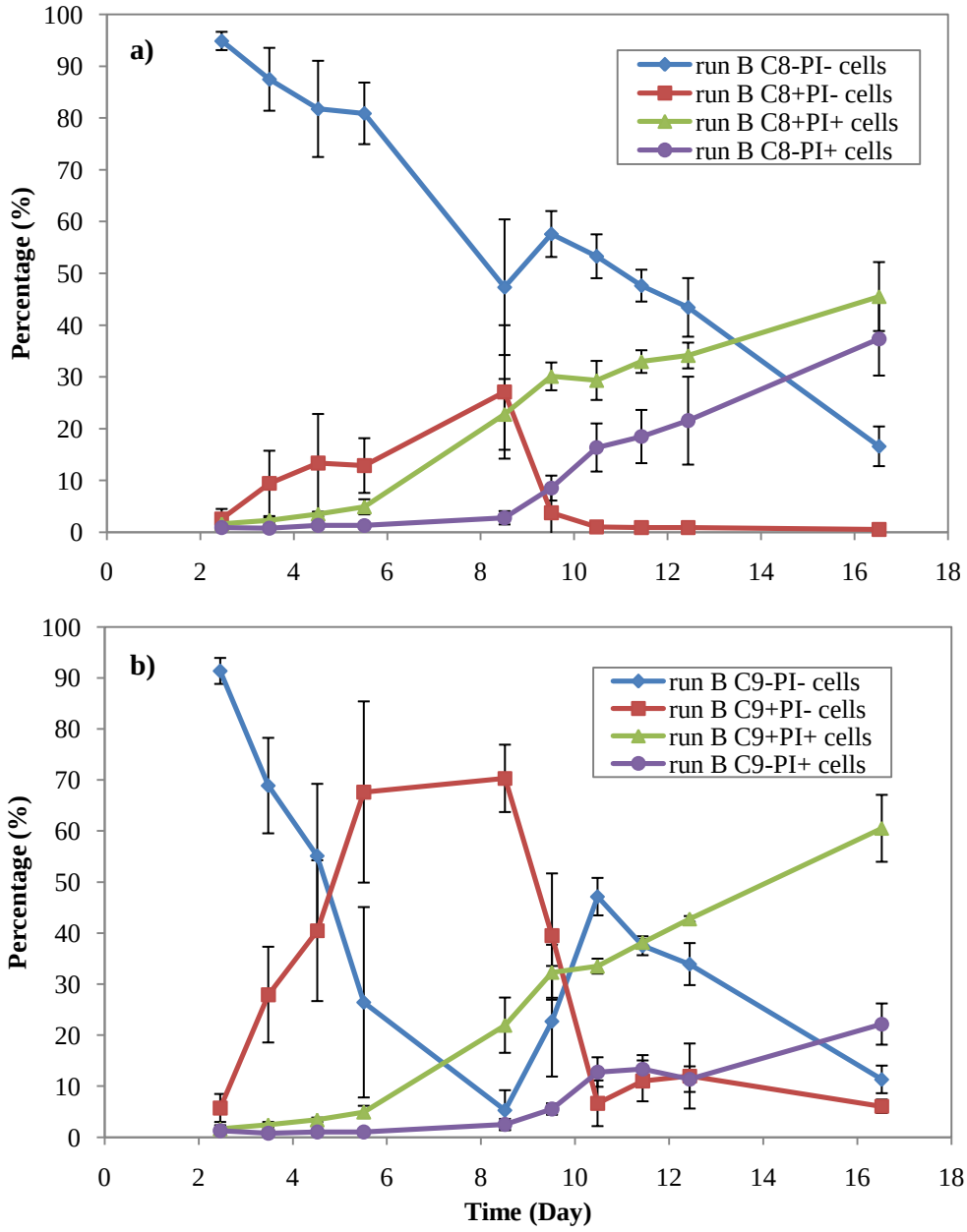

Figure A-4. Comparison between the four subpopulations based on a) caspase 8 and b) caspases 9 flow cytometry assays.

Appendix B. Proteomic Raw Data and Analysis

B.1 Statistical Analyses using the Programming Language R

Before extracting the raw standardized abundance data of all detected spots from DeCyder software, all 12 gels were analyzed together in BVA to match spots across images and assign master spot numbers that could be shared between gels. Abundance data for all protein spots was exported to R for t-test analysis using the script in section B.1.1.

For the one way ANOVA p-value extraction, the post matching BVA file was analyzed without the DeCyder built in FDR correction. The p-values calculated by the DeCyder software were imported into R and FDR corrected with R script as in section B.1.2.

B.1.1 R Scripts for T-tests Calculation

```
# Function myTTest2
# purpose: calculate t-test p-values and average ratios for each protein spot
# Abundance data table X: each row = 1 protein spot and 1st column = master spot ID
# eqVar: Boolean. TRUE = t-test variance equals, FALSE = unequal variance
# pair: Boolean. TRUE = paired t-test; FALSE = unpaired t-test will be calculated
myTTest2 <- function (X, eqVar, pair){
        ctrlInd<- c(1:4)
        treatedInd <- c(5:8)
        NApairs <- (is.na(X[treatedInd]))|(is.na(X[ctrlInd]))
        if (sum(NApairs)> 2) {    # 4 pairs, if less than 2 pairs, t.test won't work.
                return (c(NA, NA))
        }
        else{
                obj<- t.test(X[treatedInd], X[ctrlInd], var.equal = eqVar, paired = pair)
                if (pair==T){
                        temp <- 10^obj$estimate
                        ind <- which(temp <1)
                        temp [ind] <- -1/temp[ind]
                        return (c(obj$p.value, temp))}
                else  # not tested yet
                        return (obj$p.value, 10^(obj$estimate[2]/obj$estimate[1]))
        }
}
```

```
# Read in abundance data table from file into a table in R
loc <- "C:\\Users\\Catherine Wei\\Documents\\My Dropbox\\bunneh\\CHO\\Gel Images &
        data\\DIGE\\Run 8 - DIGE Apr 1 2009\\Analysis\\Run8_allProteins_3.txt"
channelNames <- read.table(loc, nrows = 1, sep ="\t")  # read in data table headings separately
blah <- read.table(loc, skip = 5, sep ="\t", header = T)    # raw abundance data
blah <-  as.matrix(blah)
channelNames <- as.matrix (channelNames)
dimnames(blah)[[2]] <- channelNames

# only obtained standardized abundancies and removed volumes columns
oddCol <- seq(1, 49, by = 2)
abund <- blah [,oddCol]

# reoder abundancies columns
orderNew <- c(1,2,3,5,4,6,7,8,9,11,10,12,13,15,14,16,17,19,18,21,20,22,23,25,24)
abund <- abund [, orderNew]

# Convert negatives abundancies to REAL abun values > 0
baddies <- which(abund<0)
abund[baddies] <- -1/abund[baddies]
unloggedAbund <- abund

# For calcualting t-test, log the standardized abundances
abund[,2:25]<- log10(abund[,2:25])

# Indices for the gel images involved in different t-tests.  Ex. D2D4 = t-test comparing day 4.5 to day
# 2.5.  Ctrl_D2DX = Day 2 control data….for X = 4.5, 5.5 or 8.5
Ctrl_D2D4 <- c(1,7,13,19) +1
Ctrl_D2D5 <- Ctrl_D2D4 + 2
Ctrl_D2D8 <- Ctrl_D2D5 + 2
allCtrl <- c(Ctrl_D2D4, Ctrl_D2D5, Ctrl_D2D8)
D4 <- Ctrl_D2D4+1
D5 <- Ctrl_D2D5+1
D8 <- Ctrl_D2D8+1

############################## T-Test pvalues ####################
# Assume un/equal variable, PAIRED t-test
# pVal [,1:2] where colume 1 = p values; colume2 = average ratios/fold change
pVal_D2D4 <- apply(abund[ , c(Ctrl_D2D4, D4)], 1, FUN = myTTest2, eqVar = F, pair = T)
pVal_D2D5 <- apply(abund[ , c(Ctrl_D2D5, D5)], 1, FUN = myTTest2, eqVar = F, pair = T)
pVal_D2D8 <- apply(abund[ , c(Ctrl_D2D8, D8)], 1, FUN = myTTest2, eqVar = F, pair = T)
pVal_D4D5 <- apply(abund[ , c(D4, D5)], 1, FUN = myTTest2, eqVar = F, pair = T)
pVal_D5D8 <- apply(abund[ , c(D5, D8)], 1, FUN = myTTest2, eqVar = F, pair = T)
pVal_D4D8 <- apply(abund[ , c(D4, D8)], 1, FUN = myTTest2, eqVar = F, pair = T)

################## False Discovery Rate ######################
fdr_D2D4 <- p.adjust(pVal_D2D4[1,], method ="fdr")
fdr_D2D5 <- p.adjust(pVal_D2D5[1,], method ="fdr")
fdr_D2D8 <- p.adjust(pVal_D2D8[1,], method ="fdr")
fdr_D4D5 <- p.adjust(pVal_D4D5[1,], method ="fdr")
fdr_D5D8 <- p.adjust(pVal_D5D8[1,], method ="fdr")
```

```
fdr_D4D8 <- p.adjust(pVal_D4D8[1,], method ="fdr")

######################## Write results to file ########################
result <- cbind(abund[,1], t(pVal_D2D4), fdr_D2D4, t(pVal_D2D5), fdr_D2D5,
        t(pVal_D2D8), fdr_D2D8, t(pVal_D4D5), fdr_D4D5, t(pVal_D5D8), fdr_D5D8,
        t(pVal_D4D8), fdr_D4D8)
colnames(result) <- c("Master No.", "pVal D2D4", "avRatio D2D4", "fdr D2D4", "pVal D2D5",
        "avRatio D2D5", "fdr D2D5", "pVal D2D8", "avRatio D2D8", "fdr D2D8", "pVal D4D5",
        "avRatio D4D5", "fdr D4D5", "pVal D5D8", "avRatio D5D8", "fdr D5D8", "pVal D4D8",
        "avRatio D4D8", "fdr D4D8")
write.table(result, paste(loc, "\\Run 8 pVal fdr ratios.txt", sep = ""), row.names = F, sep = "\t")
```

B.1.2 R Script for FDR Correction of ANOVA p-values

```
#copy the list of ANOVA p-values obtained from DeCyder into the clipboard
pvalueList <- read.table("clipboard")
fdrANOVA <- p.adjust(pvalueList, method ="fdr")
```

B.2 Raw Abundance Data for the Differentially Expressed Proteins Identified

Each figure below shows the abundance of a protein of interest at four time points of the culturing period.

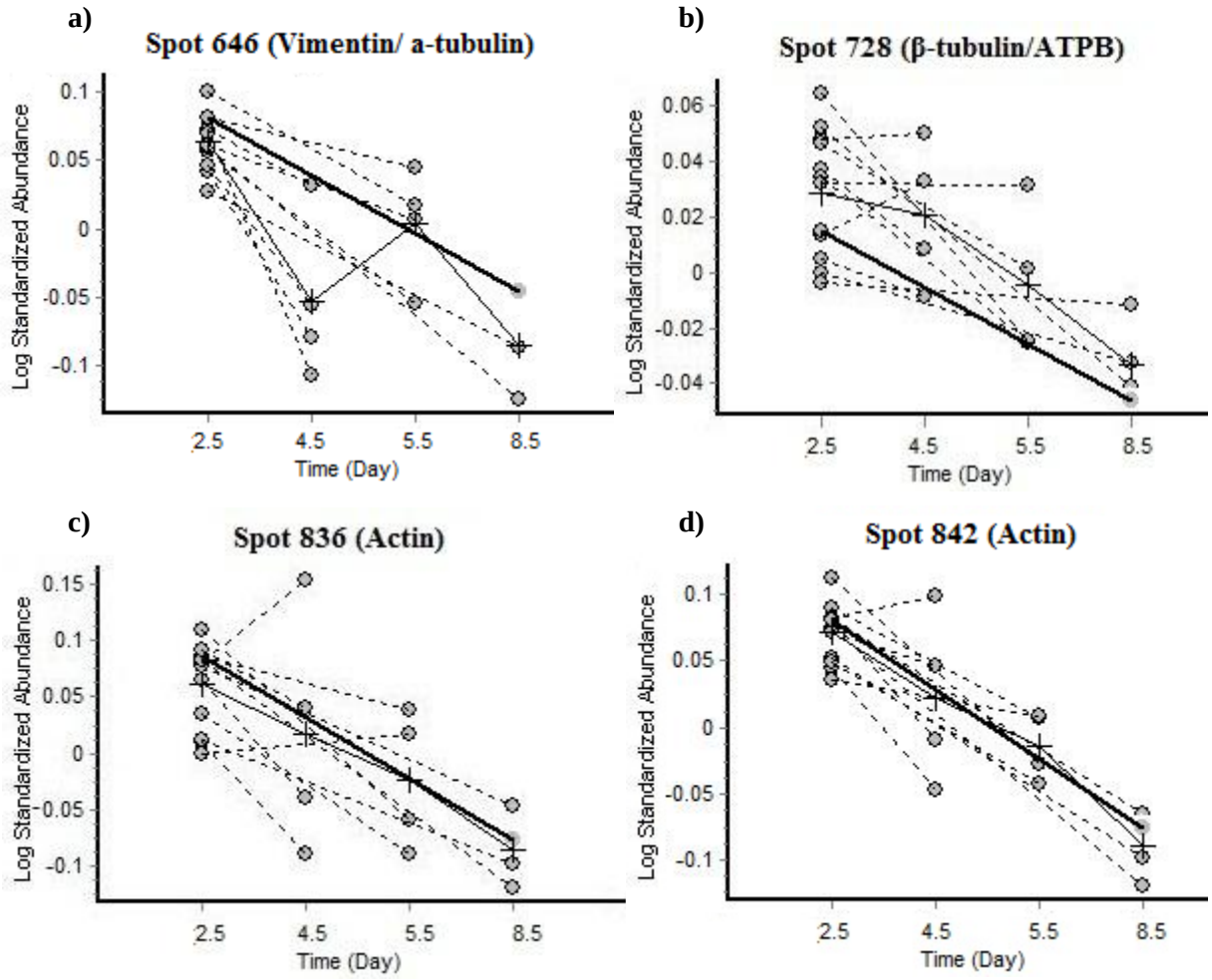

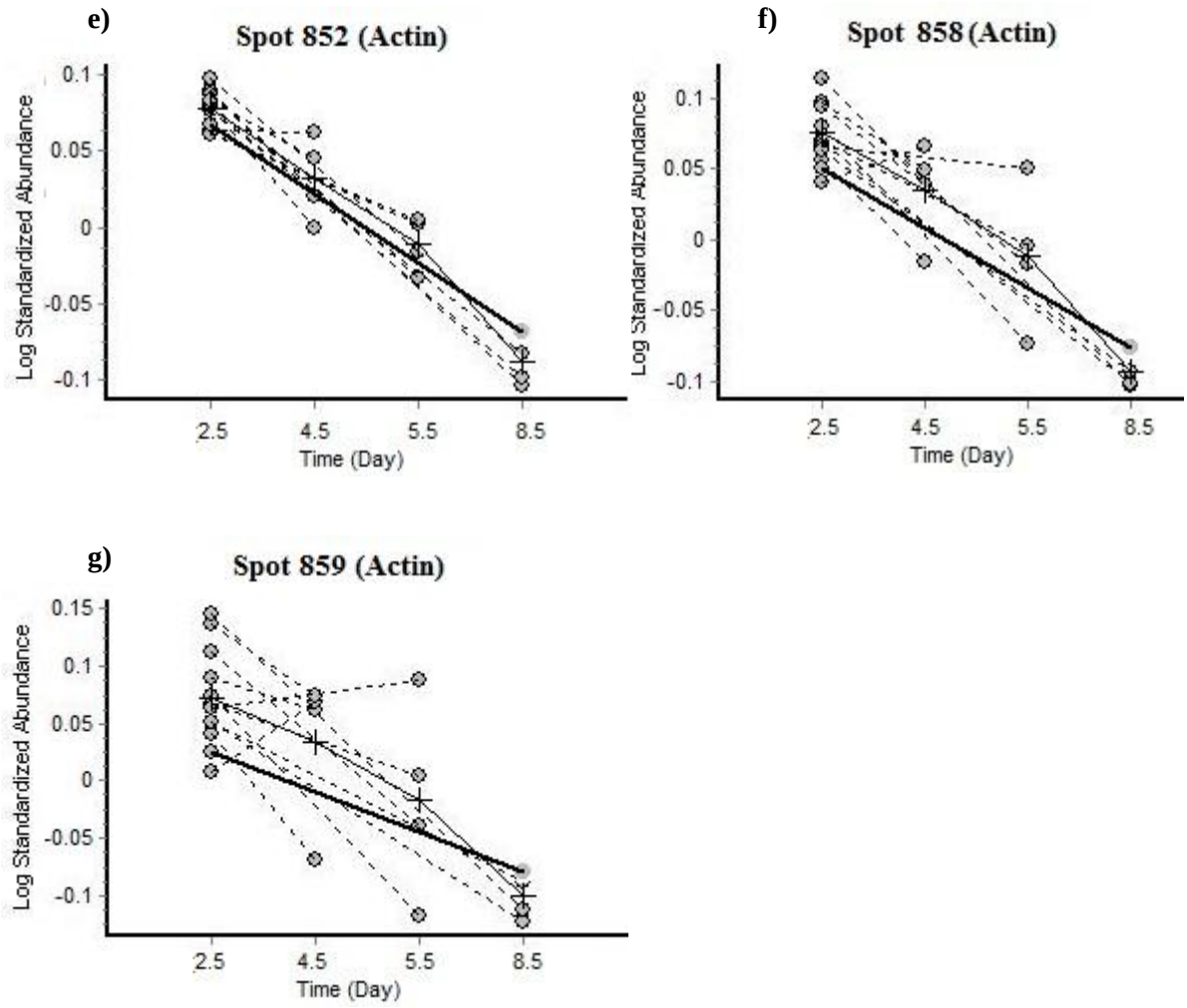

Figure B-1. Abundance data of protein spots having cytoskeletal functions.

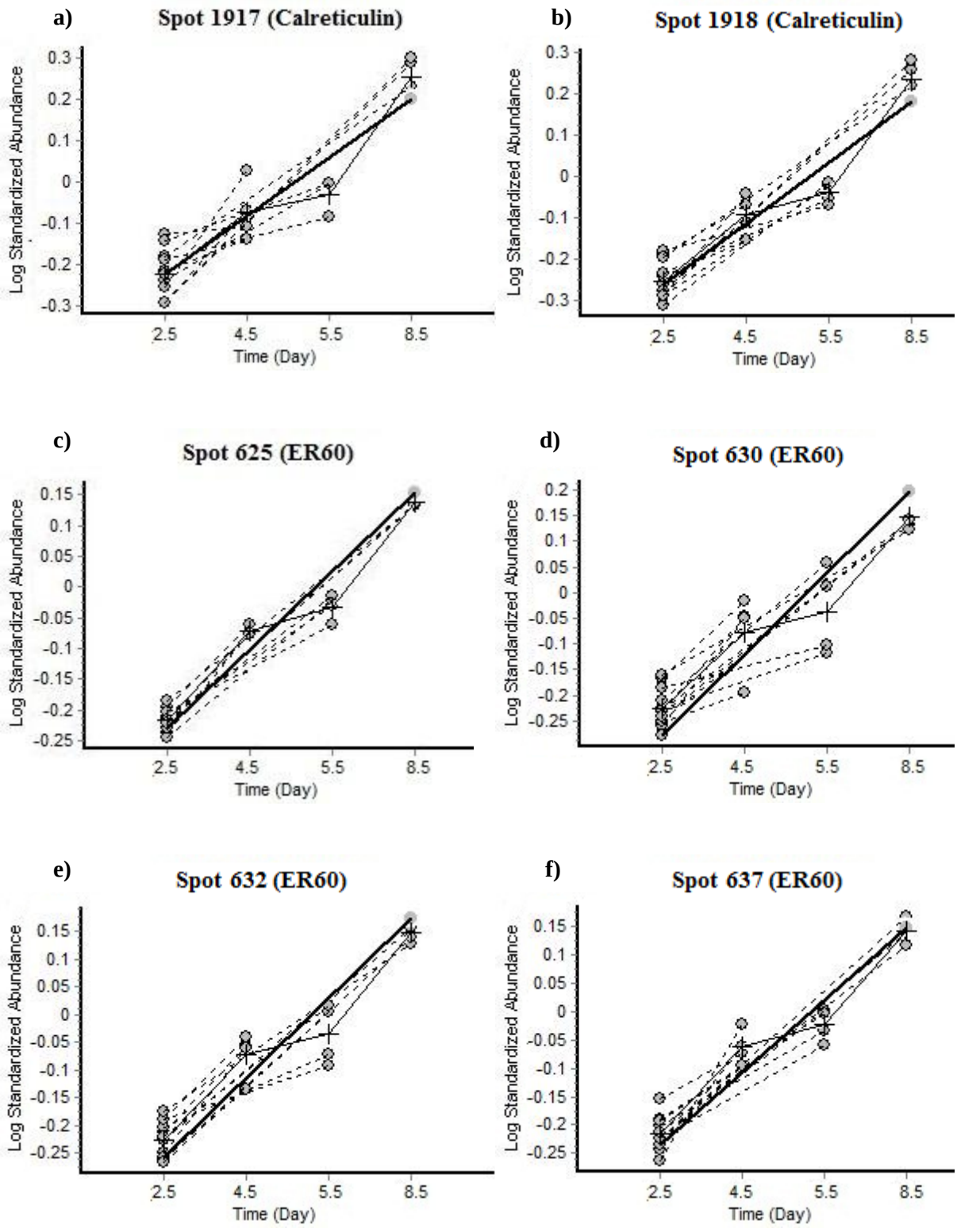
a)
Spot 1917 (Calreticulin)
b)
Spot 1918 (Calreticulin)
c)
Spot 625 (ER60)
d)
Spot 630 (ER60)
e)
Spot 632 (ER60)
f)
Spot 637 (ER60)
Log Standardized Abundance
Time (Day)
2.5
4.5
5.5
8.5

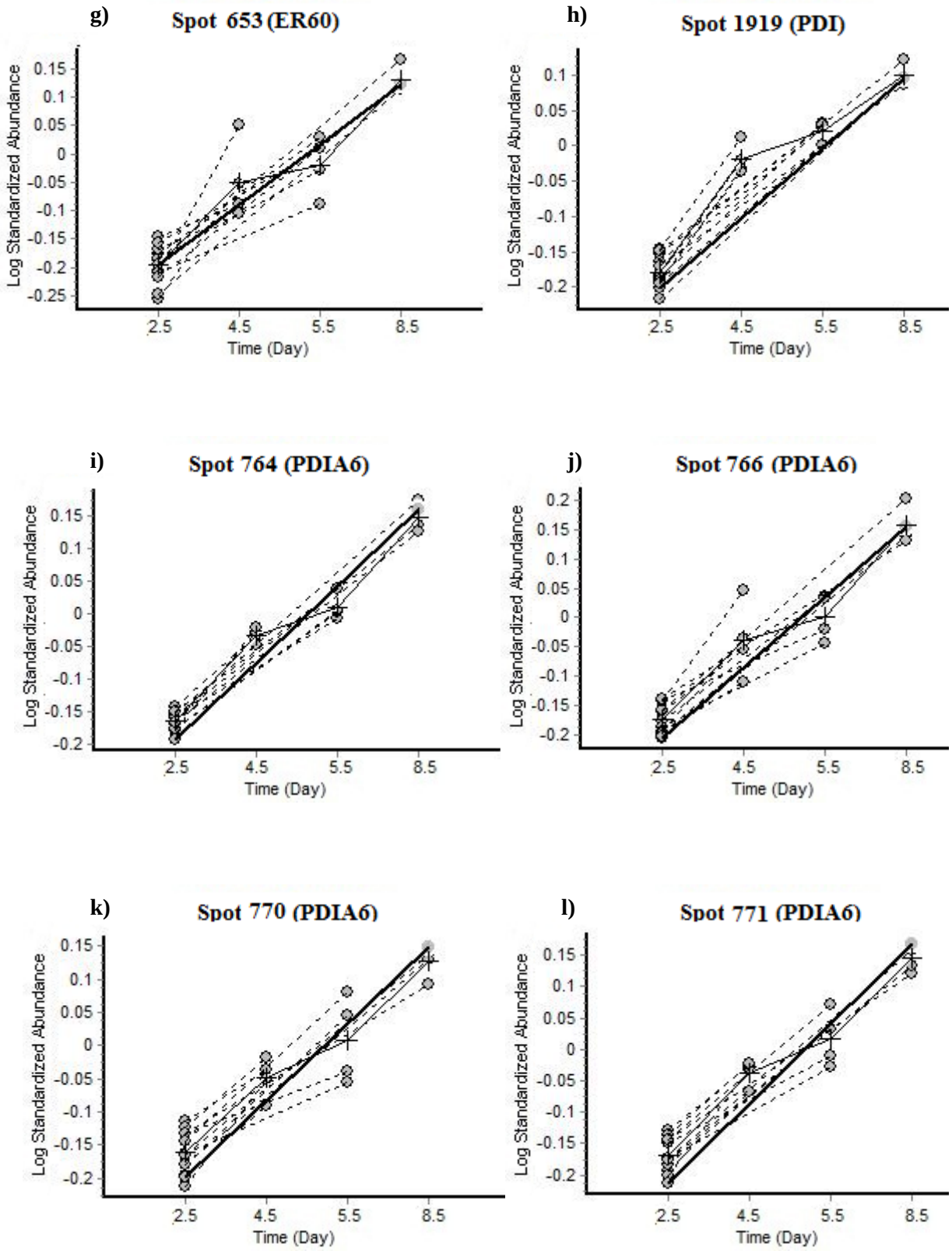
g)
Spot 653 (ER60)
h)
Spot 1919 (PDI)
i)
Spot 764 (PDIA6)
j)
Spot 766 (PDIA6)
k)
Spot 770 (PDIA6)
l)
Spot 771 (PDIA6)
Log Standardized Abundance
Time (Day)
2.5
4.5
5.5
8.5

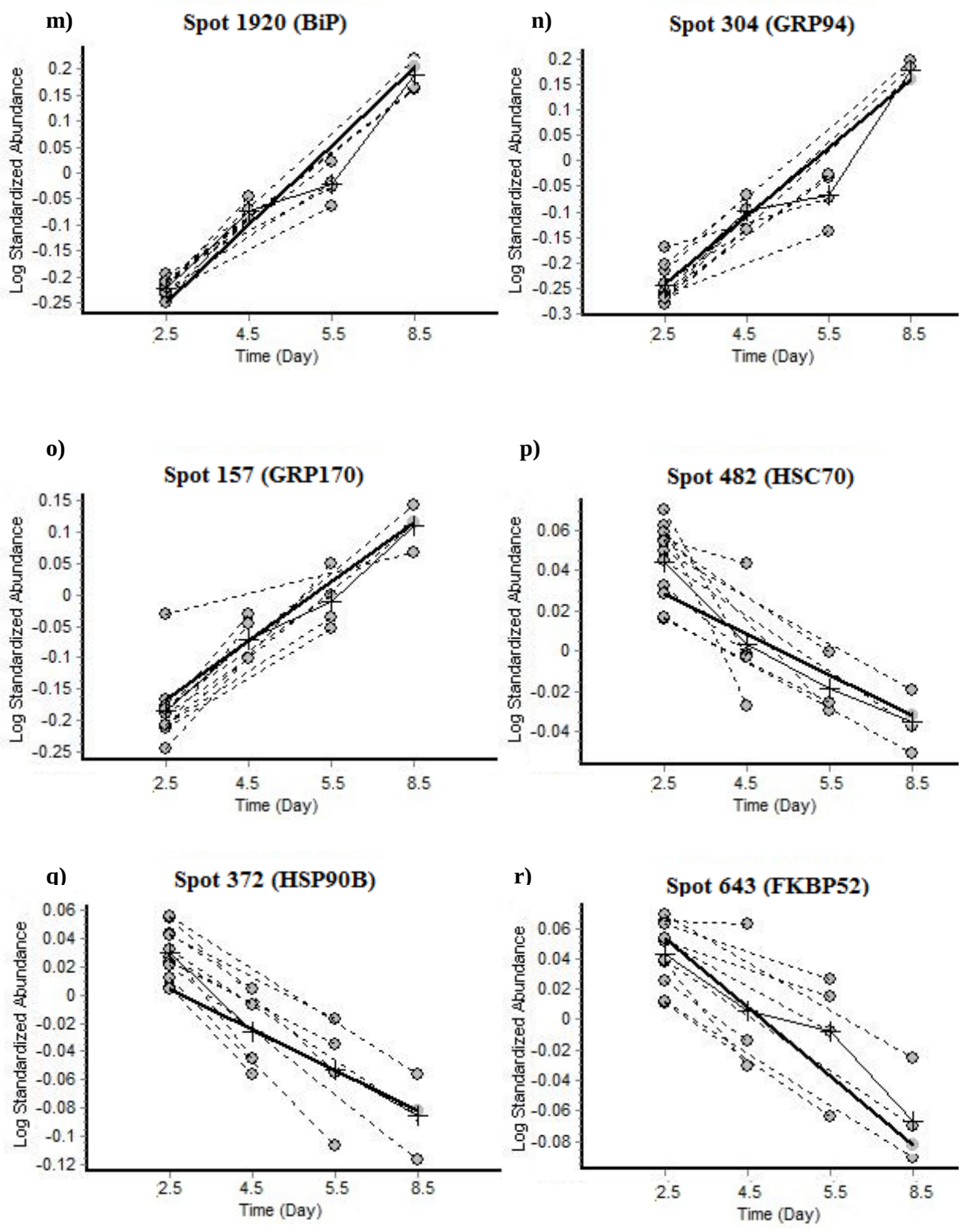

Figure B-2. Abundance data of protein spots identified as ER and cytosolic chaperones.

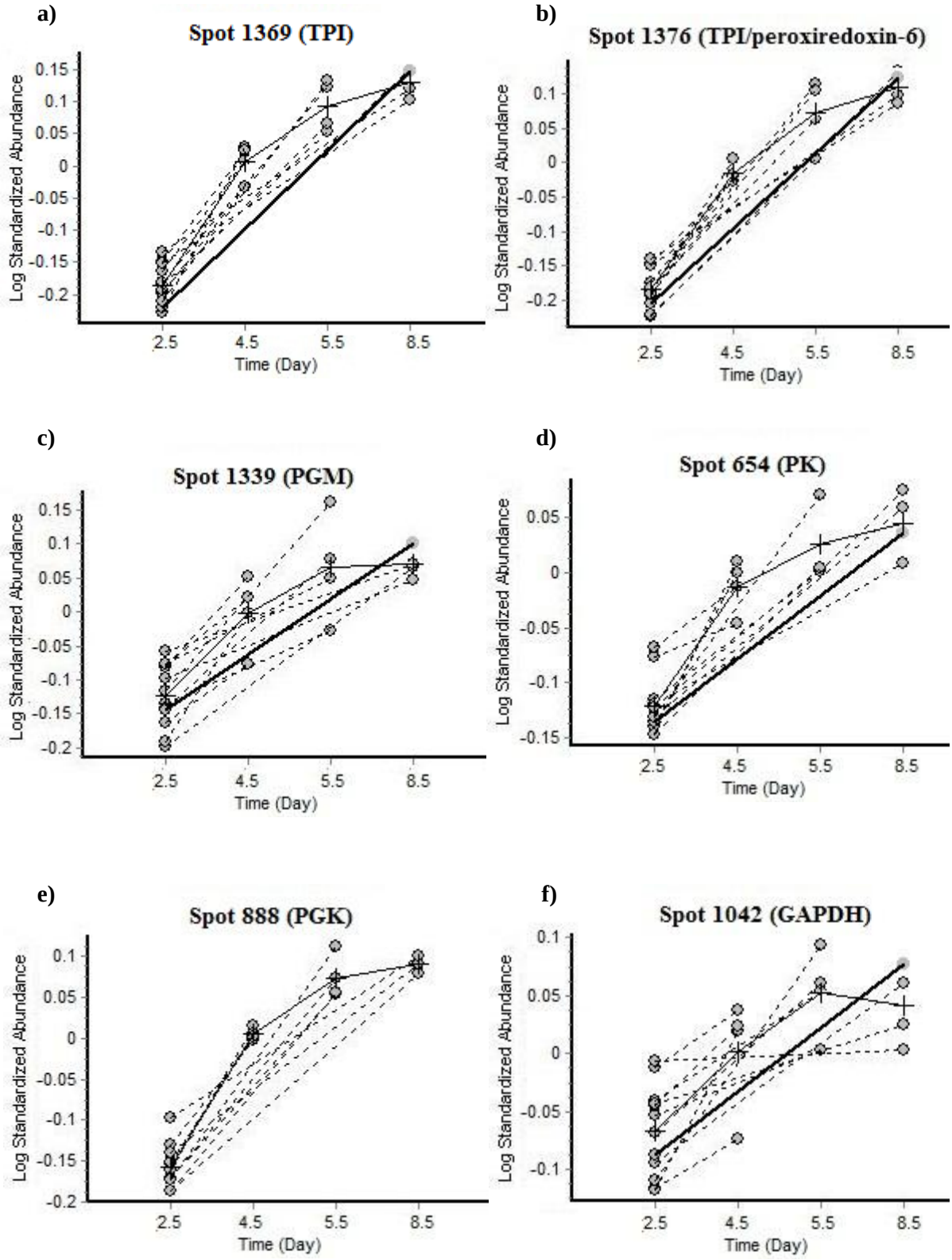
a)
Spot 1369 (TPI)
b)
Spot 1376 (TPI/peroxiredoxin-6)
c)
Spot 1339 (PGM)
d)
Spot 654 (PK)
e)
Spot 888 (PGK)
f)
Spot 1042 (GAPDH)
Log Standardized Abundance
Time (Day)
2.5
4.5
5.5
8.5

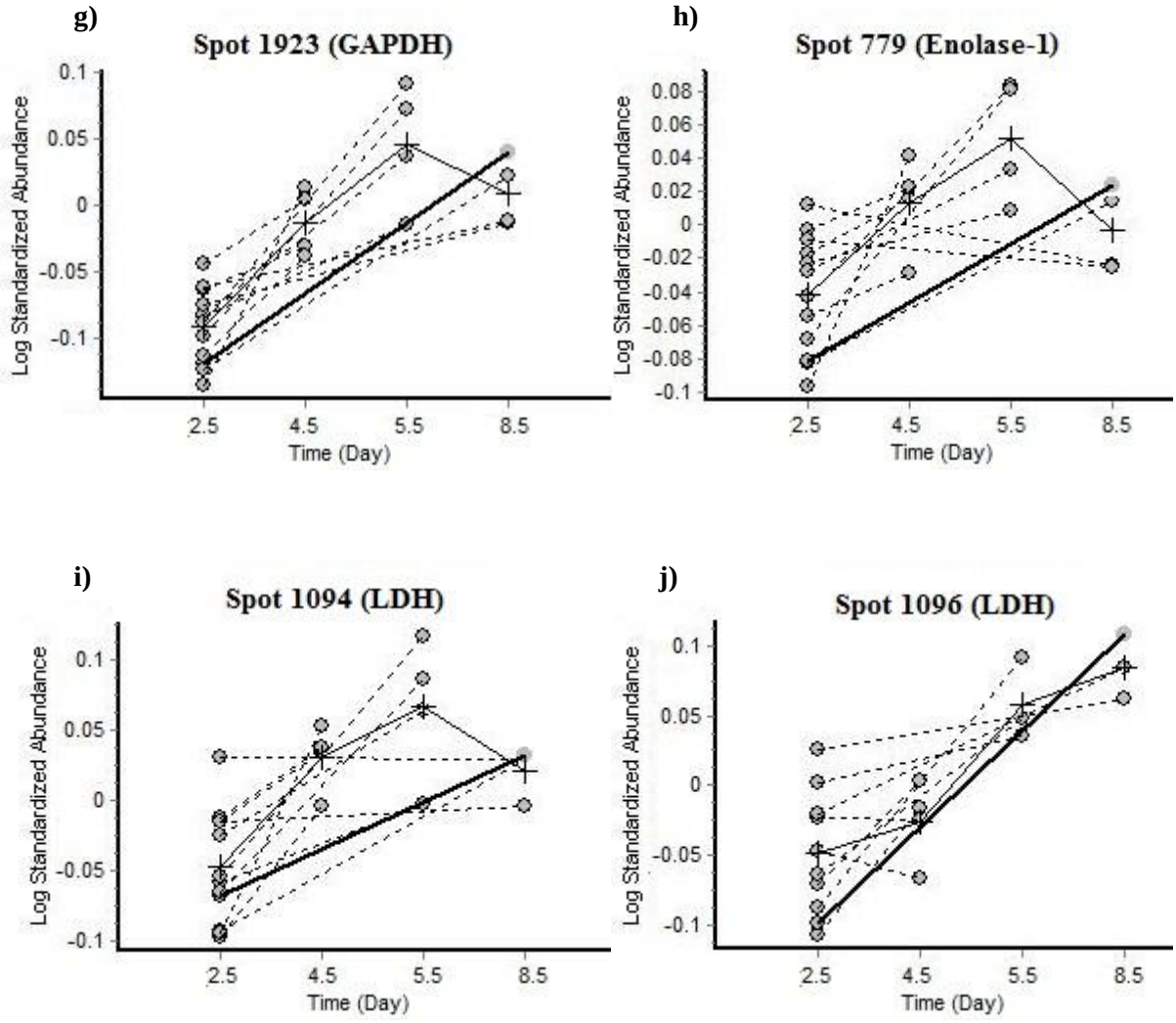

Figure B-3. Abundance data of protein spots identified as glycolytic and metabolic enzymes.

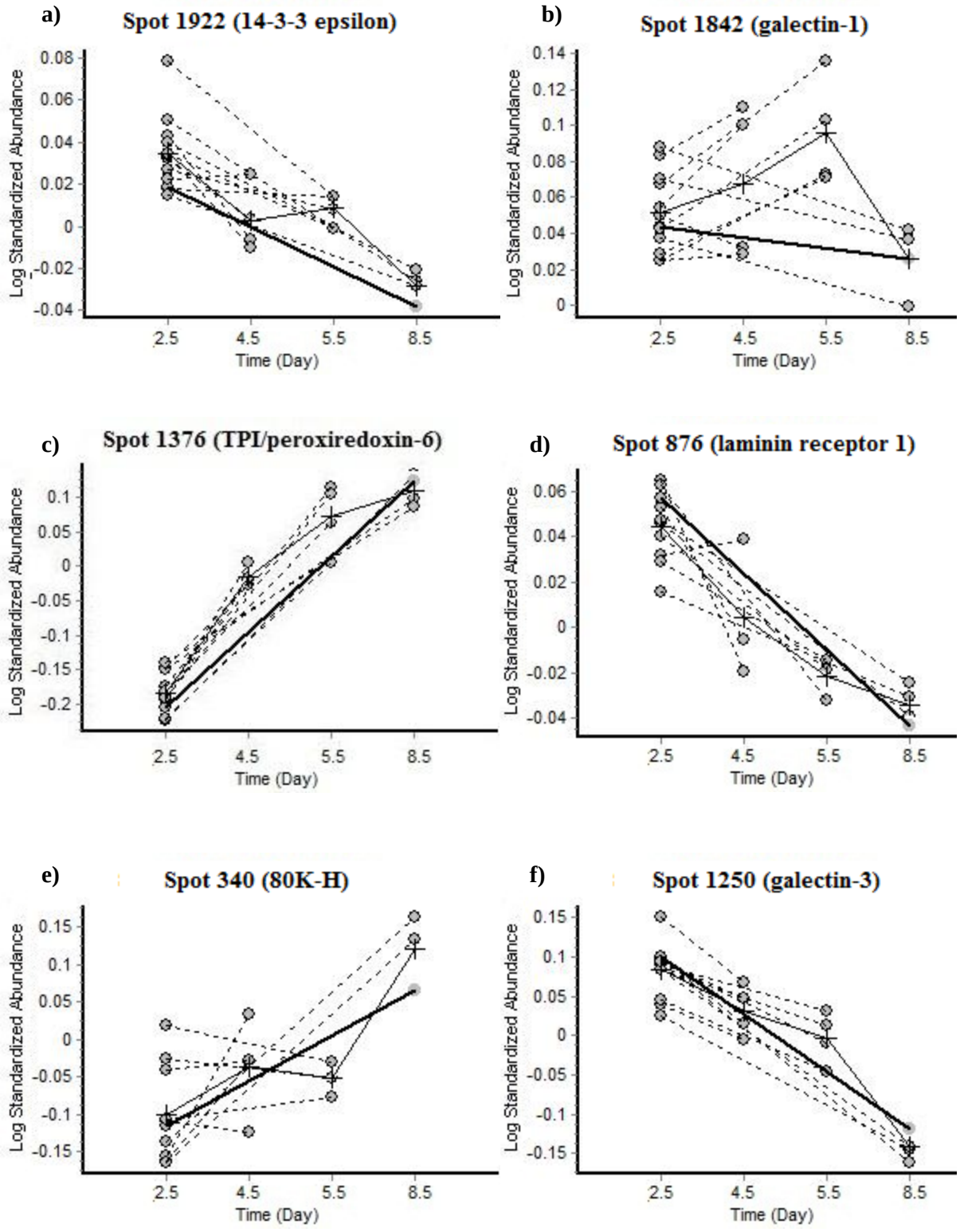
a)
Spot 1922 (14-3-3 epsilon)
b)
Spot 1842 (galectin-1)
c)
Spot 1376 (TPI/peroxiredoxin-6)
d)
Spot 876 (laminin receptor 1)
e)
Spot 340 (80K-H)
f)
Spot 1250 (galectin-3)
Log Standardized Abundance
Time (Day)
2.5
4.5
5.5
8.5

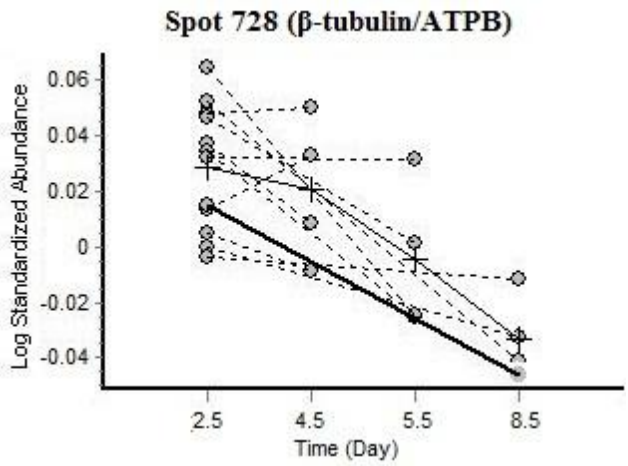

Figure B-4. Abundance data of protein spots having non-cytoskeletal, non-chaperone and non-glycolytic functions.

The detailed MS results from PEAKS and MASCOT analyses are shown in Table B-1 below.

Table B-1. Mass spectrometry results from PEAKS and MASCOT analyses

a) Cytoskeletal Proteins

Protein Name	DIGE spot ID	PEAKS					MASCOT				
		Score (%)	Accession	Mass (kDa)	No. of peptides matched	Sequence coverage (%)	score	Accession	Mass (kDa)	pI	No. of peptides matched
Vimentin	646†	93.8	BAD74030	53.6	5	12%	60	P02544	53.6	5.06	3
α-tubulin		n/a**					74	Q3TIZ0	50.6	4.96	2
β-tubulin	728††	n/a**					188	P99024	50.1	4.82	5
Actin (β/γ)	836	98.3	P83751	36.3	6	20.1%	194	Q3UGS0	42.1	5.37	5
	842	95.9	P20359	41.6	6	16%	177	O35247	42	5.37	5
	852	99.7	O76784	41.8	9	23.9%	203	O35247	42	5.37	7
	858	99.9	P60712	41.6	9	22.5%	334	O35247	42	5.37	8
	859	99.8	O76784	41.8	10	26.6%	336	Q3UGS0	42.1	5.37	10

b) ER and Cytosolic Chaperone Proteins

Protein Name	DIGE spot ID	PEAKS					MASCOT				
		Score (%)	Accession	Mass (kDa)	No. of peptides matched (+2,+3/+1)	Sequence coverage (%)	score	Accession	Mass (kDa)	pI	No. of peptides matched
Calreticulin	1917	93.1	Q8K3H7	48.2	8	23.5%	131	Q8K3H7	48.4	4.33	5
	1918	90.9	Q8K3H7	48.2	5	16.8%	84	Q8K3H7	48.4	4.33	3
ERp60	625	95	Q91Z81	56.7	8	16.8%	110	Q91Z81	57.2	5.98	5
	630	85	P11598	56.6	5	11.3%	72	P27773	57	5.98	3
	632	92.4	Q91Z81	56.7	5	9.9%	85	Q91Z81	57	5.98	4
	637	83	P11598	56.6	4	9.5%	65	P27773	57	5.98	3
	653	66.7	Q91Z81	56.7	3	6.9%	n/a				
PDI	1919	94.2	P05307	57.2	4	9%	126	P05307	57.6	4.8	4
PDIA6	764	97.3	P38660	48.1	6	19.4%	222	P38660	48.5	5.04	5
	766	89.1	P38660	48.1	4	13.7%	96	P38660	48.5	5.04	3
	770	88.3	P38660	48.1	5	16%	131	P38660	48.5	5.04	4
	771	95.8	P38660	48.1	6	21.2%	88	P38660	48.5	5.04	2
BiP	1920	99.8	P07823	72.3	11	22.5%	205	P06761	72.5	5.07	5
GRP94	304	99.6	Q3UBU0	92.4	7	11.4%	210	Q3UBU0	92.7	4.74	4
GRP170	157	92.8	Q9JKR6	111.1	6/5	6.6%	262	Q9JKR6	111.4	5.14	8
HSC70	482	73.3	Q53HF2	53.4*	8/2	16%	234	P19120	42.2*	6.62	5
HSP90β	372	n/a					53	P34058	83.6	4.95	6
FKBP52	643	n/a					168	P27124	51.7	5.34	3

C) Glycolytic Proteins and other metabolic enzymes

Protein Name	DIGE spot ID	PEAKS					MASCOT				
		Score (%)	Accession	Mass (kDa)	No. of peptides matched	Sequence coverage (%)	score	Accession	Mass (kDa)	pI	No. of peptides matched
Triosephosphate isomerise	1369	98.6	Q53HE2	26.7	10/6	31.7	153	P00939	26.9	7.1	2
	1376†††	84.4	P00939	26.6	4/2	12.5	121	P00939	26.9	7.1	3
Phosphoglycerate mutase1	1339	86.9	P18669	28.6	8	36.4	167	P18669	28.9	6.67	8
Pyruvate kinase isozyme M1/M2	654	96.2	P11980	57.7	6	12.6	147	P52480	58.3	7.42	5
Phosphoglycerate kinase	888	89.4	P50310	44.5	5	17	141	P50310	44.8	8.02	4
Glyceraldehyde-3-phosphate dehydrogenase	1042	65.5	P00355	35.7	5	21.1	225	P17244	36	8.49	5
	1923	98.3	P00355	35.7	7	28.6	218	P17244	36	8.49	5
Enolase-1	779	90.9	P04764	50.6	4	11	213	Q9PVK2	47.5	6.62	4
L-lactate dehydrogenase chain A/C	1094	77.1	P07864	28.9	2	7.9	149	P00340	36.7	8.18	2
	1096***	35.7	Q5R1W9	36.5	1/3	5.7	89	Q06BU8	36.8	7.01	2

D) Other Proteins

Protein Name	DIGE spot ID	PEAKS					MASCOT				
		Score (%)	Accession	Mass (kDa)	No. of peptides matched	Sequence coverage (%)	score	Accession	Mass (kDa)	pI	No. of peptides matched
14-3-3 epsilon	1922	72.2	Q1HPT4	29.6	2/1	9.5	213	Q4VJB6	26.7	4.76	3
Galectin-1	1842***	42.1	P48538	14.6	2	18.7	42	P48538	15.1	5.52	2
Peroxiredoxin-6	**1376†††**	49.2	O35244	24.8	3	13.8	63	O08709	24.8	5.72	3
Laminin receptor 1	876	78.5	P08865	31.8	3	11.2	165	P26452	32.9	4.8	3
80K-H	340	49.5	Q3U518	58.6	2	5.4	101	P14314	45.3	4.27	2
Galectin-3	1250	33	P08699	27	1 (+3)	5.4	n/a				
ATP synthase subunit beta, mitochondrial	728††	52.8	P46561	57.5	2	6.1	77	P00829	56.2	5.15	2

** The top hit matches to a Hsc70 fragment thus the mass is much less than 70kDa. This record was still an unreviewed UniProtKB entry.*
******* no match to this particular protein was resulted but a match to another protein for the same spot was resulted.*
**** MASCOT search with MSDB returned no hit so search was repeated with SWISS-PROT and NCBI-DB.*

† Mascot reported two different proteins from a single MS analysis. The two sets of matched peptides had no overlap. PEAKS matches to only one identification.
†† Both b-tubulin and ATP synthase beta subunit were detected in reference maps by Hayduk and Van Dyk with very similar pI. In both studies, β-tubulin had slightly heavier MW than ATP synthase beta. It is likely that overlapping of these two proteins occurred during electrophoresis or from imprecise spot picking.
††† TPI and Prx6 were identified when analyzing spot 1376 on two gels.

Note: The MASCOT mass and estimated pI were as reported by MASCOT ms/ms analysis. The PEAKS mass and sequence coverage were as reported by PEAKS analysis. In both cases, the accession numbers reported are the most current version. Some matching resulted in protein records that are obsolete due to various reasons such as deletion and record/database merging. As a result, the reported accession number might correspond to a protein with slightly different sequence from the obsolete record. In turns, this implies that the reported mass, pI and sequence coverage might not correspond perfectly to the reported accession number.